10.13147/NYME.2014.014

Nyugat-magyarországi Egyetem
Roth Gyula Erdészeti és Vadgazdálkodási Tudományok Doktori Iskola
Erdei ökoszisztémák ökológiája és diverzitása program

FACTORS INFLUENCING SEDIMENT TRANSPORT ON THE HEADWATER CATCHMENTS OF RÁK BROOK, SOPRON

HORDALÉKSZÁLLÍTÁSRA HATÓ TÉNYEZŐK A SOPRONI RÁK-PATAK FELSŐ VÍZGYŰJTŐJÉN

DOKTORI (PhD) ÉRTEKEZÉS

Készítette:
Csáfordi Péter

Témavezetők:
Dr. habil Gribovszki Zoltán PhD PhD
Dr. Kalicz Péter PhD

Sopron, 2014

10.13147/NYME.2014.014

Factors influencing sediment transport on the headwater catchments of Rák Brook, Sopron

Hordalékszállításra ható tényezők a soproni Rák-patak felső vízgyűjtőjén

Értekezés doktori (PhD) fokozat elnyerése érdekében
Készült a Nyugat-magyarországi Egyetem
Roth Gyula Erdészeti és Vadgazdálkodási Tudományok Doktori Iskolája
Erdei ökoszisztémák ökológiája és diverzitása programja keretében

Írta:
Csáfordi Péter

Témavezetők: Dr. habil Gribovszki Zoltán PhD PhD
Elfogadásra javaslom (igen / nem) .....
aláírás

Dr. Kalicz Péter PhD
Elfogadásra javaslom (igen / nem) .....
aláírás

A jelölt a doktori szigorlaton ..... % -ot ért el,
Sopron, 2011. június 28.

.....
a Szigorlati Bizottság elnöke

Az értekezést bírálóként elfogadásra javaslom (igen /nem)

Első bíráló: ..... igen / nem .....
aláírás

Második bíráló: ..... igen / nem .....
aláírás

(Esetleg harmadik bíráló ..... igen / nem .....
aláírás)

A jelölt az értekezés nyilvános vitáján ..... % -ot ért el,
Sopron, ...
a Bírálóbizottság elnöke

A doktori (PhD) oklevél minősítése .....
Sopron, ...
Az EDT elnöke

10.13147/NYME.2014.014

„ …megméretik az embernek fia
s ki mint vetett, azonképpen arat.
Mert elfut a víz és csak a kő marad,
de a kő marad.”

(Wass Albert: Üzenet haza)

„ …the man will be judged
and we reap what we sow.
Because the water runs off and only the stone remains,
but the stone remains.”

(Albert Wass: Message to home)

Contents

List of symbols and abbreviations 7
Abstract 9
Kivonat 10
1. Introduction 11
1.1. Background 11
1.2 Soil erosion by water 12
1.3 Soil erosion modelling 14
1.3.1 The Universal Soil Loss Equation and its applicability 14
1.3.2 Implementation of the USLE in Geographical Information Systems 16
1.3.3 The soil erosion prediction model EROSION-3D 17
1.4 Sediment types 19
1.4.1 Bedload transport 20
1.5 Suspended sediment transport 23
1.5.1 Physical principles of the suspended sediment transport 23
1.5.2 Temporal variability of the suspended sediment transport 23
1.5.3 Hydrological, hydrometeorological and climate parameters influencing the suspended sediment transport 27
1.5.4 Prediction of suspended sediment transport 28
1.6 Erosion and sediment dynamics under different land cover and land use 31
1.6.1 Erosion and sediment dynamics of forested catchments 31
1.6.2 Impact of the land cover alterations on the suspended sediment dynamics 34
2. Objectives and research questions 36
3. Materials and methods 38
3.1 Study area 38
3.1.1 The catchment of the Rák Brook 38
3.1.2 The Farkas Valley and the Vadkan Valley 39
3.2 Sediment and sediment control parameters 44
3.2.1 Precipitation data 44
3.2.2 Runoff data 46
3.2.3 Temperature data 48
3.2.4 Sediment data 48
3.3 Statistical analyses 52
3.4 Geodesic survey and working with GIS 53
3.5 Soil loss calculations 56
3.5.1 Determination of factors of the Universal Soil Loss Equation (USLE) 56
3.5.2 Datasets and parameters of the EROSION-3D 58
4. Results 59
4.1 Soil, rainfall and runoff conditions 59
4.1.1 Soil map of the Farkas Valley and spatial distribution of the *K* factor 59
4.1.2 Precipitation categories and the descriptive statistical variables of different rainfall parameters 59
4.1.3 Characterization of flood events in the Farkas Valley 63
4.2 Suspended sediment concentration and its control factors 66
4.3 Relation between suspended sediment and sediment control factors 71
4.3.1 Relation between suspended sediment and sediment control factors at low flow 71
4.3.2 Relation between suspended sediment and sediment control factors at high flow 75

4.4 Sediment yield calculations 85
4.4.1 Regression equations for calculating suspended sediment yield 85
4.4.2 Calculation of sediment yield at annual and event-scale 86
4.4.3 Quantification of the sediment contribution by an outwashing sediment deposit 91
4.5 Contribution of soil erosion to the sediment transport 94
4.5.1 Development of the workflow “Erosion analysis” in the ArcGIS Model Builder 94
4.5.2 Modelling of surface erosion with the USLE in the Farkas Valley 97
4.5.3 Modelling with EROSION-3D 99
5. Discussion and conclusions 102
6. Outlook 105
7. Theses of the dissertation 106
Acknowledgements 108
References 109
List of figures 121
List of tables 123
Annex 124
Annex I.III 124
Annex I.IV 125
Annex I.V 126
Annex III.I 127
Annex III.III 131
Annex III.V 133
Annex IV.I 136
Annex IV.II 140
Annex IV.III 144
Annex IV.IV 148
Annex IV.V 152

List of symbols and abbreviations

A average annual soil loss ($t \cdot ha^{-1} \cdot yr^{-1}$)
$a, b, c, d, f, j, k, m, n, o, p$ empirical (rating) coefficients (*dimensionless*)
ABF strongly acidic non-podzolic brown forest soil
A_c catchment area (km^2)
AC aggregate category
AD antecedent days (number of days elapsed since the previous flood event) (*days*)
API antecedent precipitation index (cumulative rainfall depth) (in general)
API1 antecedent precipitation of 1 day before the sampling/before the flood event (*mm*)
API3 antecedent precipitation of 3 days before the sampling/before the flood event (*mm*)
API7 antecedent precipitation of 7 days before the sampling/before the flood event (*mm*)
BY bedload yield ($t \cdot yr^{-1}$; $t \cdot month^{-1}$)
*BY** bedload yield between two measurements (*kg*)
$BY_{bf\_average}$ average baseflow bedload yield ($kg \cdot min^{-1}$)
BY_{flood_obs} bedload yield of the sampled flood event (*kg*)
C cover-management factor (*dimensionless*)
CF log-transformation bias correction factor
CS colluvial soil
$_{c1}$ tipping bucket rain gauge with 0.1 mm rainfall capacity
D mean stream depth (*m*)
DEM Digital Elevation Model
d_s diameter of sediment particle (*mm*)
e exponential function
EI rainfall erosivity index ($kJ \cdot m^{-2} \cdot mm \cdot h^{-1}$)
g acceleration due to gravity ($m \cdot s^{-2}$)
G specific gravity (*dimensionless*)
GIS Geographical Information Systems
h water stage (*cm*)
$_{hhm}$ tipping bucket rain gauge with 0.5 mm rainfall capacity
I_{max30} maximum 30-min rainfall intensity ($mm \cdot h^{-1}$)
K soil erodibility factor ($t \cdot ha^{-1} \cdot m^2 \cdot kJ^{-1} \cdot h \cdot mm^{-1}$)
L slope length factor (*dimensionless*)
LBF lessivated brown forest soil
LWD large woody debris
MD molecular diffusion coefficient ($L^2 \cdot T^{-1}$)
m, n empirical exponents
OS content of organic substance (%)
P erosion-control practice factor (*dimensionless*)
PBF podzolic brown forest soil
PC category of permeability
q, Q discharge ($m^3 \cdot s^{-1}$, $l \cdot s^{-1}$)
q_{bv} volume of gravel material in motion per unit cross-section width and time ($L^2 \cdot T^{-1}$)
q_{bv*} dimensionless volumetric unit sediment discharge
Q_d daily discharge of water ($m^3 \cdot s^{-1}$)
Q_{max} peak discharge during a flood event ($l \cdot s^{-1}$)
Q_s sediment yield ($mg \cdot s^{-1}$)

p	significance level in the statistical analyses
P	rainfall depth (mm)
r	correlation coefficient (Pearson's r)
r^2	determination coefficient (in linear regressions)
R	rainfall-runoff erosivity factor ($kJ \cdot m^{-2} \cdot mm \cdot h^{-1}$)
R_h	hydraulic radius (m)
s	energy slope of the reach (*dimensionless*)
S	slope steepness factor (*dimensionless*)
SD, Std.Dev.	standard deviation
SDR	sediment delivery ratio (*%*)
SSC	suspended sediment concentration ($mg \cdot l^{-1}$)
S_{sed}	suspended sediment supply
$ST0$	soil temperature at 0 cm depth (^oC)
$ST5$	soil temperature at 5 cm depth (^oC)
$ST10$	soil temperature at 10 cm depth (^oC)
SSY	suspended sediment yield ($t \cdot yr^{-1}$)
SSY_d	daily discharge of suspended sediment ($kg \cdot s^{-1}$)
$SumQ$	total volume of the flood event (l)
$SumQ_{hf}$	total volume of high flow periods between two bedload measurements (l)
SY	sediment yield (in general)
t	time/duration
TSY	total sediment yield (suspended sediment yield + bedload yield) ($t \cdot yr^{-1}$)
u^*	shear velocity
USLE	Universal Soil Loss Equation
x, y, z	coordinates
v	mean flow velocity in the cross-section ($m \cdot s^{-1}$)
v_b	actual flow velocity near the bed
v_c	critical velocity required to just move a particle ($m \cdot s^{-1}$)
W	stream width (m)
WT	water temperature (^oC)

Greek symbols:

$\alpha_{1,2,3,4}$, $\beta_{1,2,3,4}$	empirical coefficients
β	slope steepness (^{o})
γ	specific weight of water ($N \cdot m^{-3}$)
γ_m	specific weight of the fluid mixture ($N \cdot m^{-3}$)
γ_s	specific weight of the sediment particle ($N \cdot m^{-3}$)
ε	turbulent mixing and dispersive coefficient
ρ	mass density of water ($kg \cdot m^{-3}$)
ρ_m	mass density of the water-sediment mixture ($kg \cdot m^{-3}$)
ρ_s	mass density of sediment ($kg \cdot m^{-3}$)
σ	standard error of the regression equation
τ_0	shear stress at the bed ($N \cdot m^{-2}$)
τ_c	critical shear stress to initiate gravel motion ($N \cdot m^{-2}$)
τ^*	dimensionless shear stress – Shields parameter
ω_0	Rubey's clear-water fall velocity
Ψ	empirical rating parameter (*dimensionless*)

Abstract

The dissertation reveals the complexity of sediment dynamics and describes the reasons of the sediment stochasticity with special regard to the suspended sediment transport in the catchment of the Rák Brook in the Sopron Hills, Hungary. Based on ten-years-long dataset, the relation between suspended sediment concentration and hydrological, hydro-meteorological and meteorological variables has been evaluated at different flow conditions and different temporal resolution in the Farkas Valley and the Vadkan Valley. The results draw attention to the seasonality, the inter- and intra-event fluctuation of the parameters. As sediment outwash and replenishment may explain the low flow sediment dynamics as well, the role of days elapsed since the previous flood event has also been the investigated. As a major result of this part, different hysteresis types have been recognised on the basis of sediment rating curves under high flow conditions.

To calculate suspended sediment concentration under high flow conditions, regression models have been developed. Using the observed and modelled values, sediment yield has been computed at event and annual scale in the Farkas Valley. The reference hydrological year is 2008-2009, in order to point out the influence of a sediment deposit on the total annual sediment yield which has been outwashed between October 2008 and August 2009. The calculated total sediment yield (124.7 $t \cdot yr^{-1}$) is equal as if about 0.15 *mm* soil layer eroded from the surface of the entire catchment and reached the channel. As a stochastic process, sediment exhaustion from the deposit behind log jam increased by 15% (15.8 *t* sediment surplus) the total sediment yield.

Erosion modelling has been performed with an empirical soil loss equation (Universal Soil Loss Equation – USLE, *Wischmeier & Smith* 1978) and a physical erosion model (EROSION-3D, *von Werner* 1995). The USLE modelling, which have been supported by a self-made workflow built in the ArcGIS Model Builder, shows that surface erosion is not an important form of soil erosion in the Farkas Valley (13% proportion to the total annual sediment yield). The length-slope factor is the most important factor determining the surface erosion. Test of the EROSION-3D model can only be applied for qualitative analyses of soil erosion: the unpaved roads produced the highest average soil loss.

Although several research questions in connection with sediment dynamics in forested catchments have not been clarified yet, the results give new aspects for the sediment transport and erosion processes in the Sopron Hills. Results of the low flow sediment transport and the GIS-workflow to the USLE model can be utilized outside of the study catchment as well. To achieve more plausible and comprehensive results, development of the data collection methods is a necessary requirement in the future.

Kivonat

A disszertáció feltárja a hordalékszállítási dinamika komplex jellegét és jellemzi annak sztohaszticitásának okait, különös tekintettel a Soproni-hegységben eredő Rák-patak mellékvízgyűjtőinek lebegtetett hordalékszállítására. A szerző dolgozatában 10 éves adatsor alapján vizsgálja a Farkas-árokban és Vadkan-árokban mért lebegtetett hordalékkoncentrációk összefüggését hidrológiai, hidrometeorológiai és meteorológiai paraméterekkel különböző vízhozam-tartományok és időbeli felbontás esetén. Az eredmények rámutatnak az egyes változók szezonális változására és az egyes árhullámok alatti és közötti fluktuációjára. Mivel a hordalék árhullámok alatti kimosódása és visszatöltődése a kisvízi hordalékszállítás törvényszerűségeit is magyarázhatja, a szerző a megelőző árhullám óta eltelt napok számát is bevonta vizsgálataiba. A dolgozat egy fő eredménye, hogy az árhullámok alatti hordalékkoncentráció és vízhozam közötti kapcsolat (hordalékhozam-görbe) elemzése során több különböző hiszterézistípust sikerült azonosítani.

A szerző regressziós egyenleteket határozott meg a nagyvízi lebegtetett hordalékkoncentrációk számítására. Mért és modellezett értékek felhasználásával kiszámolta a Farkas-árok hordalékhozamát esemény és éves szinten. Referenciaként a 2008-2009-es hidrológiai év szolgált, hogy egy 2008. október és 2009. augusztus között kiürülő hordalékdepónia éves hordalékhozamra gyakorolt hatása is számszerűsíthető legyen. A számolt éves hordalékhozam (124,7 *t/év*) úgy értelmezhető, mintha a vízgyűjtőről egységesen 0,15 *mm* talaj pusztult volna le és az mind a patakmederbe került volna. A hordalékdepónia elszállítódása – sztochasztikus folyamatként – 15%-os növekedést okozott a Farkas-árok éves hordalékhozamában (15,8 *t* hordaléktöbblet).

Az eróziómodellezés egy empirikus talajvesztési egyenlettel (Általános Talajvesztési Egyenlet – USLE, *Wischmeier & Smith* 1978) és egy fizikai eróziómodellel (EROSION-3D, *von Werner* 1995) történt. Az Általános Talajvesztési Egyenlet – amelyet a szerző az ArcGIS Model Builder segítségével adaptált térinformatikai környezetbe – alapján a felületi erózió elhanyagolható jelentőségű a Farkas-árok területén (13%-os részesedés az éves hordalékhozamból). Az eróziót leginkább meghatározó tényező a lejtés-lejtőhossz faktor. Az EROSION-3D modell csak a talajpusztulás minőségi értékelésére volt alkalmazható. E modell szerint a burkolatlan közelítőutak produkálták a legmagasabb átlagos talajveszteséget.

Habár a disszertáció számos tudományos kérdésre nem ad választ, eredményei mégis egy új irányvonalat jelentenek a Soproni-hegység hordalékszállításának és talajpusztulásának vizsgálatában. A kisvízi hordalékszállítással kapcsolatos következtetések és az USLE modellhez elkészített GIS-keretrendszer pedig más vízgyűjtőkön is alkalmazhatók. Megbízhatóbb eredmények és átfogóbb megállapítások elsősorban az adatgyűjtési módszerek jövőbeli fejlesztésével lennének elérhetők.

1. Introduction

1.1. Background

Nowadays sediment transport and soil erosion processes may lead to even more serious environmental and ecological catastrophes due to the global climate changes. Precipitation scenarios for Hungary agree that intensity and frequency of extreme precipitation will increase, while the total precipitation amount will decrease. Namely the change of rainfall distribution leads to the increase of drought and heavy rainstorm frequency (*Bartholy & Pongrácz* 2007, *Gálos et al.* 2007, *Kis* 2011). The intensification of rainfall events accompanies the increase of surface runoff due to the time reduction of infiltration and infiltration excess. As the hydrological response will be faster, the rise of design flood level is also expected, especially in the small catchments. Higher raindrop energy, surface runoff and stream power have influence on the rate of soil detachment and transported *SY* as well. Several news and studies reported on disastrous flash floods and debris flows when not only the high *Q* but the meaningful *SY* was also responsible for the damages (*URL1-3*, *Vinet* 2008, *Mizuyama & Egashira* 2010, *Shieh et al.* 2010).

Soil erosion, as the main source of the sediment in the watercourses shows also a growing tendency related to the extreme precipitation. However, the role of the land use is also important considering the sediment delivery problem. Although water erosion is a natural process which is responsible for landscape degradation (*Thyll* 1992), human activities, such as road building, tree and crop harvesting and overgrazing increase the detachment of soil particles. Soil loss promotes different harmful hydrological changes in the soil (e.g. reduction of water holding capacity, infiltration capacity) and in the water bodies as well (e.g. decrease of river channel stability and siltation of channels and lakes). The decreasing reservoir capacity and flow section of channels imply higher flood risk (*Lewis* 1998). Changes of channel morphology may cause the loss or modification of aquatic habitats. Eroded material as suspended sediment enhances the turbidity altering the aquatic ecosystems (*Ma* 2001). Suspended particles can directly injure gills of fish and macroinvertebrates, impair the ability to locate food, reduce the depth at which photosynthesis can take place. Suspended particle-bond substances can lead to the contamination of aquatic ecosystems, such as eutrophication caused by the nutrients (*Clement et al.* 2009, *Rodríguez-Blanco et al.* 2009a) and acute intoxication due to contaminants, such as metals (*Rodríguez-Blanco et al.* 2009b). Sediment in the water shortens the life of irrigation systems and hydraulic structures. To avoid the multiple harmful effects, as reported by several authors (*Bogárdi* 1971, *Shen & Julien* 1993, *Gordon et al.* 2004, *Owens & Collins* 2006, *Chang* 2006), it is necessary to get detailed information about soil erosion and sediment dynamics. Nevertheless, it is a difficult question to predict sediment motion and to plausibly calculate *SY* for the future, because the sediment dynamics shows significant spatial and temporal fluctuation.

The preceding researches related to the soil erosion in forested catchments were performed by the Hungarian Forest Research Institute in the Mátra Mountains (*Bánky* 1959, *Újvári* 1981). They measured soil loss at plot-scale in different forest stands.
To calculate average soil loss and life expectancy of forest ponds, and to describe the complex dynamics of bedload and suspended sediment transport sediment researches also started in the forested catchments of Sopron Hills (*Kucsara & Rácz* 1988, *Kucsara & Rácz* 1991, *Gribovszki & Kalicz* 2003). To determine bedload yield (*BY*) and suspended sediment yield (*SSY*), *Gribovszki* (2000b) developed regression equations.

1.2 Soil erosion by water

The importance of soil erosion is well represented thereby creating the erosion maps and water management maps of Hungary (*Duck* 1955, *Stefanovits* 1964, *Kazó* 1970, *Kerényi* 1991), and including the regular soil loss measurements into the Hungarian National Information and Monitoring System for Soil Protection as a subsystem of the integrated Information and Monitoring System for Environment Management (*Várallyai* 1992, *Nováky* 2001).
Knowledge about the different erosion forms is important, in order to select the adequate model for soil loss prediction. A classic categorization basis of soil erosion types is the agricultural practice and the cultivability of plot after erosion. I describe the different types of soil erosion by water according to *Stefanovits et al.* (1999, ps. 328-331.) and *URL4* below.

Inter-rill or surface erosion: Soil loss phenomena within a plot which do not limit the horizontal (following the contour-lines) cultivation. Soil detachment occurs in a layer with homogeneous depth which remains under the tillage depth. Scales of the surface erosion are:

- *Micro-solifluction*: This form is generally invisible. It appears when more rainfall reaches the saturated soil surface which goes into a suspension with the runoff and begins to slide slowly downstream to a point of deposition in a very thin layer but at large extension.
- *Splash erosion*: This phenomenon is induced by the hitting impact of raindrops. The effect is different on dry and wet soil surface (explosive and splashing effect).
- *Sheet erosion*: This form appears due to the unconcentrated surface runoff when soil particles start to move at large extension at the same time.

Rill erosion: This type occurs when sheet flows and smaller flow paths on the soil surface start to converge into larger water rills. Its effect is not uniform leaving visible scouring on the surface. Damages cannot be corrected by shallow tillage, but the horizontal mechanical cultivation has been possible yet. The reasons can be: e.g. wheel-tracks, furrows etc.

Gully erosion: Rill erosion evolves into gully erosion as duration or intensity of rain continues to increase and runoff volumes continue to accelerate. A gully is generally defined as a scoured out area that is not crossable with tillage or grading equipment. Thus, farming activities are impeded by gully erosion (*Duck* 1969, *Stefanovits* 1999).

Although afforestation can stabilize gully development (*Gábris et al.* 2003), studies of *Jakab et al.* (2005) and *Jakab* (2008) draw the attention that gully erosion can occur in catchments with mixed land use or forested regions as well. Similarly in the Sopron Hills, primarily the rills and gullies are dominant (due to the unpaved forest roads), as for the runoff-driven erosion. However, quasi-invisible surface erosion forms can also appear in some regions where the forest cover had been removed. Besides the soil loss by water runoff, gravity combined with other forces such as soil saturation, earthquake and uprooting can lead to different **mass movements** on steep hillslopes.

Without giving detailed descriptions of mass movements and their driving forces, some examples are listed here. In the model of *Benda & Dunne* (1997), complex interaction between climatic and topographic factors had been embedded which influence the slope stability and may trigger landslides. These elements are: fire regime – root strength, precipitation regime – pore pressure in colluvium, depth of colluvium, soil strength and topography. Water can induce the downslope movements of surface material in several ways (*URL5*):

- adding weight to the soil,
- filling the pore spaces of slope material,
- exerting pressure which tends to push apart individual grains.

Landslide is a general term which can be divided into the more specialized categories, such as slump, rockslide, debris slide, mudflow and earthflow.

Sediment delivery ratio. Researches introduce that only a small fraction of the soil eroded within a basin will reach the catchment's outlet, and sediment sources of a stream are not necessarily the major soil erosion areas because different parts of a catchment has different transport capacity to convey sediment. Particles can be deposited and temporarily or permanently stored on the slope, particularly where gradients reduce downslope, at the base of the slope, in swales, on the floodplain or in the stream channel (*Walling* 1983, *Di Stefano et al.* 2000). In order to assess sediment yield (*SY*) from soil loss it is necessary to estimate the *SDR* and the time lag between basin *SY* and soil erosion as well (*Ferro & Minacapilli* 1995, *Amore et al.* 2004). The residence time of sediment in the storage elements towards the base level may increase from decades to 10000 years (*Dietrich & Dunne* 1978).

Nevertheless, *SDR* varies within a catchment, depending on geomorphological and environmental factors such as extent and location of sediment sources, relief, drainage network and channel conditions, land cover, land use and soil types (*Walling* 1983). Many authors investigated the sediment delivery problem applying empirical, statistical, physical respectively spatially lumped and distributed *SDR* equations (*Ferro & Minacapilli* 1995, *Di Stefano et al.* 2000). But in the frame of this study, only the empirical equation of *Vanoni* (1975, in *Lim et al.* 2005) is highlighted. The principle of this formula is the relation between catchment area (A_c, km^2) and *SDR* ("*SDR* curve"):

$$SDR = 0.4724 \cdot A_c - 0.125 \qquad (Eq.\ 1.1)$$

1.3 Soil erosion modelling

Many models have been developed to predict areas sensitive to water erosion, to predict soil loss, and to evaluate soil erosion-control practices. They can be classified in different ways, e.g. according to

- calculation method (empirical, semi-empirical, physical),
- spatial resolution (lumped or distributed) and extent of spatial units (plot-scale, slope-scale, watershed-scale),
- temporal resolution (event-based, continuous – integrated estimation for a given time period),
- pollution sources (non-point or point-source pollution, soil loss, nutrients),
- processes (erosion, deposition, sediment transport).

Annex I.III.1 shows examples of the different types of erosion models. Since the author applied the empirical equation of Universal Soil Loss Equation (USLE, *Wischmeier & Smith* 1978) implemented in GIS-environment and the physical-based model of EROSION-3D (*von Werner* 1995), following descriptions involve these models.

1.3.1 The Universal Soil Loss Equation and its applicability

In contrast with physically based models, *Martin et al.* (2003) noted that empirical models such as the USLE require less site specific data. Therefore, the USLE is more widely applied for predicting soil loss and for planning of soil conservation measurements, especially in developing countries (*Szabó* 1995, *Jain & Kothyari* 2000, *Lu et al.* 2004, *Onyando et al.* 2005, *Erdogan et al.* 2007, *Pandey et al.* 2007). The USLE is an empirical equation originally developed by *Wischmeier & Smith* (1978) in the USA. The Hungarian adaptation had been performed by *Kiss et al.* (1972, in *Salamin* 1982), while *Schwertmann et al.* (1987) elaborated the application in Germany. The equation computes the average specific soil loss pro unit area by multiplying the following six factors:

$$A = R \cdot K \cdot L \cdot S \cdot C \cdot P, \text{ where} \qquad (Eq.\ 1.2)$$

- A is the average annual soil loss ($t \cdot ha^{-1} \cdot yr^{-1}$);
- R is the rainfall-runoff erosivity factor ($kJ \cdot m^{-2} \cdot mm \cdot h^{-1}$) which represents the erosion potential of locally expected rainfalls on cultivated soil without vegetation cover;
- K is the soil erodibility factor ($t \cdot ha^{-1} \cdot m^{2} \cdot kJ^{-1} \cdot h \cdot mm^{-1}$) which shows the rate of soil loss per unit of rainfall for a specific soil for a clean-tilled fallow;
- L is the slope length factor (*dimensionless*), the rate of soil loss compared to the soil loss from a 22.13 *m* length slope;
- S represents the slope steepness factor (*dimensionless*), the rate of soil loss compared to the soil loss of a slope with a 9% inclination;
- C is the cover-management factor (*dimensionless*) which shows the influence of plants in contrast with bare fallow;
- P is the erosion-control practice factor (*dimensionless*) where control practices are usually contours, strip cropping or terraces (*Centeri* 2001, *Amore et al.* 2004).

Dettling (1981) and *Centeri* (2001) drew the attention to the importance of the proper harmonization of American and SI units at the European USLE adaptations. The calculated soil loss can be compared to the tolerable soil loss which indicates the maximum level of soil erosion that still allows a high level of crop productivity over the years (*Stone & Hilborn* 2000).

Many authors discussed the applicability of the USLE in different study areas. Originally, the USLE allows the long term prediction of soil loss only for standardised agricultural plots (*Wischmeier & Smith* 1978, *Schwertmann et al.* 1987). The adaptation of the equation to a wider scale and to other land usages (e.g. forest) is not recommended by *Wischmeier & Smith* (1978). The predicted soil loss may exceed the observed values by one order of magnitude in forested areas (*Risse et al.* 1993). The reasons of the overestimation can be that the soil distribution is mostly irregular and surface runoff is often prevented by organic debris such as logs, twigs and leaves. In addition, the rate of macropore infiltration is also high (*Gribovszki* ex verb.). However, several other authors proved that USLE is capable for estimating soil loss under different conditions (*Jain & Kothyari* 2000, *Onyando et al.* 2005, *Khosrowpanah et al.* 2007, *Beskow et al.* 2009). *Rácz* (1985) suggested factor values to the USLE adaptation in forested catchments of Hungary.

Considering the *C* factor, the international studies give a wide range of its value even for the similar land cover types. *Wischmeier & Smith* (1978) classifies the *C* factor according to the canopy type and height, the % cover by the vegetative canopy and the cover that contacts the soil surface. Minimal *C* factor is 0.003 independently on the canopy, if the cover consists of grass, grasslike plants or decaying compacted litter, and ground cover is higher than 95%. However, *C* factor is not lower than 0.011, if the cover consists of broadleaf herbaceous plants and undecayed residues. In case of 75-100% canopy or undergrowth cover and 90-100% litter cover, *C* factor can decrease to 0.0001 in forested catchments. Some authors agree that mean annual *C* factor has 0.1 orders of magnitude for different crop rotation systems (*Márkus & Wojtaszek* 1993a, *Gabriels et al.* 2003, *Tetra Tech* 2007, *Khanal & Parajuli* 2013). *Schwertmann et al.* (1987) specify "advantageous" cases when *C* factor can be 0.01 orders of magnitude on arable land as well. Furthermore, mulch cover can also reduce the values. This value is 0.001 order or magnitude in forests or pasture (*Khanal & Parajuli* 2013). Other authors work with higher values for the pasture: 0.01 order of magnitude in *Ma* (2001) and *Tetra Tech* (2007). In the study of *Kosky* (1999), cropland, forest and wetland have *C* factor in the same order of magnitude contradicting the previous researches relating the croplands. Some researchers distinguish *C* factor in deciduous and evergreen/coniferous forest, where evergreen/coniferous forest produces almost by 50% lower values than deciduous forests (*Ma* 2001).

The USLE had been developed for the prediction of sheet and rill erosion. However, the results show no separate values for rill and inter-rill erosion, but overall soil loss only. The USLE is also not feasible for estimating the amount of deposition and for calculation of sediment yield (*SY*) from gully, streambed and streambank erosion (*Wischmeier & Smith* 1978, *Fistikoglu & Harmancioglu* 2002). The equation was primarily designed for calculating

long-term average annual rates of erosion (*Stone & Hilborn* 2000). It is therefore necessary to develop techniques to estimate soil loss for individual storm events (*Jain & Kothyari* 2000). *Andersson* (2010) noted that interactions between USLE factors are not taken into account.

1.3.2 Implementation of the USLE in Geographical Information Systems

Soil erosion risk differs spatially because of heterogeneous topography, geology, geomorphology, soil types, land cover, and land use. Geographical Information Systems (GIS) are able to handle these spatially variable data easily and efficiently. The estimation of soil erosion with GIS techniques reduces costs and improves accuracy (*Ma* 2001, *Erdogan et al.* 2007, *Khosrowpanah et al.* 2007). State-of-the-art GIS provides the necessary mapping and interpolation methods to create a database, which includes all input datasets for erosion modelling. The resolution should reflect the spatial variation of the hydrological and erosion processes (*Fistikoglu & Harmancioglu* 2002, *Beskow et al.* 2009). Decreasing cell size and increasing scale requires a large amount of data for accurate prediction. GIS is therefore most appropriate for the management of a huge amount of data. It reduces time and costs for accessing and handling a database (*De Roo & Jetten* 1999). *De Roo et al.* (1996), *Fistikoglu & Harmancioglu* (2002), *Khosrowpanah et al.* (2007), and *Pandey et al.* (2007) described even more advantages of GIS, such as the production of complex input maps and the combination of soil, land use and coverage information. With GIS techniques, the calculation of soil loss rates for alternative land management scenarios becomes easier.

The required data for the prediction of soil loss (rainfall erosivity, soil data, digital elevation model, land use) has to be converted into a GIS-format in order to implement the USLE in GIS. Different authors have used GIS-based techniques to model USLE factors for predicting soil loss for larger watersheds on a grid cell basis (*Erdogan et al.* 2007, *Andersson* 2010). According to *Martin et al.* (2003), a combined USLE/GIS approach is able to identify discrete locations with precise spatial boundaries with high erosion potential. *Beskow et al.* (2009) validate that the combined USLE/GIS technique shows an acceptable accuracy and allows mapping of the most susceptible areas. The studies by *Onyando et al.* (2005) and *Erdogan et al.* (2007) contradicted this: upscaling of the USLE-applications from plots to large watersheds is limited depending on the reliability and availability of direct field measurements. As *Fistikoglu & Harmancioglu* (2002) mentioned, the results of erosion risk assessment are more plausible for small grid sizes and smaller areas. Therefore larger watersheds must be analysed as sub-basins. A comprehensive USLE/GIS application was accomplished in the frame of the Balaton Project in Hungary, where *Kertész et al.* (1992, 1997) divided the Örvényes Catchment into “erotopes” which indicate the inclined parts of the relief with an unconcentrated runoff approximately in the same direction. This technique ensures to analyse the impact of unconcentrated runoff and to model soil erosion in a larger catchment at quasi-plot scale or in slope segments.

The combined USLE/GIS approach is also limited by each input factor. *Auerswald* (1987) stated that the calculated soil loss is highly sensitive to the slope factor. To provide a more

accurate slope length prediction, the ArcInfo Arc Macro Language (AML) scripts of *Van Remortel et al.* (2001) calculates the cumulative uphill length from each cell. All convergent flow paths and depositional areas are integrated in this model. *Van Remortel et al.* (2004) presented another GIS-model based on the revised USLE. The AML processing code solves the difficulty in obtaining the *LS* factor grid at regional scales using ANSI C++ software.
Modern GIS-based procedures support the calculation of other USLE factors as well. Many studies applied remote sensing data to develop values for the *C* and *P* factors, to classify land cover categories and land use units (*Ma et al.* 2003, *Beskow et al.* 2009). These studies confirmed that the original spatial limitations of the USLE can be avoided by using remote sensing data and GIS. *Márkus & Wojtaszek* (1993a, 1993b) conducted the USLE calculation in ArcInfo environment and compared the density differences of aerial photographs and satellite images with the erosion sensitive areas. The results proved that remote sensing is a suitable method to check the modelled soil erosion categories and to follow the actual stage of the erosion processes.

According to the literature overview, integration of GIS-based techniques with the USLE is useful to describe areas that are vulnerable to soil erosion, enabling immediate conservation planning (*Lee* 2004, *Beskow et al.* 2009).

1.3.3 The soil erosion prediction model EROSION-3D

EROSION-3D (*von Werner* 1995) is a process-based model, which means that it predominantly operates based on physical principles of the following erosion processes:

- runoff generation;
- particles detachment by raindrop impact and runoff;
- transport of eroded particles by runoff;
- routing of runoff and sediment through the catchment;
- sediment deposition.

The model considers critical shear strength of the soil and transport capacity of the runoff as physical principles of the particles detachment and transport, which are expressed in a form of a critical momentum flux. Rainfall infiltration excess is calculated by the modified Green & Ampt equation, which shortcoming is the reliable simulation of macropore flow.
The model works on the basis of a regular grid where the grid size is variable, but must be consistent within a matrix of a catchment (more than $5 \cdot 10^5$ raster cells). The model operates on an event basis, and the temporal resolution ranges from 1 to 15 min. Grid-based processing requires the model applicability in Geographical Information Systems (GIS) (e.g. ArcInfo, GRASS) (*Schmidt et al.* 1999).

Figure 1.1 represents the model structure referring also to the calculation process. Input parameters are described in *Sect. 3.5.2*. The model consists of two modules, the GIS and the erosion component. The GIS module performs the preprocessing of Digital Elevation Model (DEM), generating the flow direction and flow accumulation for each grid and creating the

channel network. The erosion component determines the rate of surface runoff and soil loss. In detail, EROSION-3D is able to calculate:

- erosion and deposition by rill and inter-rill erosion;
- particle transport and deposition for nine soil fractions from fine clay to coarse sand;
- sediment volume and sediment concentration in the channels' grid.

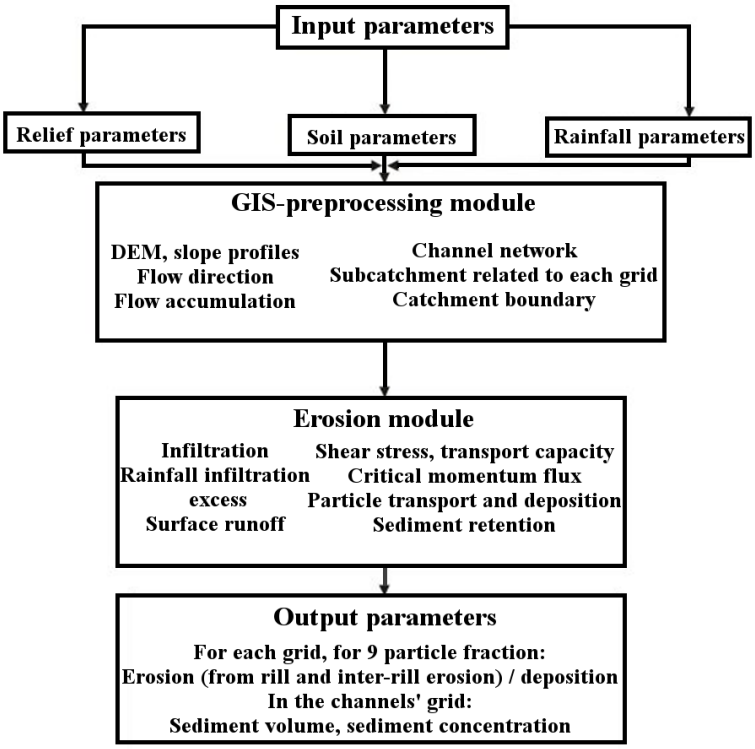

Figure 1.1. Model structure of the EROSION-3D (from Kitka 2009)

Thus, EROSION-3D enables to analyse the effect of erosion-control practices (e.g. changes in the agricultural techniques and plants), the sediment retention in basins and ditches, nutrient inlet to the streams through soil particles, snowmelt erosion, etc. (*Kitka* 2009).

Nevertheless, EROSION-3D has also several shortcomings. Besides the high data requirements and quantitative overestimation due to the neglected macropore flow and surface crusting, reliability of qualitative and quantitative soil loss prediction from linear erosion (rill erosion) is limited as well. For instance, as *Bug* (2011) found, modelling the location of erosion forms was not entirely accurate. The model indicated soil loss reduction in a thalweg, but the field observation proved high erosion damages in that place.

1.4 Sediment types

Physical and chemical weathering plays a major role in the decomposition of bedrock. The products of weathering, such as smaller particles, soil minerals and dissolved constituents, are removed by erosion processes, where the main agent is the water. Since residual materials formed by weathering are usually eroded and transported to the streams, water quality is also influenced by erosion processes (*Bricker et al.* 1992). Sediment in streams can be classified in many different ways. In order to describe sediment in general, total sediment yield can be categorized as bedload and suspended sediment. Bedload has an almost permanent contact with the streambed while moving, and suspended sediment is in suspension (*Bogárdi* 1971). The threshold distinguishing bedload from suspended load depends on the particle size and flow magnitude. In the technical practice only fractions larger than 0.002 *mm* are reckoned as sediment. One of the sediment classification methods separates sediment types according to the origin. Sediment in the streams comes from the slopes of watershed (washload) or the channel itself (bed-material load), where washload contains particles are finer than the bed-material.

Considering the several different types of sediment movements, origins and other characters the following complex classification has been defined. Total sediment yield of the stream is the amount of dissolved and particulate organic and inorganic material. Although there are no sharp boundaries, total load can be divided into three groupings: flotation load, dissolved load, sediment yield (*Figure 1.2*) (*Gordon et al.* 2004).

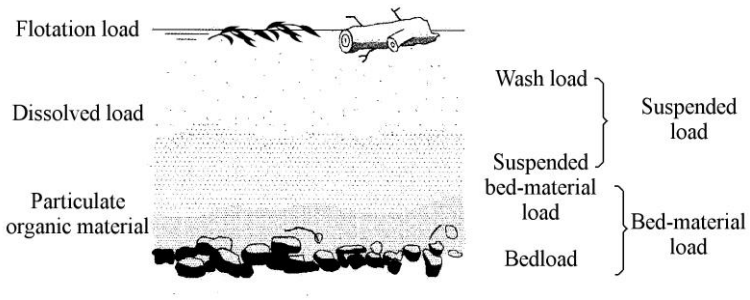

Figure 1.2. Classification of the transported material in streams (from Gordon et al. 2004)

Logs, leaves, branches and other organic debris, which are generally lighter than water, compose the *flotation load*. The organic debris is supplied from the vegetation along the banks, bank failure and tree fall. The *dissolved load* is the material transported in solution. Origins of dissolved load can be the sea salts dissolved in the rainwater, the chemical weathering of rocks – sometimes enhanced by organic acids from the decay of vegetation, industrial effluents and agricultural solutes. *Sediment*, which is usually considered to be the solid inorganic material load according to *Gordon et al.* (2004), can be further separated into the following categories: washload, bed-material load, which can be transported as suspended load or bedload.

Washload refers to the smaller sediments, primarily clays, silts and fine sand fractions washed into the stream from the banks and upland areas. The size ranges from 0.0005 *mm* to 0.0625*mm*, where the smallest grain size is the distinguishing value between dissolved load

and washload. Only low velocities and minor turbulences enable that washload may never settle out, and its concentration is considered constant over the depth of a stream. As *Hjulstrom* (1939, in *Gordon et al.* 2004) said, streams cannot become saturated with sediment as they can with dissolved solids. High washload concentration may typify streams with banks of high clay-silt content, and catchments after fire denudation, volcanic eruptions, road or dam building and agricultural practices.
Bed-material load is the material in motion which has approximately the same size range as the streambed particles. Depending on flow conditions, the portion of bed-material load remaining in suspension for an appreciable length of time is called *suspended bed-material load*. *Bedload* is that portion which moves by rolling, sliding or 'hopping' in a narrow region near the bottom of the stream. Based on the method of data collection, washload and suspended bed-material are often grouped into the single category, *suspended load*. Another conventional separation of suspended load from bedload is based on the sand particle size threshold at 0.0625 *mm*. However, this threshold value may differ according to other authors. According to the review of *Gomi et al.* (2005) sediment particles carried in suspension are fine sand, silt and clay with the diameter less than 0.2 *mm*. Nevertheless, depending on flow magnitude, particles which have diameters 0.2 to 2 *mm* may move either in suspension or as bedload. Particles which are finer than sands tend to be evenly distributed in the cross-section, while coarser material is more concentrated near the bed (*Julien* 2010).

This dissertation follows the general sediment separation and discusses bedload and suspended sediment forms. Although bedload can play a major role in the alteration of channel geometry and destruction of water structures, this work focuses primarily on the suspended sediment transport, because generally less bedload than suspended load is transported over a year. The ratio of bedload to suspended load is in the range 1:30 to 1:40 in summer and 1:2 to 1:3 in winter in the headwater catchments of the Rák Brook (*Gribovszki* 2000a).

1.4.1 Bedload transport

Principles of incipient sediment motion. *Stream power* describes the erosive capacity of streams, and it is related to the shape of the longitudinal profile, channel pattern, the development of bed forms and sediment transport. According to the *Bagnold*'s definition (1966, in *Gordon et al.* 2004), stream power

per unit of streambed area is equal to ($N \cdot m^{-1} \cdot s$): $\omega_a = \tau_0 \cdot v$ (*Eq. 1.3*)

per unit of stream length ($kg \cdot m \cdot s^{-3}$): $\omega_l = \rho \cdot g \cdot q \cdot s$ (*Eq. 1.4*)

per unit mass of water ($m^2 \cdot s^{-3}$): $\omega_m = g \cdot v \cdot s$ (*Eq. 1.5*)

per unit weight ($m \cdot s^{-1}$): $\omega_a = \tau_0 \cdot v$ (*Eq. 1.6*)

In the equations, τ_0 is the shear stress at the bed ($N \cdot m^{-2}$); v is the mean flow velocity ($m \cdot s^{-1}$) in the cross-section; ρ is the density of water ($kg \cdot m^{-3}$); g ($m \cdot s^{-2}$) is the acceleration due to gravity; q is the discharge of water ($m^3 \cdot s^{-1}$); s is the energy slope of the reach (*dimensionless*). ω_l is also called total stream power in the literature.

Leopold & Maddock (1953, in *Gordon et al.* 2004) found that *hydraulic geometry* of a channel varies with the streamflow, and the changes can be well demonstrated by the following relationships:

$$W = a \cdot Q^b \qquad D = c \cdot Q^f \qquad v = k \cdot Q^m \qquad Q_s = p \cdot Q^j, \qquad (Eq.\ 1.7)$$

where the unknown units are: Q is the discharge ($l \cdot s^{-1}$); W is the stream width (m); D is the mean depth (m); Q_s is the sediment yield in a given time-period ($mg \cdot s^{-1}$); a, b, c, f, k, m, p and j are empirical coefficients.

Lift and drag forces act on a sediment particle when pressure and velocity differences exist from top to bottom or front to back of the grain. The Hjulstrom curves describe the *critical velocities* required for particles detachment, transport and deposition; however, they are only valid for idealized conditions (uniform material, $D>1m$). Jowett's *relative bed stability* defines the suitability of a streambed, as the ratio of the critical velocity required to just move a particle (v_c) to the actual flow velocity near the bed (v_b).

Bedload equations. Bedload indicates the transport of sediment particles which frequently maintain contact with the bed, where the bed layer thickness is the double of the grain diameters as commonly used. Bedload delivery can be treated as a deterministic and probabilistic problem as well. Deterministic approaches are the equation of *Du Boys* and *Meyer-Peter Müller*, while the probabilistic equations were developed by *Kalinske* and *Einstein*. In the followings, basic bedload equations are overviewed according to *Bogárdi* (1971) and *Julien* (2010). Since the dissertation discusses mainly the suspended sediment transport, further bedload equations can be found in the *Annex I.IV.1*.

As the beginning of theoretical development of the bedload movement can be considered the *Du Boys equation* (1879, in *Julien* 2010) which is based on the concept that sediment moves in thin layers along the bed. The applied bed shear stress τ_0 must exceed the critical shear stress τ_c to initiate motion, where

$$\tau_0 = \gamma \cdot R_h \cdot s, \text{ and} \qquad (Eq.\ 1.8)$$

$$\tau_c = c \cdot d_s \cdot (\gamma_s - \gamma), \text{ where} \qquad (Eq.\ 1.9)$$

γ is the specific weight of water ($N \cdot m^{-3}$); γ_1 is the specific weight of the sediment particle ($N \cdot m^{-3}$); R_h is the hydraulic radius (m); c is a constant; d_s is the particle size (mm).
The volume of gravel material in motion per unit cross-section width and time equals (q_{bv}; $L^2 \cdot T^{-1}$):

$$q_{bv} = \frac{0.173}{d_s^{3/4}} \cdot \tau_0 \cdot (\tau_0 - 0.0125 - 0.019 \cdot d_s). \qquad (Eq.\ 1.10)$$

According to the *Du Boys theory*, only the bed shear stress is accounted for the gravel mobilisation. However, internal power of the stream can also contribute to the bedload transport (*Bogárdi* 1971).
Shields (1936, in *Bogárdi*, 1971) substituted the c constant in *Eq. 1.9* with a nonconstant resistance coefficient which depends on the Reynolds number. Therefore, the resistance coefficient and the critical shear stress depend on the viscosity and the water temperature as

well. It means that the critical shear stress related to a sediment particle, with d_s gravel diameter and ρ_s density, will increase if the water temperature decreases.

Processes and phenomena influencing the bedload motion. Particle-size distribution and channel features may influence the grain movement. The *pool-riffle sequences* are most common bedforms in streams with mixed bed materials, where the pool is a region of deeper, slower-moving water, whereas the riffle is a region with shallower, faster-moving water (*Figure 1.3*). Due to the differences of shear stress in pools and riffles, fine bed materials are concentrating in pools, while coarser particles mostly appear in riffles. Sediment from riffles is mobilized only under large floods, at which time the coarse bed materials are transported from riffle to riffle. However, very coarse fragments will still remain or accumulate in the deepest region of pools (*Gordon et al.* 2004).
Armouring and imbrication are also accounted for the intermittent character of bedload movement (*Figure 1.3*). *Armouring* is the development of a surface layer that is coarser than the bed material beneath it. If the streambed is armoured, the sub-surface particles are protected from channel erosion until the armour layer is broken up. *Particle imbrication*, which also induces that higher shear stress is required to mobilize the gravels, can occur in streams primarily with disc-shaped pebbles, where particles are stacked against each other, nose-down into the oncoming current. This kind of accumulation may happen because of a sudden fall in the stream's transport capacity when particles tend to be deposited in their position of transport (*Gordon et al.* 2004).

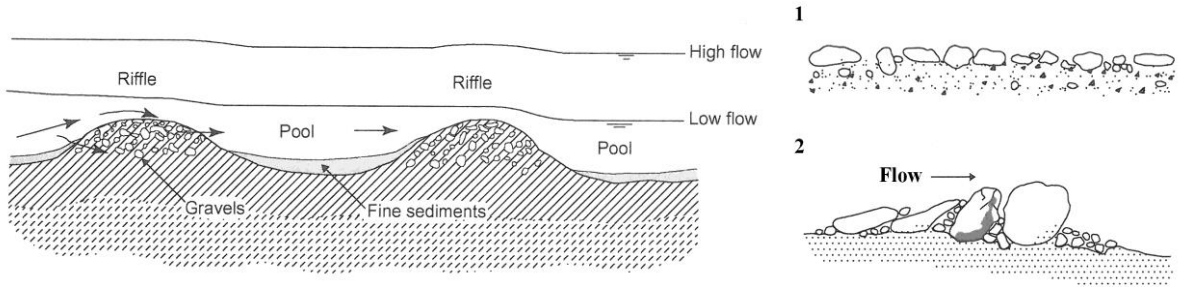

Figure 1.3. Channel bed features contributing to the postponement of bedload yield: pool-riffle sequences (left), armouring (1) and imbrication (2) (right) (from Gordon et al. 2004)

If the shear stress or flow velocity exceeds the critical values, e.g. during large flood events, delaying bedload yield (*BY*) can show a sudden increase due to the following reasons (*Gribovszki* 2000b):

- breaking up of the armour layer on a long stream section,
- exhaustion of sediment deposit behind obstructions after their disruption,
- changes of the channel geometry,
- connection of floodplain sediment sources to the stream channel.

1.5 Suspended sediment transport

1.5.1 Physical principles of the suspended sediment transport

The condition of finer particles delivery in suspension is that turbulent velocity fluctuations have to be sufficiently large to maintain the particles within the mass of fluid without frequent bed contact. This subsection sums up the physical principles according to *Julien* (2010) and *Bogárdi* (1971). The general physical processes governing the conservation of suspended sediment mass are advection, molecular diffusion, mixing and dispersion. From the sediment continuity equation:

$$\underbrace{\frac{\partial SSC}{\partial t}}_{mass\_change} + \underbrace{\frac{\partial v_x \cdot SSC}{\partial x} + \frac{\partial v_y \cdot SSC}{\partial y} + \frac{\partial v_z \cdot SSC}{\partial z}}_{advective\_terms} = \underbrace{\dot{SSC}}_{phase\_change} + \underbrace{\left(MD \cdot \left(\frac{\partial}{\partial x}\left(\varepsilon_x \cdot \frac{\partial SSC}{\partial x} \right) + \frac{\partial}{\partial y}\left(\varepsilon_y \cdot \frac{\partial SSC}{\partial y} \right) + \frac{\partial}{\partial z}\left(\varepsilon_z \cdot \frac{\partial SSC}{\partial z} \right) \right) \right)}_{diffusive\_and\_mixing\_terms}$$

(*Eq. 1.11*)

In *Eq. 1.11 SSC* is the suspended sediment concentration ($mg \cdot l^{-1}$); *t* is the time; *MD* is the molecular diffusion coefficient ($L^2 \cdot T^{-1}$); ε is the turbulent mixing and dispersive coefficient; *x, y* and *z* are coordinates. "Phase change" includes possible internal mass changes such as chemical reactions, phase changes, adsorption, dissolution, flocculation, radioactive decay, etc.

The advective fluxes describe the sediment transport by velocity currents. Molecular diffusion indicates the scattering of sediment particles by random molecular motion according to the Fick's law. Turbulent mixing generates the particles motion due to turbulent fluid motion, which effect is by three orders of magnitude higher than the molecular diffusion. Therefore, the molecular diffusion can be neglected.

Regarding the viscosity/temperature-dependency of suspended sediment motion, other relation can be determined. At bedload transport, increasing viscosity induces the stream energy decline due to the thickening laminar layer near the streambed, thus gravel motion will decrease. In contrast, finer particles concentration will decrease according to the temperature dependency of Stokes law, if the temperature declines (*Bogárdi* 1971).

1.5.2 Temporal variability of the suspended sediment transport

Sediment availability in the channel plays a major role in the suspended sediment dynamics. Sediment availability is determined by the hydrological parameters, such as the catchment characters and the climatic variables (*Bogárdi* 1971). Due to the spatial and temporal variability of the hydrological parameters, suspended sediment yield (*SSY*) shows fluctuation as well. As *Walling* (1983) summarized, problems of temporal lumping or aggregation can be viewed ranging from the single storm through to a long-term perspective of the erosion–delivery–sediment yield system. Furthermore, problems of the spatial resolution relate to the accurate representation of the sediment transport characteristics within a basin: the spatial diversity of topographic, land use and soil conditions. This session gives an overview how the

suspended sediment transport varies at different time scales and at different flow conditions, and which factors can be accounted for the changes.

Temporal variations occur over a wide range of time scales, and the *SSY* can vary over a number of orders of magnitude at any one discharge (*Q*) in the same stream according to *Morehead et al.* (2003). *Albert* (2004) and *Gao et al.* (2011) investigated the long-term sediment time series of large rivers (Rio Grande and Yellow River) using breakpoint analyses, and pointed out that human activities, such as terrace building, dam and reservoir construction, afforestation and grass planting were the main factor for the transition of suspended sediment transport during the studied decades.

Morehead et al. (2003) listed more reasons, which can lead to the *intra-annual* variability of suspended sediment flux. These are the seasonal changes of water sources (rain versus snowmelt), the altering channel morphology due to the changing climatic conditions, variability of the sediment supply processes and the unstable availability of the fine material in the channel. The authors emphasized that suspended load on smaller rivers tend to have smaller annual variations, and the alteration is smaller on snowmelt-dominated rivers than on rain-dominated basins. The latter statement is also confirmed by *Lenzi & Marchi* (2000). Nevertheless, they pointed out that *SSY* has also noticeable differences depending on the timing and extent of snow cover and snowmelt. Early snowfalls combined with permanent snow cover throughout the winter and slow snowmelt without important rainfall led to negligible *SSY*, while snowmelt periods which followed a mild winter and late snowfalls caused abundant *SSY*. According to *Alexandrov et al.* (2007), the different rainfall types can also be accounted for the inter-seasonal variability of the *SSY*. Convective or convectively-enhanced storms with high intensity generally led to higher *SSC*, while the frontal rainfalls with long duration but low intensity induced comparatively lower *SSC*.

Bronsdon & Naden (2000) have analysed the *monthly* fluctuation of suspended solid concentration on three rivers in Scotland and identified the control factors. The processes, influencing the amount of easily available fine material in the channel month by month, can be wetting and drying of the catchment, cattle trampling, diatom growth and death, sediment exhaustion, erosion protection by the snow cover, freeze-thaw action, ice-crystal growth along the river banks.

Duvert et al. (2010) found, the analysis of *sub-daily* (or *inter-event*) variability of sediment fluxes in small mountainous catchments is inevitably necessary for the accurate calculation of annual *SSY*. They reported that between 63 and 97% of the annual load is exported in 2% of time, and strong bias (i.e. up to 1000% error) were obtained on annual *SSY* estimation based on daily sampling due to the very short hydrologic response (1-3 h) of the small catchments (3-12 km^2). The significance of event-based suspended sediment sampling in small streams is also confirmed by other authors. *Thomas* (1985) wrote in his methodological study that most suspended solids are transported during infrequent high flows that are generally underrepresented by the manual sampling strategies. It is not a specific case when the 15% of total *Q* transfers the 50% of the total *SSY* in 2% of the reference period. *Estrany et al.* (2009)

gave a more extreme example where 50% of the total load occurred in only 0.13% of the time, and 90% of the total flow delivered only 1% of the total suspended sediment flux in the 1.03 km^2 area of the studied Mediterranean catchment. The absolute peak of the *SSC* was more than 120 time higher than the average concentration and the coefficient of variation was >300%. *Xu et al.* (2005) and *Antonelli et al.* (2008) also highlighted the role of large floods in the solid transport on the Yangtze River respectively the Rhone River. *Xu et al.* (2005) obtained 6.5 time higher sediment flux during the simulated event than the normal flood season averaged over the last 50 years, and they held responsible the increasing human activities (e.g. deforestation and slope farming) in the basin for the rising sediment availability. Nevertheless, *Antonelli et al.* (2008) drew the attention to that the highest flow does not lead to the highest suspended sediment export due to the sediment removal effect of the previous moderate flood events. *Sadhegi et al.* (2008) pointed out the large difference of one to four orders of magnitude in *SSC* in different forest stands, the wide scatter of data on the rating curve and the low correlation between *SSC* and *Q* for the entire dataset. These facts confirm that reliable prediction of *SSY* in highly variable or dynamic streams is only achievable through the stormwise (event-based) analyses.

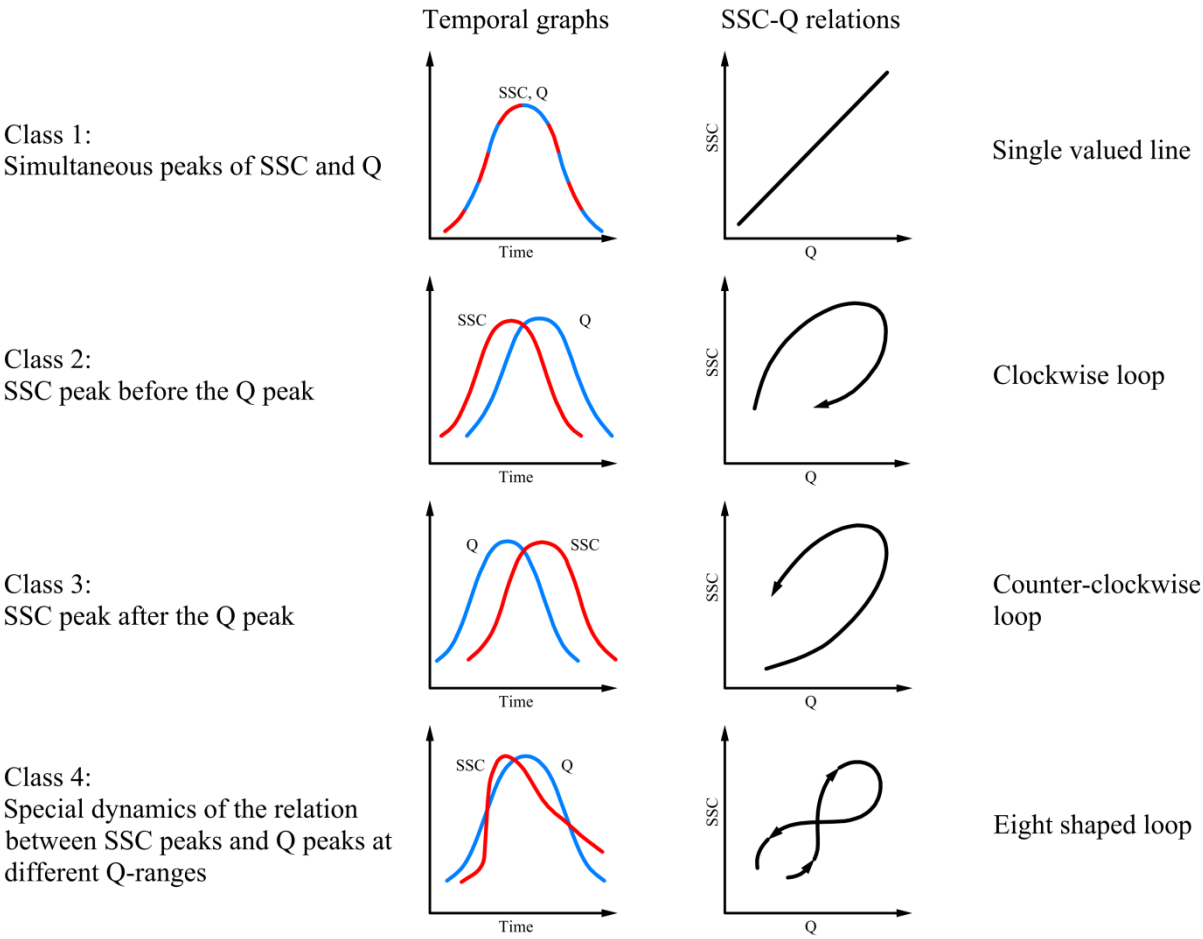

Figure 1.4. Basis types of the relationship between suspended sediment concentration (SSC) and discharge (Q) during a single flood event (from Williams 1989)

To indicate the *intra-event* variability of suspended sediment transport, and to reveal the overall pattern of erosion and sediment delivery (i.e. the processes responsible for the supply

of easily available fine material) operating in the basin, *Walling & Webb* (1982) and *Williams* (1989) analysed the sediment rating curve (*SSC* against *Q*). *Williams* (1989) described the distinguishing criterion and sole requirement for hysteresis loops to form on the basis of the *SSC*-*Q* relationship (*Figure 1.4*). If any *SSC*/*Q* ratio on the rising limb of the hydrograph is equal to the *SSC*/*Q* ratio on the falling limb, for the same value of *Q*, we obtain the simplest type of SSC-*Q* relation: the *single-valued line*. If *SSC*/*Q* ratio on the rising limb of the *Q*-graph is consistently greater than *SSC*/*Q* ratio on the falling limb, there is a *clockwise loop*, and if *SSC*/*Q* ratio for each and any value of *Q* is less on the rising limb than those on the falling limb, there is a *counter-clockwise loop*. If the *SSC*/*Q* ratios for one *Q*-range of the rising limb of the *Q*-graph are larger and smaller for another *Q*-range on that limb, compared to the same *Q* values on the falling limb, the *eight-shaped hysteresis loop* will be formed.

Numerous authors used the same technique, to identify sediment sources within the catchment and the reasons of the variable suspended solid flux. The clockwise sedigraph (positive hysteresis or in-advance sedigraph) may indicate that the area contributing to suspended sediment transport is the channel itself or an adjacent area, and the sediment supply shows an exhausting tendency (*Sadhegi et al.* 2008, *Rodríguez-Blanco et al.* 2010a).
The counterclockwise sedigraph (negative hysteresis or delayed sedigraph) refers to that the upper part of the slopes is the sediment source area, or particles can also derive from processes which dynamics are slower than the *Q* rising (e.g. bank collapse may happen when bank material is sufficiently saturated) (*Lenzi & Marchi* 2000).
Proving also by the studies where no counterclockwise hysteresis were found (e.g. *Lefrancois et al.* 2007, *Sadhegi et al.* 2008), the most common hysteresis type is the clockwise loop caused by the early sediment depletion (*Lenzi & Marchi* 2000). In contrast, the anticlockwise hysteresis dominated the total number of events (48%) in the study of *Marttila & Klove* (2010) performed on a drained catchment where mostly the snow/ground frost melt or snowmelt combined with rainfall are dominating. Furthermore, they found that clockwise hysteresis represented 34%, random variations 10% and eight-shaped hysteresis 7% of sampled events.
The eight-shaped hysteresis loop is a combination of the clockwise and counterclockwise loops (*Williams* 1989), and this type may appear when the flood is associated with multiple peaks in *SSC* coinciding with the highest peaks of rainfall intensity (*Nadal-Romero et al.* 2008). As for the conditions of the eight-shaped hysteresis, not all studies agree with each other. While the eight-shaped loops occurred mainly in spring under wet conditions when the baseflow and antecedent precipitation values were high in a small Central Spanish Pyrenees catchment with badlands (*Nadal-Romero et al.* 2008), the same hysteresis type appeared only in summer when the soil moisture was lower and high rainfall intensity dominated in the Basque Country, Spain (*Zabaleta et al.* 2007).

1.5.3 Hydrological, hydrometeorological and climate parameters influencing the suspended sediment transport

After all, suspended sediment flux in a stream primarily depends on the fine material availability in the channel. However, hydrological, hydrometeorological and climate parameters can be also accounted for the *SSC*-control.

Analyses of sediment rating curves by *Sadhegi et al.* (2008) pointed out the combined effects of sediment availability on hillslopes, *rainfall intensity* and *rainfall depth*. Higher rainfall intensity led to earlier *SSC* and flow peak, but higher rainfall depth was associated with higher *SSC* and *Q*. Variation of surface runoff generation depends on the *antecedent soil moisture* as well, which showed significant relationship with the *SSC-Q* hysteresis loops. Similarly to the antecedent soil moisture, antecedent precipitation index (*API*) can be also applied to predict the rainfall-runoff response (*Fedora & Beschta* 1989, *Bousfield* 2008), which is an important factor of sediment preparedness on hillslopes. Through drying processes and biological activity (e.g. soil fauna or cattle trampling as revealed by *Lefrancois et al.* 2007), also the dry periods can provide fine material to the stream channels.
Sadhegi et al. (2008) found that the *sequential occurrence of storm events* may influence the *SSC*. Surface runoff and previous floods can outwash and thus reduce the fine material eroded on hillslopes and deposited in the channel, resulting in limited sediment resources for the subsequent flooding periods. As a consequence, it could be reasonable to analyse the relationship between *SSC* and number of days elapsed since the previous flood event.

To identify the significant control factors of *SSC* and *SSY*, several authors generated a Pearson correlation matrix. The involved factors were:

- rainfall variables: total rainfall depth, rainfall duration, maximum *x*-min rainfall intensity, average rainfall intensity, kinetic energy of the maximum rainfall intensity over an *x*-min period;
- runoff variables: storm-flow depth / total volume of the event (*mm* / m^3), maximum flood discharge, average flood discharge, initial discharge (baseflow at the beginning of the event), duration of the flood, runoff coefficient, stream power;
- antecedent moisture variables: antecedent precipitation of 1 hour before the event and 1, 3, 5, 7, 15 and 21 days before the event;
- sediment variables: average *SSC*, maximum *SSC*, total *SSY*.

According to *Nadal-Romero et al.* (2008), suspended sediment parameters showed strong relationship with rainfall depth, *peak Q* and *storm-flow depth*; weaker linear correlations with maximum rainfall intensity; and no significant correlation with *API* which refer to the antecedent moisture conditions. This fact contradicts the results of *Sadhegi et al.* (2008) who performed the investigation in a reforested catchment, where soil moisture has higher importance than in an active badland region which may almost induce Hortonian overland flow. Pearson correlation coefficients and principal component analysis by *Zabaleta et al.* (2007) also confirmed that no relationship with antecedent conditions means a direct hydro-sedimentary response to rainfall events (flash flood conditions). Conditions at *López-Tarazón et al.* (2010), such as no significant correlation between *SSC* and rainfall intensity but

significant correlation between *SSC*, total precipitation and *API*, refer that the study catchment in the analysed period is better explained by the theory of *Dunne* than by the theory of *Horton*. (Concepts of storm runoff mechanisms according to *Dunne* and *Horton* are described in the *Annex I.V.1*)
In some cases, good correlation was obtained between rainfall, runoff and sediment variables despite of the wide scatter in the data (*Rodríguez-Blanco et al.* 2010b). The wide scatter reflects the non-linearity in the hydro-sedimentary response of the catchment, and points out that other factors influence the suspended sediment transport besides the rainfall and runoff parameters.

Concluding from the studies above, it is not eligible for a comprehensive evaluation to analyse only the relationship between sediment, hydrological, hydrometeorological and climate factors. Further examples of the complexity of suspended sediment delivery are the followings. Sediment unavailability can cause a paradox on the relationship between sediment and runoff variables. While *SSY* shows strong relation with *Q* variables, *SSC* parameters has no significant correlation with them, because the increase of *Q* cannot be associated with *SSC*-increase (*Zabaleta et al.* 2007). In addition, complex trends in the *SSC*-*Q* scatterplots, such as

- a horizontal line up to a flow threshold followed by a steep linear increase in the suspended solid with flow, or
- a decrease in *SSC* with *Q* up to a threshold followed by a linear increase,

indicate the role of high flows in sediment mobilizing and transport but the multiplicity of other impacts at low flows (e.g. bank collapse, sediment exhaustion during the falling limb) (*Bronsdon & Naden* 2000).

It is not a frequent issue of sediment researches when external sediment sources do not exist, although periods between flood events represent much longer times. *Salant et al.* (2008) have reported that *SSC* depends on the in-channel supply besides the *Q*-capacity. Furthermore, bed composition may also have a significant influence on the changes to in-channel supply.

1.5.4 Prediction of suspended sediment transport

Empirical equations describing the *SSC* and *SSY* include principally the hydraulic variables of the stream such as flow velocity (*v*), *Q*, energy slope (*S*) and water stage (*h*). The concept of these equations is that higher hydraulic variables may cause higher sediment fluxes. Nonetheless, these kind of relations are valid only for a given stream section or a given time period, until the sediment availability and sediment dynamics have not been modified by the change of hydraulic conditions (*Bogárdi* 1971). The most widespread empirical relation is the *sediment rating curve* method derived from the stream hydraulic geometry relationships according to *Leopold & Maddock* (1953, in *Gordon et al.* 2004):

$$SSC = a \cdot Q^b \text{, where} \qquad (Eq.\ 1.12)$$

SSC is the suspended sediment concentration at a given cross-section ($mg \cdot l^{-1}$); *Q* is the discharge ($l \cdot s^{-1}$); *a*, *b*: empirical coefficients.

Eq. 1.12 serves as a basis of numerous upgraded calculation method of *SSC*. *Gribovszki* (2000a) completed the model with the water temperature in his study performed in the Sopron Hills. In certain computer-based models such as the RIVER3 by *Syvitski & Alcott* (1995) and the HYDROTREND by *Syvitski et al.* (1998), the *SSY* module also applies the modified *Eq. 1.12*. The authors separated the sediment sources associated with the water sources thus describing more accurately the different rating relationships in intra-annual scale:

$$SSY = \alpha_1 \cdot Q_n^{\beta_1} + \alpha_2 \cdot Q_r^{\beta_2} + \alpha_3 \cdot Q_i^{\beta_3} + \alpha_4 \cdot Q_g^{\beta_4}, \text{ where} \qquad (Eq.\ 1.13)$$

$\alpha_{1,2,4}$ and $\beta_{1,2,4}$ are local or regional empirical coefficients; α_3 and β_3 differ with the level of glaciations; *n*, *r*, *i* and *g* indices refer to the nival, rain, ice and groundwater sources.

The variable *SSC*-*Q* relations during a flood event, i.e. the hysteresis loops lead to the different *SSC* dynamics in rising limb and falling limb of the hydrograph. To calculate *SSC* in the case of clockwise hysteresis loops, *Richards* (1984) revised the *Eq. 1.12* using the first derivative of *Q* with respect to time:

$$SSC = a \cdot Q^b \left(c \cdot \frac{\partial Q}{\partial t} \right), \qquad (Eq.\ 1.14)$$

where the unknown letter *c* is an empirical coefficient.

As the sediment exhaustion in the stream channel may occur quasi-continuously through a *Q* season, *Moog & Whiting* (1998) developed a model including the seasonally summed discharge (*ΣQ)* (and *d* is an empirical coefficient):

$$SSC = a \cdot Q^b \cdot \left(\sum Q \right)^d. \qquad (Eq.\ 1.15)$$

To define the initial sediment supplies for each flood event, i.e. the in-channel sediment storage at low flow and sediment exhaustion due to subsequent storm events, *Van Sickle & Beschta* (1983) introduced the storage/washout function, *G(S)*:

$$SSC = a \cdot Q^b \cdot G(S), \text{ where} \qquad (Eq.\ 1.16)$$

$$G(S) = n \cdot exp\left(o \cdot \frac{S}{S_0} \right). \qquad (Eq.\ 1.17)$$

In *Eq. 1.17* S_0 is the total available sediment mass; S_{sed} is the real sediment supply; *n* and *o* are empirical coefficients. Combination of *Eq. 1.16* and *1.17* gives the temporal change of the *SSC*, and the suspended sediment supply is equal to:

$$\frac{dS_{sed}}{dt} = -Q \cdot SSC. \qquad (Eq.\ 1.18)$$

It means that S_{sed} through time equals to the *SSY* with negative sign.

Lidén (1999) applied the semi-distributed conceptual HBV-SED model to predict the *SSC* and the total annual *SSY* at catchment scale. The model follows the supply-based approach by *Van Sickle & Beschta* (1983), and gave better results both for the calibration and validation periods compared to the standard sediment rating curve (*Eq. 1.12*).

The dimensionless general model of *Morehead et al.* (2003) captures the *SSY*-trend and its variability:

$$\left(\frac{SSY_d}{\overline{SSY_d}}\right) = \psi \cdot \left(\frac{Q_d}{\overline{Q_d}}\right)^c \text{, where} \qquad (Eq.\ 1.19)$$

SSY_d is the daily discharge of suspended sediment ($kg \cdot s^{-1}$); Q_d is the daily discharge of water ($m^3 \cdot s^{-1}$); $\overline{SSY_d}$ and $\overline{Q_d}$ are the long-term average of SSY_d and Q_d; Ψ and c are the rating parameters (which are expected to vary on an annual time scale).

Numerous statistical techniques were used for computing suspended sediment fluxes. The *Bayesian dynamic linear model* is a useful tool to generate *SSY* on the basis of intermittent sediment data and continuous flow data that are responsible for changes in the *SSY*-*Q* relation over time (*Krishnaswamy et al.* 2001). Based on daily rainfall, streamflow and *SSC* data, *Cobaner et al.* (2009) calculated the current *SSC* with a *neuro-fuzzy technique* and compared its potential to three different *artificial neural network techniques* and two sediment rating curves. Besides of the conventional sediment rating curve, the authors applied the following equation:

$$SSC = CF \cdot a \cdot Q^b, \qquad (Eq.\ 1.20)$$

$$CF = e^{2.65\sigma^2},$$

where *CF* is the log-transformation bias correction factor, e is the exponential function and σ is the standard error of the regression equation.

1.6 Erosion and sediment dynamics under different land cover and land use

1.6.1 Erosion and sediment dynamics of forested catchments

Suspended sediment concentration (*SSC*) data in the streams of undisturbed rain-dominated forested catchments can be divided into two periods. During the storms, discharge (*Q*) and *SSC* show wide fluctuations, while *SSC* are relatively low and steady between the storm periods. In snowmelt-dominated regions, these fluctuations are lower (*Thomas* 1985).

Besides the flooding periods, *forest management activities* can lead to the increase of soil loss by water erosion, the complexity of *SSC*-patterns and the suspended sediment yield (*SSY*) through addition of woody debris to the stream, triggering mass movements, increasing and/or redirecting surface runoff and modifying channel geometry (*Lewis* 1998). *Figure 1.5* demonstrates the conceptual diagram how the different logging activities influence the stream sediment transport.

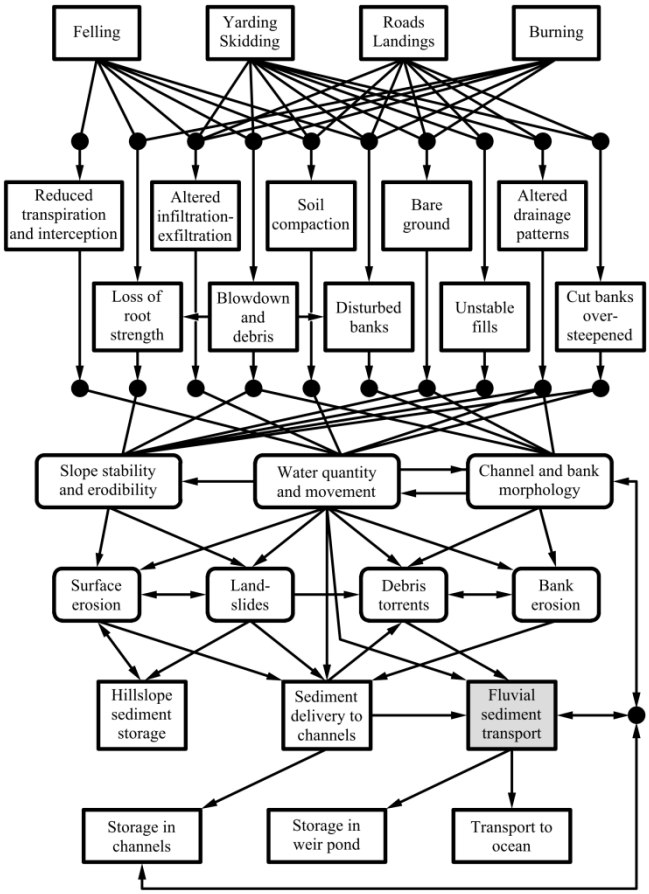

Figure 1.5. Conceptual flow chart of the major pathways through which forestry activities affect the stream sediment delivery (from Lewis 1998)

Removing trees reduces evapotranspiration and rainfall interception, leading to increased surface runoff. Soils become vulnerable to surface erosion without vegetation cover. Uprooting or root decay as well as road cuts may decrease slope stability and cause mass movements. Heavy equipment can compact soils during roadwork, log skidding, construction

and use of roads and landings which decreases infiltration, increases and concentrates overland flow. Linear structures alter drainage paths and redirect water to more erodible areas. The construction of stream crossings and roads, due to the low permeability of the road surface, are one of the primary sources of erosion in forested catchments (*Lewis* 1998, *Chang* 2006).

Several authors, especially in the USA, studied the sediment delivery problem of forested catchments, where soil erosion and thus fine material supply to the streams grew to considerable size due to the forestry activities, which can be responsible for direct physical disturbances and long-term post treatment effects as well. *Beschta* (1978) reported on the significant increase of *SSC* in three small forested catchments as a post-treatment effect of logging activities, where the average annual sediment yield (*SY*) became 1.4-times higher in a 25% patch-cutted creek and 2.8-times higher in a 82% clear-cutted catchment, and the change is obvious compared to an untreated adjacent basin as well. However, the statistically significant changes in *SSC* are not confirmed in all cases and for all watersheds, because of its large annual variation for a given sampling point in a basin (*Brown & Krygier* 1971). Nevertheless, according to a 30-years investigation, *Grant & Wolff* (1991) also proves the suspended sediment increase after timber harvesting. Moreover, annual differences of sediment delivery are well demonstrated within a catchment and between the treated watersheds. In the "catchment 1", *SSY* increased rapidly and remained elevated in the first 10 years after the forestry activities. The average *SSY* started to decline after 7 years following an exponential trend. In the other treated catchment, where the suspended sediment form are more dominated partly due to the debris flows, the early *SSY*-increase was even more rapidly, and the highest load was produced by a storm event within several hours after 3 years of the treatment.

Debris slides and associated *debris flows* are special types of fine material supply in forested basins. On those catchments where debris-flow-prone gullies are connected to the streams, episodic fine material inlet may contribute to the *SSC*-variability in compliance with the flow threshold and the sediment replenishment-exhaustion phases (*Nistor & Church* 2005).
Besides of the fine woody debris, the impact of the *large woody debris* (*LWD*) on the stream sediment delivery is also a specific characteristic of forested catchments. Natural processes of the forest ecology and forest operations can also add *LWD* to the streams directly. The sediment retention effect of these debris (including branches, leaves and twigs) and log jams (*Figure 1.6*) accounts for the changed flow and sediment characters, likewise the alteration of channel morphology such as widening, lateral shifts and downcutting of channels (*Lisle & Napolitano* 1998, *Nakamura & Swanson* 1993). As *Megahan* (1982) reported, 3.6 obstructions were found per 30 *m* of channel with 0.8 m^3 of sediment storage per obstruction, averaging every years and streams. Although the number of obstructions and stored sediment volumes varied year by year and between streams, data emphasize the importance of channel-sediment storage in small forest streams: sediment amount stored behind the obstructions was an average of 15-times higher than the annual average *SY* transported to the stream mouth. Similarly, the role of channel-sediment storage is pointed out in the study of *Beschta* (1979). The author wrote that a debris removal activity led to the exhaustion of 3800 *t* of sediment

along 100 *m* of channel, where the greatest increase in turbidity was measured during the first autumn and winter storms.

Figure 1.6. Sediment retention behind log jam in a forested catchment (Sopron Hills)

Unpaved *forest roads* and skid trails, which may redirect and accelerate the surface runoff, can be the primary place of soil erosion and may contribute to the stream sediment budget (*Figure 1.7*). Certainly, produced sediment flux depends on several factors, such as length, slope, soil texture, vegetation cover, road maintenance-disturbance of the road surface and the traffic (*Luce & Black* 1999). During the experiments of *MacDonald et al.* (2001), runoff from the road surface started in response to most storms with at least 6 *mm* of rainfall depth, and the runoff ratio exceeded the runoff from undisturbed hillslopes by least an order of a magnitude.
As for the *SY*, again the unpaved roads were the dominant sediment sources (annual *SY*: 8-15 $kg \cdot m^{-2}$), even though they occupy a very small portion of the catchment area. In contrast, analysed the spatial distribution of fully connected pathways to the stream, *Croke et al.* (2005) drew the attention to that total sediment yield (*TSY*) from these pathways are relatively low, and the highest mass of sediment reach the channel at a few locations (e.g. at direct stream crossings and disperse pathways with large contributing area and small available hillslope length).

Notwithstanding, *mass movements* (*Figure 1.7*) due to high intensity rainfall events can also provide abundant *SY* from the steep hillslopes (*MacDonald et al.* 2001). However, as *Beschta* (1983) reported, sediment from mass failures were carried downslope only to be deposited on alluvial fans, in topographic depressions or on river terraces in many cases, and thus had little impact on stream *SY*. This fact also indicates well the complexities of hillslope sediment delivery component, floodplain storage and channel routing which lead to inaccurate *SY* estimations and increasing sediment variability.

Figure 1.7. Erosion processes in forested catchments: soil loss from an unpaved forest road (left) and mass movement (right) (Sopron Hills)

1.6.2 Impact of the land cover alterations on the suspended sediment dynamics

In the case of forest land cover, different land use types can be distinguished which influence differently the fine material availability in the stream channels. Research of *Surfleet & Ziemer* (1996) confirm that large organic debris input depends on the tree harvest method: a watershed with 60% *clear-cut* and riparian buffer strips showed slower recruitment from large organic debris than a second basin where 60% of the timber volume had been *selectively harvested*. *Stott et al.* (2001) investigated the effects of site-specific harvesting techniques (e.g. machine never drove on bare, unprotected ground, minimized number of stream crossings) to the *SSC*, and found that *SSC*-increase show a delay compared to the traditional forestry methods. Although in the case of an agricultural field, but *Mosimann et al.* (2007) pointed out that soil loss from tractor tracks can be reduced by up to 80% due to intermittent planting. In addition, conservation tillage provided sufficient soil protection up to 5% slope.
Hossain et al. (2002) made a comparison between the suspended sediment exports of three adjacent subcatchments, concluding on clear *SSY* response to the *different ratio of* forest *coverage*. Two of the subcatchments (22% and 42% forest) produced > 93% of the *SSY* during the study period, while sediment flux from the third subcatchment (75% forest) remained low due to its extensive forest cover and relatively flat terrain. Different land cover and topography induced different *SSC-Q* relationships as well: clockwise hysteresis loops were obtained in the subcatchments with lower forest coverage, and anti-clockwise hysteresis appeared in the third basin, in the case of studied floods. To criticize this study, the authors would have to separately analyse the effect of forest cover and different topography. The role of different ratio of a land cover type is also emphasized by *Bartley et al.* (2010), who pointed out that pasture rehabilitation through reduced utilisation and resting led to the increase of ground cover, and thus to the decline of *SY* where the vegetation cover exceeded 10%. In short term, surface runoff was less sensitive to land use change compared to erosion rate.
Sorriso-Valvo et al. (1995) detected that experimental plots with well-developed *grass cover* produced negligible runoff and *SY*, and plot with *Eucalyptus* forest and 100% litter cover generated rapidly high rate of runoff but virtually no erosion. In contrast, based on a 12-years-

long experiments performed in three small (< 2 ha) control catchments with different aspect, slope and vegetation but uniform lithology, *Iovino & Puglisi* (1991, in *Sorriso-Valvo et al.* 1995) observed highest annual runoff in the grassed catchment and lowest in the undisturbed forested catchments. Highest erosion rate was measured in the logged and undisturbed forested catchment, querying numerous erosion studies which neglect the soil loss in forest regions.

García-Ruiz et al. (2008) gave a good example of different rainfall-runoff and erosion processes at small catchments (<3 km^2) with different land cover (dense forest, agricultural land and catchment consisting in part of active badlands). As for the average *SSC* in the three experimental catchments, the highest value was obtained from the badlands which exceeded 200-times the average *SSC* in the forested catchment. Similarly to the above cited studies, land cover determined the seasonality and intensity of floods, and the annual volume of *Q* as well.

Considering the consequences of the changes in land cover, researches related to soil erosion and sediment delivery processes have to be even more stressed due to the expected climate change and forest decline.

2. Objectives and research questions

The dissertation aims to complete the previous results related to the sediment transport and soil erosion processes on the headwater forested catchments of the Rák Brook. Based on the ten-years-long dataset (2000-2010), the author describes the spatial and temporal alterations of suspended sediment concentration (*SSC*) and its control factors in the Farkas Valley and Vadkan Valley.

Temporal fluctuations are discussed under different flow conditions and at different time scales: annual, seasonal, inter-event and intra-event scale. To reveal which factors are responsible for the variability of sediment dynamics, different type of statistical analyses have been performed. The study also focuses on the calculation of sediment yield (*SY*), therefore regression models have been developed. Using the observed and modelled values, this work gives quantitative estimation at event scale and annual scale. The two selected flood events occurred on 18.07.2009 and 04.08.2009, while the reference hydrological year is 2008-2009, in order to point out the stochastic effect of a sediment deposit to the total annual sediment yield (*TSY*) which has been outwashed between October 2008 and August 2009.

As soil erosion is one of the main sediment sources of the streams, the proportion of soil loss to the annual *TSY* and the erosion endangered regions have been also determined using erosion models, such as the empirical Universal Soil Loss Equation (USLE – *Wischmeier & Smith* 1978) and the physically-distributed model EROSION-3D (*von Werner* 1995) in the Farkas Valley for the hydrological year 2008-2009. To implement the analysis of soil erosion with the USLE into a Geographical Information System, a new workflow has been developed with the ArcGIS Model Builder. The aim of this four-part workflow is to accelerate data processing and to ensure comparability of soil erosion risk maps.

Table 2.1 summarizes the main objectives of the dissertation and the applied methods.

Table 2.1. Main objectives of the dissertation and the applied methods

Objectives	Methods
To demonstrate the spatial and temporal fluctuation of the suspended sediment concentration and its control factors	Descriptive statistical analysis
To determine the significant sediment control factors at low and high flow conditions and at different time scales	Pearson correlation analysis Factor analysis
To develop regression equations and to calculate sediment yield • for the flood events 18.07.2009 and 04.08.2009 • for the hydrological year 2008-2009 in the Farkas Valley	Stepwise multiple regression analysis Sensitivity analysis

To examine the influence of an outwashing sediment deposit to the sediment dynamics as a stochastic processes (in the Farkas Valley)	Geodesic survey and data preprocessing in Geographical Information Systems Time series analysis
To identify the role of soil erosion in the Farkas Valley as sediment sources of the stream	Soil analyses Geodesic survey and data preprocessing in Geographical Information Systems Erosion modelling • Surface erosion calculation using an empirical equation (USLE – *Wischmeier and Smith* 1978) • Erosion calculation using a physically-distributed model (EROSION-3D – *von Werner* 1995)

3. Materials and methods

3.1 Study area

3.1.1 The catchment of the Rák Brook

The dissertation focuses on the sediment transport of the headwater catchments of the Rák Brook, such as the Farkas Valley and Vadkan Valley. The Rák Brook is the second largest stream of Sopron town, and it takes its source in the prealpine Sopron Hills and flows through the rarely disturbed forested catchment part until it reaches the urbanised flow-sections in the Sopron Basin (*Figure 3.1*). From NW and SW, the catchment boundary is located directly on the Hungarian-Austrian border on a long section. The 18.5 *km* long brook has a 38 km^2 catchment area with diversified geomorphology, geology and land cover. The highest peak of the catchment is 556 *m* a.s.l. (Magasbérc) and the lowest altitude is 189 *m* a.s.l. at the stream mouth resulting in the 367 *m* relief (*Marosi & Somogyi* 1990, *Dövényi* 2010).

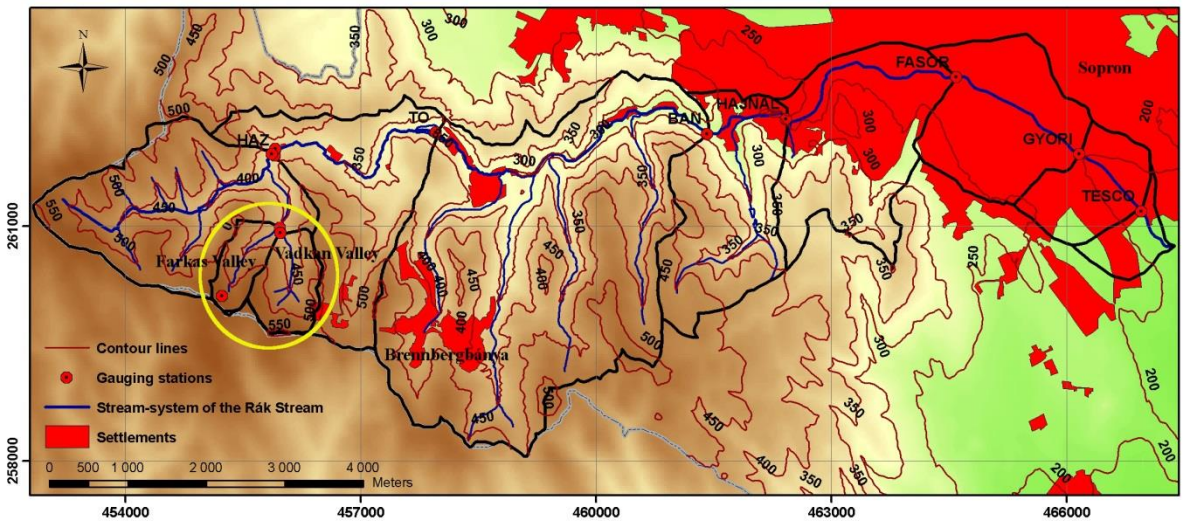

Figure 3.1. Catchment of the Rák Brook with settlements, gauging stations and subcatchments belonging to the stream gauging stations (The yellow circle represents the two headwater study catchments)

Geological and geomorphological conditions in the catchment of the Rák Brook. The main part of the catchment is located in the Sopron Hills which is mostly a crystalline block-mountain developed in the Palaeozoic Era. The metamorphic crystalline rocks (e.g. gneiss, muscovite and schist) can be found on the surface to the Köves Valley. On the west side of Köves Valley (in the Brennberg Basin), crystalline bedrocks are covered with strongly unclassified Tertiary (Miocene period) fluvial sediment (e.g. metamorphic pebbles, conglomerates, gravel, sand and loam). Mountain ridges, uplifted blocks, deep stream valleys and steep rocky slopes divide the terrain. Catchment of the Rák Brook divides into a number of subcatchments, and the geologic conditions, such as the impermeable crystalline bedrock

and the good aquifer in fluvial sediments, explain the dense stream network. The stratums are strongly displaced by the geologic faults determining the flow direction of watercourses. The Rák Brook follows an almost West-East fracture. On the South side of the catchment, the hills incline to the stream, while on the North side the hills incline away from the stream resulting in the strong catchment asymmetry (*Kárpáti* 1955, *Kisházi & Ivancsics* 1981-1985). The Sopron Basin is bordered by sharp tectonic lines from the surrounding geographical regions on the East and South side, while the NW border is a low watershed ridge divided into remnant hills and covered with gravels. The wide NW-SE basin has also crystalline bedrock capped by Tertiary loam and Quaternary sediments (Pleistocene gravel, loam, loess; Holocene fluvial sediments) (*Marosi & Somogyi* 1990, *Dövényi* 2010).

Soil types in the catchment of the Rák Brook. Forest soils have evolved on the basis of schist and fluvial sediments in the region of Sopron Hills. Lessivated or partly lessivated, acidic and non-podzolic brown forest soils are dominating. In the Sopron Basin, alluvial meadow soils and raw alluvial soils have a high ratio due to the floodplain character. However, the main soil group is the lessivated brown forest soil in this region as well. Water-driven erosion and mass movement erosion play an important role among the geomorphologic processes shaping the surface of the catchment of Rák Brook (*Marosi & Somogyi* 1990, *Dövényi* 2010).

Climatic conditions in the catchment of the Rák Brook. In the Sopron Hills region, the average annual temperature is 8.5-9.2 ^{o}C, the average temperature in January is -2,0 ^{o}C and 19.0 ^{o}C in July. The region belongs to the continental climate zone with four seasons; however Mediterranean, continental and ocean currents also influence the local climate. The NE and Adriatic cyclones increase the rainfall amount mostly in summertime. The heaviest rainfall intensities occur mostly in summer due to the thunderstorms, and the winter precipitation is dominantly snow. The annual precipitation is 700-750 *mm* (430-480 *mm* in the vegetation period). In the Sopron Basin, the average annual temperature is higher than the hilly regions, it is 9.5-9.8 ^{o}C, while the annual precipitation decrease to 640-660 *mm* (390-410 *mm* in the vegetation period) (*Dövényi* 2010). From the forestry climate classes according to *Járó*, the catchment of the Rák Brook belongs to the beech climate.

3.1.2 The Farkas Valley and the Vadkan Valley

The Farkas Valley and Vadkan Valley (latitude 47^{o}40’24’’N, longitude 16^{o}27’49’’E) (*Figure 3.2*) belong to the Hidegvíz Valley Experimental Watershed which has been established by the Institute of Geomatics and Civil Engineering (University of West Hungary, Faculty of Forestry) and its predecessor departments at the end of the 1970s (*Gribovszki & Kalicz* 2012).

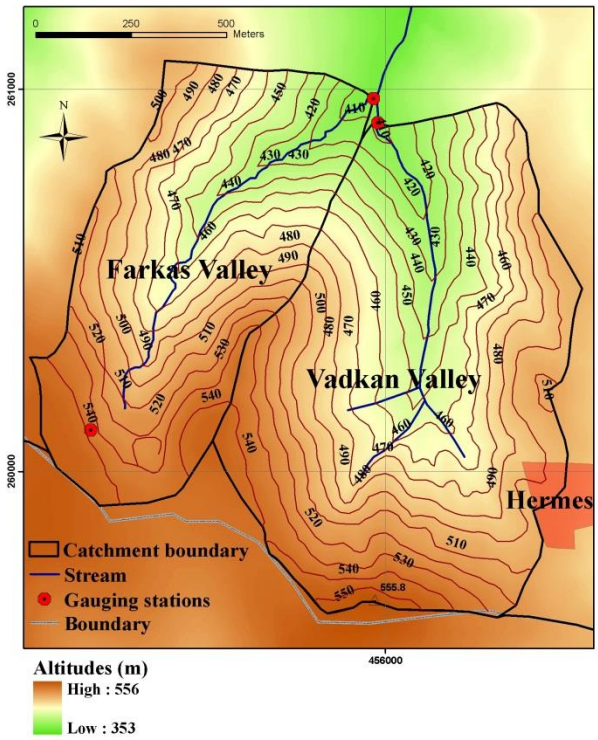

Figure 3.2. The Farkas Valley and the Vadkan Valley with the location of gauging stations

Geology of the Farkas Valley and Vadkan Valley

In the region of the Farkas and Vadkan Valley, five rock layers have deposited on the crystalline shale bedrock under different siltation conditions which are categorized as two Formations (*Kárpáti* 1955, *Kisházi & Ivancsics* 1981-1985).

Ligeterdő Gravel Formation. This formation is a 400-500 *m* thick fluvial sandy-gravel layer which is divided into four layers. The lower beds of the Ottnangian ages, with prevailing metamorphic pebbles and conglomerates, has the name Alsóligeterdő Formation while the subsequent bundles of beds are the Felsőligeterdő Formation. Only the two upper layers of the Carpathian ages can be found on the surface. The middle part of the formation with lignite strings and Congeria-bearing beds is called the Magasbérc Sand Formation which finer material appears on the valley bottom. Hilltops and hill-slopes are covered by the letter formation, the strongly unclassified Felsőtödl Gravel Formation which contains conglomerate, coarser gravels and finest loam. The thickness is 10-50 *m*. These layers are a good aquifer, therefore both valleys have a perennial streamflow. The streams never dry out, not even in driest periods.

Brennberg Lignite Formation. The lowest layer is called Brennberg Lignite Formation which is 60-180 *m* thick. Lignite-bearings were settled on unclassified sediments and they are covered by grey sand and loamy-sand.

Geomorphology of the Farkas Valley and Vadkan Valley

Table 3.1 represents the main physical parameters of the two catchments modified on the basis of *Gribovszki et al.* (2006). Values have been recalculated based on the DDM-5 digital elevation model using the ArcGIS/ArcMap 9.3 geoinformatical software.

Table 3.1. Characteristic physical parameters of the two catchments (after the modification of the table by Gribovszki et al. (2006))

Physical parameters	**Farkas Valley**	**Vadkan Valley**
Catchment area (*A*) (km^2)	0.59	0.91
Catchment length (*L*) (*m*)	1320	1340
Catchment perimeter (*m*)	4680	5140
Form factor (catchment area/catchment length^2 [km^2/km^2])	0.34	0.51
Average width (*A/L*) (*m*)	470	690
Greatest width (*m*)	602	880
Average length of overland flow (*A/L·1/2*) (*m*)	235	343
Average height (*m* a.s.l.)	488.8	484.9
Lowest point (*m* a.s.l.)	404.0	407.6
Highest point (*m* a.s.l.)	548.8	555.8
Total relief (*m*)	144.8	148.2
Average slope steepness (° and %)	12.3° (22.0%)	11.8° (21.1%)
Greatest slope steepness (° and %)	27.3° (51.5 %)	29.0° (55.4 %)
Average slope length	200-250	300-400
Main stream channel length [total] (*m*)	1190 [1190]	1060 [1440]
Channel slope (° and %)	4.4° (7.7%)	3.2° (5.5%)
Drainage density (length of cannel/surface area [km/km^2])	2.0	1.58
Valley direction	NE-SW	N-S
Average exposure of catchments	W-NW	N-NW

The physical parameters of the two catchments are similar, but the Farkas Valley is narrower and has higher average slope steepness than the Vadkan Valley. *Annex III.I.1* represents the relief conditions and the slope categories according to *Ad-hoc-AG Boden* (2005): flat terrain (<2%), very gentle slope (2-3.5%), gentle slope (3.5-9%), moderate slope (9-18%), strong slope 18-27%), very strong slope (27-36%), steep slope (36-58%) and very steep slope (>58%). The relief is relative high considering both catchment areas. Steepest slopes are located at the upper part of the catchments and next to the streams where the channels are similar to gullies. Consequently, morphological characteristics may play an important role in triggering the runoff and erosion processes, and erosion risk is locally very high in both catchments. Log jams and sediment deposits evolve frequently in the stream channel of both catchments resulting in pool and riffle sequences which interrupt the channel slope in the length profile.

Soils of the Farkas Valley and Vadkan Valley

According to *Bellér* (1996) and the *Forestry management plan* (2004), the following soil types can be found in the study catchments: podzolic brown forest soils (Luvisol, PBF),

strongly acidic non-podzolic brown forest soils (Luvisol, ABF), lessivated brown forest soil (Luvisol, LBF). To a small extent eroded skeletal soils (Regosol) and, on the bottom of the slopes, colluvial soils (Cambisol, CS) can also be found. *Table 3.2* shows the proportion of soil groups in both catchments.

Table 3.2. Percentual distribution of the soil groups in the Farkas Valley and the Vadkan Valley

Soil group	Farkas Valley (%)	Vadkan Valley (%)	Total (%)
PBF	79.7	92.5	87.3
ABF	5.7	-	2.3
LBF	14.6	-	5.9
CS	-	7.5	4.5

The dominant soil group, similarly in both catchments, is the PBF which is prone to erosion because of its texture. The CS appears in the Vadkan Valley due to the gentler valley bottoms but this soil type is not significant in the Farkas Valley. The ABF and LBF (with more advantageous water capacity) soil groups are expected to be found also in the Vadkan Valley; however, it requires further examinations to detect them.

These soils are generally strongly acidic and the deeper horizons generally show higher pH(H_2O) values. Regarding four soil sections (*Bellér* 1996):

- LBF (between 0-72 *cm*; A_1, A_3, B_1, B_2 and C horizon): 4.8, 4.7, 5.0, 5.0, 5.1
- ABF (between 0-110 *cm*; A, A, B, B and C horizon): 4.6, 4.7, 4.9, 4.9, 5.1
- ABF (between 0-90 *cm*; A, A, B, B, and C horizon): 4.3, 4.9, 4.9, 4.9, 5.0
- CS (between 0-120 *cm*; 1^{st}, 2^{nd}, 3^{rd} and 4^{th} horizon): 5.1, 4.8, 4.9, 5.1

According to the *Forestry management plan* (2004) the tilth depth is 60-100 *cm* and 70-90 *cm* based on the analyses of *Bellér* (1996) making more precise this range. The physical soil textures are loam and loam with clastic elements. Fine sandy fraction (50-70%) is very characteristic in the upper soil layer referring to the high erosion risk. In the C-level of soils, 70-80 *cm* deep a thin impermeable clayey layer can be locally found. This layer can contribute to water retention supporting the water balance and producing subsurface flow. However, clay-bearing layer can also promote the mass movement activities on steep slopes increasing the *SY* in the streams. Under the clayey layer unclassified gravelled ferrous fluvial sediment can be found. The humus content in the surface level is 6-7% at LBF and CS while 2-3% at PBF and ABF.

A-level of all soil types have less erosion resistance in both catchments, therefore vegetation cover plays a significant role of in erosion protection. Without land cover the A-level can be quickly eroded. B-levels have more compact texture resulting in lower erodibility but higher rate of surface runoff. Due to the steep slopes near to the channels and soil conditions, landslides activity has high frequency in both catchments. The whole channel segment is endangered by mass movement erosion in the Farkas Valley while the upper steepest parts of the main channel show obviously high landslide risk in the Vadkan Valley.

Land cover and forestry activities

Both catchments and their surroundings have been covered by forest and frequently managed by forestry activities. There are differences in the ratio of deciduous-coniferous stands considering the forest coverage of the two catchments. The Vadkan Valley is dominantly covered with deciduous stands, while the Farkas Valley has more coniferous than deciduous forest. The main conifer species is spruce (*Picea abies*) and the main deciduous is beech (*Fagus sylvatica*). These species have different hydrological behaviours and they also have different forest floor cover. In the bottom of the valleys another species, the alder (*Alnus glutinosa*) is dominant. The increasing damages by wood-borer in the spruce stands motivate forest maintenance in even more area of the catchments, therefore a lot of clear-cutting have taken place in the region since the last decade. *Annex III.I.2/a-b* summarizes the main forest activities in the subcompartments of Farkas Valley and Vadkan Valley.
Cutting areas were sometimes very close to the stream system probably affecting to the sediment transport processes. Coarse woody debris can promote the formation of log jams and sediment deposits in the stream channels.

There is a difference between the shares of road areas within the two catchments. The road area is more than twice larger in the Farkas Valley (6.2%) than in the Vadkan Valley (2.7%). These roads can modify runoff processes and lead to significant soil losses caused by accelerated and concentrated runoff from the unpaved forest roads. *Annex III.I.3* shows the major characters of land cover in the Farkas Valley, such as forest subcompartments, vegetation types and forest road network.

3.2 Sediment and sediment control parameters

3.2.1 Precipitation data

The central meteorological station is located approximately 1.5 *km* from the headwater catchments in the Hidegvíz Valley in front of the main research building. The precipitation data have being measured using two recording tipping buckets rain gauge (0.5 *mm* and 0.1 *mm* rainfall capacity) (*Figure 3.3*). The rain gauge 0.1 *mm* (marked as "$_{c1}$") collects data at 1-min intervals, while the rain gauge 0.5 *mm* (marked as "$_{hhm}$") registers the time of the tips. Records of the "$_{c1}$" instrument have been available since 2003. *Rainfall depth* data (*P* or P_{c1} and P_{hhm}, *mm*) by both of the rain gauges have been applied to the calculation of *antecedent precipitation index* and *rainfall erosivity index.*

Figure 3.3. The central meteorological station (left) and the tipping bucket rain gauges (right; white: "$_{c1}$", gray: "$_{hhm}$") in front of the main research building in the Hidegvíz Valley

Data gaps, data inaccuracies and deviations between the records by the two rain gauges can be related to the intermittent failure of the instruments (e.g. clogging, power outage, evaporated snow due to overheating) and the different data recording method of the two rain gauges. Since the "$_{c1}$" instrument registers data in each minutes and the "$_{hhm}$" instruments registers only the time when 0.5 *mm* capacity bucket tipped, more than six hours (the time limit without rainfall which marks a new rainfall event) may elapse between two records resulting in a following rainfall event. The distance between the central meteorological station and the study catchments may also cause inaccuracies in the real rainfall depth due to the high spatial heterogeneity of precipitation distribution. Although a long and difficult manual verification has preceded the synchronization of the database of the two rain gauges and the water stage recorders, a further type of the possible data inaccuracies are the consequence of the regularly change between winter time (*CET*) and summer time (*CEST*) or the delay/gain of the data recorders. If the server time has not been updated in the computer which serves for

downloading the raw data from the data recorders, the delay/gain can also cause the same synchronization problems.

Rainfall erosivity index (*EI*; EI_{c1} and EI_{hhm}, $kJ \cdot m^{-2} \cdot mm \cdot h^{-1}$) has been determined on the basis of the SI adaptation of the *Wischmeier & Smith* (1978) equation (*Dettling* 1989, *Centeri* 2001). The *EI* ($kJ \cdot m^{-2} \cdot mm \cdot h^{-1}$) is the product of the storm kinetic energy times the maximum 30-min intensity for each storm:

$$EI = E \cdot I_{max30} = \left[\sum_{k=1}^{m} e_r \cdot P_r \right] \cdot I_{max30}, \text{ where } e_r = \qquad \text{(Eq. 3.1)}$$

$$0.1189 + 0.0873 \cdot log_{10} i_r, \text{ if } 0.05 < i_r < 76.2,$$

$$0, \text{if } 0.05 \geq i_r,$$

$$0.283, \text{if } 76.2 \leq i_r.$$

In the *Eq. 3.1* *E* is the total storm kinetic energy ($kJ \cdot m^{-2}$); I_{max30} is the maximum 30-min rainfall intensity ($mm \cdot h^{-1}$); e_r is the rainfall energy per unit depth of rainfall per unit area ($kJ \cdot m^{-2} \cdot mm^{-1}$); P_r is the depth of rainfall (*mm*) for the r^{th} increment of the storm hyetograph which is divided into *m* parts, each with essentially constant rainfall intensity (i_r) ($mm \cdot h^{-1}$).

The separation base of the single rainfall events is, if there is no precipitation in 6 hours-long period. If the rainfall duration is less than 30 *min*, the maximal 30-min rainfall intensity is equal to the total rainfall depth. 30-min rainfall intensities have been applied to the kinetic energy calculation of the rainfall increments. According to *Jakab* (ex verb.), we have not distinguished erosive and non-erosive rainfalls at the rainfall separation, setting out from the fact that the non-erosive rainfalls also contribute to the saturation of the soil, thus accelerating later the starting of rainfall-runoff at another rainfall event.

EI have been computed for each rainfall events recorded in the ten-years-long period in the Hidegvíz Valley, and to each suspended sediment concentration (*SSC*) value sampled in the Farkas Valley and Vadkan Valley during the flood events. In winter, the soil becomes increasingly more erodible as the soil moisture profile is being filled, the surface structure is being broken down by repeated freezing and thawing, thus the early spring runoff from snowmelt or light rain on frozen soil can induce increased soil loss and sediment yield (*SY*). Therefore, a subfactor has to be added to the rainfall erosivity values in these periods (*Wischmeier & Smith* 1978). However, we did not have snow data, thus the *EI* values in winter, spring and at annual scale are lower than the real values.

Antecedent precipitation index (*API*) has been calculated with the accumulation of rainfall depth of 1 ($API1_{c1}$, $API1_{hhm}$; *mm*), 3 ($API3_{c1}$, $API3_{hhm}$; *mm*) and 7 ($API7_{c1}$, $API7_{hhm}$; *mm*) days before the water sampling:

$$APId = \sum_{i=1}^{d \cdot 1440} p_i \text{ , where} \qquad \text{(Eq. 3.2)}$$

p_i is the rainfall depth in the i^{th} minute; *d* is the number of days (in this case 1, 3 and 7) ; *1440* is the multiplication factor for the unit conversion of *day* to *min*. We accepted the simplified

calculation method of *API* (*Zabaleta et al.* 2007), thus weight factor has not been applied to the rainfall depths as given for the small Hungarian catchments according to *Kontur et al.* (2003). Adaptation of this method can be a next step in the future research.

3.2.2 Runoff data

The stream gauging stations at the outlet of Vadkan Valley and Farkas Valley (401 *m* a.s.l.) consist of a 1.5 m^3 volumetric capacity stilling basin with weir (*Figure 3.4*). The weir had a trapezoid cross section to 22.05.2007, when a V-weir has been constructed. This rebuilding plays an important role in the water stage-discharge relation.

Figure 3.4. Stream gauging station at the outlet of the Farkas Valley (1: low flow; 2: high flow) and the Vadkan Valley (3: high flow; 4: low flow; 5: data logger)

Water stage (*h, cm*) has been recorded by a pressure sensor connected to a data logger with 2 minute frequency to 31.12.2007 and with 1 minute frequency from 01.01.2008. The pressure sensor is the "DLCMDU-P DA-23" model made by the DATAQUA 2002 Electronics Ltd. Water stage has been also measured manually with weekly frequency or linked to the rainfall events.

As the rainfall depth time series, neither the water stage time series are continuous due to data gaps. Pressure sensors cannot be heated, and the frost can damage the membrane of the instruments, therefore they are removed from the gauging stations in wintertime. In order to

clean out the sediment from the stilling basins, water has to be run off for a short period. A number of unplanned reasons can also lead to the interruption of *h* time series, such as flat batteries, water drop in the capillary tube, short circuit due to the vapour inside of the instrument box, self-restarting of the data recorder and plugging due to high sediment level in the stilling base.

Discharge (*Q*, $l \cdot s^{-1}$)**.** Parallel to the manual water stage measurements, discharge has been measured using volumetric method. The volumes of the chests or pots applied to the *Q* measurement during the ten-years-long period were variable, depending on the *Q*-ranges: 1.5 *l*, 5.5 *l*, 12.5 *l*, 15 *l*, 16.5 *l*, 26 *l*, 37 *l* and 90 *l*.
The strong correlation between the manually measured *h* and *Q* data pairs enables to produce long-term *Q* time series on the basis of the automatic *h* records. *Eq. 3.3* describes the regression equation of the water stage-*Q* relationship for the trapezoid weir and *Eq. 3.4* for the V-weir (where $r^2 > 0.99$):

$$Q = 0.086 \cdot (h + 0.568)^{2.049} \qquad (Eq.\ 3.3)$$

$$Q = 0.024933 \cdot h^{2.3818} \qquad (Eq.\ 3.4)$$

On the basis of the available automatic *h* and derived *Q* time series the main descriptive *Q* values are the following in the Farkas Valley (*Table 3.3*). The hydrological year 2008-2009 (the basis period for sediment yield calculations) produced higher descriptive values than the entire period between 2000 and 2010, representing a more humid period. Seasonal data point at the major role of stormflow in summer (the highest maximum *Q*) and the deflating groundwater stocks in summer and autumn (the lowest minimum *Q*). Despite of the data gaps in the automatic *Q* time series, the long term observation enables us to apply these results to the further calculations.

Table 3.3. The main descriptive Q values in the Farkas Valley based on the automatic h-records

Q ($l\ s^{-1}$)	2000-2010	2008-2009	Autumn	Winter	Spring	Summer
Normal	2.5	4.7	1.9	1.6	2.7	3.2
Average	1.9	2.7	1.9	1.0	1.9	2.0
Minimum	0.0	1.3	0.0	0.4	0.2	0.0
Maximum	281.4	281.4	109.7	68.5	66.4	281.4

Flood wave separation. Since the sediment dynamics show significant variability in the different *Q*-ranges according to the literature, "*low flow*" and "*high flow*" conditions are distinguished. Separation of low and high flow is simplified: if there is no precipitation contribution, the flow condition is considered as "*low flow*", while "*high flow*" periods indicate the flood events. This simplification can lead to relative higher *Q*-ranges of low flow, when high groundwater level increases the baseflow stage or subsurface runoff contributes to the stream *Q* at the end of a flood event.
The flood events have been manually separated. The beginning of the flooding period has been identified as the increase of the *Q* caused by the rainfall, while the end of the event is when the straight line (with the same upward slope as the hydrograph slope before the starting of direct runoff) from the beginning of the hydrograph intersects the falling limb of the

hydrograph (*Figure 3.5*). The description of the flood wave separation method in detail can be found at *Kontur et al.* (2003). The *peak discharge* (Q_{max}, $l \cdot s^{-1}$) and the *total volume of the flood event* (*SumQ*, *l*) have been determined for each flood event. If the *SSC* sampling occurred during the flood event, Q_{max} and *SumQ* has been calculated for the period between the beginning of flood event and sampling time.

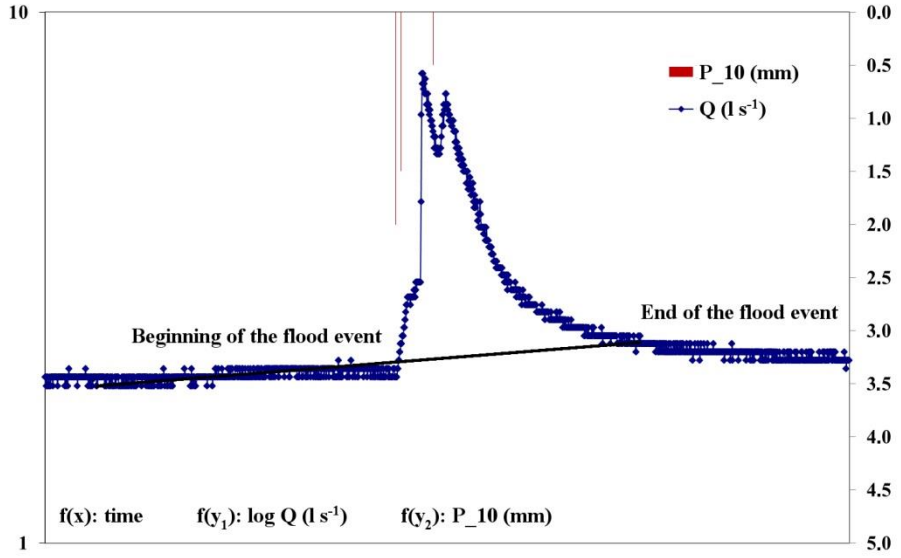

Figure 3.5. Method of the flood wave separation according to Kontur et al. (2003) – example of the flood event 15.10.2010 in the Farkas Valley (Q: discharge, P_10: 10-min rainfall depth)

3.2.3 Temperature data

The water temperature has been registered in every 10 minutes by the sensor installed in the stilling basins, and measured manually with weekly frequency linked to the water sampling. First of all the manual data have been applied to the further analyses.

Thermometers for measuring the soil temperatures are placed in the beech interception garden established in the upper part of the Farkas Valley (in the subcompartment *171H*). Soil temperatures were measured at three depths: 0 cm (*ST0*, ^{o}C), -5 cm (*ST5*, ^{o}C) and -10 cm (*ST5*, ^{o}C). Data have been available since May 2006; however, remarkably data failures have been obtained in the years 2008 and 2009.

3.2.4 Sediment data

Suspended sediment and bedload data has been gathered in the Farkas Valley and Vadkan Valley since 1996. In the frame of this work, the sediment dataset between the hydrological years 2000 and 2010 has been analysed.

Suspended sediment data

Water samples have been manually collected into plastic bottles at the gauging stations with weekly frequency or linked to the flood events. One sample means 1 *l* water: according to the recommendation of WMO 1981 (*Gordon et al.* 2004), if suspended sediment concentration (*SSC*, $mg \cdot l^{-1}$) exceeds 100 $mg \cdot l^{-1}$ in the stream, 1 *l* water sample is sufficient to determine *SSC*. The *SSC* have been quantified by filtering of the water samples. The filter papers containing sediment have been dried in an oven for 24 hours at 90-105 ^{o}C and weighed on a precision scale before and after the drying. As the weight of filter papers increases fast due to the air humidity after their removal from the oven, empty filter papers have been applied as control papers to diminish the inaccuracies due to the weight increase. *Figure 3.6* shows the process of gathering *SSC* data.

Figure 3.6. The process of gathering SSC data: water sampling (1), filtering (2-3), drying (3) and weighing (4) of the filter papers

Suspended sediment yield (*SSY*, $mg \cdot s^{-1}$ or $t \cdot yr^{-1}$ after unit conversion) is the total mass that leaves the catchment in a given time and can be estimated by integrating the suspended sediment transport rate over time:

$$SSY = \int_{\tau} Q(t) \cdot SSC(t) dt \qquad (Eq.\ 3.5)$$

where τ is the time interval of interest; *Q(t)* is the stream discharge ($l \cdot s^{-1}$) at time *t*; and *SSC(t)* ($mg \cdot l^{-1}$) is the suspended sediment concentration at time *t*.

To calculate *SSY* on the basis of *Eq. 3.5* for every 1 or 2 minute, as having *Q* values by the automatic water stage recorders in that time resolution, more frequent *SSC* values are necessary as well. To generate *SSC* data for the automatic *Q* time series, regression equations have been developed. For those intervals when

- neither *SSC* nor *Q* data have been available with high frequency,
- no reasonable *SSC* values have been obtained by the regression equations,

SSY have been calculated using average *SSC* and *Q* values:

$$SSY = \int_{\tau} Q_{average} \cdot SSC_{average} dt \qquad (Eq.\ 3.6)$$

where $Q_{average}$ is the normal discharge ($l \cdot s^{-1}$) and $SSC_{average}$ ($mg \cdot l^{-1}$) is the average suspended sediment concentration for the given season when no continuous data series were available; *t* in *dt* refers to the duration of data gap.

Flow conditions, control factors and time scales for the suspended sediment concentration analyses. Since sediment dynamics has a significant temporal fluctuation according to the literature, this work examines *SSC* and its control factors at different time scales. Moreover, as the regression analyses, similarly the descriptive statistical assessment of *SSC* and *SSC* control factors has been divided into low flow and high flow conditions. Low flow database has been separated on the basis of the number of days elapsed since the previous flood event (*antecedent days*, *AD*) resulting in four arbitrary categories:

- if $AD < 2$ (the previous flood event can directly influence the low flow *SSC*),
- if $2 \leq AD < 8$,
- if $8 \leq AD$ (effect of the in-channel supply processes due to the long dry period may increase).

The high flow database has also been separated according to the rising and falling limb of the hydrograph.

The following factors controlling *SSC* and *SSY* have been examined *under low flow conditions*:

- discharge (*Q*),
- antecedent days (*AD*),
- water temperature (*WT*),
- soil temperature at a depth of 0 cm (*ST0*), 5 cm (*ST5*) and 10 cm (*ST10*).

Relations between the sediment variables and control factors have been analysed at different time scales:

- for the entire study period – from 1st November 2000 to 31th October 2010,
- at seasonal scale – autumn, winter, spring and summer,
- and for the hydrological years.

The list below represents the factors controlling *SSC* and *SSY* involved in the analyses *under high flow conditions*:

- *Q*, *WT*, *ST0*, *ST5*, *ST10*,
- rainfall erosivity index (EI_{c1}, EI_{hhm}),
- antecedent precipitation index for 1 day ($API1_{c1}$, $API1_{hhm}$), 3 days ($API3_{c1}$, $API3_{hhm}$) and 7 days ($API7_{c1}$, $API7_{hhm}$),
- total volume of the flood event (*SumQ*) and
- peak discharge at the given flood event (Q_{max}).

Relations between hydrological, hydrometeorological and sediment variables have been investigated at the following time resolution:

- for the entire study period – from 1st November 2000 to 31th October 2010,
- at seasonal scale – autumn, winter, spring and summer,
- and at event scale – with especial regard to the flood events on 18th July 2009 and 4th August 2009.

No *SumQ* and Q_{max} values are available for the Vadkan Valley.

Bedload data

Although the analysis of bedload dynamics is not the objective of the dissertation, the short description of bedload is important to be able

- to calculate the total annual sediment yield (*TSY*) of the Farkas Valley in the hydrological year 2008-2009,
- to compare the *TSY* of two flood events (18.07.2009 and 04.08.2009) in the Farkas Valley and Vadkan Valley,
- to assess stochastic effect of the outwash of a sediment deposit to the sediment transport in the Farkas Valley.

Bedload has being trapped in the stilling basins at the outlet of Farkas Valley and Vadkan Valley (*Figure 3.4*). The bedload yield (*BY*, $t \cdot yr^{-1}$) is a cumulative value which is measured weekly using volumetric method, simultaneously to the water stage and/or *Q* measurement.
Stilling basins are generally open in winter in order to avoid the damages by the frozen water, thus bedload trapping is also limited in winter period. *BY* of great floods exceed sometimes the 1.5 m^3 capacity of the stilling basin causing quantitative underestimation. Organic debris, such as periphyton, leaves and logs may lead to *BY* overestimation. Suspended sediment may accumulate in the basin at very low *Q*, while a part of the bedload may behave as suspended sediment at high *Q* because of the turbulent conditions. To determine the *SY* leaving the stilling basin, not only the inflow *SSC* but also the outflow *SSC* has being sampled since April 2009. The average value of the SSC_{inflow}-$SSC_{outflow}$ difference has been applied as a correction factor of the *BY*.

BY has been calculated with a simple summation of the observed data for a longer time period. However, the weekly or longer measuring intervals cause problems in the determination of *BY at event scale*, because bedload of more flood events and low from period may accumulate in the stilling basin between the measurements. *Eq. 3.7* was applied to subtract the *BY* of the irrelevant high and low flow periods in the cases of the flood event 18.07.2009 and 04.08.2009:

$$BY_{flood\_obs} = (BY - (BY_{bf\_mean} \cdot t)) \cdot \left(\frac{SumQ}{SumQ_{hf}} \right) \qquad (Eq.\ 3.7)$$

where BY_{flood_obs} is the bedload yield of the sampled flood event (*kg*), *BY** is the total bedload yield accumulated in the stilling basin between two measurements (*kg*); $BY_{bf\_average}$ is the average baseflow bedload yield ($kg \cdot min^{-1}$) – it has been determined on the basis of *BY* values observed in long dry periods when no flood events occurred between two bedload measurements; *t* is the duration of the low flow periods between two bedload measurements (*min*); *SumQ* is the total volume of the sampled flood event (*l*); $SumQ_{hf}$ is the total volume of the high flow periods between two bedload measurements (*l*) (*Csáfordi et al.* 2010a).
The method is based on the simplification that there is a direct proportionality between the cumulative *Q* and *BY* of the flood events. As this assumption neglect the strong stochasticity in the bedload dynamics due to the sediment availability (breakage of the armoured streambed, sudden outwash of sediment deposits, landslides) and the power law between *Q*

and *BY*, *BY* values for the sampled flood events have to be recalculated using other methods in the future.

The sum of suspended sediment yield and bedload yield for a given time period is equal to the total sediment yield (*TSY*, $t \cdot yr^{-1}$).

3.3 Statistical analyses

Statistical analyses have been performed with the STATISTICA, the MS Office and the R software. Detailed description of the statistical methods used in the dissertation can be found in the *Annex III.III*.

Pearson correlation analysis was applied to reveal linear relationship between suspended sediment concentration and hydrological, hydrometeorological and climatic variables. Besides the correlation analysis, *stepwise multiple regression analysis* and *factor analysis* supported the selection of suspended sediment control factors involved in the regression-equation-based sediment yield models.

To check the consistency of *BY* data over time and to demonstrate the influence of the outwashing sediment deposit on the bedload dynamics in the Farkas Valley, the *mass curve* (MC) and *double mass curve analysis* (DMC) have been applied. Cumulative values of *BY*, precipitation and *Q* have been compared on the basis of the time period from January 2006 to October 2009. Data gaps have been completed with average values. On the basis of the plots, it can be identified when the outwash of sediment deposit has begun and terminated, and breaks in slope refer to the changing trends of the outwash process as well.

3.4 Geodesic survey and working with GIS

To monitor the morphological changes of the stream channel and to reveal the potential sediment sources (e.g. landslides, gully erosion on forest roads), geodesic surveys have been accomplished in the Farkas Valley.

The *outwash of sediment deposits* are considered as major but stochastic sediment sources in small forest streams. To identify the most important suspended sediment control factors in the Farkas Valley, the outwash of a sediment deposit behind a log jam has been examined. The surface of the sediment deposit and its surroundings has been surveyed with a Trimble total station in October 2008 before the sediment outwash has begun, and in October 2009 when the sediment outwash has terminated. Major breakpoints of the terrain and the stream channel have been recorded as parallel cross sections 2 *m* distance from each other. *X*, *y* and *z* coordinates of the measured points have been processed in the Digiterra Map software resulting in two surface models. The elevation difference between the two surface models indicates the volume of the outwashed sediment yield.
Figure 3.7 shows the outwashed sediment deposit with a remarkable channel incision and the GPS-survey of the eroded areas.

Figure 3.7. The outwashed sediment deposit (left) and GPS-survey at a shallow landslide (right)

The *eroded areas* have been mapped with a Thales Mobile Mapper GPS. Horizontal inaccuracy of the positioning using this instrument is not higher than 1 *m* due to the WAAS/EGNOS correction and the external real time RTCM differential correction. On the basis of the GPS-points, an erosion map has been created for the Farkas Valley which verifies the results of the erosion models. Since neither the Universal Soil Loss Equation (USLE) nor EROSION-3D is suitable to predict gully erosion and landslides, the erosion map serves for completing these model shortcomings as well.

Creating the *dataset for the erosion modelling and the evaluation of the model results* also need a GIS-environment for both of the erosion models. The ArcGIS/ArcMap 9.3 software has been applied to generate the required parameters for the soil erosion prediction, where the following input data have been pre-processed:

- a 5·5 *m* raster resolution Digital Elevation Model (DEM) (*FÖMI, DDM-5*),
- a 1:10000 scale georeferred rasterized topographic map (*FÖMI, DTA-10*),
- aerial photographs in 0.5 *m/px* resolution (*FÖMI, ortophoto*),
- *Forestry management plans* (1994, 2004) and
- a soil map based on the analysis of soil samples from the Farkas Valley.

The DEM is the input for modelling the catchment boundary, the stream network and the *LS* factor. A specific threshold is needed to model the stream network in the USLE. A grid cell is considered to be a channel if the catchment above the point is greater than the specific threshold (*Jain & Kothyari* 2000). On the basis of topographic maps, aerial photographs, forest management plans and soil map, vector layers have been digitalised (as polygons and linear elements) which involve the different land cover types, land use units and forest roads. The attribute tables of these vector layers will include the *R*, *K*, *C* and *P* factors for the USLE, and the "soil dataset" for the EROSION-3D.

While the EROSION-3D needs GIS-environment only as an interface to prepare input and to analyse output dataset, and the *soil erosion computation* runs automatically in the model software, the *implementation of the USLE into a GIS* means that the whole model process runs in the GIS-environment. Land units in the vector layers such as land cover and land use maps provide the spatial distribution of the six USLE factors. To integrate the USLE in an ArcGIS/ArcMap environment, each factor must be available as a thematic raster layer. Therefore vector datasets must be converted into a grid format with the same raster resolution as the DEM. The USLE-calculation is a raster-based function, where the model multiplies the unique value of each spatially corresponding grid cell in the six thematic raster layers based on the *Eq. 1.2* (*Figure 3.8*). The model output is the average annual soil loss (*Andersson* 2010).

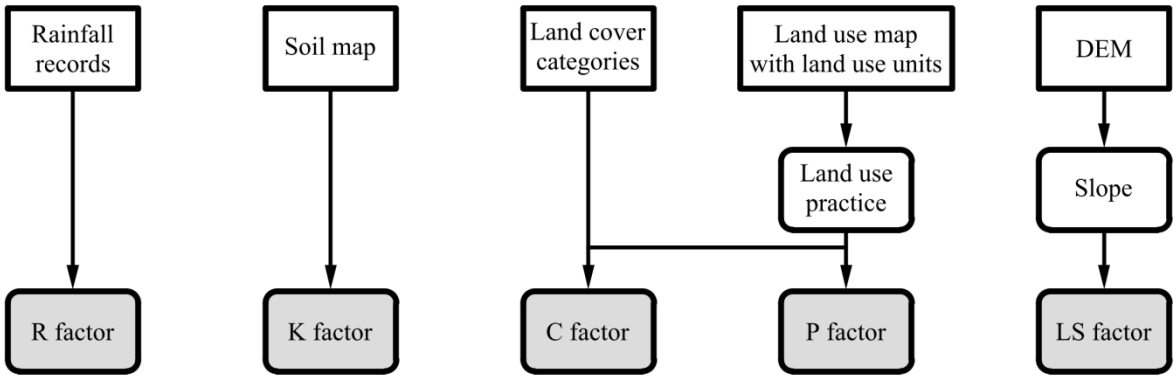

Figure 3.8. Conceptual flow chart for determining the USLE factors

To accelerate the data processing for the soil erosion modelling with the USLE in a GIS environment and to ensure comparability of soil erosion risk maps, a new *workflow* has been

developed *with the ArcGIS Model Builder*. The ArcGIS/ArcMap Model Builder is a visual interface that combines several GIS operations in a user-defined sequence and runs these modules with different datasets (*Pfaff & Glennon* 2004). A model consists of three fundamental elements: input parameters, geoprocessing tools and output data. Model parameters are specific model inputs which need to be defined by the user. For example, the user has to define the specific location of input data, or has the opportunity to specify thresholds. The workflow built in this study requires ArcGIS 9.3 Desktop with ArcInfo license involving Spatial Analyst and 3D-Analyst Extensions. The model consists of the following tools of ArcMap/ArcToolbox: Spatial Analyst Tools, Conversion Tools, Analysis Tools and Data Management Tools.

3.5 Soil loss calculations

3.5.1 Determination of factors of the Universal Soil Loss Equation (USLE)

There are several methods to determine the USLE factors, but this section only presents which was applied in the dissertation.

The *R* factor ($kJ \cdot m^{-2} \cdot mm \cdot h^{-1}$) is equal to the annual summation of the rainfall erosivity index (*EI*) of the single rainfall events, which has been determined on the basis of the "$_{hhm}$" rainfall data recorded in the 2008-2009 hydrological year in the Hidegvíz Valley rain gauge station.

The *K* factor ($t \cdot ha^{-1} \cdot m^{2} \cdot kJ^{-1} \cdot h \cdot mm^{-1}$) is based on the physical soil texture, the water content measurement and the organic substance analysis of 25 soil samples collected from the upper soil layer in the Farkas Valley. Soil analyses have been performed in the laboratory of Institute of Physical Geography and Landscape Ecology, Faculty of Natural Sciences, Leibniz University of Hannover.
The physical soil texture has been determined on the basis of grain size distribution and extrapolated for the whole Farkas Valley where erosion modelling has been performed. Extrapolation method is based on the assumption that physical soil texture may depend on the altitudes and follow the contour lines (*Meer ex verb.*). Physical soil textures have been distinguished and grain size limits have been taken according to the *Ad-hoc-AG Boden* (2005) (KA4/KA5 classification, see also the *DIN 4220:2008-11 standard*). Grain size analyses have been conducted on the basis of the *ISO 11277:2009 standard* (*Figure 3.9*).

Figure 3.9. Surface soil sampling in the Farkas Valley (1-2), pounding the soil samples (3) and analysis of particle size distribution using Köhn pipette (4)

Soil erodibility has been calculated with the following equation according to *Schwertmann et al.* (1987):

$$K = 2.77 \cdot M^{1.14} \cdot 10^{-6} \cdot (12 - OS) + 0.043 \cdot (AC - 2) + 0.033 \cdot (4 - PC) \quad (Eq.\ 3.8)$$

where *M* = (particle fraction between 0.063 *mm* and 0.002 *mm* (%) + particle fraction between 0.1 *mm* and 0.063 *mm* (%)) · (particle fraction between 0.063 *mm* and 0.002 *mm* (%) + particle fraction between 2.0 *mm* and 0.063 *mm* (%)); *OS* is the percentual content of organic substance (if *OS* > 4% *OS* = 4 %); *AC* = aggregate category; *PC* = category of permeability.

In this case A = 2 (soil aggregates are between 1-2 *mm*) and PC = 3 (infiltration rate is between 10-40 $cm \cdot day^{-1}$) (*Schwertmann et al.* 1987).

The *LS* factor is based on the DEM and the unit stream power theory of *Moore & Burch* (1986), as *Eq. 3.9* shows. The calculation has been performed with the ArcMap 9.3 Spatial Analyst Tools.

$$LS = \left(FlowAccumulation \cdot \frac{CellSize}{22.13} \right)^{m} \cdot \left(\frac{\sin \beta}{0.0896} \right)^{n} \qquad (Eq.\ 3.9)$$

In *Eq. 3.9* the *FlowAccumulation* is a raster layer representing the upslope cell number contributing to the surface runoff of a certain raster cell; *CellSize* refers to the resolution of the DEM; β is the slope steepness in *degree* (^{o}); *m* and *n* are empirical exponents; *22.13* is the standard slope-length (*m*); *0.0896* is the factor for the unit conversion of *degree* to *radian*. Due to the lack of detailed digital elevation data, the values m = 0.4 and n = 1.3 have been applied, in correspondence to other international studies such as *Lee* (2004) and *Demirci & Karaburun* (2011). Values of *m* and *n* have been suggested by *Moore & Burch* (1986) for standard reference conditions of USLE, where the slope-length is 22.13 *m* and slope is 9%.
Spatial distribution of the *LS* factor is represented by the *Annex III.V.1*.

Although recommendations of *Ma* (2001) and the *US EPA* (2009) concern to some regions of the USA, erosion analysis is based on these normative values in this work:

- pasture/hay 0.05,
- deciduous forest 0.009,
- evergreen/coniferous forest 0.004,
- mixed forest 0.007,
- forest/woody wetland 0.003
- and grass 0.000-0.004.

Afterwards the *C* factors have been locally modified (reduced or increased) on the basis of field experiences, the forestry management plans and the visual interpretation of aerial photographs. *Annex III.V.2* shows the spatial distribution of the *C* factor.

Recommendations by *Rácz* (1985) based on the tree harvesting and planting techniques have been applied to determine the *P* factor:

- finished berming or terracing reforestation after clear cutting: 0.20,
- finished pitting reforestation clear cutting: 0.40,
- shelterwood cutting: 0.35,
- selective cutting: 0.30.

The normative *P* values above have also been redefined for each subcompartment in the Farkas Valley on the basis of field experience, forestry management plans and visual interpretation of aerial photographs, similarly to the determination of the *C* factor. In this study, *P* factor value is equal to 1 if the forest has been directly clear cutted. Since all of the cutting areas have been already reforested in the Farkas Valley, reduced *P* values are applicable. *Annex III.V.3* presents the *P* factor in the Farkas Valley.

To detect the most sensitive regions to soil erosion, the author classified the soil loss map according to the tolerance categories for the annual soil loss. The tolerable soil loss values according to *Rácz* (1985) depend on the depth of the soil:

- 1.0 $t \cdot ha^{-1} \cdot yr^{-1}$ at 20 *cm*,
- 2.2 $t \cdot ha^{-1} \cdot yr^{-1}$ at 40 *cm*,
- 4.1 $t \cdot ha^{-1} \cdot yr^{-1}$ at 60 *cm*,
- 6.4 $t \cdot ha^{-1} \cdot yr^{-1}$ at 80 *cm*,
- 9.0 $t \cdot ha^{-1} \cdot yr^{-1}$ at 100 *cm*,
- 11.*8* $t \cdot ha^{-1} \cdot yr^{-1}$ at 120 *cm*,
- 15.0 $t \cdot ha^{-1} \cdot yr^{-1}$ at 140 *cm*.

According to the *Forestry management plan* (2004), the average depth of the soil in the Farkas Valley is between 60 and 100 *cm*, thus the tolerable annual soil loss would be not higher than 6.4 $t \cdot ha^{-1}$ (assuming 80 *cm* average depth of the soil in the catchment). However, the field assessment shows that the soil depth can be lower or higher due to the local heterogeneity of the soil characters. Therefore each tolerance category is applied to enable us to create suitable erosion risk maps.

Whereas the USLE does not compute deposition along hillslopes, it is necessary to estimate the sediment delivery ratio (*SDR*; *%*), in order to assess stream sediment yield (*SY*) from soil loss. *Eq. 1.1* has been chosen in this work for calculating *SDR* in the Farkas Valley. Notwithstanding, the application of a watershed specific *SDR* curve would be better for the accurate calculation. Reduction of the soil loss by the *SDR* plays an important role in the comparison of surface soil loss with the total sediment yield (*TSY*) in the hydrological year 2008-2009 in the Farkas Valley.

3.5.2 Datasets and parameters of the EROSION-3D

Previously described source data, such as DEM, 1-min resolution "$_{c1}$" rainfall time series, land cover and soil map, serve to create the three groups of dataset for the EROSION-3D model: relief, rainfall and soil parameters. Soil dataset consists of seven variables: bulk density ($kg \cdot m^{-3}$), organic matter (*%*), initial moisture (*%*), erodibility ($N \cdot m^{-2}$), cover (*%*), Manning's roughness coefficient ($s \cdot m^{-1/3}$), skin factor for the corrections (*dimensionless*) and nine particle fractions (*Annex IV.I.1*).

In the absence of own soil parameters, such as bulk density, initial moisture, erodibility, roughness and skin factor, due to the time consuming and expensive measurements, data of the *Parameter catalogue for Saxony* (1996) have been used. As the parameter catalogue is primarily developed for the agricultural land cover, relating values are simplified at different surfaces, such as forest stands and roads. To test the EROSION-3D model and to complete the knowledge about sediment dynamics with the regions susceptible for soil erosion, the author accepted these values (*Annex III.V.4/a-b*).

4. Results

4.1 Soil, rainfall and runoff conditions

4.1.1 Soil map of the Farkas Valley and spatial distribution of the K factor

Figure 4.1 represents the map of physical soil texture (for the upper soil layer) and the spatial distribution of *K* factor in the Farkas Valley where the legendary indicates: very loamy sand (*Sl4*), slightly sandy loam (*Ls2*), moderate sandy loam (*Ls3*) and silty-loamy sand (*Slu*). Same texture categories appear more than one, referring to the different proportion of clay, silt and sand within the same categories. *Annex IV.I.1* shows the extrapolated percentual values of particle fractions such as coarse sand (*gS*), middle sand (*mS*) fine sand (*fS*), coarse silt (*gU*), middle silt (*mU*), fine silt (*fU*), coarse clay (*gT*), middle clay (*mT*) and fine clay (*fT*). *C* means the organic material content.

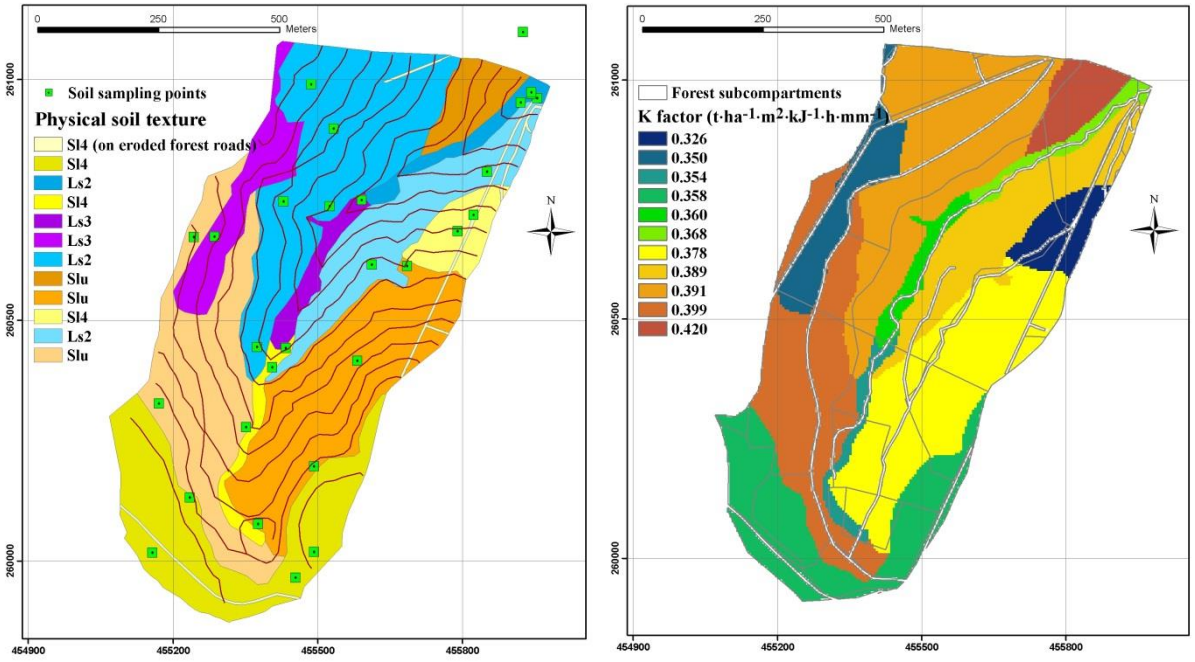

Figure 4.1. Physical soil texture of the upper soil layer (left) and the spatial distribution of K factor in the Farkas Valley (right)

4.1.2 Precipitation categories and the descriptive statistical variables of different rainfall parameters

989 rainfall events have been separated based on the records of the tipping bucket rain gauge "$_{hhm}$" during the hydrological years 2000-2010 and 1123 rainfall events have been observed according to the "$_{c1}$" rain gauge during the hydrological years 2003-2010. Deviations have also been obtained between the rainfall variables, due to the previously described failures of the instruments. However, this work primarily focuses on the impact of some selected rainfall

events on the sediment transport, thus the ten-years-long precipitation database has not been corrected in the frame of the dissertation.

Description of the rainfall conditions are based on five precipitation categories according to *Kucsara* (1996), where the classes are: 0.0-2.0 *mm*, 2.1-5.0 *mm*, 5.1-10.0 *mm*, 10.1-20.0 *mm* and > 20.0 *mm*. Precipitation events with 0.5 *mm* or lower rainfall depth (*P*) are considered as trace of precipitation, but they are errors in several cases. Therefore, it would be necessary to neglect these data in the future, to make the evaluation more plausible. Precipitation categories in the different time scales give a comprehensive view of rainfall depth, intensity and erosivity distribution and also reflect the relation of the rainfall variables.

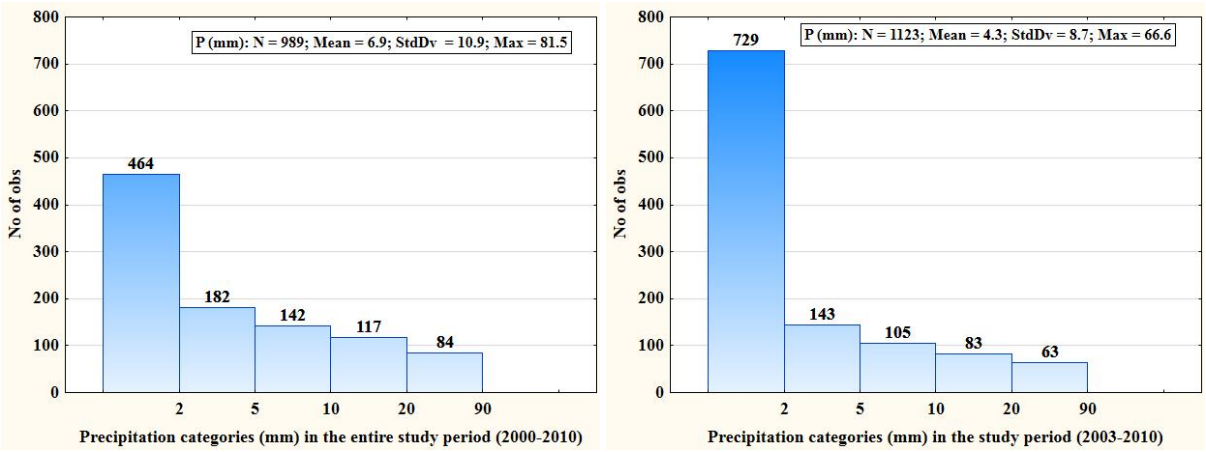

Figure 4.2. Precipitation categories and number of precipitation events according to the records of "$_{hhm}$" rain gauge (left) and "$_{c1}$" rain gauge (right)

According to the *Figure 4.2* the frequency of precipitation events increases in the higher categories. Disregarded the 0.0-2.0 *mm* category, the number of observations are comparable based on the two rain gauges:

- As the histogram of "$_{hhm}$" shows, 35% of the rainfall events belong to the 2.1-5.0 *mm* category, 27% to the 5.1-10.0 *mm* category, 22% to the 10.1-20.0 *mm* category and 16% to the > 20.0 *mm* category.
- Rainfall distributions are similar according to the "$_{c1}$", as for the 36% proportion of the 2.1-5.0 *mm* precipitation class, 27% proportion of the 5.1-10.0 *mm* category, 21% proportion of the 10.1-20.0 *mm* category and 16 % proportion of the > 20.0 *mm* category.

Since the contribution of precipitations lower than 2.0 *mm* to the total annual erosivity index (*EI*) are not higher than 0.8% at "$_{c1}$" and 0.9% at "$_{hhm}$", the lowest category could be omitted in the sediment transport examinations.

Considering the seasonal distribution of precipitation events according to the database of "$_{hhm}$" (*Figure 4.3*), the rate of heavy rainfalls are dominant in summer (September-November): 31% all of the precipitation events are observed in summer (45% of the total rainfall amount in the ten-years-long study period) and 29% of the summer rainfalls belong to the >10.1 *mm* precipitation category. The ratio of the >10.1 *mm* category is 17% in autumn (September-November), 14% in winter (December-February) and 16% in spring (March-

May). As expected, the descriptive statistical variables also prove the high frequency of summer storms and the major role of the summer season in soil erosion (*Annex IV.I.2*), as well the records by the "$_{c1}$" rain gauge.

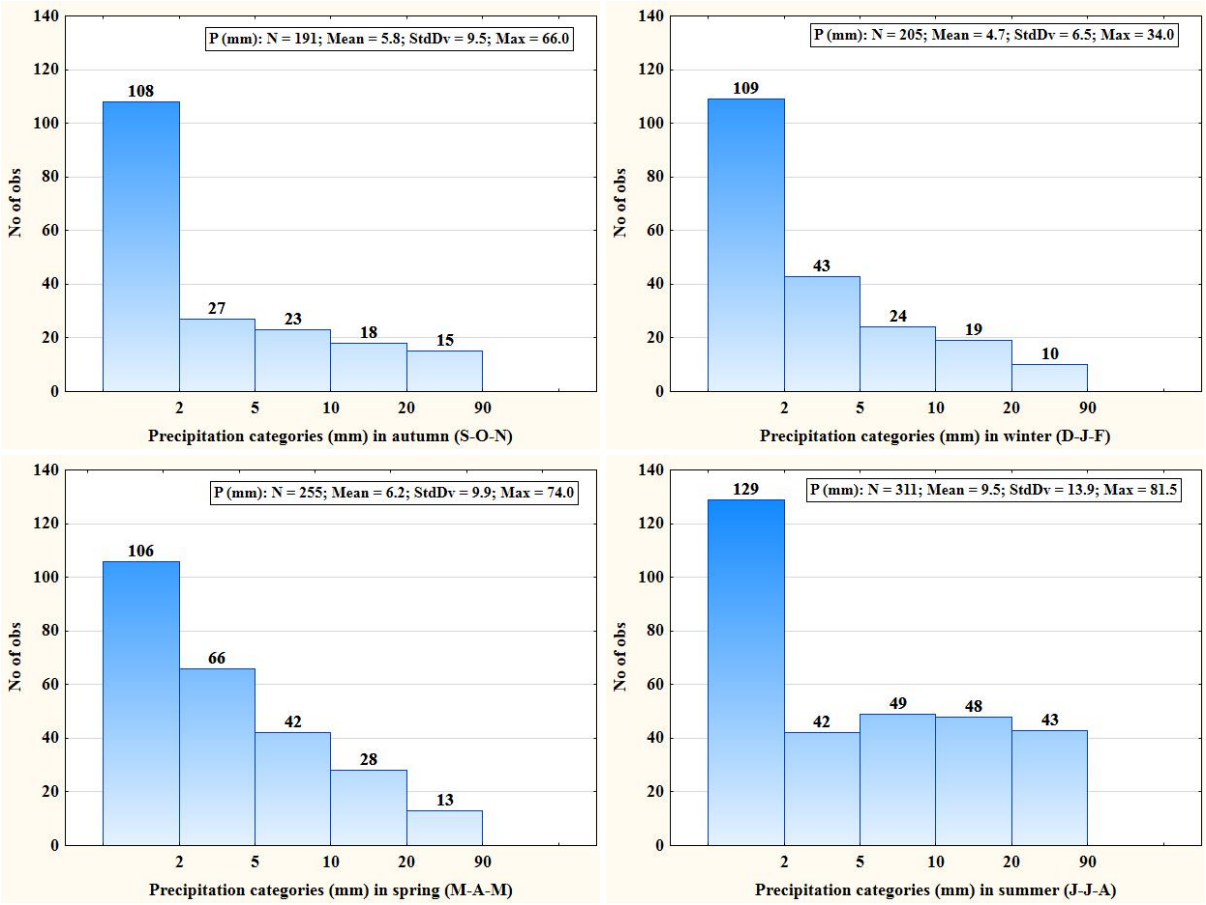

Figure 4.3. Seasonal distribution of the precipitation categories according to the records of "$_{hhm}$" rain gauge

Average and maximal values of maximal 30-min rainfall intensity (I_{max30}) and *EI* are the highest in summer and the lowest in winter. Despite of the bit higher ratio of the upper two precipitation category in autumn (17% vs. 16%), the late spring storms indicate higher erosion risk regarding the maximum rainfall depth (66.0 *mm* vs. 74.0 *mm*), I_{max30} (58.0 $mm \cdot h^{-1}$ vs. 74.0 $mm \cdot h^{-1}$) and *EI* (47.2 $kJ \cdot m^{-2} \cdot mm \cdot h^{-1}$ vs. 92.0 $kJ \cdot m^{-2} \cdot mm \cdot h^{-1}$). The sum of *EI* in summer represents 71.5% of the total *EI* in the entire study period, while the proportion of the sum of *EI* to the total *EI* is 16.5% in spring, 9.5% in autumn and 2.5% in winter. Knowledge of these ratios is especially useful in the mirror of the vegetation cover. Since heavy rainfall events are the most frequent in late spring and summer, forestry activities should be avoided in these periods, to ensure the soil protection role of the vegetation.

Suspended sediment dynamics have also been evaluated at annual scale. To describe the rainfall conditions for these examinations, this section summarizes the precipitation categories for each hydrological year from 2000 to 2010 according to the records of "$_{hhm}$" rain gauge (*Annex IV.I.3*). A detailed precipitation analysis of the hydrological year 2008-2009 has been

represented according to the "*hhm*" rain gauge, because the sediment yield (*SY*) calculations and the assessment of an outwashing sediment deposit have been accomplished for this period.

Considering the *Annex IV.I.3*, the average annual precipitation is 746 *mm* in the study period based on the "*hhm*" rain gauge and omitted the inaccurate rainfall depth in 2002-2003. This value coincides well with the average annual precipitation of Sopron Hills according to *Dövényi* (2010). The average annual *EI* is 187.2 $kJ \cdot m^{-2} \cdot mm \cdot h^{-1}$; furthermore, the sum of *EI* remarkably exceeds the average value in the hydrological years 2007-2008 and 2009-2010. The extremely heavy rainfall events have a major role for providing high *EI* and triggering high rate of soil erosion. Rainfall events with rainfall depth higher than 20.0 *mm* have an 89.8% contribution to the annual sum of *EI* in 2008 and 88.1% in 2010.

Table 4.1. Rainfall events with high EI from the years 2008-2010 based on the "hhm" rain gauge (List of symbols: P – rainfall depth; I_{max30} – maximal 30-min rainfall intensity; EI – erosivity index)

Start	**End**	**Duration** (*h*)	***P*** (*mm*)	I_{max30} ($mm \cdot h^{-1}$)	***EI*** ($kJ \cdot m^{-2} \cdot mm \cdot h^{-1}$)	**% *EI*-ratio to the annual sum of *EI***
04.06.2008 18:30	05.06.2008 10:27	16.0	57.5	35.0	43.0	11.7
26.06.2008 16:41	27.06.2008 5:13	12.5	81.5	46.0	89.6	24.5
20.07.2008 13:45	21.07.2008 11:39	21.9	59.0	48.0	62.8	17.2
02.08.2008 14:09	02.08.2008 16:09	2.0	41.0	42.0	42.8	11.7
04.08.2008 15:56	04.08.2008 17:06	1.2	30.0	45.0	33.9	9.3
18.07.2009 8:11	*18.07.2009 15:40*	*7.5*	*23.0*	*21.0*	*10.5*	*7.8*
03.08.2009 20:54	*04.08.2009 14:55*	*18.0*	*42.0*	*21.0*	*17.7*	*13.2*
27.05.2010 12:12	27.05.2010 18:53	6.7	50.0	74.0	92.0	19.2
15.07.2010 21:33	16.07.2010 1:09	3.6	43.5	72.0	81.5	17.0
05.08.2010 23:16	06.08.2010 6:45	7.5	31.0	44.0	32.1	6.7
13.08.2010 19:43	13.08.2010 22:48	3.1	63.0	83.0	134.0	28.0
14.08.2010 21:23	15.08.2010 7:47	10.4	35.0	39.0	33.2	6.9

As an example, *Table 4.1* shows some selected events from the years 2008 and 2010 which compose a large proportion to the annual sum of *EI*. The two rainfall events from 2009 in the marked by *italic* numbers generated the sampled flood events which are analysed in detail (examination of suspended sediment dynamics and *SY* calculation at event-scale).

The hydrological year 2008-2009 can be considered as an average year as for the annual sum of *P* (723.5 *mm*) and *EI* (133.9 $kJ \cdot m^{-2} \cdot mm \cdot h^{-1}$), thus it is ideal for the *SY* calculation. In this period, 96 single rainfall events have been observed, from which 38.5% of the precipitations belong to the <2.0 *mm* category, 20.8% to the 2.1-5.0 *mm* category, 19.8% to the 5.1-10.0 *mm* category, while the proportion of the upper two categories are similarly 10.4%. Rainfalls with rainfall depth higher than 10.0 *mm* have 66.6% ratio to the annual precipitation and 80.1% ratio to the annual *EI* pointing at the importance of heavy rainfalls in soil destruction. Considering the seasonal distribution of *P*, I_{max30} and *EI* (*Table 4.2*), trends are mostly similar to the seasonal fluctuation of rainfall variables based on the entire study period. Although in the hydrological year 2008-2009 the autumn is the driest season, intensity and erosivity

parameters follow the "usual" order: winter < autumn < spring < summer. Sum of *EI* of the summer rainfalls compose the 82.7% proportion of the annual *EI*.

Table 4.2. Seasonal fluctuation of the descriptive statistical variables of the rainfall parameters in the hydrological year 2008-2009 based on the "$_{hhm}$" rain gauge (List of symbols: P – rainfall depth; I_{max30} – maximal 30-min rainfall intensity; EI – erosivity index)

	Valid N	Average	Sum	Maximum	Std.Dev.
autumn					
P *(mm)*	15	4.7	70.0	22.5	6.0
$\boldsymbol{I_{max30}}$ $(mm \cdot h^{-1})$	11	3.6	40.0	10.0	2.7
EI $(kJ \cdot m^{-2} \cdot mm \cdot h^{-1})$	11	0.5	5.7	3.3	1.0
winter					
P *(mm)*	12	7.1	85.5	26.5	8.3
$\boldsymbol{I_{max30}}$ $(mm \cdot h^{-1})$	10	3.1	31.0	8.0	2.0
EI $(kJ \cdot m^{-2} \cdot mm \cdot h^{-1})$	10	0.4	3.6	0.9	0.4
spring					
P *(mm)*	30	4.9	147.5	32.5	6.9
$\boldsymbol{I_{max30}}$ $(mm \cdot h^{-1})$	25	4.0	100.0	16.0	3.4
EI $(kJ \cdot m^{-2} \cdot mm \cdot h^{-1})$	25	0.6	13.8	3.6	1.0
summer					
P *(mm)*	39	10.8	420.5	80.0	15.5
$\boldsymbol{I_{max30}}$ $(mm \cdot h^{-1})$	34	9.5	323.0	23.0	6.8
EI $(kJ \cdot m^{-2} \cdot mm \cdot h^{-1})$	34	3.3	110.8	17.7	4.6

4.1.3 Characterization of flood events in the Farkas Valley

426 flood events have been separated on the basis of the water stage time series registered in the Farkas Valley. Flow conditions of the Farkas Valley can also be correlated with the Vadkan Valley based on the method of equivalent water-levels. *Annex IV.I.4* represents the strong relation between the discharges in Farkas Valley and Vadkan Valley (Q_{FA} and Q_{VA}).

Although the time series are interrupted by relative long data gaps (especially in winter as described previously), the flood database gives a comprehensive view of the flood characteristics of the studied catchments. Nevertheless, this dissertation can not undertake to evaluate flood parameters and their distributions as detailed as given for the rainfall events, but the previously described precipitation database and the flood database can underlie for further rainfall-runoff research.

To describe the variables of flood events, the author used the previous time scales. *Table 4.3* represents the major descriptive statistical variables of flood parameters, such as discharge at the beginning and the end of flood events (Q_{start} and Q_{end}), total volume of the flood event (*SumQ*) peak discharge (Q_{max}), for the entire study period and at seasonal scale. Q_{start} may refer to the antecedent rainfall conditions and water storage of the catchment. If the catchment is saturated, the baseflow can be durably stable and relative high, increasing the value of

Q_{start}. *SumQ*, Q_{max} and the ratio of Q_{max}-Q_{start} indicate the extent of rainfall intensity and rainfall depth. Heavy rainfalls can theoretically generate higher flood peaks and total volume of the flood event.

Table 4.3. Descriptive statistical variables of the flood parameters for the entire study period and at seasonal scale (List of symbols: Q_{start} – discharge at the beginning of the flood event; Q_{end} - discharge at the end of the flood event; SumQ – total volume of the flood event; Q_{max} – peak discharge; Valid N – sample size)

	Valid N	Average	Median	Min	Max	Std.Dev.
all						
Q_{start} $(l \cdot s^{-1})$	421	1.8	1.4	0.1	11.4	1.4
Q_{end} $(l \cdot s^{-1})$	425	2.2	1.8	0.2	19.2	2.1
SumQ *(l)*	426	361473	88264	5267	14752272	1200774
Q_{max} $(l \cdot s^{-1})$	426	14.3	4.6	0.5	281.4	32.3
autumn						
Q_{start} $(l \cdot s^{-1})$	102	1.6	1.4	0.2	3.5	0.9
Q_{end} $(l \cdot s^{-1})$	102	1.8	1.9	0.2	5.0	0.9
SumQ *(l)*	102	258773	104952	5267	4381220	528320
Q_{max} $(l \cdot s^{-1})$	102	8.6	3.9	0.5	109.7	15.7
winter						
Q_{start} $(l \cdot s^{-1})$	21	1.5	1.3	0.7	3.5	0.8
Q_{end} $(l \cdot s^{-1})$	23	1.9	1.4	0.9	6.4	1.2
SumQ *(l)*	23	264070	76486	33823	3142955	653505
Q_{max} $(l \cdot s^{-1})$	23	6.6	3.0	1.5	68.5	13.9
spring						
Q_{start} $(l \cdot s^{-1})$	111	1.9	1.4	0.5	8.1	1.4
Q_{end} $(l \cdot s^{-1})$	112	2.2	1.5	0.7	13.0	1.7
SumQ *(l)*	113	381471	70652	20033	14272352	1430747
Q_{max} $(l \cdot s^{-1})$	113	6.7	3.8	1.2	66.4	8.8
summer						
Q_{start} $(l \cdot s^{-1})$	178	1.9	1.4	0.1	11.4	1.6
Q_{end} $(l \cdot s^{-1})$	179	2.6	2.1	0.0	19.2	2.7
SumQ *(l)*	179	421886	92750	7227	14752272	1387604
Q_{max} $(l \cdot s^{-1})$	179	23.6	6.7	0.8	281.4	46.0

The seasonal values of the *Table 4.3* partly confirm the previous assumptions. Averages of Q_{start} seem to follow the theoretical fluctuation of groundwater level which reaches the minimum to November and the maximum to spring. In some cases, Q_{start} can be much higher than the average value due to the flood separation method. If two flood events follow each other very fast, they have been sometimes separated, even if the subsurface runoff has not descended yet and it has being contributed to the *Q*. Highest average and maximal *SumQ* and Q_{max} have been obtained in summer coinciding well with the seasonal trend of rainfall parameters. However, only the *SumQ* shows the expected trend in spring, because the average and maximal Q_{max} in autumn and the maximal Q_{max} in winter exceed the spring values. As for the Q_{max}-Q_{start} ratio, the summer produces the highest average value, but the second highest

average and the highest maximum value have been obtained in autumn. To reasonable explain these unexpected characters, connected rainfall and flood events and the vegetation cover should be simultaneously examined in the future.

Annex IV.I.5 shows the main descriptive statistical variables of the flood parameters at annual resolution. Setting out from the previous hypotheses (and neglecting the data gaps), drier (2000-2005) and more humid (2007-2010) periods can be distinguished, when average Q_{start} values are remarkably higher. According to the average and maximal Q_{max} values, which indirectly refer to the heavy rainfall events when the soil detachment and *SY* can also be potentially high, flash floods were especially frequent in the hydrological years 2005-2006, 2007-2008, 2008-2009 and 2009-2010. *SumQ* also indicates this trend; however, if *SumQ* is high, it does not mean unequivocally a flash flood, because rainfalls with long duration, and thus with high rate of runoff, generate long-lasting floods, high *SumQ* and relative low Q_{max}.

4.2 Suspended sediment concentration and its control factors

This section describes the fluctuation of suspended sediment concentration (*SSC*) and its control factors, which have been applied as a basis of the correlation analysis and sediment yield (*SY*) calculations, using descriptive statistical variables for different flow conditions and at different time scales as given in the *Sect. 3.2.4*. *Annex IV.II.1/a-b* represents the time series of the observed *SSC* and manually measured discharge (*Q*) values in the Farkas Valley and the Vadkan Valley under low flow conditions.

Figure 4.4 represents the boxplots of *SSC* values for the low flow categories based on the antecedent days (*AD*), respectively for the rising and falling limb of flood waves. Main descriptive statistical parameters as tables can be found in the *Annex IV.II.2*.

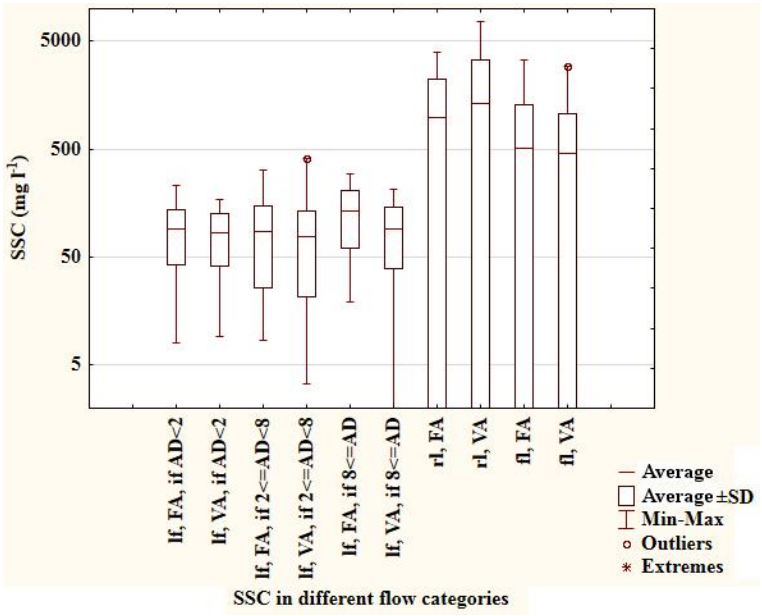

Figure 4.4. Boxplots of the suspended sediment concentration (SSC) in different flow categories in the Farkas Valley (FA) and Vadkan Valley (VA) (Scale type of the y-axis is logarithmic.)
(List of abbreviations: AD – antecedent days, lf – low flow, rl – rising limb of the hydrograph, fl – falling limb of the hydrograph)

Descriptive statistical values of *SSC* show special trend in both catchments: highest values have been obtained at the rising limb, when easily available sediment sources are being outwashed by the rising *Q*. *SSC* values are lower at the descending limb, referring to the limited sediment availability in the channels. Compared the average *SSC*s at different low flow conditions with each other, value of the category "*AD≤2*" are higher than value of the category "*2≤AD<8*" in both catchments, suggesting the direct impact of previous flood events in the form of residual sediment stocks. If the *AD* increases, the average *SSC* values decrease at first probably due to the outwash, and then unambiguously rise due to the in-channel supply (see the category "*8≤AD*").
Considering the descriptive statistical values of *SSC* in the Farkas and Vadkan Valley, an outstanding difference is notable. Average *SSC* is the highest in the Vadkan Valley at the

rising stage of the flood waves. However, all of the average *SSC* values for the other flow conditions are lower than in the Farkas Valley. This trend may refer to the quicker sediment exhausting or the more effective sediment trapping in the Vadkan Valley. Higher average *SSC* under low flow conditions in the Farkas Valley can be explained by the more effective sediment replenishment in the dry periods due to the in-channel supply. Different morphological characters of the valleys can induce the different sedimentary response: the Farkas Valley is narrower and steeper slopes are dominant, therefore the hydrological processes can be quicker than in the Vadkan Valley. This fact contradicts the first hypothesis for the lower average *SSC* values in the Vadkan Valley, that is, the quicker sediment outwash. The following sections below represent further examinations, to find the right answer to the different sediment dynamics of the two adjacent valleys. However, the results should be handled with care because suspended sediment samplings are underrepresented for some flow categories (see the *N* values).

Annex IV.II.3 shows the main descriptive statistical variables of the observed *SSC* and its control factors at low flow for the entire study period and at seasonal scale. (*Q* and water temperature (*WT*) values in the table are based on the manual observations directly linked to the sediment samplings.) Seasonality of the descriptive statistical values, especially the deviations between the summer and winter values emphasize the necessity to evaluate sediment dynamics for larger time resolution than the entire study period. Lower average *SSC* values in the Vadkan Valley are noticeable at seasonal scale as well confirming the slower sediment replenishment or more efficient sediment trapping. Higher descriptive statistical values of *Q* refer to the larger catchment area. There is no essential difference in relation to *WT* and soil temperature (*ST*); moreover, the Vadkan Valley is a little warmer than the Farkas Valley in winter and colder average temperatures have been obtained in the other seasons.

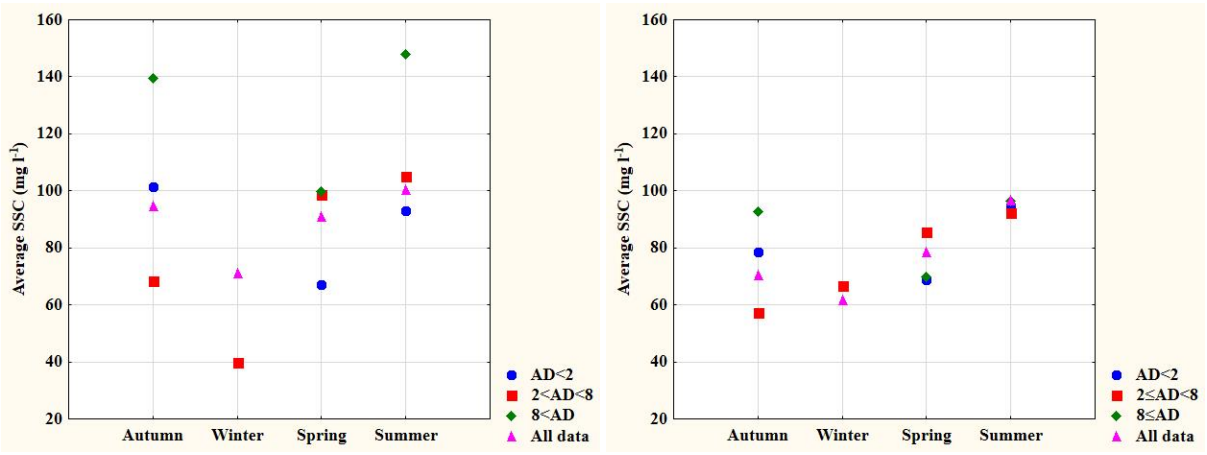

Figure 4.5. Seasonal variability of the average suspended sediment concentration (SSC) in different low flow categories (AD – antecedent days) in the Farkas Valley (left) and in the Vadkan Valley (right)

Figure 4.5 is the combination of the previously described variability of the average *SSC* at different low flow conditions (*Annex IV.II.2*) and at seasonal scale (*Annex IV.II.3*) in both catchments. In the Farkas Valley, lowest average *SSC* values have been obtained in winter,

regarding the plots based on the entire low flow database and the "*2≤AD<8*" category. (Values are missing at the other categories, because not enough samples were collected in these periods). The highest average *SSC* values have been observed predominantly in summer. The only exception is the "*AD<2*" category, where the average *SSC* in autumn exceeds the summer value which may refer to the faster fine material outwash after the higher floods in summer. In the Vadkan Valley, the average *SSC* peaks appear in summer without exception, but the lowest average *SSC* in one plot has been obtained in winter only at the entire low flow database. Higher *SSC* in summer can be explained by the more organic material (e.g. periphyton), while the SSC-decrease in winter can be caused by the interrupted vegetation growth and the reduced soil detachment due to frozen soil. Nevertheless, the hypotheses for the reason of seasonal *SSC*-fluctuation have not been confirmed in the frame of this research yet.

Figure 4.6 shows the boxplots of the low flow *SSC* at inter-annual scale representing the obvious *SSC*-variability in both catchments year by year. The basic statistical evaluation of the *SSC* and *SSC*-control factors can be found in the *Annex IV.II.4* as tables. Farkas Valley has higher average and maximal *SSC* values than the Vadkan Valley almost in each hydrological year. Hydrological year 2005-2006 shows outstanding values in both catchments. Forestry activities, especially the clear cutting and shelterwood cutting have been accomplished on a relative large area between 2005 and 2006 (10.0 *ha* in the Farkas Valley and 4.7 *ha* in the Vadkan Valley according to the *Annex III.I.2/a-b* which may induce the disturbances of the low flow sediment motion. Relative high average *SSC* values in 2009-2010 need explanation. This hydrological year produced the highest annual rainfall in the study period (1035.0 *mm* according to the *Annex IV.I.3*). Although rainfall events do not influence low flow sediment dynamics directly, intense rainfalls and high surface runoff can connect more particles from the external catchment regions into the channel. These sediment stocks are available for the lower *Q* ranges as well.

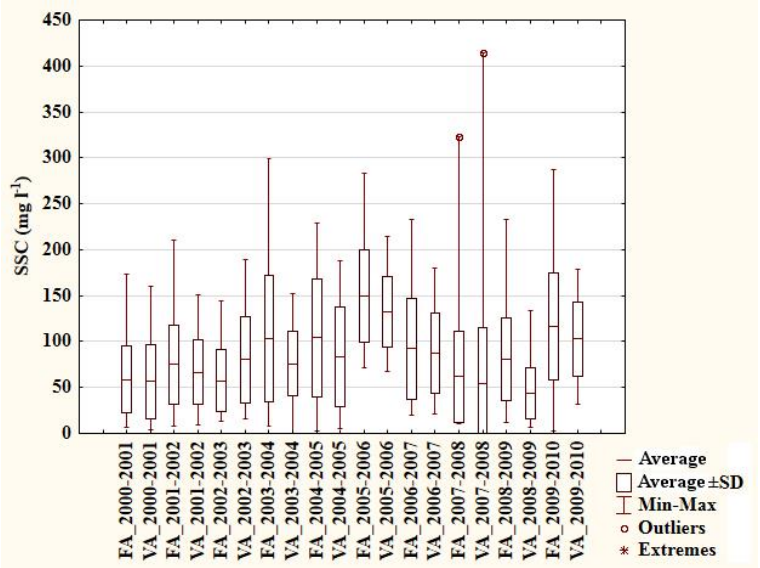

Figure 4.6. Boxplots of the suspended sediment concentration (SSC) at low flow for the hydrological years in the Farkas Valley (FA) and Vadkan Valley (VA)

To introduce the *SSC* database and its control factors under high flow conditions for the further analyses, the main descriptive statistical variables have been summarized in the *Table 4.4*. Since the high flow periods are underrepresented at larger time scales (e.g. seasonal, annual), basic statistical values have been evaluated only for the summer season, when enough data are available. Moreover, data derived from two flood events dominate over the summer database reducing the representativeness of the analysed variables.
As for the average, median and maximum of the high flow *SSC* data, higher values have been obtained in the Vadkan Valley. A possible explanation can be, that higher runoff from the larger catchment area of the Vadkan Valley can set more particles in motion than in the Farkas Valley.

Table 4.4. Descriptive statistical variables of suspended sediment concentration (SSC) and its control factors at high flow for the entire study period (List of symbols: Q – discharge; WT – water temperature; ST0, ST5, ST10 – soil temperature at the depths 0 cm, 5 cm, 10 cm; API1, API3, API7 – antecedent precipitation index for 1, 3 and 7 days; EI – erosivity index; SumQ – total volume of the flood event; Q_{max} – peak discharge)

	Farkas Valley				Vadkan Valley			
	Average	**Median**	**Min**	**Max**	**Average**	**Median**	**Min**	**Max**
SSC *($mg \cdot l^{-1}$)*	695.9	212.5	24.9	4005.3	797.9	226.2	7.5	7635.9
Q *($l \cdot s^{-1}$)*	11.7	4.6	0.5	144.3	11.4	7.7	1.0	69.2
WT *(^oC)*	8.3	8.4	0.1	15.9	8.1	8.1	0.1	15.6
ST0 *(^oC)*	13.0	15.2	1.8	17.0	12.9	15.2	1.8	17.0
ST5 *(^oC)*	13.2	15.9	2.3	16.8	13.2	15.9	2.3	16.8
ST10 *(^oC)*	13.4	15.9	2.7	16.8	13.4	15.9	2.7	16.8
API1$_{c1}$ *(mm)*	20.5	17.3	0.0	50.8	21.4	18.3	0.1	51.0
API3$_{c1}$ *(mm)*	22.5	20.2	0.3	94.6	22.7	20.2	0.2	94.8
API7$_{c1}$ *(mm)*	28.0	24.5	3.6	108.5	28.2	25.1	3.6	108.7
EI$_{c1}$ *($kJ \cdot m^{-2} \cdot mm \cdot h^{-1}$)*	4.2	1.1	0.0	37.1	4.3	1.2	0.0	40.0
API1$_{hhm}$ *(mm)*	17.3	12.5	0.0	53.5	18.0	12.5	1.0	54.0
API3$_{hhm}$ *(mm)*	27.6	20.3	0.0	132.0	28.1	20.5	3.0	132.5
API7$_{hhm}$ *(mm)*	33.0	25.3	4.0	171.0	33.2	26.0	4.0	171.0
EI$_{hhm}$ *($kJ \cdot m^{-2} \cdot mm \cdot h^{-1}$)*	5.2	2.2	0.0	22.4	5.2	2.3	0.0	22.4
SumQ *(l)*	836865	188726	805	14632032	-	-	-	-
Q_{max} *($l \cdot s^{-1}$)*	1609.3	633.1	57.7	16885.5	-	-	-	-

(Notes: Descriptive statistical values are based only on those values of SSC-control factors which were measured or registered in the time of SSC-sampling.)

In the followings, information for the hydrological year 2008-2009 is summarized. *SSC* shows a wide range, the minimum value (11.9 $mg \cdot l^{-1}$) has been measured on 20.07.2009, while the maximum *SSC* has been observed during the flood wave 18.07.2009. The minimum follows the maximum in two days, which can be explained by the outwashing effect of the flood event.

Although the *Q* of small streams, like the brook of the Farkas Valley, generally exceeds the average *Q* only during the flood events (high flow), *Q* values exceeding the average *Q* were obtained after the flood wave separation as well (primarily between the end of March 2009 and early May 2009). Average *Q* is 2.7 $l \cdot s^{-1}$ on the basis of the automatic time series (*Table 3.3*) and 3.2 $l \cdot s^{-1}$ based on manual data in the hydrological year 2008-2009. Average *SSC* for the different discharge-ranges is:

- under the average *Q*: 78.1 $mg \cdot l^{-1}$ (the average *Q* in this flow range is 6.1 $l \cdot s^{-1}$);
- and above the average *Q*: 75.2 $mg \cdot l^{-1}$ (the average *Q* in this flow range is 2.0 $l \cdot s^{-1}$).

4.3 Relation between suspended sediment and sediment control factors

4.3.1 Relation between suspended sediment and sediment control factors at low flow

Analysing the database for the entire study period

Table 4.5 shows the correlation coefficients between suspended sediment concentrations (*SSC*) measured under low flow conditions and the sediment control variables considering the whole period in the Farkas Valley and Vadkan Valley, where the correlations marked by ***bold italic*** letters are significant at $p<0.05$ and *N* shows the sample size.

Table 4.5. Correlation coefficients between the suspended sediment concentration (SSC) data under low flow conditions and the sediment control variables for the entire study period (List of symbols: Q – discharge; AD – antecedent days; WT – water temperature; ST0, ST5, ST10 – soil temperature at the depths 0 cm, 5 cm, 10 cm)

		Q	*AD*	*WT*	*ST0*	*ST5*	*ST10*
Farkas Valley	***SSC***	-0.03	***0.30***	***0.25***	***0.19***	***0.20***	***0.19***
	N	417	269	403	158	158	158
Vadkan Valley	***SSC***	***-0.12***	0.11	***0.30***	0.15	***0.16***	0.15
	N	396	271	406	160	160	160

Correlation between *SSC* and discharge (*Q*) is not significant in the Farkas Valley, but significant in the Vadkan Valley. However, the strength of relation is weak (*Figure 4.7*), referring to other variables influencing the suspended sediment dynamics. Moreover, weak negative correlation may represent the limited sediment sources in the stream channel due to the sediment outwashing effect of flood events before the sampled low flow period. Thus, less suspended sediment is available for relative higher *Q*.

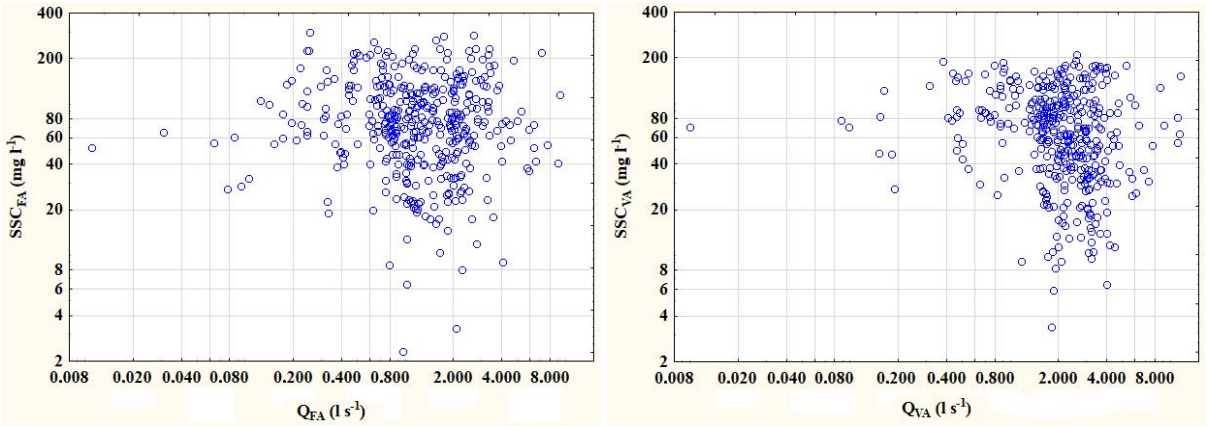

Figure 4.7. Log-log plot of suspended sediment concentration (SSC) against discharge (Q) at low flow for the entire study period in the Farkas Valley (FA) (left) and the Vadkan Valley (VA) (right)

Regarding the values in the *Table 4.5*, the strongest significant correlation has been obtained between *SSC* and antecedent days (*AD*) in the Farkas Valley. This correlation confirms that number of days elapsed since the previous flood event can be determinant for the in-channel

sediment supply, when no sediment sources contribute to the stream sediment yield (*SY*) from the farther catchment regions. After the recession of flood events *SSC* show increasing trend against the *AD* because more fine materials can accumulate depending on time in the channel in dry periods (*Figure 4.8*).

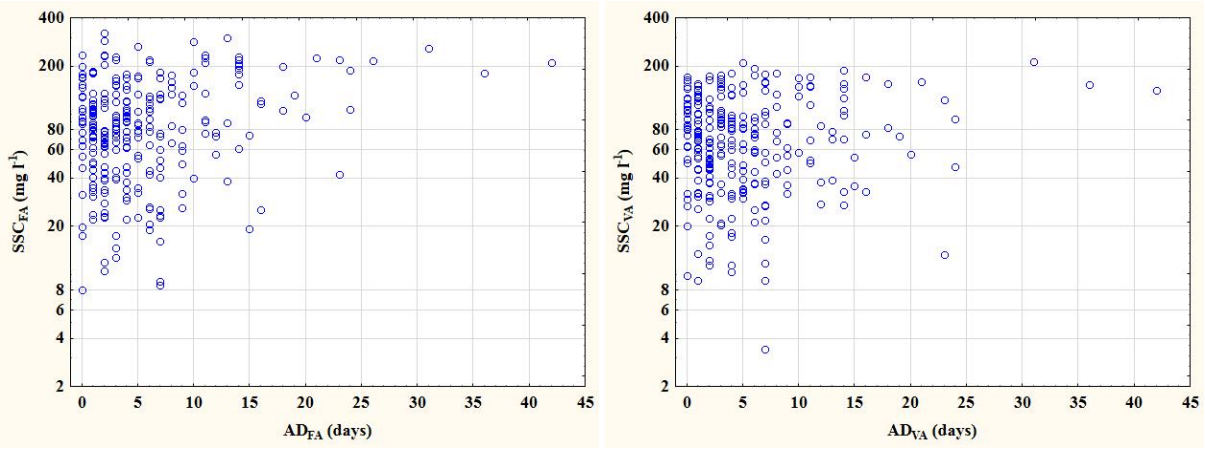

Figure 4.8. Semi-log plot of suspended sediment concentration (SSC) against antecedent days (AD) under low flow conditions for the entire study period in the Farkas Valley (FA) (left) and the Vadkan Valley (VA) (right)

Contradicting the *SSC-AD* relation in the Farkas Valley, *AD* is not a significant control factor in the adjacent Vadkan Valley. Furthermore, the higher negative correlation coefficient between *SSC* and *Q* suggests higher limitation of sediment availability than in the Farkas Valley. Considering the average *SSC* and *Q* values in both catchments, the difference of suspended sediment dynamics is also noticeable: relative lower *SSC* values belong to the relative higher *Q* values in the Vadkan Valley, resulting in the steeper decreasing trend of *SSC* and the stronger negative correlation. Two possible but contradictory explanations may exist:

1. The Vadkan Valley is a larger catchment with gentler slopes and wider stream channel, where more residual fine materials can be trapped on the catchment area or in the channel (e.g. behind log jams) after flood events, diminishing the sediment availability and the effect of *AD*.
2. The larger Vadkan Valley can generate higher *Q* which outwash more fine material and less residual sediment remain in the channel, reducing sediment availability and the possibility of in-channel supply.

To check these hypotheses, it is required to examine several separated flood events, where the hysteresis types refer to the dominant conditions of fine material availability.

Assuming that *AD* can also have effect to the *SSC-Q* relationship, $r_{SSC\text{-}Q}$, $r_{SSC\text{-}AD}$ and $r_{Q\text{-}AD}$ correlation coefficients were examined for the three different *AD*-categories. Obtained *r* values do not confirm that *AD* significantly influences the *SSC-Q* relationship. Weak but significant linear relationship was obtained only in the Farkas Valley if $8 \leq AD$ (*Annex IV.III.1*).

Statistically significant relationship was obtained with water temperature (*WT*) (*Figure 4.9*) in both catchments. Since the viscosity decreases exponentially with the water temperature, if the water temperature rises, the fluid resistance of fine material transport is reduced. Water and soil temperature are strong correlation in each other ($r_{WT\text{-}ST0}$ = 0.96, $r_{WT\text{-}ST5}$ = 0.95, $r_{WT\text{-}ST10}$ = 0.94 in the Farkas Valley, $r_{WT\text{-}ST0}$ = 0.96, $r_{WT\text{-}ST5}$ = 0.96, $r_{WT\text{-}ST10}$ = 0.95 in the Vadkan Valley), therefore the relationship between *ST* and *SSC* is similar to the *WT-SSC* relationship. Weaker correlations between *SSC* and soil temperature (*ST*) in the Vadkan Valley can be explained by the different geomorphology of the study catchments. Since the Farkas Valley is narrower and steeper, lower temperatures can be characteristic on the valley bottom, which may have an impact on the strength of *SSC-ST* correlation.

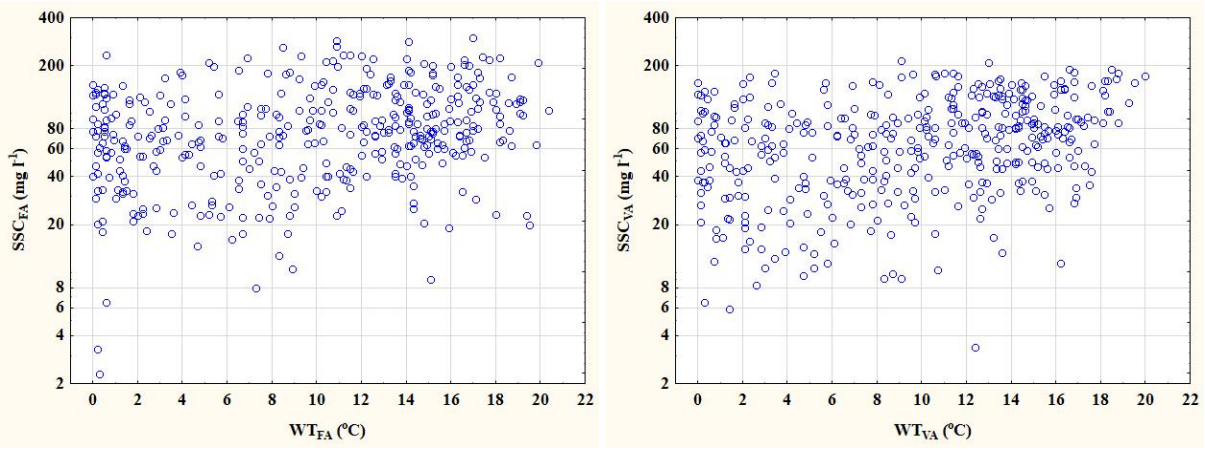

Figure 4.9. Semi-log plot of suspended sediment concentration (SSC) against water temperature (WT) under low flow conditions for the entire study period in the Farkas Valley (FA) (left) and the Vadkan Valley (VA) (right)

As the paper (*Csáfordi et al.* 2011) suggests, it can be reasonable to separate the database according to different *Q*-ranges (e.g. under and above the average *Q*) and to accomplish the correlation analyses also for these categories. However, the conclusions will be the same: no strong correlation is obtained between *SSC* and involved control factors under low flow conditions for the entire study period, referring to other variables and processes (such as sediment trapping, forestry activities, freeze-thaw effect, algae growth) influencing the suspended sediment dynamics. To reveal special *SSC* control forces the author continues the analyses at lower time scales.

Analysing the database at seasonal time scale

Different correlation characteristics have been obtained at seasonal scale, due to the supposedly different sediment transport dynamics and lower sample size. *Table 4.6* summarizes the significant correlation coefficients for the Farkas Valley and the Vadkan Valley. *Annex IV.III.2/a-d* presents the detailed correlation matrices.

AD has the strongest correlation coefficient with *SSC* in the Farkas Valley **in autumn**, similarly to the entire study period. *Q* is also significantly correlated with *SSC* showing

decreasing tendency as previously described at the data analysis of entire study period. Increasing *SSC* due to the assumed in-channel sediment supply and decreasing sediment availability seem to contradict each other, but the different speed of the antagonistic processes such as fine sediment replenishment and exhaustion may explain this problem.
AD is also the strongest control factor in the Vadkan Valley in autumn. Compared the relations of *SSC-AD* in different seasons in both catchments, the strongest impact of *AD* in autumn is clear. The *SSC-WT* relation is significant in the Vadkan Valley, but the very weak negative relation between *SSC* and *ST* suggest again differences between the two catchments (*Csáfordi et al.* 2013).

No significant correlation has been obtained **in winter** between *SSC* and its control variables in the study catchments.

Table 4.6. Significant correlations between suspended sediment concentration (SSC) at low flow and sediment control variables at seasonal scale (r correlation coefficients are significant at p<0.05 and N shows the sample size in parentheses) (List of symbols: Q – discharge; AD – antecedent days; WT – water temperature; ST0, ST5, ST10 – soil temperature at the depths 0cm, 5cm, 10cm)

	Farkas Valley		**Vadkan Valley**	
	Sediment control variable	***r* (*N*)**	**Sediment control variable**	***r* (*N*)**
Autumn	*Q*	-0.23 (111)		
	AD	0.48 (92)	*AD*	0.30 (93)
			WT	0.20 (109)
Spring	*WT*	0.27 (100)	*WT*	0.25 (100)
	ST0	0.33 (44)		
	ST5	0.44 (44)		
	ST10	0.45 (44)		
Summer	*AD*	0.35 (92)		
			WT	0.22 (98)

Suspended sediment transport has a special dynamics **in spring** in the Farkas Valley. *SSC* shows increasing trend as a function of *Q*. In contrast with other seasons, *AD* is not relevant control factor for *SSC*. As a hypothesis, the freeze-thaw effect may explain these changes of correlation characteristics. After the winter period abundant fine material is available for each low flow *Q*-range in the stream channel because of bank collapses due to the freeze-thaw processes, remarkably reducing the role of *AD*. Considering the significant relationship between *WT-SSC* and *ST-SSC*, previous theories seem to be confirmed: if the temperature rises, melting processes promote fine material availability in the channel. Regarding the other seasons, no significant relationship has been obtained between *WT-SSC* and *ST-SSC*.
The freeze-thaw effect is not as clearly identifiable on the basis of correlation coefficients in the Vadkan Valley, nevertheless the negative sign of *SSC-AD* relation may refer to the exhaustion of abundant fine material stocks, and the 0.23-0.25 values of *SSC-WT* and *SSC-ST* correlation coefficients may suggest the role of temperature in the sedimentary processes (*Csáfordi et al.* 2013).

Only the *AD* shows significant correlation with *SSC* in the Farkas Valley **in summer**, and *SSC* has increasing tendency as a function of *Q*, referring to the quasi-unlimited fine material availability in the stream channel. In summertime, the frequency of landslides may be higher when the heavy rainfalls saturate the upper sandy soil layers. Therefore, besides the in-channel supply processes the residual fine material due to high flood events, landslides and bank collapses can be the possible sources of suspended sediment yield (*SSY*).
The Vadkan Valley shows again limited sediment availability (negative sign of the *SSC-Q* relation), *AD* is not determinant, but *WT* is statistically significant for controlling the *SSC*.

Season by season varying *r* values represent the complexity of suspended sediment dynamics. Analyses at seasonal scale point at

- the strongest role of *AD* in autumn, referring to the impact of flood wave dynamics on *SSC*,
- the freeze-thaw effect in spring, when the *SSC-ST* relations are stronger than the *AD-SSC* relation,
- the spatial fluctuation of *SSC* which appears on the different correlation characteristics between the Farkas and Vadkan Valley and presumedly refers to the role of the geomorphological complexity of a catchment.

Analysing the database for the hydrological years

Analyses at annual scale can reveal alterations in the sediment dynamics which are hidden at other temporal resolution and mostly based on stochastic factors. Regarding the correlation coefficients of *Annex IV.III.3*, temporal and spatial fluctuation of fine material transport is noticeable as well.
No significant correlation has been obtained in the Farkas Valley from 2008 to 2010, when an exhausting sediment deposit was the main sediment control process not far from of the sampling point.

4.3.2 Relation between suspended sediment and sediment control factors at high flow

In comparison with low flow conditions, suspended sediment transport has different dynamics at high flow, when rainfall characters, alteration of rising and descending *Q* and availability of external sediment sources may play major role controlling the *SSC*.
Table 4.7 summarizes the significant correlations obtained between *SSC* at high flow and hydrological, hydrometeorological and climate variables in the Farkas Valley and Vadkan Valley at different temporal scales. Detailed tables representing also the non-significant relations can be found in the (*Annex IV.III.4/a-i*).

Table 4.7. Significant correlations between suspended sediment concentration (SSC) at high flow and sediment control variables at different temporal scale

	Farkas Valley		**Vadkan Valley**	
	Sediment control variable	***r* (*N*)**	**Sediment control variable**	***r* (*N*)**
2000-2010 entire period	*Q*	0.65 (86)	*Q*	0.62 (81)
	WT	0.46 (42)	*WT*	0.38 (42)
	ST0	0.30 (61)	*ST0*	0.26 (59)
	ST5	0.32 (61)		
	ST10	0.34 (61)		
	$API1_{c1}$, $API1_{hhm}$	0.46 (48), 0.35 (79)	$API1_{c1}$, $API1_{hhm}$	0.60 (46), 0.42(76)
	$API3_{c1}$, $API3_{hhm}$	0.35 (60), 0.30 (80)	$API3_{c1}$, $API3_{hhm}$	0.56 (59), 0.61 (78)
	$API7_{hhm}$	0.23 (80)	$API7_{c1}$, $API7_{hhm}$	0.40 (59), 0.56 (79)
	EI_{c1}, EI_{hhm}	0.39 (59), 0.33 (80)	EI_{c1}, EI_{hhm}	0.42 (58), 0.29 (79)
	Q_{max}	0.31 (79)		
2000-2010 summer	*Q*	0.62 (50)	*Q*	0.59 (48)
	WT	0.66 (10)		
	$API1_{hhm}$	0.30 (51)	$API1_{hhm}$	0.38 (51)
	$API3_{c1}$, $API3_{hhm}$	0.43 (32), 0.31 (51)	$API3_{c1}$, $API3_{hhm}$	0.56 (32), 0.66 (51)
	$API7_{hhm}$		$API7_{c1}$, $API7_{hhm}$	0.45 (32), 0.61 (51)
			EI_{c1}	0.38 (32)
2000-2010 rising limb	*Q*	0.68 (33)	*Q*	0.54 (32)
	WT	0.62 (18)	*WT*	0.49 (18)
	$API1_{c1}$, $API1_{hhm}$	0.61 (19), 0.59 (27)	$API1_{c1}$, $API1_{hhm}$	0.77 (15), 0.59 (28)
	$API3_{hhm}$	0.52 (27)	$API3_{c1}$, $API3_{hhm}$	0.75 (20), 0.81 (29)
	$API7_{hhm}$	0.44 (27)	$API7_{c1}$, $API7_{hhm}$	0.51 (20), 0.76 (29)
	EI_{hhm}	0.57 (27)	EI_{hhm}	0.46 (29)
	SumQ	0.53 (28)		
	Q_{max}	0.64 (28)		
2000-2010, falling limb	*Q*	0.68 (53)	*Q*	0.86 (49)
	ST10	0.31 (41)		
	$API1_{c1}$	0.48 (32)	$API1_{c1}$, $API1_{hhm}$	0.60 (38), 0.43 (48)
	$API3_{c1}$	0.35 (41)	$API3_{c1}$, $API3_{hhm}$	0.42 (39), 0.28 (29)
	EI_{c1}, EI_{hhm}	0.53 (40), 0.31 (53)	EI_{c1}, EI_{hhm}	0.59 (39), 0.48 (50)
2000-2010, summer rising limb	*Q*	0.67 (20)	*Q*	0.55 (19)
	$API1_{c1}$, $API1_{hhm}$	0.70 (9), 0.64 (20)	$API1_{hhm}$	0.64 (21)
	$API3_{hhm}$	0.55 (20)	$API3_{c1}$, $API3_{hhm}$	0.65 (10), 0.86 (21)
			$API7_{hhm}$	0.79 (21)
	EI_{hhm}	0.71 (20)	EI_{hhm}	0.49 (21)
	SumQ	0.56 (20)		
	Q_{max}	0.62 (20)		
2000-2010, summer falling limb	*Q*	0.63 (30)	*Q*	0.89 (20)
			$API1_{hhm}$	0.38 (30)
			$API3_{c1}$	0.56 (22)
			$API7_{c1}$	0.52 (22)
			EI_{c1}, EI_{hhm}	0.54 (22), 0.38 (30)

Flood wave 18.07.2009	*Q*	0.88 (23)	*Q*	0.77 (24)
	ST0	-0.63 (24)	*ST0*	-0.52 (24)
	ST5	-0.62 (24)	*ST5*	-0.52 (24)
	ST10	-0.58 (24)	*ST10*	-0.47 (24)
	$API1_{hhm}$	0.78 (24)	$API1_{hhm}$	0.74 (24)
	$API3_{hhm}$	0.78 (24)	$API3_{hhm}$	0.74 (24)
	EI_{hhm}	0.72 (24)	EI_{hhm}	0.70 (24)
	SumQ	0.63 (24)		
	Q_{max}	0.75 (24)		
Flood wave 18.07.2009 rising limb	*Q*	0.97 (10	*Q*	0.74 (11)
	ST0	-0.66 (10)		
	$API1_{hhm}$	0.71 (10)	$API1_{hhm}$	0.74 (11)
	$API3_{hhm}$	0.71 (10)	$API3_{hhm}$	0.74 (11)
	EI_{hhm}	0.70 (10)	EI_{hhm}	0.75 (11)
	SumQ	0.72 (10)		
	Q_{max}	0.98 (10)		
Flood wave 18.07.2009 falling limb	*Q*	0.93 (13)	*Q*	0.99 (13)
	ST0	-0.70 (14)	*ST0*	-0.71 (13)
			ST5	-0.69 (13)
			ST10	-0.65 (13)
	$API1_{hhm}$	0.89 (14)	$API1_{hhm}$	0.97 (13)
	$API3_{hhm}$	0.89 (14)	$API3_{hhm}$	0.97 (13)
	EI_{hhm}	0.84 (14)	EI_{hhm}	0.99 (13)
	SumQ	0.78 (14)		
	Q_{max}	0.86 (14)		
Flood wave 04.08.2009 falling limb	*Q*	0.99 (12)	*Q*	0.99 (12)
	$API1_{c1}$, $API1_{hhm}$	-0.98 (12), -0.93 (12)	$API1_{c1}$, $API1_{hhm}$	-0.99 (12), -0.80 (12)
	EI_{c1}, EI_{hhm}	-0.98 (12), -0.93 (12)	EI_{c1}, EI_{hhm}	-0.99 (12), -0.80 (12)
	SumQ	-0.93 (12)		

Notes: r correlation coefficients are significant at $p<0.05$ and N shows the sample size in parentheses. List of symbols: Q – discharge; WT – water temperature; ST0, ST5, ST10 – soil temperature at the depths 0 cm, 5 cm, 10 cm; API1, API3, API7 – antecedent precipitation index for 1, 3 and 7 days; EI – erosivity index; SumQ – total volume of the flood event; Q_{max} *– peak discharge;* $_{c1}$ *–rain gauge 0.1mm;* $_{hhm}$ *rain gauge 0.5mm*

Analysing the database for the entire study period

As the correlation matrix (*Annex IV.III.4/a*) shows, each factor involved in the analyses has significant correlation with the *SSC* in the Farkas Valley, except for the $API7_{c1}$ and *SumQ*. The strongest correlation is obtained between *SSC* and *Q*, as it was expected before. Higher *Q* can set higher sediment yield (*SY*) in motion if sediment is unlimitedly available. According to the *Figure 4.10*, *SSC* against *Q* do not show explicit trend, which can be explained with inter- and intra-event fluctuation of *SSC*. Significant correlation between *SSC* and *API* confirms the determinant role of soil saturation conditions before the flood events. Since top soil saturation can lead to landslides, bank collapses and rainfall runoff, *SSC* rises with increasing *API*. Moreover, the strength of relationship between *SSC* and *API* decreases with

the number of antecedent days which could be responsible the calculation method of *API* (calculation without weighting) for. In the elapsing time the catchment is drying out and more other factors start contributing to the sediment transport diminishing the correlation between *SSC* and *API*.

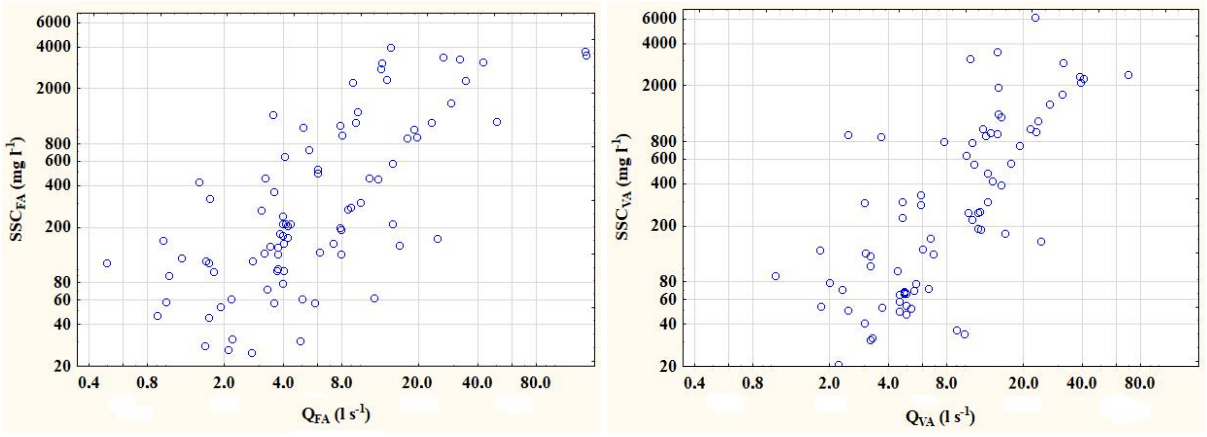

Figure 4.10. Log-log plot of suspended sediment concentration (SSC) against discharge (Q) at high flow for the entire study period in the Farkas Valley (FA) (left) and the Vadkan Valley (VA) (right)

In the Vadkan Valley, *Q* has also the highest influence on the *SSC*, but *API* plays a strong significant role too (especially $API1_{c1}$, $API3_{c1}$, $API3_{hhm}$ and $API7_{hhm}$), exceeding the importance of *API* in the adjacent study catchment. If the increase of *SSC* depends strongly on the previous rainfall conditions, which provide external sediment for the stream, it may reflect the limited fine material availability due to the fast sediment outwash or sediment trapping, confirming the hypothesis derived from the database analyses under low flow conditions.

SSC increases with *EI* in both catchments, because rising rainfall depth and kinetic energy generates higher rate of soil saturation, surface runoff and stream power. Nevertheless, varying inter- and intra-event suspended sediment dynamics makes the *SSC*-trend non-explicit and reduces the strength of *SSC–EI* relationship. *SumQ* is not determinant to control *SSC* at high flow. A plausible reason can be found on the basis of the separated evaluation of samples from rising and descending limb. Q_{max} represents the maximal power of flood wave till the sampling time, thus the increasing trend of *SSC* with Q_{max} is expectable. Notwithstanding, the analysed factors, such as *API*, *SumQ* and Q_{max} can lead to contradicting *SSC* dynamics, on the basis of effect-counter-effect:

1. If high previous runoff brings new sediment sources into the stream and/or sediment is easily available, *SSC* show increasing trend as a function of *API*, *SumQ* and Q_{max}.
2. If the previous runoff is relatively high due to the increased *API*, *SumQ* and Q_{max}, but sediment stocks are limited for the given *Q*-ranges, channel outwash reduces available fine material and *SSC* starts to decrease.

Therefore, the strength of correlation depends on the different dynamics and phase of flood events. To resolve this complexity of *SSC*-evaluation under high flow conditions, the author has also analysed *SSC* data separately for rising and falling limb of the hydrograph (inter- and intra-event fluctuation of *SSC*) (*Csáfordi et al.* 2013).

Analysing the database at seasonal scale – summer

Because of the limited *SSC*-sampling under high flow conditions, seasonal statistical evaluation has only been accomplished for summer eliminated the snowmelt-induced floods. *SSC* data derive dominantly from two floods in summer (24 pairs of data sampled on 18.07.2009 and 14 pairs of data sampled on 04.08.2009), resulting in the outstanding effect of inter- and intra-event fluctuation to the strength of correlations and trends (*Annex IV.III.4/b*). Significant correlation of *SSC* with *Q* and *API* are demonstrated in both catchments, and the *API* plays more important role in the Vadkan Valley again, similarly to the results based on the analyses of entire study period. The importance of *API3* is higher than *API7* for controlling *SSC*, which can be based not only on the data quality but also the saturation-drying out phase due to the number of elapsing days. Increasing trend of *SSC* is obvious in any cases, but the trend is non-explicit.

Figure 4.11 gives an example how the different flood events influence the relation between *SSC* and *API*. To conclude, it is not enough to separate and analyse the high flow *SSC* data at seasonal scale for the exact correlation results and suspended sediment model construction, but it also required to examine *SSC*-dynamics at event-scale.

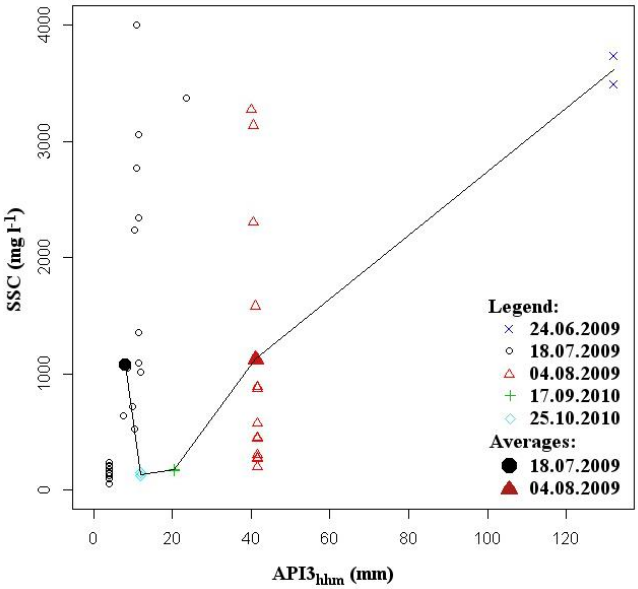

Figure 4.11. Scatterplot of suspended sediment concentration (SSC) against antecedent precipitation of 3-days ($API3_{hhm}$) at different flood events in the Farkas Valley (The line links the average SSCs per flood event demonstrating the SSC variability at intra-event scale.)

Analysing the database at the rising and descending limb in the entire study period

Compared the correlation coefficients at the rising (*Annex IV.III.4/c*) and descending limb (*Annex IV.III.4/d*) to each other, some essential difference are to be realized in both catchments. (The $r_{APIhhm\text{-}SSC}$ values have been disregarded in the Farkas Valley because of the significant deviation from the $r_{APIc1\text{-}SSC}$ values.) Depending on the number of elements *Q*, *API* and *EI* show statistically significant correlation with *SSC*, and the strength of correlation are

diminished by the inter-event *SSC* fluctuation as before, but *SumQ* and Q_{max} are important only at rising limb to influence *SSC* (*Annex IV.III.5/a-b*). At the rising stage, higher *SumQ* and Q_{max} set even more sediment in motion and bring new sediment stocks into the stream channel, resulting in the significant correlation and increasing trend of *SSC* as a function of *SumQ* and Q_{max}. Moreover, the strength of correlation is reduced by the inter-event *SSC* fluctuation. At the falling limb two main processes can impact on the *SSC* dynamics: exhaustion of fine material and sediment replenishment into the stream. No significant correlation was obtained at falling limb between *SSC-SumQ* and *SSC-*Q_{max} because of this antagonistic character of sediment dynamics. In point of fact, the decreasing trend of *SSC* with *SumQ* points at the sediment outwash.

Relation between *SSC* and control factors have also been examined at **seasonal scale** for rising and falling limb, but enough sample was collected only in **summer**. Correlation coefficients lead to the similar conclusions as given by the data of entire study period (*Annex IV.III.4/e-f*). *Q, API, EI, SumQ* and Q_{max} can also be important control factor for *SSC* at the rising stage, and the increasing rainfall and runoff variables lead to the increase of *SSC* due to the higher stream power and external sediment sources provided by surface runoff, landslides and bank collapse at saturated topsoil. Some correlation coefficients reflect the exhausting trend of fine material at the descending limb (e.g. $API1_{c1}$, *SumQ* and Q_{max} in the Farkas Valley). However, the results are inconsistent, suggesting data uncertainties. The inconsistency of correlation coefficients at *API* points out that the applied *API*-calculation method is not always capable for describing the sedimentary processes at the descending limb of flood events.

Analysing the database at event scale

Relation between *SSC* and control factors at two flood events 18.07.2009 and 04.08.2009 has been investigated at event-scale. Correlation analyses have been accomplished for the entire event and also separated for the rising and descending limb on 18.07.2009. Only 2 samples were collected from the rising limb of flood wave 04.08.2009, thus analyses are limited to the descending limb in this case.

Annex IV.III.4/g represents the strength of correlation between *SSC* and control factors for the entire database derived from the flood event 18.07.2009 in both catchments. In comparison with the correlation coefficients at larger temporal scale, stronger relations have been obtained at event-scale. It confirms that every flood event has a special sediment dynamics and standardized regression equations for the *SSC*-modelling are not able to give reasonable results. *SSC* shows increasing trend with *Q, API,* EI, *SumQ* and Q_{max} referring to the fact, that higher runoff, antecedent rainfall depth and rainfall erosivity and can set more fine material in motion and connect new sediment sources to the stream channel. Negative significant correlations between *SSC* and *ST* demonstrate that soil temperature and *SY* have a declining trend from the starting point of flood wave: temperatures generally decrease during a rainfall event and *SY* will also be lower due to the outwash processes to the end of flooding. Moreover, increasing or decreasing trends are not explicit at all. Local *SSC*-maximums, which

may follow the fluctuation of rainfall intensity or fine material availability, break them in each case, as represented by the *Figure 4.12*. (Data from the Vadkan Valley show similar relations.)

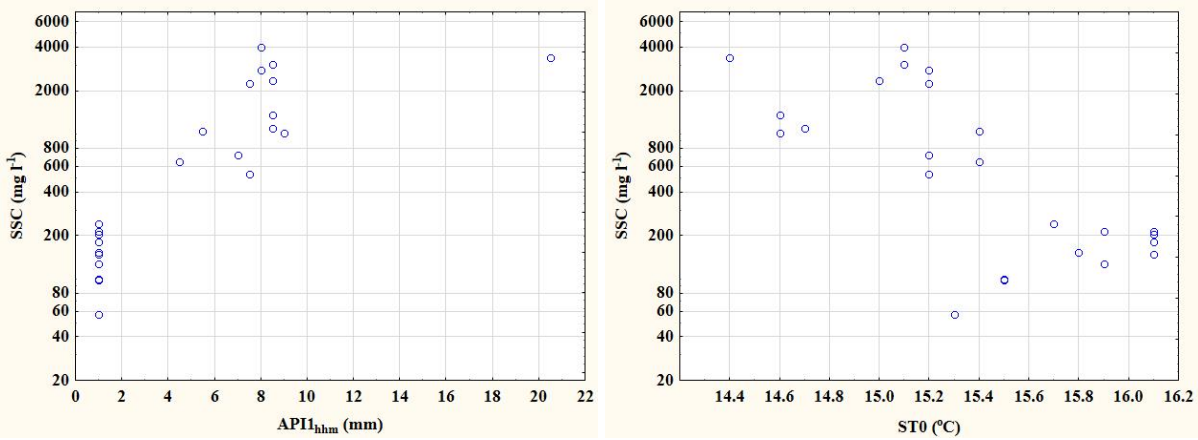

Figure 4.12. Semi-log plot of suspended sediment concentration (SSC) against antecedent precipitation of 1-day ($API1_{hhm}$) (left) and semi-log plot of SSC against soil temperature at 0cm depth (ST0) (right) at the flood event 18.07.2009 in the Farkas Valley

Regarding the relations between *SSC* and control factors separately for the rising and descending limb (*Annex IV.III.4/h*), the change of correlation coefficients are noticeable. In some cases, such as between *SSC* and *Q*, *SumQ* and Q_{max} at the rising limb, reduced data number and thus lower scatter can be responsible for stronger relations (change of standard deviation (SD) from the database of entire flood event to the database of separated rising limb: *Q*: 5.59 vs. 3.89; *SumQ*: 32675.27 vs. 17236.44; Q_{max}: 456.97 vs. 233.35). Moreover, lowering of the SD is not verified at the database of descending limb, therefore merely the separation of different dynamics of rising and falling limb can also strengthen the correlation.

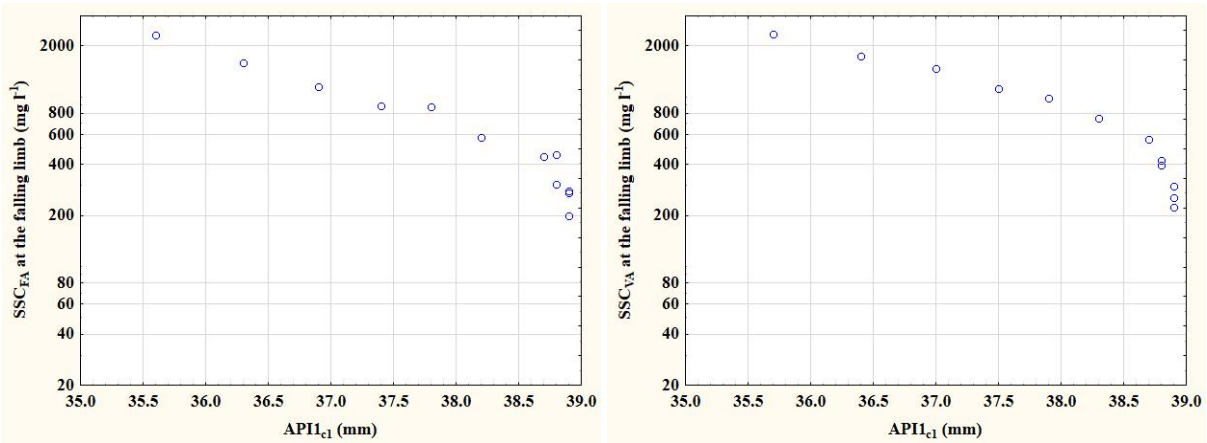

Figure 4.13. Semi-log plot of suspended sediment concentration (SSC) against antecedent precipitation of 1-day ($API1_{c1}$) at the descending limb of flood event 04.08.2009 in the Farkas Valley (FA) (left) and the Vadkan Valley (VA) (right)

Strong relations have also been obtained at the flood event 04.08.2009 in both catchments, where the descending limb of hydrograph is single and quasi-linear and non-intermitted by

local *SSC*-maximums (*Figure 4.13*). The negative correlation between *SSC* and *API*, *EI* and *SumQ* (*Annex IV.III.4/i*) suggest a clear sediment outwash at the falling limb, when no more external fine material have already reached the stream channel despite of the increasing soil saturation and cumulative runoff.

In some cases, correlation between *SSC* and *Q* (and the other sediment control variables) is not even reasonable strong after the separated data analyses at event-scale, for rising and falling limb. The subsection below describes what kind of effect reduces the strength of *SSC-Q* correlation.

Intra-event variability of suspended sediment concentration-discharge relation: the hysteresis effect. Suspended sediment transport has a fluctuation not only flood event by flood event, but also may show a special dynamics during one event, resulting in the hysteresis loops of suspended sediment concentration-discharge (*SSC-Q)* graphs. According to the samplings in the summer 2009, three types of hysteresis have been obtained in the Farkas and Vadkan Valley: clockwise, counter-clockwise and eight-shaped (*Csáfordi et al.* 2010a).

The *SSC-Q* relation shows **clockwise loop** at the flood event sampled on 18th July 2009 in the Vadkan Valley, because the *SSC* peak arrives at the stream cross section before the maximal *Q* (*Figure 4.14*). As the temporal graphs of *SSC* and *Q* prove, the ratio SSC_i/Q_i at any chosen time on the rising limb of the water-discharge graph is greater than that for the same *Q* on the falling limb. This kind of *SSC-Q* relationship may appear when the rainfall event does not produce enough surface runoff, which enables the arrival of more distant particles. This hysteresis type may refer to the removal of sediment deposited in the channel. The availability of sediment supply is restricted during the event for the concerned range of *Q*. Antecedent rainfall-runoff conditions may also explain the limited sediment availability, because a smaller flood event triggered by 3.5 *mm* rainfall depth, 2.5 days before the studied event could outwash the sediment stocks from the channel without any sediment replenishment, and neither the shorter dry period provides the in-channel sediment supply as well.

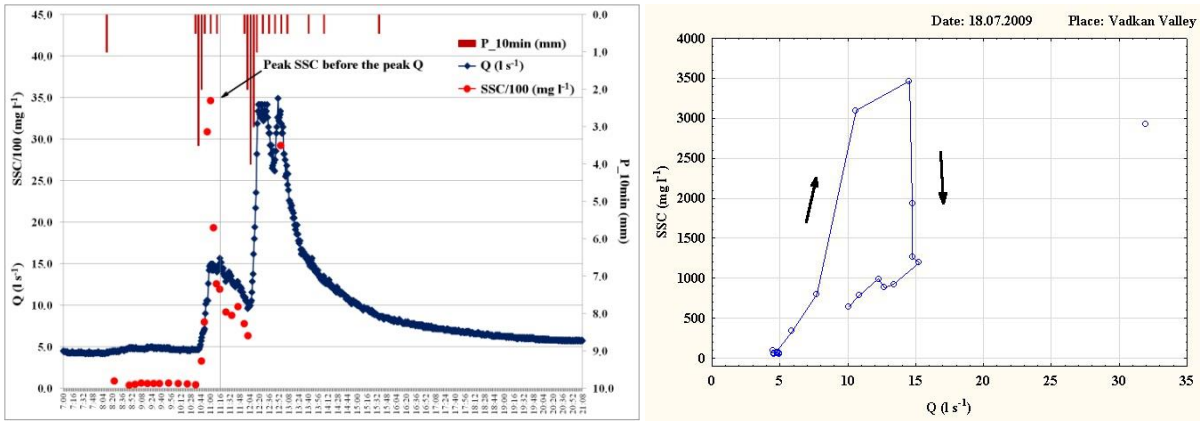

Figure 4.14. The hydrograph, the sedigraph and the rainfall data (P) (left) and the suspended sediment concentration-discharge (SSC-Q) relationship (right) during the flood event in the Vadkan Valley on 18th July 2009

The points of *SSC*-*Q* plot of the flood sampled on 18th July 2009 in the Farkas Valley describe an **eight-shaped hysteresis loop** (*Figure 4.15*). This class of *SSC*-*Q* relationship can be interpreted as the variable rainfall intensity, which produces two peaks during the sampling period. A smaller flood wave is registered before the studied one, which may reduce the available sediment supply. The amount of surface runoff is not satisfactory to resupply the stream by mobilization of particles from more distant regions. In addition the preceding dry period is too short to bring sediment by bank collapse induced by trampling and rooting of forest animals. As a result of supply removal processes and limited sediment availability the *SSC* decreases at the beginning of the flood event, to the sample *no.17*. The trend of hysteresis loop turns at the samples *no.18* and *19*, that phenomenon may indicate the mobilization of a smaller sediment deposit or arrival of particles coming from more distant areas. The sediment supply for the concerned *Q*-range decreases again after the sample *no.20*.

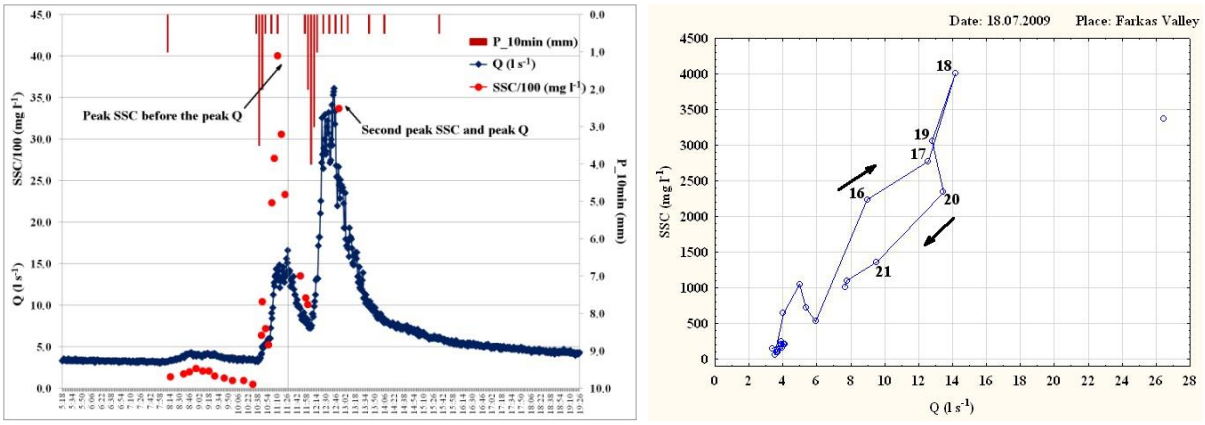

Figure 4.15. The hydrograph, the sedigraph and the rainfall data (left) and the SSC-Q relationship (right) during the flood event in the Farkas Valley on 18th July 2009

The distinguishing criterion for the **anti-clockwise hysteresis** is that SSC_i/Q_i ratios on the rising limb of the *Q*-graph has to be consistently less those on the falling limb for each and any value of *Q*. Although the collected *SSC* data are not enough to unambiguously fulfil this criterion, the *Figure 4.16* gives an example of the anti-clockwise loop. In this case, the peak *Q* arrives at the sampling station of Vadkan Valley before the *SSC* peak at the flood wave on the 4th August 2009. Several flood waves induced by intensive storms can be seen before the studied event. The antecedent precipitations saturate the soil, and the reduced infiltration capacity may promote enough amount of surface runoff, that can transport sediment into the channel from farther catchment regions. Sediment contribution of these zones is ensured only by long-lasting and more intensive rainfall events, because of the gentler hillslope conditions and sediment traps of Vadkan Valley. Processes, having slower dynamics than the *Q* rise, can provide significant sediment supply into the stream, also explaining this hysteresis type. These phenomena are e.g. the bank collapse after sufficient saturation of the bank material, and smaller landslide-activities, which have high risk in the Vadkan Valley because of the sandy-loamy soil layers.

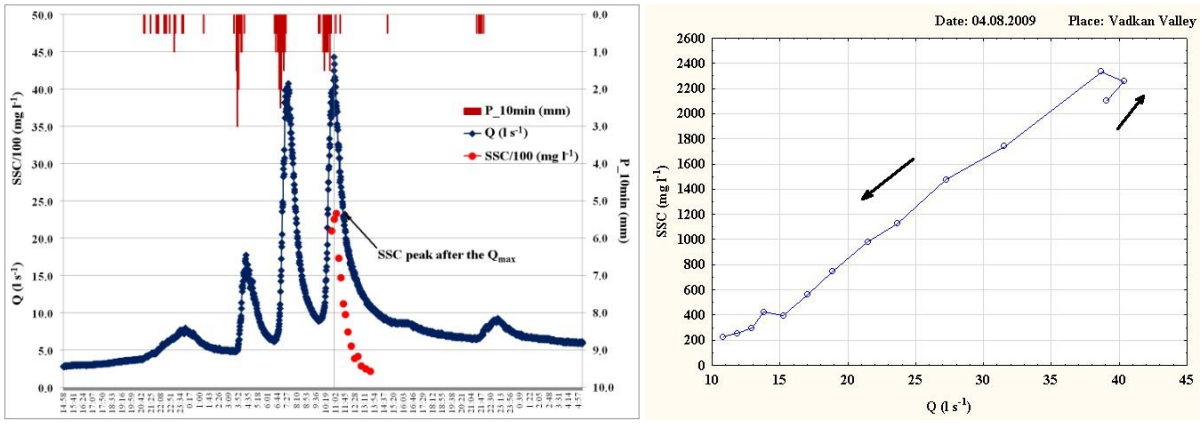

Figure 4.16. The hydrograph, the sedigraph and the rainfall data (left) and the SSC-Q relationship (right) during the flood event in the Vadkan Valley on 4th August 2009

The *SSC-Q* relation represents **clockwise loop** in the Farkas Valley at the flood wave registered on 4th August 2009 *(Figure 4.17)*. This class describes again the removal of sediment deposited in the channel, with a decreasing availability for the concerned range of *Q* during the flood event quite like at the event measured on 18th July 2009 in the Vadkan Valley. According to the hypothesis, the sediment supply, that is transported by surface runoff triggered by an intensive storm superposed on high antecedent rainfall depth, reaches the local base level faster from the steeper slopes of Farkas Valley, and leaves the gauging cross section earlier than in the Vadkan Valley. Thus, the quicker catchment response may explain the decreasing sediment availability and the clockwise hysteresis.

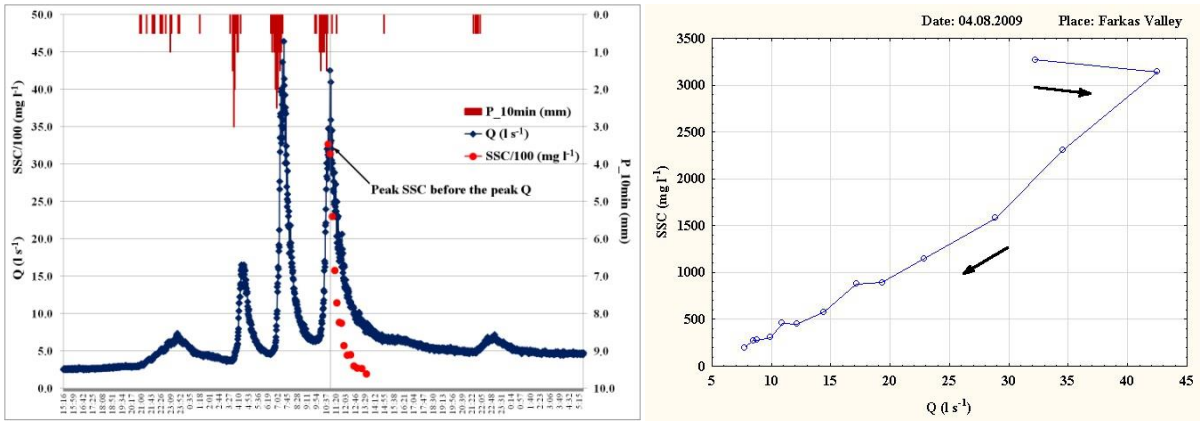

Figure 4.17. The hydrograph, the sedigraph and the rainfall data (left) and the SSC-Q relationship (right) during the flood event in the Farkas Valley on 4th August 2009

The event-scale examination of the *SSC*-dynamics confirms the assumptions, that correlation between *SSC* and control factors under high flow conditions are stronger if we eliminate the inter- and intra-event variability of *SSC* separating the database according to flood events, rising and falling limb. These establishments support the results of the following section.

4.4 Sediment yield calculations

4.4.1 Regression equations for calculating suspended sediment yield

Results of the correlation analysis at different temporal scales motivate us to develop regression equations for each season at low flow. Under high flow conditions, regression models have been separately created for the rising and falling limb, but not enough available suspended sediment concentration (*SSC*) data are available to fulfil the seasonal assessment.

To recognize the complex system of the relationships between the sediment control factors to be involved in the regression models, the author applied the factor analysis before the stepwise multiple regression analysis. According to the factor analysis the *SSC* control variables can be grouped into several factors (main groups of variables) wherein the variables have strong correlation with each other. Three factors have been identified under low flow conditions which explain more than 98.2% of the cumulative total variance in both catchments: temperatures, runoff and antecedent days. At high flow, variables can be grouped as antecedent saturation, temperature and variables influenced by direct rainfall. Three main factors explain more than 93.6% of the total variance in both catchments.
However, the results of factor analysis could not be applied to the regression models, thus the *Annex IV.IV.1/a-b* contains the supplementary informations.

Regression models for predicting *SSC* under low flow conditions (*Annex IV.IV.2/a-b*). Developed regression equations are not suitable for the *SSC* calculation, because

- the determination coefficient (r^2) and Nash-Sutcliffe coefficient (*NSCE*) remains under 0.40,
- or the involved variables are not independent on each other,
- or the dataset is limited to represent plausibly the entire study period.

Instead of these equations, suspended sediment yield (*SSY*) is calculated on the basis of *Eq. 3.6* using the seasonal averages of observed *SSC* (*Annex IV.II.3*) (and average *Q* on the basis of *Table 3.3*, where no continuous time series is available).

<u>Regression models for predicting *SSC* under high flow conditions</u>

Rising limb:

- Farkas Valley: $SSC = b_0 + b_1 \cdot Q^{b_2} + b_3 \cdot API3_{hhm}^{b_4} + b_5 \cdot EI_{hhm}^{b_6}$ (*Eq. 4.1*)
- Vadkan Valley: $SSC = b_0 + b_1 \cdot Q^{b_2} + b_3 \cdot API1_{hhm}^{b_4} + b_5 \cdot API3_{hhm}^{b_6}$ (*Eq. 4.2*)

Falling limb:

- Farkas Valley: $SSC = b_0 + b_1 \cdot Q^{b_2} + b_3 \cdot API1_{hhm}^{b_4} + b_5 \cdot EI_{hhm}^{b_6}$ (*Eq. 4.3*)
- Vadkan Valley: $SSC = b_0 + b_1 \cdot Q^{b_2} + b_3 \cdot API1_{hhm}^{b_4} + b_5 \cdot EI_{hhm}^{b_6}$ (*Eq. 4.4*)

In the equations *Q* is the discharge, $API1_{hhm}$ and $API3_{hhm}$ are the antecedent precipitation index of 1 and 3-days, EI_{hhm} is the rainfall erosivity index, b_0-b_6 are the empirical model parameters (*Csáfordi et al.* 2013).

For the more accurate *SSC* calculation at event scale, specific equations have been created for the flood wave on 18.07.2009 and 04.08.2009. Whereas *SSC* data are limited for the rising limb of the flood wave 04.08.2009, the regression model is not separated for rising and falling limb in this case.

Flood event 18.07.2009, Farkas Valley (where Q_{max} is the peak discharge):

- Rising limb: $SSC = b_0 + b_1 \cdot API1_{hhm}^{b_2} + b_3 \cdot API3_{hhm}^{b_4} + b_5 \cdot Q_{max}^{b_6}$ (*Eq. 4.5*)
- Falling limb: $SSC = b_0 + b_1 \cdot Q^{b_2} + b_3 \cdot API1_{hhm}^{b_4} + b_5 \cdot Q_{max}^{b_6}$ (*Eq. 4.6*)

Flood event 18.07.2009, Vadkan Valley:

- Rising limb: $SSC = b_0 + b_1 \cdot Q^{b_2} + b_3 \cdot API1_{hhm}^{b_4} + b_5 \cdot EI_{hhm}^{b_6}$ (*Eq. 4.7*)
- Falling limb: $SSC = b_0 + b_1 \cdot Q^{b_2} + b_3 \cdot API1_{hhm}^{b_4} + b_5 \cdot EI_{hhm}^{b_6}$ (*Eq. 4.8*)

Flood event 04.08.2009:

- Farkas Valley: $SSC = b_0 + b_1 \cdot Q^{b_2} + b_3 \cdot API1_{hhm}^{b_4} + b_5 \cdot EI_{hhm}^{b_6}$ (*Eq. 4.9*)
- Vadkan Valley: $SSC = b_0 + b_1 \cdot Q^{b_2} + b_3 \cdot API1_{hhm}^{b_4} + b_5 \cdot EI_{hhm}^{b_6}$ (*Eq. 4.10*)

Annex IV.IV.3 summarizes the values of r^2, *NSCE*, sample size (*N*), standard deviation (*SD*) of residuals and the empirical coefficients for each regression equation. Although the regression models for high flow conditions show also some limitations, such as the involved variables may be dependent on each other, or the dataset consist of limited number of data, these models are acceptable to compute *SSC* in the rising and falling limb of the flood events considering the relative high model efficiency values.

4.4.2 Calculation of sediment yield at annual and event-scale

To determine the quantitative impact of the outwashing sediment deposit on the sediment dynamics and the proportion of the extra sediment to the annual sediment yield (*SY*), total sediment yield (*TSY*) has been calculated for the hydrological year 2008-2009. Quantification of the *SY* at event-scale has also benefits for the detection of temporal (low flow-high flow, inter-event and intra-event) and spatial variability of the sediment dynamics.

Sediment yield calculation for the hydrological year 2008-2009 in the Farkas Valley

Bedload calculations. The amount of total bedload is 4.0 m^3 in the hydrological year 2008-2009, based on the volumetric bedload measurements in the stilling basin at the outlet of Farkas Valley. Monthly bedload yield (*BY*) and precipitation are represented by the *Annex IV.IV.4*. Since the mean bulk density of bedload is 1.6 $t \cdot m^{-3}$ in summer and 1.3 $t \cdot m^{-3}$ in winter, when mostly finer material accumulate in the stilling basin, the average bulk density is about 1.5 $t \cdot m^{-3}$ (*Gribovszki* 2000b). Using the average value of bulk density, the total *BY* is 5.9 *t* in the given time period.

BY contains some inaccuracies. In some cases, when the *BY* of a flood event is too high, sediment can partly overpass the stilling basin due to its finite storage capacity, resulting in the underestimation of bedload cubature. Large woody debris may have an overestimating

impact on bedload quantification. According to previous assumptions, suspended sediment can also accumulate in the stilling basin under low flow conditions. Furthermore, coarser particles (in general the bedload) can behave as suspended material, and they can be easily washed out from the stilling basin. Control samples have been collected since April 2009 at the stilling basins, to detect the deviation between the *SSC* of inflow and outflow. The average deviation is -0.6 *t*, that means one part of the bedload is lifted up due to the turbulent flow conditions in the stilling basin and leave the sediment trap. Therefore 0.6 *t* has to be added to the observed *BY* to correct the *BY* in the study period. After the modification *BY* amounts 6.5 *t* in the hydrological year 2008-2009.

Calculation of the suspended sediment yield. *Table 4.8* shows the *SSY* in monthly resolution and in winter when no continuous water stage data were available.

Table 4.8. Suspended sediment yield (SSY) in the hydrological year 2008-2009 (Csáfordi et al. 2013)

Time period	***SSY** (t)*
/October 2008 (from 22.10.2008)	0.2/
November 2008. (to 24.11.2008)	0.6
24.11.2008 – 02.03.2009	1.0
March 2009 (from 02.03.2009)	42.0
April 2009	1.5
May 2009	0.9
June 2009	66.0
July 2009	2.6
August 2009	2.2
September 2009	0.8
October 2009 (to 16.10.2009)	0.2
October 2009 (from 16.10.2009)	0.3
$\sum$*SSY* (in the hydrological year 2008-2009)	**118.2**
/$\sum$*SSY* (in the outwashing period of the sediment deposit)	**118.1/**

The data demonstrate well that the intensive sediment motion is connected to the snowmelt floods in the early spring and the heavy stormflows in the early summer. Aggregating the values in the relating time periods, 118.2 *t SSY* was obtained in the hydrological years 2008-2009 and 118.1 *t SSY* in the outwashing period of the sediment deposit.

Eq. 4.1 and *Eq. 4.3* underestimate the *SSC* in numerous cases (minus or unreal low values), therefore the regression models have been modified at some single flood events. These corrections are:

- neglecting some of the model variables, such as *EI* and/or $API3_{hhm}$ in the rising limb, *EI* and/or $API1_{hhm}$ in the falling limb,
- replacing the first *EI* values with higher *EI* values at the beginning of the rainfall events. (As the "$_{hhm}$" rain gauge records only the tipping time, thus not giving information of the starting time of the rainfall event, no *EI* can be calculated to the first rainfall depth record.)
- replacing the negative model values with acceptable local minimum of *SSC* values,
- completing data gaps in the "$_{hhm}$" dataset with the "$_{c1}$" dataset, assuming the same correlation between API_{c1} and *SSC*.

Whereas *Eq. 4.5-4.6* and *Eq. 4.9* calculate *SSC* only for the sampled section of the flood events reliably, *SSC* have been predicted for the other sections using the general rising and falling limb models (*Eq. 4.1* and *4.3*). Overestimation has locally been obtained at the application of *Eq. 4.9*, thus some modification have to be introduced as listed above.
As the regression models have serious limitations, future developments are required to predict *SSC* plausibly. First of all more water samples have to be collected during the flood events, which can be realized with automatic instruments. However, the author did not have possibility to use automatic samplers and turbidimeters in this phase of the sediment research.

The sum of bedload yield (6.5 *t*) and suspended sediment yield (118.2 *t*) is equal to the total sediment yield, thus the stream of the Farkas Valley transported 124.7 *t* sediment at the sampling cross section in the hydrological year 2008-2009.

Sensitivity analysis. For changes of one variable at a time, *Annex IV.IV.5* demonstrates results of the sensitivity analysis for *SSY* under high flow conditions in the hydrological year 2008-2009. The directions of change in outputs are as expected at the *Q*, *EI* and Q_{max} variables: rising parameter values induce rising *SSY*. Nevertheless, the relation system of the *SSY* and influencing factors is more difficult if the sediment availability is limited. Higher rainfall and runoff can accelerate the sediment outwash resulting in the fast decrease of *SSY*, or connect new sediment sources into the stream increasing the *SSY* in the descending limb of the hydrograph. Negative relation at the *API1* and *API3* may refer to the sediment outwash, when increasing rainfall is not able to contribute to the sediment availability and cannot increase the *SSY*. On the other hand, contrasting direction of the change of *API* and other variables, which are not independent on each other, may point at the incorrect coding of the model. Thus, *API* should be neglected or recalculated in the future using another method.

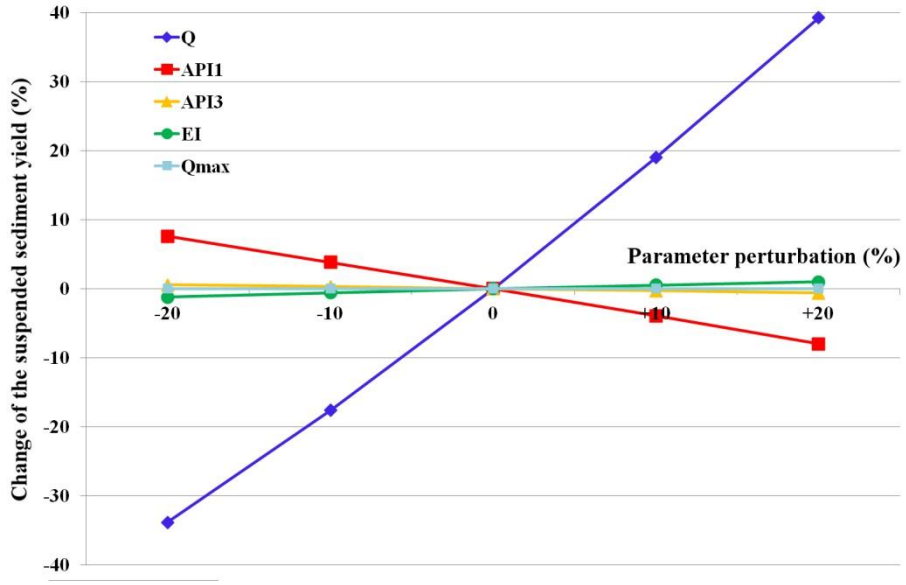

Figure 4.18. High flow suspended sediment yield response to the hydrological parameter perturbations in the year 2008-2009 in the Farkas Valley (List of symbols: Q – discharge; API1, API3 – antecedent precipitation of 1 and 3-days; EI – erosivity index; Q_{max} – peak discharge)

SSY shows the greatest sensitivity to perturbations in *Q*, because this variable appears twice in the *SY* calculation: first in the *SSC* estimation (not in all of the applied regression models but the most of them), secondly in the multiplication of *SSC* and *Q*. Q_{max} has a less important role to affect the *SSY*, since this parameter has only been applied at the *SSC* computation of a section of a flood event (*Eq. 4.5* and *4.6*). *Figure 4.18* represents the output response to the hydrological parameter perturbations.

Sediment yield patterns during two flood events

SY calculation at event-scale is based on two flood waves sampled in the Farkas Valley and Vadkan Valley on 18.07.2009 and 04.08.2009. Variables of the flood inducing rainfall events are demonstrated in the *Table 4.1*. *SSY* based on the regression equations and *BY* calculated with the *Eq. 3.7* are represented in the *Table 4.9*. To detect quantitative differences between the sediment transport at high flow and low flow conditions, *SY* of the two flood events have been compared with the *SY* of the average baseflow periods with the same duration as the flood events. *SSY* and *BY* for baseflow have been determined using average sediment and *Q* values observed in summer at low flow periods. (Since the automatic water stage records have not been processed, the normal *Q* value for the Vadkan Valley in summer has been calculated on the basis of the method of equivalent water-levels.)
Specific *SY* (**bold** values) in the *Table 4.9* enable the better comparison of the catchments. However, the effective catchment zones, which really contribute to the stream sediment transport as sediment sources, are unknown. This shortcoming reduces the accuracy of the specific values.

Table 4.9. Sediment yield during the two flood events in the Farkas Valley and the Vadkan Valley (for better comparison kg units are applied)

	18.07.2009		**04.08.2009**	
	Farkas V.	**Vadkan V.**	**Farkas V.**	**Vadkan V.**
Reference time (*min*)	429	449	280	273
SSY of the flood event (*kg*)	426	474	302	322
Specific SSY of the flood event ($kg \cdot ha^{-1}$)	**7.22**	**5.21**	**5.13**	**3.54**
SSY of the low flow period (*kg*)	8.3	11.5	5.4	7.0
Specific SSY of the low flow period ($kg \cdot ha^{-1}$)	**0.14**	**0.13**	**0.09**	**0.08**
SumQ / Total volume of the flood event (*l*)	305078	407794	858139	1128439
Peak discharge / Q_{max} ($l \cdot s^{-1}$)	36.1	34.9	42.5	44.3
BY of the flood event (*kg*)	60	44	21	51
Specific BY of the flood event ($kg \cdot ha^{-1}$)	**1.02**	**0.48**	**0.36**	**0.56**
BY of the low flow period (*kg*)	1.1	0.4	0.7	0.3
Specific BY of the low flow period ($kg \cdot ha^{-1}$)	**0.017**	**0.004**	**0.011**	**0.003**

Suspended sediment yield. Considering the *specific SSY* of the sampled flood waves, deviation between the two catchments is obvious: *specific SSY* is 1.4-times higher in the Farkas Valley than the Vadkan Valley in July and August as well. Some possible reasons of the spatial *SSY* variability based on two flood events can be as follows:

- As the Vadkan Valley is a larger catchment, *SDR* is lower due to the more sediment traps, thus less particles reach the stream channel.
- Since the Farkas Valley has steeper slopes, detached soil may connect faster into the stream due to the surface runoff.

Compared the high flow and low flow *specific SSY* values to each other, the following rates have been received. Flood waves transported 40-60-times higher *SSY* in each studied case, and the Farkas Valley shows higher sediment increase due to the floods. As for the low flow *SSY* in the both catchments, similar specific values have been computed. Whereas average low flow *SSC* are higher in the Farkas Valley, the higher average *Q* of the Vadkan Valley compensates this deviation, resulting in the almost equal specific *SSY*.

Bedload yield shows different dynamics during the two flood events than the suspended sediment. Since the flood wave in July yielded 2-times higher *specific BY* in the Farkas Valley than the Vadkan Valley, contrasting ratio has been obtained in August when the Vadkan Valley transported 1.5-times higher *BY*. Steeper slopes and channel inclination may responsible for the higher bedload values of the Farkas Valley in July, when effective rainfall was lower. The faster bedload outwash due to the high antecedent rainfalls may also account for the reverse relation between the *BY* of the two catchments in August. This explanation can contradict some results of the correlation analyses. To clarify the answers more flood events should be investigated in the future.
Specific BY of the flood wave exceeds 60-times the low flow value in July and 30-times higher *BY* in August in the Farkas Valley. Declining *BY* rate may reflect to the decreasing sediment availability at the second flood wave due to the increased outwash effect, when the antecedent rainfall and runoff was higher than in July. These ratios are 120 and 190 in the Vadkan Valley, which may confirm the previous explanations: sediment response is slower in the Vadkan Valley, thus higher antecedent rainfall reduces the *BY* in the Farkas Valley and increases in the Vadkan Valley. Considering the anti-clockwise loop in the case of *SSC*, this assumption can be confirmed at least at the flood wave on 04.08.2009.

Sensitivity analysis. *Figure 4.19* shows the *SSY* response in the Farkas Valley and the Vadkan Valley in the case of the two flood waves above, if one of the hydrological variables changes at a time.

Regarding the *Q* and Q_{max}, the direction of change in outputs coincides well with the results from the hydrological year 2008-2009. Furthermore, *SSY* shows the greatest sensitivity to perturbations in *Q* on 18.07.2009 in both catchments. *API1* has the most important role on 04.08.2009, and its impact on the sediment response is outstanding at the other flood events as well. Neither the direction of change in *API* or *EI* factors is permanent, higher values can also induce the *SSY* increase and decrease. Especially the flood wave 04.08.2009 in the Vadkan Valley shows contrasting *SSY* response, where anti-clockwise hysteresis has been obtained, indicating that new sediment stocks reached the stream from farther catchment regions or due to the landslides after the streambank saturation.

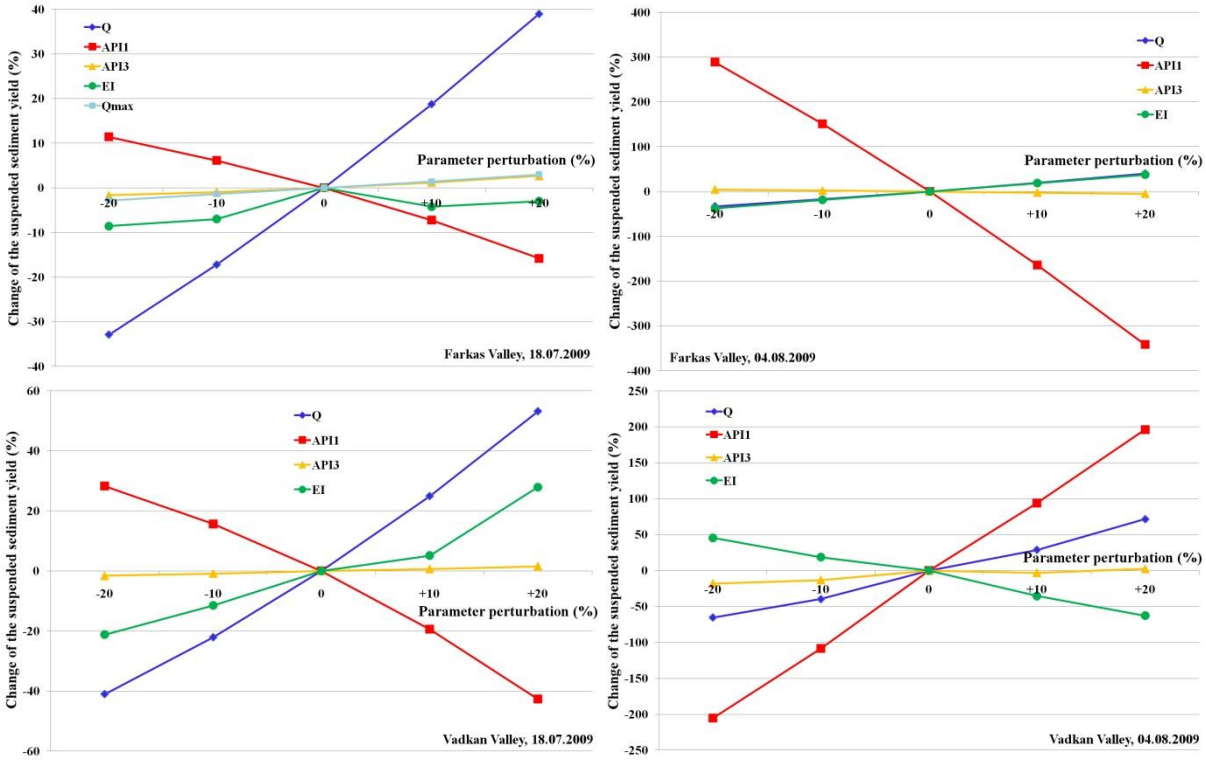

Figure 4.19. Suspended sediment yield (SSY) response to the hydrological parameter perturbations at the flood waves on 18.07.2009 and 04.08.2009 in the Farkas Valley (1-2) and the Vadkan Valley (3-4)

To better understand the inaccuracies in the description of sediment dynamics of small forest streams, it is necessary to examine the sediment deposits behind log jams upstreams to the sampling points in both catchments. The outwash of sediment deposits (e.g. after the decomposing of logs or due to human intervention) stochastically influences the sediment transport, reducing the plausibility of any model.

4.4.3 Quantification of the sediment contribution by an outwashing sediment deposit

One of the characteristic processes in the small forested catchments is the sediment accumulation behind log jams on the upstream side of different structures. The outwashing of sediment deposits may provide significant sediment surplus for the stream. Although the dissertation focuses primarily on the suspended sediment dynamics, the effect of sediment deposit is mostly analysed on the basis of bedload data, because they are almost continuously available (some data gaps only in wintertime); nevertheless, *SSC* time series are provided with regression modelling.

The 72 m^2 accumulation area on the upstream side of a culvert in the Farkas Valley has been surveyed on 22.10.2008 and on 16.10.2009, and two relief models have been produced on the basis of each survey. According to the geoinformatical calculation, 10.53 m^3 sediment has been outwashed (in bedload and suspended form together) from the channel during the study period. Applying the average bulk density by *Gribovszki* (2000b), the outwashed *TSY* amounts 15.8 *t*. Compared this value to the *TSY* of the Farkas Valley in the study period

(124.6 *t*), the studied sediment deposit has 13% proportion to the annual *TSY*, which is equal to 15% *SY* increase (*Csáfordi et al.* 2011).

The results of mass curve and double mass curve analysis graphically represent the surplus effect of the outwashing sediment deposit. *Figure 4.20* shows the cumulative bedload against the cumulative *Q*. A regression line has been fitted to the data points of bedload before and after the outwash period. Higher slope of the second trend line demonstrates well the increased *BY* during the outwash period. Other changes in the slope of cumulative bedload, which are presumably related to the seasonal fluctuation, have been neglected at this analysis. Fitting of the second trend line and the geomorphological changes observed in the field demonstrate that the outwash process was active to August 2009, according to the bedload dynamics. Since continuous *SSC* observations are not available from the sediment outwashing period, changes in suspended sediment dynamics are not recognizable due to the sediment deposit.

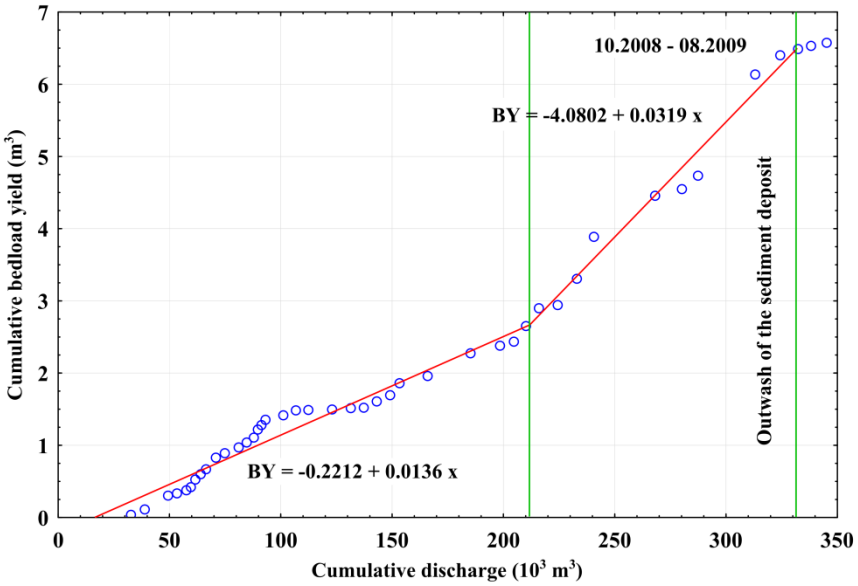

Figure 4.20. Double mass curve of bedload yield (BY) against the discharge from January 2006 to October 2009 in the Farkas Valley

Figure 4.21 represents the double mass curve of *BY* and *Q* against the precipitation depth (*P*). There are several breakpoints on the graph which separate the winter and summer seasons. Relative large increase of *Q* and *BY* is registered from autumn to spring, when the increase of *P* remains relative small. Larger increase of the *P* and smaller increase of the *Q* and the *BY* are observed from spring to autumn, therefore the slope of mass curves decreases.
Trends of the *BY* corresponds with the *Q* referring to the correlation between *BY* and *Q*. Moreover, precipitation recording has serious inaccuracies in winter increasing the slope of *Q* and *BY* mass curve. Slope of both mass curves rises from October 2008 again, and this trend remains also in the summer season, contradicting the usual trends. Moreover, *BY* increase per unit time is larger than in the previous periods. Total *BY* amounts 2.4 m^3 from March 2006 to October 2008, while 4.1 m^3 between October 2008 and August 2009, confirming the sediment surplus effect of the outwashing deposit from October 2008.

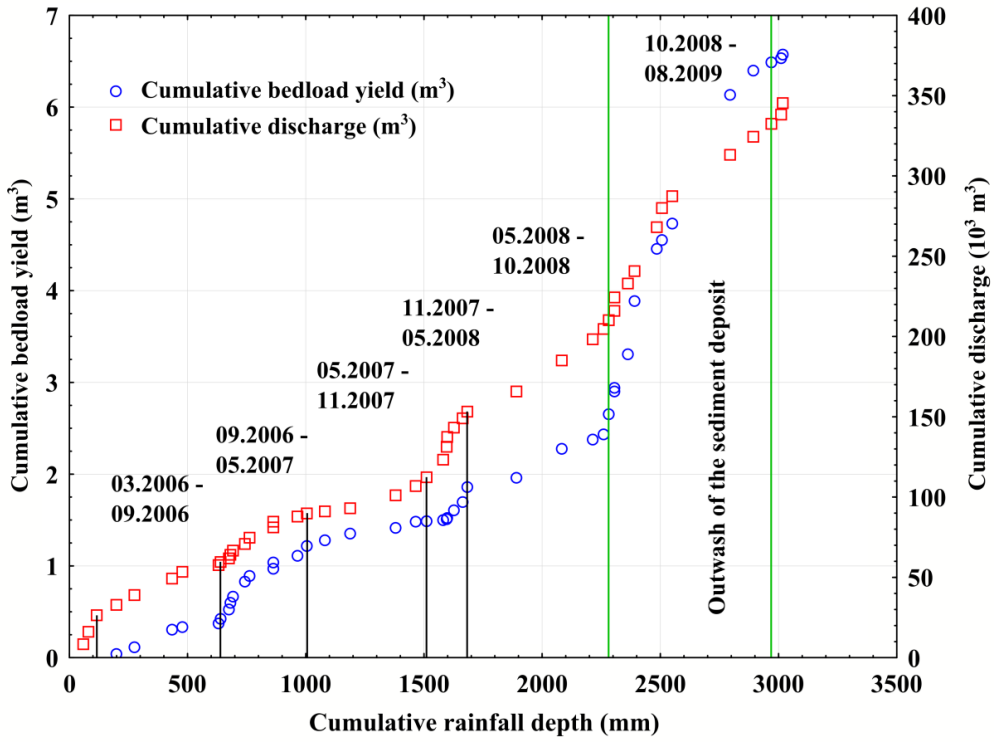

Figure 4.21. Double mass curve of bedload yield and discharge against the rainfall depth between January 2006 and October 2009 in the Farkas Valley

Annex IV.IV.6 represents the mass curve of *Q* and *BY*. As it is expected, the cumulative *Q*-graph does not show the influence of the sediment deposit. However, the suddenly rising slope of the cumulative *BY*-graph indicates the impact of the outwashing sediment deposit. Average monthly *BY* was 0.081 m^3 (0.12 *t*) before the outwash period, and it has risen to 0.368 m^3 (0.55 *t*; 4.5-times higher) during the outwash process. Exhausting of the sediment deposit can also be divided for more phases. The most active periods were between January and March 2009 related to the floods triggered by snow melts, respectively in June 2009 related to heavy rainfall events. Since the material has been mostly removed from the channel and slope of the mass curve of the bedload shows expressive decrease after August 2009, this date can be reckoned as the termination of sediment outwashing.

Although the applied database, surveying and calculation methods have some inaccuracies, the qualitative analysis of the impact of an exhausting sediment deposit on the *SY* is an advance in the sediment research, especially in the small headwater forested catchments. Results have benefits not only for the basic science but also for the forest practice. Knowledge of the dynamics of sediment accumulation and sediment outwashing from a log jam, which are very frequent problem e.g. on the upstream side of culverts, harmful consequences, such as reduction of stream cross section, road destruction by stormflow, can be more easily avoided.

4.5 Contribution of soil erosion to the sediment transport

4.5.1 Development of the workflow "Erosion analysis" in the ArcGIS Model Builder

This section describes the four-part workflow for surface erosion analysis with the Universal Soil Loss Equation (USLE) in the ArcGIS environment as represented in *Csáfordi et al.* (2012). "*Erosion analysis*" consists of the four submodels: "*Relief analysis*", "*Soil and land cover*", "*Soil loss and statistics*", and "*Regionalisation*".

The submodel "*Relief analysis*" generates a flow accumulation grid, the channel network with connected catchments, and computes slope features and the *LS* factor. *Figure 4.22* presents the conceptual flow chart of the first submodel.
The user must provide the *threshold area* for channel initiation in order to create an adequate channel network. In this study, the threshold area has been determined using the trial and error method, the comparison between the results of testing different values and the real channel network observed on the field. The model generates the catchment boundaries, the selection basis of the study catchment according to the channel network. The modelled stream networks and catchment boundaries are only usable if the DEM supplies reliable outputs, therefore they have to be checked by the user.
LS factor is computed on the basis of *Eq. 3.9.* For the calculation of *LS* factor, the terrain was simplified, and the slope-length modifying effect of artificial linear elements such as roads and ditches was neglected.

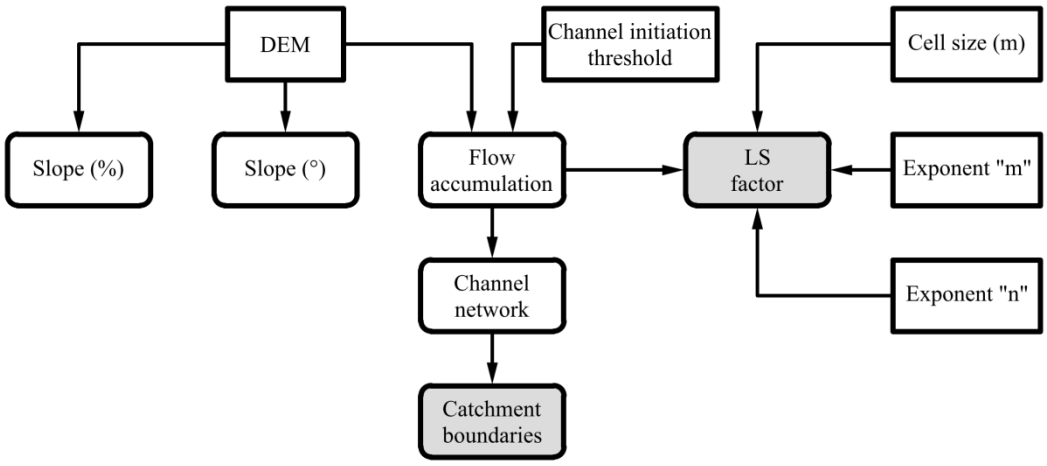

Figure 4.22. Conceptual flow chart of the first submodel "Relief analysis" (Input parameters are symbolized by the rectangles)

The submodel "*Soil and land cover*". The layers catchment boundary, channel network, roads, land cover, land use, and soil map are the result of pre-processing. The submodel "*Soil and land cover*" (*Figure 4.23*) integrates these input layers and generates a layer containing all spatial information for uploading the USLE factors which are manually calculated. The layer of the complete spatial database ("*Full soil and land cover dataset*") has the following attributes: *Object ID, Soil type, K factor, Land use unit, Land use practice, P factor, Code*

number of land cover category, *Land cover category*, *C factor*, *Polygon area* and *R factor* (*Annex IV.V.1*).

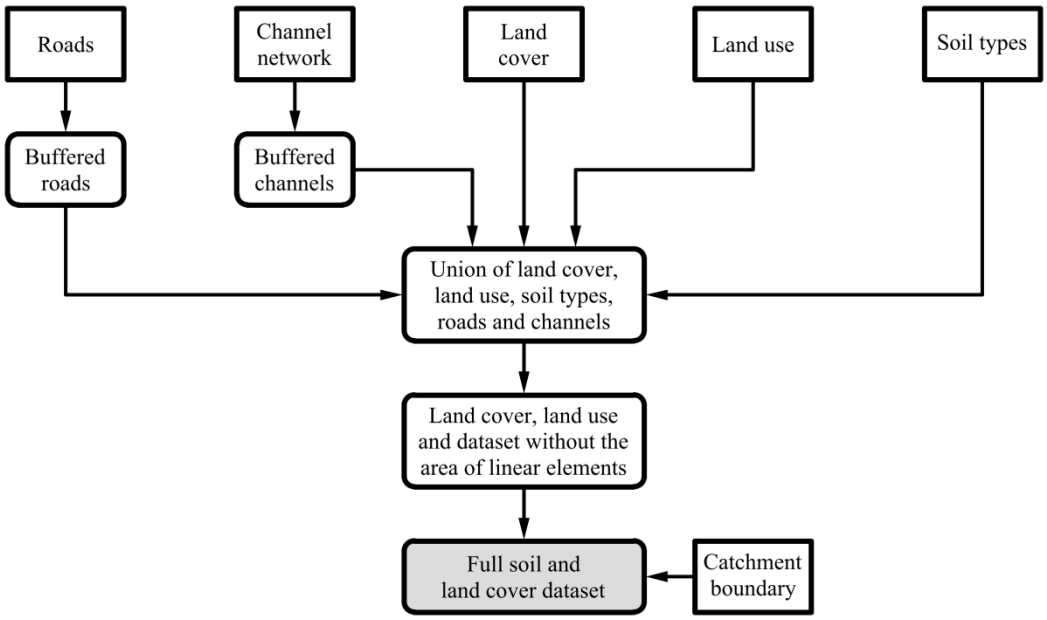

Figure 4.23. Conceptual flow chart of the second submodel "Soil and land cover" (Input parameters are symbolized by the rectangles)

C and *P* factors have to be filled in manually in the attribute table based on visual interpretation of aerial photographs and field experience. Because of this drawback the workflow is recommended principally for catchments smaller than 1 km^2. The benefit of the submodel is that several small polygons are produced with multiplied intersections, and different factor values can be given for each small polygon. This leads to a higher spatial resolution and to a more precise prediction of soil loss.
The unpaved roads are mostly damaged by gully erosion caused by concentrated runoff in the experimental catchment. Since the USLE normally predicts only the impact of unconcentrated runoff (*Kertész et al.* 1997), erosion calculation has not been conducted on the surface of dirt roads and channels. Therefore all linear elements must be removed from the study area and be replaced as hollows.

The submodel "*Soil loss and statistics*" (*Figure 4.24*) computes the soil loss and calculates zonal statistics as maps and tables per each land use unit and land cover category. The layer "*Full soil and land cover dataset*" contains the attribute fields of *R*, *K*, *C* and *P* factors. These attributes are converted into separate thematic raster layers, using the cell size determined by the digital elevation model (DEM). The model multiplies the rasterised USLE factors on cell-by-cell basis resulting in the potential specific annual soil loss by surface erosion for each cell.

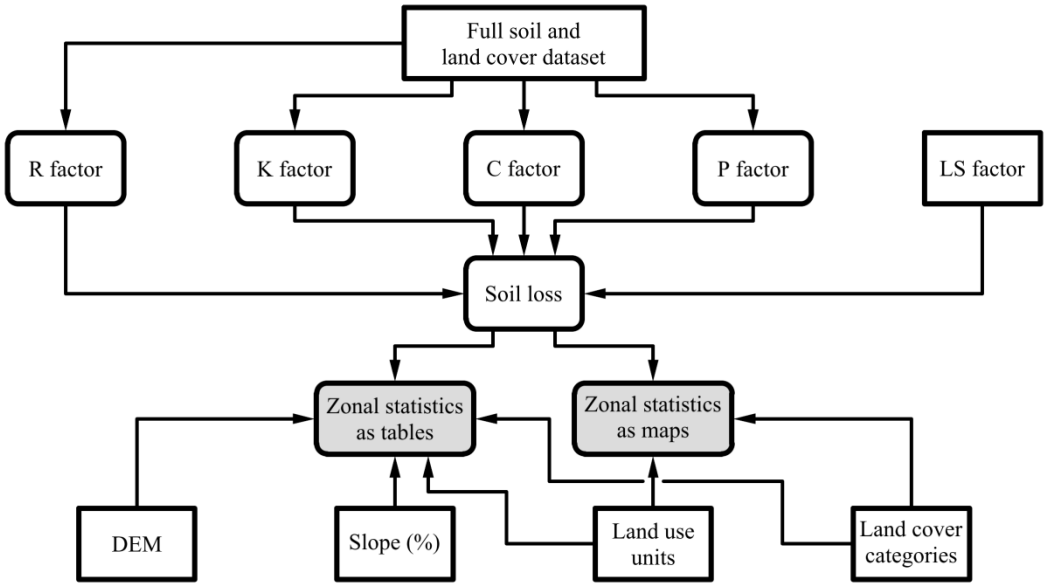

Figure 4.24. Conceptual flow chart of the third submodel "Soil loss and statistics" (Input parameters are symbolized by the rectangles)

The submodel "*Regionalisation*". To enable an area-based comparison between modelled and measured soil erosion, the calculated soil loss is converted from raster into vector format. This allows:

- the comparison of the location of potential and real eroded surfaces,
- the comparison of the size of modelled and observed eroded surfaces.

The submodel "*Regionalisation*" converts the classified raster layer of soil loss to polygons, keeping the soil loss categories of *Rácz* (1985). *Figure 4.25* shows the raster map of modelled soil erosion on the left and the soil loss classes as polygons after conversion on the right.

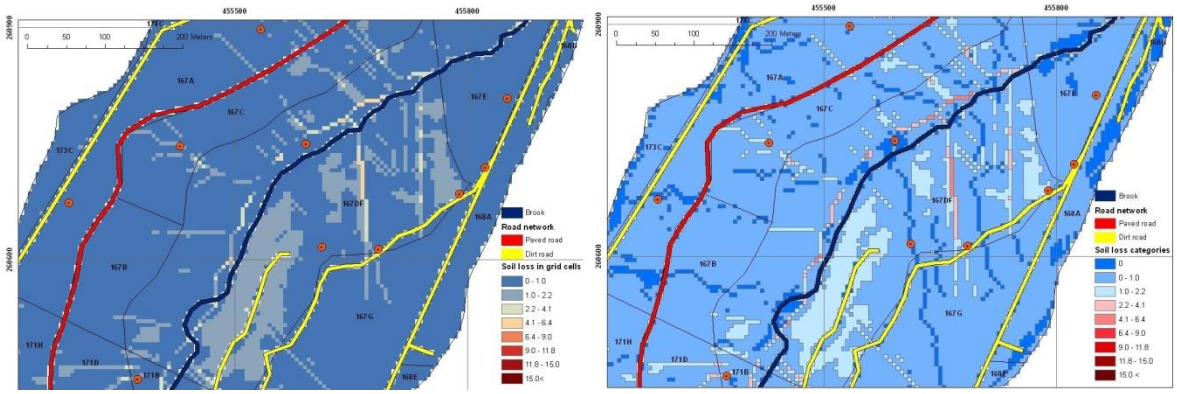

Figure 4.25. The raster map of modelled soil erosion and polygons after conversion

The workflow "Erosion analysis" may have new scientific and practical benefits as well. The model ensures a faster working process and enables to compare the surface soil erosion of different regions providing the similar structure of results (attribute tables, statistical values, and maps). The workflow is a good support for modelling the effect of different rainfall, land cover and land use scenarios to the surface soil erosion. In addition, the erosion risk maps on the basis of different scenarios point at the necessary soil protection interventions.

4.5.2 Modelling of surface erosion with the USLE in the Farkas Valley

A surface soil erosion scenario was modelled for the hydrological year 2008-2009 in the Farkas Valley. *Table 4.10* summarizes the USLE factors and the specific soil loss.

Table 4.10. The factors of USLE and the predicted soil loss by surface erosion

	Factors of the USLE					A ($t \cdot ha^{-1} \cdot yr^{-1}$)
	R ($kJ \cdot m^{-2} \cdot mm \cdot h^{-1}$)	K ($t \cdot ha^{-1} \cdot m^2 \cdot kJ^{-1} \cdot h \cdot mm^{-1}$)	LS	C	P	
Value per cells/ Interval	133.9 (constant)	0.32-0.42	0.0008-95.6	0.003-0.01	0.2-0.4	0-7.5
Average	–	0.36	6.9	0.006	0.24	0.6

Figure 4.25 represents a part of the soil erosion risk map with the most endangered zones. *Figure 4.26* shows the percentual proportion of the area of each soil loss category according to *Rácz* (1985) to the total catchment area, proving that the predicted average soil loss exceeds 6.4 $t \cdot ha^{-1} \cdot yr^{-1}$ (the limit value at 80 *cm* soil depth) only on a negligible area. Moreover, average soil loss remains below 2.2 $t \cdot ha^{-1} \cdot yr^{-1}$ on 98.4% in the Farkas Valley. The total predicted surface erosion is 32.3 *t* from the 0.56 km^2 area of the Farkas Valley without roads and channels.

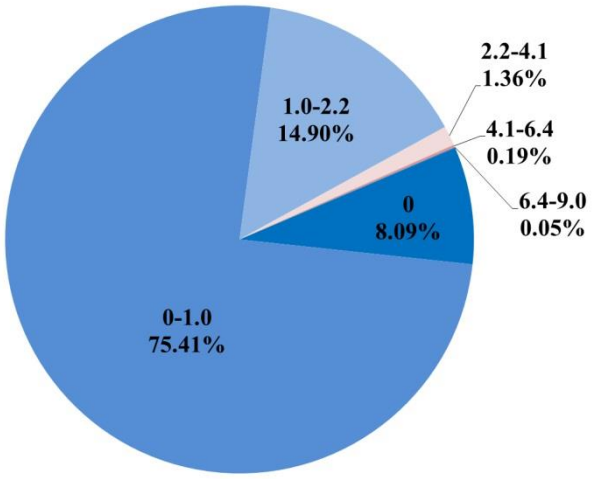

Figure 4.26. Percent area of the soil loss categories

Average and total surface erosion have been calculated for each land use unit (*Figure 4.27*) and land cover type (*Annex IV.V.2*). The predicted specific soil loss does not rise above the tolerance limit in any area unit, but spatial variability of the erosion risk can be observed. The triangles represent the average *LS* factor in each area unit, suggesting that slope-length conditions influence surface soil loss in the forest subcompartments.

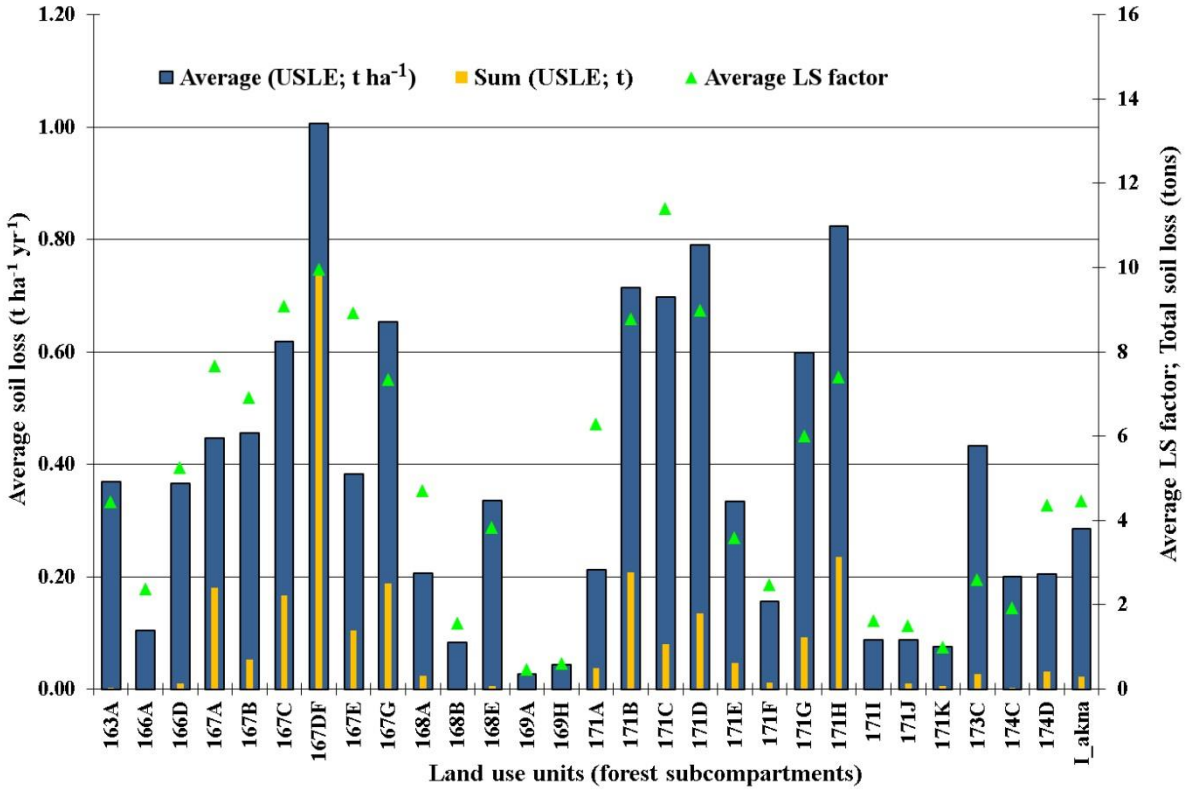

Figure 4.27. Average and total surface soil loss with the average LS factor at each land use unit

Significant control factors of surface erosion in the subcompartments of Farkas Valley have been determined using correlation analysis (*Table 4.11*). More factors show significant correlation with the soil loss, but the *LS* factor has the strongest influence aside from the unit area. *Annex IV.V.3* reports on similar analysis in case of land cover categories.

Table 4.11. Correlation coefficients between soil loss and the USLE factors in case of land use units (Marked correlations are significant at p<0.05)

	Area	***LS*-average**	***LS*-max**	***K*-average**	***K*-max**	***C*-average**	***C*-max**	***P*-average**	***P*-max**
Soil loss-average	***0.73***	***0.87***	***0.78***	***0.52***	***0.69***	0.30	0.29	0.21	0.23
Soil loss-sum	***0.94***	***0.62***	***0.72***	0.26	***0.53***	0.18	0.26	0.17	0.16

Due to the lack of direct field measurements of surface soil erosion, total sediment yield (*TSY*) has been applied to verify the reliability of predicted soil loss. The total surface soil loss reduced with 50% sediment delivery ratio (16.2 *t*) has a 13% proportion to the annual *TSY* (124.6 *t* in the hydrological year 2008-2009 in the Farkas Valley). Consequently, the surface erosion does not represent the major part of sediment sources in the Farkas Valley in the reference period, therefore other erosion phenomena, such as mass movement and erosion by concentrated runoff have to be calculated as the continuation of the present dissertation. Notwithstanding, erosion modelling for the headwater catchment of Rák Brook is a supplementary scientific work which completes the sediment analyses.

Sensitivity analysis. Analysing the response of total surface soil loss to the perturbation of any variable at a time does not make sense due to the simple multiplication character of the USLE. Thus, minimum and maximum values of each USLE factor (*Table 4.10*) have been applied to determine which variable has the greatest effect to the total soil loss between the hydrological years 2000-2010. *Figure 4.28* shows the response of total soil loss if any USLE factor would reach its minimum or maximum value. Minimum (61.7 $kJ \cdot m^{-2} \cdot mm \cdot h^{-1}$) and maximum (478.8 $kJ \cdot m^{-2} \cdot mm \cdot h^{-1}$) of *R* factor are based on the period 2000-2010.
According to the analysis, total soil loss is the less sensitive to the *K* factor and most sensitive to the *LS* factor due to the range of factor values. Maximum factor values have higher impact on the output than the minimum values except for the *K* factor. As a conclusion, length-slope conditions are the most important control factors for the surface soil erosion in the Farkas Valley between the hydrological years 2000-2010.

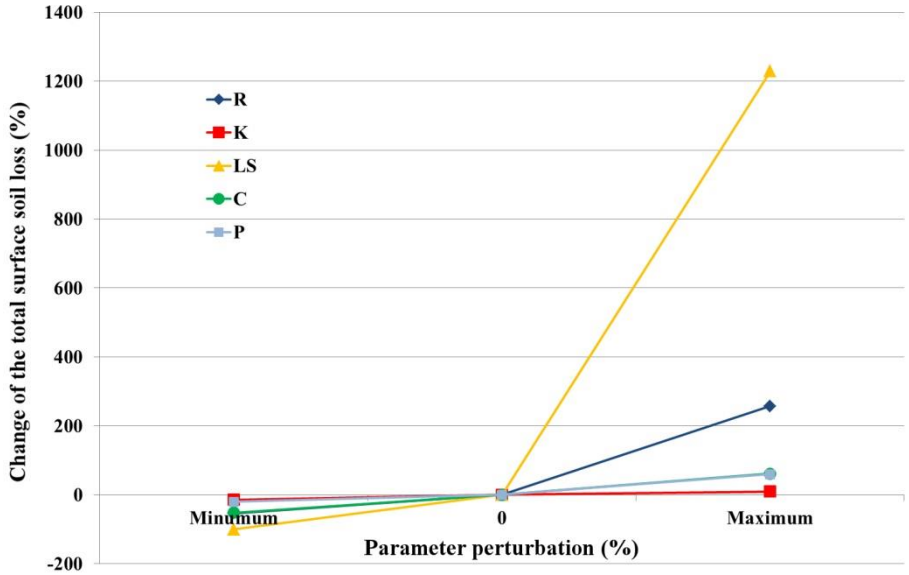

Figure 4.28. Changes of total soil loss in case of minimum or maximum USLE factor values (The reference total soil loss without perturbation is 32.3 $t \cdot ha^{-1} \cdot yr^{-1}$.)

4.5.3 Modelling with EROSION-3D

To evaluate the soil detachment by concentrated runoff from dirt roads and skid trails, and to assess the effect of single rainfall events, the physically distributed model EROSION-3D has been applied. Since the quantitative results of EROSION-3D show expressive overestimation compared to the soil loss predicted by the USLE (four orders of magnitude higher values), this section primarily focuses on the qualitative evaluation.

Erosive effects of rainfall events. Those rainfall events, where maximal 1-hour precipitation exceeded the 90th percentile value (6 *mm*), have been classified as intensive rainfall events. The erosion model has been run for three intensive and three unintensive rainfall events (*Annex IV.V.4*).

Figure 4.29 and *4.30* represent the predicted erosive effects of the selected rainfall events in January and July, where the darker red colours mark the higher potential soil loss. The erosion-accumulation maps and the graph (*Figure 4.31*) demonstrate that rising maximal 1-hour precipitation values lead to higher erosion risk on larger areas (*Csáfordi & Gálos* 2012).

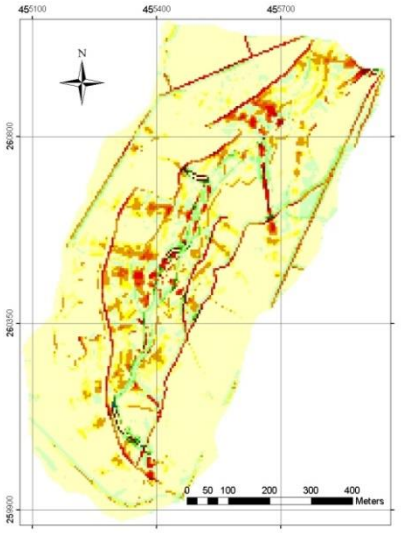

Figure 4.29. Erosion-accumulation risk during the rainfall event on 27-29.01.2009

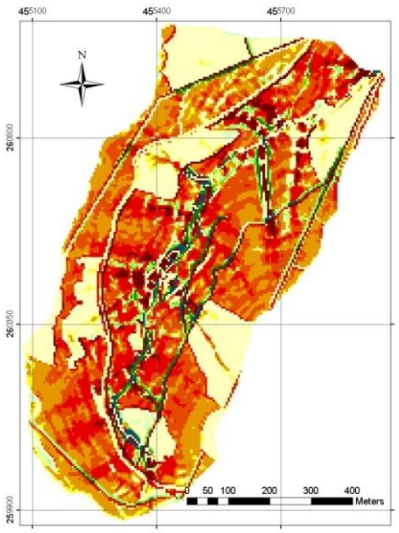

Figure 4.30. Erosion-accumulation risk during the rainfall event on 18.07.2009

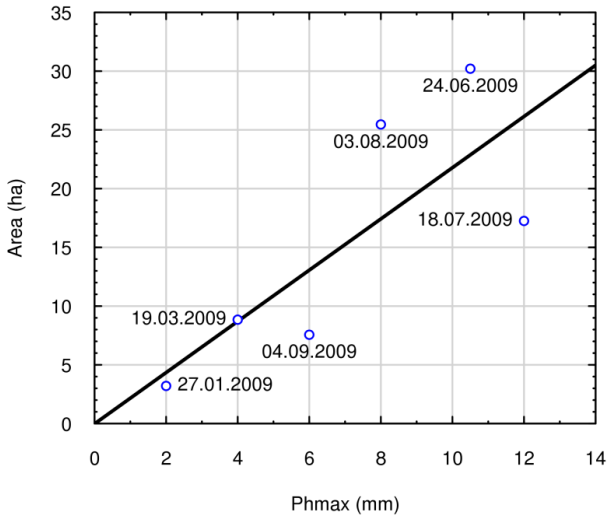

Figure 4.31. Area endangered by erosion as a function of maximal 1-hour precipitation (Phmax)

Soil erosion risk at different land cover. Aggregating the raster values of erosion-accumulation maps for single rainfalls, soil erosion has been calculated for the hydrological year 2008-2009 as well. Average and total surface erosion have been determined for each land cover type (*Annex IV.V.5*), similarly to the analyses with the USLE.

Despite of the expressive overestimation of the soil loss by the EROSION-3D, the results indicate that the average soil loss from unpaved forest roads is six times higher than the average soil loss in the forest subcompartments, and exceeds 2-times the average soil loss in

the land cover categories. Consequently, soil detachment by concentrated runoff (linear erosion) has higher importance as an erosion source in the Farkas Valley than surface erosion.

Although soil loss values are not calibrated, modelled erosion maps can be used for qualitative evaluation of erosion risk, because the most endangered regions agree with the real eroded areas observed on the field. *Annex IV.V.6* contains the GPS-points of the erosion mapping in autumn 2010. The dots localize the visible soil loss by concentrated runoff, mass movement erosion (shallow landslides) and partly the splash and sheet erosion as well. According to the field experiences the most erosion endangered zones in the Farkas Valley are the stream banks, forest roads, thalwegs, gullies and regions with steep slopes, where the canopy closure, undergrowth or litter cover is sparse.

Regarding these results, soil erosion risk can also be predicted in the knowledge of rainfall, land use and land cover projections for the future, providing an important basis to the adaptation and mitigation strategies for the climate change.

5. Discussion and conclusions

The study proved that Farkas Valley and Vadkan Valley, two adjacent headwater forested catchment of the Rák Brook in the Sopron Hills show spatial and temporal variability not only in the sediment parameters but also in the hydrological, hydro-meteorological and climate factors influencing the sediment delivery.
Under low flow conditions, the temporal fluctuation includes the inter-annual and seasonal variation of suspended sediment concentration and the correlation coefficients between suspended sediment concentration and its control factors. Since the inter-annual changes may refer to impact of forestry activities in the catchments, seasonal changes indicate assumedly the alteration in organic matter content and the different in-channel sediment supply processes. Results of *Bronsdon & Naden* (2000), that is, multiple impact of sediment control factors are responsible for the variability of suspended sediment concentration at low flow, corresponds with the finding of this thesis. According to the seasonal Pearson correlation matrices, major sources of fine material can be generated by the freeze-thaw effect in spring, but sediment exhaustion and replenishment after the flood events are primarily accounted for the suspended solids in autumn. Although *Salant et al.* (2008) have not investigated the seasonal trends of sediment delivery, but they also drew the attention to the important role of fine material replenishment during the falling limb of the hydrograph. Nevertheless, differences between the sediment dynamics of the two catchments can be explained by the deviations in the catchment geomorphology, and thus in the speed of sediment replenishment or in the efficiency of sediment trapping.

Hysteresis loops, relation between suspended sediment concentration and control factors, suspended sediment yield and bedload yield during flood events also reflect the variable sediment supply within a catchment and an event. Similarly to *Sadhegi et al.* (2008), this study confirms that reliable sediment yield prediction is only to be performed by regression equations which are developed for single events, or rather for the rising limb and falling limb. Three types of suspended sediment concentration-discharge relation identified in the study catchments, such as clockwise, counter-clockwise and eight-shaped, refer to the dynamics of sediment availability in the channel, similarly to other international studies (*Lenzi & Marchi* 2000, *Zabaleta et al.* 2007, *Nadal-Romero et al.* 2008, *Sadhegi et al.* 2008, *Marttila & Klove* 2010, *Rodríguez-Blanco et al.* 2010a).
Based on the observed data and the developed regression equations, the predicted specific suspended sediment yield is 200.3 $t \cdot km^{-2} \cdot yr^{-1}$ (118.2 *t* per 0.59 km^2) in the hydrological year 2008-2009 in Farkas Valley. This value exceeds the 120 $t \cdot km^{-2} \cdot yr^{-1}$ sediment output of the densely forested mountainous Mediterranean catchment San Salvador (0.92 km^2) in the Central Spanish Pyrenees (*Garcia-Ruiz et al.* 2008), but it has the same order of magnitude. Although the suspended sediment model in this study have not been calibrated, the calculated *bedload-suspended sediment* ratio (1:18) coincides well with previous results from the catchments (*Gribovszki* 2000a), and represents the higher quantitative importance of suspended sediment forms.

Wide scatter in the data and insignificant correlation coefficients are evidences of other factors which have impact on the suspended sediment flux. Stochastic forces such as outwash of a sediment deposit behind log jam, channel dredging and runoff inlet to the stream from an unpaved forest road, can be important processes as further sediment sources. Early sediment researches in the USA (*Beschta* 1979, *Megahan* 1982) also point out the importance of sediment stored in the channel and the fluctuating dynamics of sediment outwash year by year.

A number of international studies describe USLE/GIS implementation, and the self-developed ArcGIS workflow provides evidence that erosion modelling with the USLE can be adapted to a GIS-environment. Producing thematic raster layers of USLE factors in GIS and calculation of soil erosion using them is discussed among others by *Kertész et al.* (1992, 1997), *Márkus & Wojtaszek* (1993a,b), *Jain & Kothyari* (2000) and *Erdogan et al*. (2007). More authors, such as *Andersson* (2010) and *Demirci & Karaburun* (2011) performed their analyses within an ArcGIS/ArcMap workflow. The workflow of *Khosrowpanah et al.* (2007) achieved a more accurate prediction, because a C++ executable program (*Van Remortel et al.* 2004) computes the *LS* factor to each grid cell of the DEM input. This dissertation is limited to erosion prediction, but *Jain et al.* (2010) calculated *SY* and deposition besides soil loss, using spatially distributed sediment transport capacity.
The USLE workflow has also been tested in the Apátkút Valley of the Visegrád Mountains, and the model was capable for determining regions which are susceptible to soil erosion (*Kiss* 2013).

According to the erosion modelling using the USLE, forest vegetation plays a determinant role in the surface soil protection, because soil loss did not exceed the limit value in any land use units. Nevertheless, grassy ground cover may provide a better soil loss prevention than the forest. *Erdogan et al.* (2007) demonstrated the same results as this study in the Kazan watershed, Turkey, that soil erosion potential of the poorly managed pastures was lower as in the land of the dense forest due to relatively higher *C* values. Researches of *Iovino & Puglisi* (1991, in *Sorriso-Valvo et al.* 1995) doubted the eligible soil-protection role of forest cover, as they observed the highest erosion rate in the logged and undisturbed forested catchment compared to a grassy catchment.
In the Farkas Valley, regions with high length-slope conditions are the most sensitive to soil erosion, drawing the attention to the significance of soil conservation forestry in these endangered zones. Topographical properties of the watershed also had greater influence on the magnitude of soil loss than land use/land cover types according to *Erdogan et al.* (2007). The significance of slope conditions was also confirmed by *Demirci & Karaburun* (2011), where 73% of the mostly agricultural Buyukcekmece Lake watershed had low and slight erosion risks with values < 3 $t \cdot ha^{-1} \cdot yr^{-1}$. The majority of land with low and slight soil erosion risks have slope < 5%. Nevertheless, predicted surface soil loss remains below 2.2 $t \cdot ha^{-1} \cdot yr^{-1}$ on 98.4% of the Farkas Valley, while this rate was only about 60% in the Kazan watershed. There is a significant difference in the judgement of erosion tolerance limits according to the soil depth, because *Erdogan et al.* (2007) marked the > 1 $t \cdot ha^{-1} \cdot yr^{-1}$ soil loss as an irreversible

change, whereas soil loss below 6.4 $t \cdot ha^{-1} \cdot yr^{-1}$ means tolerable risk in the Sopron Hills (*Rácz* 1985).

Sediment mass stored in a pond can be a good basis to compare and validate the predicted sediment yield or the surface soil loss. The Brennberg Reservoir (10 km^2 catchment area) is located in the Sopron Hills and fed by the Rák Brook. According to *Csáfordi et al.* (2009), 15700 *t* of sediment has accumulated in the reservoir between the years 1981 and 2006, which is equal to 0.6 $t \cdot ha^{-1} \cdot yr^{-1}$ soil loss. The Farkas Valley shows the same value of surface soil loss calculated with the Universal Soil Loss Equation. If 124.7 *t* sediment yield had been accumulated in each year in the reservoir, the total load would be 3242.2 *t*. Considering that Farkas Valley is only one of the tributaries of the Brennberg Reservoir, the strongly fluctuating character of annual sediment yield, and the unknown ratio of outflowing suspended sediment yield from the reservoir, only the order of magnitude can be validated. According to this validation, sediment modelling performed in the thesis is plausible.
The calculated total sediment yield is equal as if about 0.15 $mm \cdot yr^{-1}$ soil layer eroded from the surface of the entire catchment and reached the channel. Average soil loss by surface erosion is even lower, only 13% of the sediment yield. However, *Kiss & Volford* (2013) point out on the basis of depth distribution of Cs-137 in the soil of some catena of the Farkas Valley that vertical migration speed of the soil profile reached the 4.4-6.6 $mm \cdot yr^{-1}$ referring to the locally stronger rate of soil loss than this dissertation reports on.

Regarding to the total annual sediment yield in the Farkas Valley, neither the mobilization of the sediment deposit nor surface erosion, is the primary factor which contributes to the stream sediment supply. It refers that other erosion phenomena such as road erosion and mass movements have to be investigated in the study catchment in the future. *Lee et al.* (2004) compared the surface erosion potential map with landslide location data and found that many landslides occurred where the *LS* factor is 0 and the soil loss value is 0. This fact draws the attention to the possible errors of *LS* factor calculating process, to the requirement of digital elevation model with higher raster resolution, and that it is not sufficient to evaluate surface and linear erosion in the Farkas Valley where landslides are frequent.

Results of the physically-distributed model EROSION-3D can be only qualitatively evaluated. However, it was obvious that unpaved forest roads can be a major place of soil detachment in the Farkas Valley. These results harmonize with the findings of *Lewis* (1998) and *Luce & Black* (1999) who also demonstrated the great influence of unpaved forest roads on stream sediment yield. Calculations with the EROSION-3D also pointed out that increasing rainfall intensity in summer due to the expected climate changes will induce higher erosion risk on larger area.

6. Outlook

The dissertation continued the previous erosion and sediment researches performed in Hungarian forested catchments, especially in the Sopron Hills. Notwithstanding, only a few studies concerned the sediment delivery in small forested catchments in Hungary, therefore this project can be considered as a supplementary work. Methods, such as hysteresis, mass curve and double mass curve analysis are novel or at least rarely applied techniques from the point of view of the Hungarian forest hydrological research. The discussed problems, such as

- low flow suspended sediment dynamics at different time-scales,
- variable suspended sediment concentration-discharge relation during flood events,
- channel sediment storage behind log jam,
- soil erosion contribution to the total annual sediment yield of a forest stream

are important and actual topics not only for the natural scientists but also for the responsible sylviculturist. These information and research results are useful, if we would like

- to protect aquatic ecosystems from the harmful effects of the increased turbidity;
- to eliminate the economic damages by the high bedload yield;
- to determine the expected life expectancy of forest ponds and reservoirs;
- to adapt soil protecting forestry technologies on the erosion threatened catchment regions;
- to prepare for the impacts of the expected climate change on erosion and sediment processes.

Nevertheless, this dissertation could not find answer for some questions. The future research needs are:

- to analyse the variability of organic matter content of suspended sediment samples, which can be accounted for the highest average suspended sediment concentration in summer;
- to implement the continuous suspended sediment concentration-sampling with turbidity sensors at the headwater catchments, which could clarify the accurate reasons of the spatial variability between the suspended sediment delivery of the Farkas Valley and the Vadkan Valley;
- to check the erosion modelling results with erosion plots (quantitative validation) besides the on-site erosion mapping (qualitative validation).

Compared the sediment yield from surface erosion and outwash of sediment deposit to the total annual sediment yield of the stream in the Farkas Valley, the dissertation pointed out that other sediment sources contribute to the stream sediment delivery as well. Thus, this work drew the attention to the role of unpaved road erosion and mass movements, which analyses should have to be an important part of the future investigations.

Secondary benefits of this project are the processing of ten-years-long dataset of precipitation, runoff and sediment for the Farkas Valley. This database could underlie numerous scientific establishments in the future, related to the rainfall-runoff processes in a small forested catchment.

7. Theses of the dissertation

1. The author introduced a new variable "antecedent days" (*AD*) which represents the number of days elapsed between the water sampling and the previous flood event. This variable refers to the sediment-outwash effect of previous flood events and the sediment supply processes during dry periods. Since the correlation is significant between *AD* and suspended sediment concentration (*SSC*) under low flow conditions, *AD* is a useful variable to better understand the low flow suspended sediment dynamics in small catchments. Freeze-thaw effect has also been identified as another significant impact on the low flow sediment dynamics: significant correlation was only obtained between *SSC* and temperature variables in spring. (*Csáfordi et al.* 2013).

2. The author identified three types of hysteresis loops relating the relation between suspended sediment concentration (*SSC*) and discharge (*Q*): clockwise, counterclockwise and eight-shaped loops. These phenomena refer to the temporal fluctuation of *SSC*-*Q* ratio during a flood event and the fine material availability in the channel. Knowing the conditions of sediment availability in a stream for different *Q*-ranges, it is also possible to identify catchment regions which contribute to the sediment load into a channel. These findings can be considered as novel results in the Hungarian forest hydrological researches related to small catchments (*Csáfordi et al.* 2010a).

3. The author found significant correlation between the suspended sediment concentration (*SSC*) and rainfall, runoff and climate parameters, such as discharge, water temperature, soil temperature, antecedent precipitation index, rainfall erosivity, peak discharge and total volume of the flood event depending on the examined time scale and flow dynamics under high flow conditions. Based on these relations between the *SSC* and its control factors, regression equations have been developed to calculate suspended sediment yield. Temporal variability of *SSC* reduces the strength of correlation between *SSC* and environmental parameters and the reliability of regression equations as well. The strongest relations have been obtained at event scale. Separation of rising and falling limb provided even higher Pearson's correlation coefficients. Thus, regression models were developed for single flood events or for the rising and falling limb of each flood. These models are suitable to calculate suspended sediment yield for high flow periods at annual and event scale (*Csáfordi et al.* 2011, *Csáfordi et al.* 2013).

4. The author developed a four-part workflow in the ArcGIS Model Builder in order to implement the empirical Universal Soil Loss Equation (*Wischmeier & Smith* 1978) into GIS-environment. The model accelerates and makes uniform the calculation of surface soil loss in small catchments. Soil loss prediction confirms the soil protection role of forest vegetation, as the predicted average surface soil loss remained under the tolerance limit in each subcompartments, and surface soil loss was not the major source of the sediment load in the small forested catchment (*Csáfordi* 2010, *Csáfordi et al.* 2010b, *Csáfordi et al.* 2012).

5. The author pointed out that other sediment sources determine the annual sediment yield in a forested catchment beside the surface erosion. Despite of the expressive quantitative overestimation of soil loss, application of the physical erosion model EROSION-3D (*von Werner* 1995) for a small forest catchment, as novel results for the Hungarian forest hydrological research, demonstrated the outstanding impact of unpaved forest roads on stream sediment budget. Geodesic survey, geoinformatical calculations and mass curve analysis were suitable methods to determine another sediment source of small forest streams, that is, an outwashing sediment deposit behind log jam. This experiment is a good recommendation to analyse stochastic processes of the sediment delivery (*Csáfordi* 2010, *Csáfordi et al.* 2011).

Acknowledgements

First of all I would like to thank the useful advices and instructions for my supervisors, Dr. Zoltán Gribovszki and Dr. Péter Kalicz, who helped me to find my own path to the scientific research and established my project with their previous work. As leading and encouraging me to take part in the related conferences, to apply for research scholarships abroad and to write publications, they contributed to enhance the level of this dissertation.

I am very grateful to all of my colleagues and friends, especially to Dr. Borbála Gálos and Dr. Norbert Móricz. This dissertation would not have been finished without their encouragement and sharing with me the practical experiences in connection with writing a PhD-thesis. I also appreciate the technical support of Balázs Kisfaludi in creating figures, of Tamás Makrai in taking photos in the field, of István Juhász in geoinformatics, and the useful advices of Dr. Mihály Kucsara and Dr. Gábor Brolly. Furthermore, I would like to say thanks to Dr. Csaba Centeri and Dr. Gergely Jakab. They gave me essential support in rainfall event separation and calculation of soil loss. Data collection in the field and data processing is a long-term work performed by the current staff and students of the Institute of Geomatics and Civil Engineering, who remained unknown to me. Besides all of them, special thanks to Tibor Barna, Mihály Erős, Gergely Jóna and Zsuzsanna Válint for the field measurements, to Amina Dahili, Kitti Gyimóthy, Tamás Pálfy, Anna Rétlaki and Kinga Sermaul for the data preprocessing and data entry.

Spending nine month in the Institute of Physical Geography and Landscape Ecology, University of Hannover in the frame of the scholarship "Deutsche Bundesstiftung für Umwelt" promoted my knowledge and scientific career to a high degree. Owing to the help of the German colleagues, especially of Prof. Dr. Thomas Mosimann, Dr. Uwe Meer, Dr. Jens Gross, Dr. Jan Bug, Heiko van Wensen and Frank Beisiegel, I learned the basis of soil analyses, soil erosion mapping and modelling. In addition, I am grateful for the support of the scholarship "Aktion für Österreich-Ungarn" which gave me possibility to study fluvial sediment transport and laboratory sediment analysis under the supervision of Prof. Dr. Helmut Habersack, Marlene Haimann and Verena Schabus in the Institute of Water Management, Hydrology and Hydraulic Engineering, University of Natural Resources and Life Sciences Vienna for a four-month-long period.

This dissertation would not have been completed without the financial support of the projects TÁMOP-4.2.1/B-09/KONV-2010-0006, TÁMOP-4.2.2.B-10/1-2010-0018, TÁMOP-4.2.2.A-11/1/KONV-2012-0013 and TÁMOP-4.2.2.A-11/1/KONV-2012-0004 supported by the European Union with the co-financing of the European Social Fund.

In addition, I am thankful my family who ensured me a reliable background for the engrossed writing of this work. At last but not least, I would like to express my thanks to the reviewers of the manuscript, Dr. Sándor Baranya, Dr. Csaba Centeri, Dr. Bálint Heil, for their helpful comments and suggestions.

References

Ad-hoc-AG Boden (2005): Bodenkundliche Kartieranleitung. [Guidance to the soil characterization.] Bundesanstalt für Geowissenschaften und Rohstoffe und Niedersächsisches Landesamt für Bodenforschung. Hannover, Germany. (in German)

Albert, J.M. (2004): Hydraulic analysis and double mass curves of the middle Rio Grande from Cochiti to San Marcial, New Mexico. MSc Thesis. Colorado State University, Fort Collins, Colorado.

Alexandrov, Y. – Laronne, J.B. – Reid, I. (2007): Intra-event and inter-seasonal behaviour of suspended sediment in flash floods of the semi-arid northern Negev, Israel. Geomorphology 85: 85-97.

Amore, E. – Modica, C. – Nearing, M.A. – Santoro, V.C. (2004): Scale effect in USLE and WEPP application for soil erosion computation from three Sicilian basins. J. Hydrol. 293: 100-114.

Andersson, L. (2010): Soil loss estimation based on the USLE/GIS approach through small catchments. A minor field study in Tunisia. Technical report TVVR 10/5019. Division of Water Resources Engineering, Department of Building and Environmental Technology, Lund University. 5-14 ps.

Antonelli, C. – Eyrolle, F. – Rolland, B. – Provansal, M. – Sabatier, F. (2008): Suspended sediment and 137Cs fluxes during the exceptional December 2003 flood in the Rhone River, Southeast France. Geomorphology 95: 350-360.

Auerswald, K. (1987): Sensitivität erosionsbestimmender Faktoren. Wasser und Boden 39 (1): 34-38.

Bánky, Gy. (1959): A kisnánai eróziómérő állomás három évi munkásságának eredményei. [Three-year results of the soil erosion gauging station in Kisnána.] Erdészeti Kutatások 6 (3): 139-160. (in Hungarian)

Bartholy, J. – Pongrácz, R. (2007): Regional analysis of extreme temperature and precipitation indices. Global Planet. Change 57: 83-95.

Bartley, R. – Corfield, J.P. – Abbott, B.N. – Hawdon, A.A. – Wilkinson, S.N. – Nelson, B. (2010): Impacts of improved grazing land management on sediment yields, Part 1: Hillslope processes. J. Hydrol. 389: 237-248.

Bellér, P. (1996): Meszezési kísérletek a Soproni-hegységben. [Soil liming experiments in the Sopron Hills.] Research report. University of Sopron. (in Hungarian)

Benda, L. – Dunne, T. (1997): Stochastic forcing of sediment supply to channel networks from landsliding and debris flow. Water Resour. Res. 33 (12): 2849-2863.

Beschta, R.L. (1978): Long-term patterns of sediment production following road construction and logging in the Oregon Coast Range. Water Resour. Res. 14 (6): 1011-1016.

Beschta, R.L. (1979): Debris removal and its effects on sedimentation in an Oregon Coastal Range Stream. Northwest Sci. 53: 71-77.

Beschta, R.L. (1983): Channel changes following stream-induced hillslope erosion in the Upper Kowai Basin, Torlesse Range, New Zealand. Journal of Hydrology New Zealand 22 (2): 93-111.

Beskow, S. – Mello, C.R. – Norton, L.D. – Curi, N. – Viola, M.R. – Avanzi, J.C. (2009): Soil erosion prediction in the Grande River Basin, Brazil using distributed modeling. Catena 79: 49-59.

Bogárdi, J. (1971): Vízfolyások hordalékszállítása. [Sediment transport of water-courses.] Akadémiai Kiadó, Budapest, Hungary. (in Hungarian)

Bousfield, G. (2008): Peakflow prediction using an antecedent precipitation index in small forested watersheds of the Northern California coast range. MSc Thesis. Humboldt State University.

Brauner, M. (1999): Modelling the sediment budget of an alpine catchment within GIS environment. In: Proceedings of the 28th IAHR Congress. Graz, Austria. 1999.

Bricker, O.P. – Pačes, T. – Johnson, C.E. – Sverdrup, H. (1992): Weathering and erosion aspects of small catchment research. In: Moldan, B. – Cerny, J. (ed.): Biogeochemistry of small catchments – A tool for environmental research. John Wiley and Sons. 85-103 ps.

Bronsdon, R.K. – Naden, P.S. (2000): Suspended sediment in the Rivers Tweed and Teviot. Sci. Total Environ. 251-252: 95-113.

Brown, G.W. – Krygier, J.T. (1971): Clear-cut logging and sediment production in the Oregon Coast Range. Water Resour. Res. 7 (5): 1189-1198.

Bug, J. (2011): Modellierung der linearen Erosion und des Risikos von Partikeleinträgen in Gewässer – Entwicklung und Anwendung von entscheidungsbasierten Modellen zur flächenhaften Prognose der linearen Erosionsaktivität und Gewässeranschlusses von Ackerflächen (Niedersachsen und Nordwestschweiz). [Modelling of linear erosion and risk of soil particle inlet to the streams.] PhD thesis. University of Hannover. (in German)

Centeri, Cs. (2001): Az általános talajveszteség becslési egyenlet (USLE) K tényezőjének vizsgálata. [Investigation of the K factor of the Universal Soil Loss Equation.] PhD thesis. Szent István University, Gödöllő. (in Hungarian)

Chang, M. (2006): Forest hydrology. Taylor and Francis, Boca Raton. 237-282 ps.

Clement, A. – Buzás, K. – Fetter, É. (2009): Measuring and modelling of stormwater runoff and associated nutrient load at an experimental catchment near Lake Balaton, Hungary. In: Proceedings of the 7th International Symposium on Ecohydraulics. Concepción, Chile. 12-16.01.2009. Paper X.

Cobaner, M. – Unal, B. – Kisi, O. (2009): Suspended sediment concentration estimation by an adaptive neuro-fuzzy and neural network approaches using hydro-meteorological data. J. Hydrol. 367: 52-61.

Croke, J. – Mockler, S. – Fogarty, P. – Takken, I. (2005): Sediment concentration changes in runoff pathways from a forest road network and the resultant spatial pattern of catchment connectivity. Geomorphology 68: 257-268.

Csáfordi, P. (2010): Erózióveszélyeztetettség vizsgálata a Soproni-hegység erdősült kisvízgyűjtőjén az USLE és az EROSION-3D modellekkel. [Erosion risk assessment in the forested catchment of Sopron Hills using the USLE and the EROSION-3D models.] In: Kovács Gy., Gelencsér G., Centeri Cs. (eds.): Az Élhető Vidékért 2010 környezetgazdálkodási konferencia, Konferenciakötet. Koppányvölgyi Vidékfejlesztési Közhasznú Egyesület, Törökkoppány: 189-198. (in Hungarian)

Csáfordi, P. – Kalicz, P. – Gribovszki, Z. – Kucsara, M (2009): A Brennbergi-tározó hordaléklerakódás-vizsgálata [Estimation of sediment accumulation in the Brennberg Reservoir.] Hidrológiai Közlöny 89 (3): 33-37. (in Hungarian)

Csáfordi, P. – Gribovszki, Z. – Válint, Zs. – Kalicz, P. (2010a): Kisvízfolyások anyagszállításának vizsgálata két árhullám példáján. [Examination of sediment- and iontransport of small streams during two floods.] Hidrológiai Közlöny 90 (2): 55-61. (in Hungarian)

Csáfordi P., Gribovszki Z., Kalicz P. (2010): Contribution of surface erosion to sediment transport in a small forested headwater catchment in the Sopron Hills. Journal of Landscape Management 1 (2): 3-11.

Csáfordi, P. – Kalicz, P. – Gribovszki, Z. (2011): Erdősült kisvízgyűjtő éves hordalékhozamának becslése és egy hordalékkúp hatásának vizsgálata. [Estimation of annual sediment load of a forested catchment and examination of the effect of an alluvial fan.] Hidrológiai Közlöny 91 (3): 46-54. (in Hungarian)

Csáfordi, P. – Gálos, B. (2012): The erosive effects of precipitation and their changing frequency in the future. In: Schmidt, P. (ed.): Környezeti problémák a Kárpát-medencében II., Nemzetközi Klímakonferencia. PTE-TTK, Földtudományok Doktori Iskola, Publikon Kiadó, Pécs: 262-266.

Csáfordi, P. – Pődör, A. – Bug, J. – Gribovszki, Z. (2012): Soil erosion analysis in a small forested catchment supported by ArcGIS Model Builder. Acta Sylv. Lign. Hung. 8: 39-55.

Csáfordi, P. – Kalicz, P. – Gribovszki, Z. (2013): What did we learn from the ten-years-long sediment dataset from the Rák Brook? In: Gribovszki, Z. – Hlavčová, K. – Kalicz, P. – Kohnová, S. (eds.): Catchment processes in regional hydrology: from experiment to modeling in Carpathian drainage basins. Nyugat-magyarországi Egyetem Kiadó, Sopron: 6-1-6-16.

Demirci, A. – Karaburun, A. (2011): Estimation of soil erosion using RUSLE in a GIS framework: a case study in the Buyukcekmece Lake watershed, northwest Turkey. Environ. Earth Sci. 66 (3): 903-913.

Dettling, W. (1989): Eine mathematische Betrachtung des R-Faktors. [Mathematical analysis of the R factor.] Z. Geomorphol. 33 (2): 373-377. (in German)

De Roo, A.P.J. – Jetten, V.G. (1999): Calibrating and validating the LISEM model for two data sets from the Netherlands and South Africa. Catena 37: 477-493.

Dietrich, W.E. – Dunne, T. (1978): Sediment budget for a small catchment in mountainous terrain. Z. Geomorphol. 29: 191-206.

DIN 4220:2008-11 standard: Deutsches Institut für Normung. [German Organization for Standardization.] Bodenkundliche Standortbeurteilung – Kennzeichnung, Klassifizierung und Ableitung der Bodenkennwerten (normative und nominale Skalierungen). [Pedologic site assessment – Designation, classification and deduction of soil parameters (normative and nominal scaling)]. 2008.

Di Stefano, C. – Ferro, V. – Palazzolo, E. – Panno, M. (2000): Sediment delivery processes and agricultural non-point pollution in a Sicilian Basin. J. Agr. Eng. Res. 77 (1): 103-112.

Dövényi, Z. (ed.) (2010): Magyarország kistájainak katasztere. [Cadastre of the Hungarian regions.] MTA Földrajztudományi Kutatóintézet. Budapest, Hungary. 345-353 ps. (in Hungarian)

Duck, T. (1955): Az erózió térképezése és eddigi eredményei Magyarországon [Mapping of erosion and its results until now in Hungary.] Földrajzi Közlemények 5. (in Hungarian)

Duck, T. (1969): Alapfokú talajvédelem a mezőgazdasági üzemekben. [Fundamental soil protection in the farming activities.] Mezőgazdasági Kiadó. Budapest, Hungary. pp. 191 (in Hungarian)

Duvert, C. – Gratiot, N. – Némery, J. – Burgos, A. – Navratil, O. (2010): Sub-daily variability of suspended sediment fluxes. Hydrol. Earth Syst. Sc. 15: 703-713.

Erdogan, E.H. – Erpul, G. – Bayramin, I. (2007): Use of USLE/GIS Methodology for Predicting Soil Loss in a Semiarid Agricultural Watershed. Environ. Monit. Assess. 131: 153-161.

Estrany, J. – Garcia, C. – Batalla, R.J. (2009): Suspended sediment transport in a small Mediterranean agricultural catchment. Earth Surf. Proc. Land. 34 (7): 929-940.

Fedora, M.A. – Beschta, R.L. (1989): Storm runoff simulation using an antecedent precipitation index (API) model. J. Hydrol. 112: 121-133.

Ferro, V. – Minacapilli, M. (1995): Sediment delivery processes at basin scale. Hydrolog. Sci. J. 40: 703-717.

Fistikoglu, O. – Harmancioglu, N.B. (2002): Integration of GIS with USLE in Assessment of Soil Erosion. Water Resour. Manage. 16: 447-467.

Forestry management plan (1994): Állami Erdészeti Szolgálat. [Hungarian State Forestry Service.]

Forestry management plan (2004): Állami Erdészeti Szolgálat. [Hungarian State Forestry Service.]

FÖMI, DDM-5: Digital elevation model in 5 m resolution. Földmérési és Távérzékelési Intézet. [Institute of Geodesy, Cartography and Remote Sensing.] 2005.

FÖMI, DTA-10: Georeferred rasterized topographic map 1:10000. Földmérési és Távérzékelési Intézet. [Institute of Geodesy, Cartography and Remote Sensing.] 2002.

FÖMI, ortophoto: Ortophoto in 0.5 m/px resolution. Földmérési és Távérzékelési Intézet. [Institute of Geodesy, Cartography and Remote Sensing.] 2008.

Gabriels, D. – Ghekiere, G. – Schiettecatte, W. – Rottiers, I. (2003): Assessment of USLE cover-management C-factors for 40 crop rotation systems on arable farms in the Kemmelbeek watershed, Belgium. Soil Till. Res. 74: 47-53.

Gábris, Gy. – Kertész, Á. – Zámbó, L. (2003): Land use change and gully formation over the last 200 years in a hilly catchment. Catena 50: 151-164.

Gao, P. – Mu, X.-M. – Wang, F. – Li, R. (2010): Changes in streamflow and sediment discharge and the response to human activities in the middle reaches of the Yellow River. Hydrol. Earth Syst. Sc. 15: 1-10.

Gálos, B. – Lorenz, Ph. – Jacob, D. (2007): Will dry events occur more often in Hungary in the future? Environ. Res. Lett. 2 034006 doi: 10.1088/1748-9326/2/3/034006 (online journal)

García-Ruiz, J. M. – Regüés, D. – Alvera, B. – Lana-Renault, N. – Serrano-Muela, P. – Nadal-Romero, E. – Navas, A. – Latron, J. – Martí-Bono, C. – Arnáez, J. (2008): Flood generation and sediment transport in experimental catchments affected by land use changes in the central Pyrenees. J. Hydrol. 356: 245-260.

Gomi, T. – Moore, R.D. – Hassan, M.A. (2005): Suspended sediment dynamics in small forest streams of the Pacific Northwest. J. Am. Water Resour. As. 41 (4): 877-898.

Gordon, N.D. – McMahon, T.A. – Finlayson, B.L. – Gippel, C.J. – Nathan, R.J. (2004): Stream hydrology. John Wiley and Sons, Chichester. 169-200 ps.

Grant, G.E. – Wolff, A.L. (1991): Long-term patterns of sediment transport after timber harvest, Western Cascade Mountains, Oregon, USA. In: Proceedings of the Vienna Symposium "Sediment and Stream Water Quality in a Changing Environment: Trends and Explanation". Vienna, Austria. August 1991. IAHS Publ. 203: 31-40.

Gribovszki, Z. (2000a): Forest stream sediment transport in Sopron Mountain. In: Tóth, L. (ed.): Hungarian Agricultural Engineering 13. Gödöllő. 78-80.

Gribovszki, Z. (2000b): Erdősült kisvízgyűjtők vízfolyásainak hordalékszállítása – Vizsgálatok két soproni kisvízgyűjtőn. [Stream sediment delivery of small forested catchments – Examinations in two small catchments in the Sopron Hills.] PhD thesis. University of West Hungary, Sopron. (in Hungarian)

Gribovszki, Z. – Kalicz, P. – Kucsara, M. (2006): Streamflow characteristics of two forested catchments in the Sopron Hills. Acta Sylv. Lign. Hung. 2: 81-92.

Gribovszki, Z. – Csáfordi, P. – Herceg, A. – Kalicz, P. (2011): A városiasodás vízminőségi hatásai a soproni Rák-patak vízrendszerén. [Water quality change due to urbanisation along the stream system of Rák Brook, Sopron.] In: Lakatos, F. – Szabó, Z. (ed.): Proceedings of the Scientific Conference on the Faculty of Forestry. Sopron, Hungary, University of West Hungary. 5. October 2011. 173-178. (in Hungarian)

Gribovszki, Z. – Kalicz, P. – Csáfordi, P. – Szita, R. – Király, G. – Pődör, A. – Ambrus, A. (2012): Hydrological changes due to urbanization along the Rák Stream in Sopron. In: Neményi, M. – Heil, B. (ed.): The Impact of Urbanization, Industrial, Agricultural and Forest Technologies on the Natural Environment. University of West Hungary, Sopron, Nemzeti Tankönyvkiadó, Budapest. 161-170.

Gribovszki, Z. – Kalicz, P. (2003): Analysis of headwater stream sediment parameters. In: Geophysical Research Abstracts. European Geophysical Society, 28th Joint Assembly. Nice, France. April 2003.

Hossain, S. – Eyre, B. – McConchie, D. (2002): Spatial and temporal variations of suspended sediment responses from the subtropical Richmond River catchment, NSW, Australia. Aust. J. Soil Res. 40: 419-432.

ISO 11277:2009 standard: International Organization for Standardization. Soil quality – Determination of particle size distribution in mineral soil material – Method by sieving and sedimentation. 2009.

Jain, M.K. – Mishra, S.K. – Shah, R.B. (2010): Estimation of sediment yield and areas vulnerable to soil erosion and deposition in a Himalayan watershed using GIS. Curr. Sci. India 98 (2): 213-221.

Jain, M.K. – Kothyari, U.C. (2000): Estimation of soil erosion and sediment yield using GIS. Hydrolog. Sci. J. 45 (5): 771-786.

Jakab, G. (2008): Természeti tényezők hatása a talajpusztulás vonalas formáinak kialakulására. [Influence of natural factors on the development of linear erosion types.] PhD thesis. Hungarian Academy of Sciences, Research Institute of Geographic Sciences, Budapest. (in Hungarian)

Jakab, G. – Kertész, Á. – Papp, S. (2005): Az árkos erózió vizsgálata a Tetves-patak vízgyűjtőjén. [Assessment of the gully erosion in the catchment of Tetves Brook.] Földrajzi Értesítő 54 (1-2): 149-165. (in Hungarian)

Julien, P.Y. (2010): Erosion and sedimentation. Cambridge University Press. Cambridge, UK.

Kárpáti, L. (1955): Adatok Sopron környékének geomorfológiájához. [Data for the geomorphology of Sopron surroundings.] Földrajzi Értesítő 4 (3): 21-40. (in Hungarian)

Kazó, B. (1970): Vízgazdálkodási kartogram szerkesztése mesterséges esőztetéssel mért eredmények felhasználásával [Creating water management map using the results of artificial raining.] Agrokémia és Talajtan 19 (4): 481-502. (in Hungarian)

Kerényi, A. (1991): Talajerózió – térképezés, laboratóriumi és szabadföldi kísérletek. [Soil erosion – mapping, laboratory and field experiments.] Akadémiai Kiadó, Budapest. ps. 219 (in Hungarian)

Kertész, Á. – Márkus, B. – Mezősi, G. (1992): Soil erosion assessment using GIS methods. In: 3rd European Conference on Geographical Information Systems. Munich, Germany. March 1992. 885-893.

Kertész, Á. – Richter, G. – Schmidt, R.G. (eds.) (1997): The Balaton project. In: European Society for Soil Conservation, Newsletter 2-3: 3-36.

Khanal, S. – Parajuli, P. B. (2013): Evaluating the impacts of Forest clear cutting on water and sediment yields using SWAT in Mississippi. JWARP 5: 474-483.

Khosrowpanah, S. – Heitz, L.F. – Wen, Y. – Park, M. (2007): Developing a GIS-based soil erosion potential model of the UGUM watershed. Technical Report No. 117. Water and Environmental Research Institute of the Western Pacific, University of GUAM, UOG station, Mangilao, Guam. 9-33 ps.

Kis, A. (2011): Csapadékindexek várható trendjei Magyarországon az ENSEMBLES szimulációk alapján. [Expected trends of precipitation indices in Hungary according to the ENSEMBLES simulations.] BSc thesis. Lóránd Eötvös Univeristy of Sciences, Budapest. (in Hungarian)

Kisházi, P. – Ivancsics, J. (1981-1985): Sopron környéki üledékek összefoglaló földtani értékelése. [Comprehensive geologic assessment of the sediments in Sopron surroundings.] Központi Bányászati Fejlesztési Intézet Petrográfia, Sopron: 48. (in Hungarian)

Kiss, B. (2013): Az erózió kialakulásának és mérséklésének lehetősége az Apátkúti-völgyben. [Formation of erosion and possibilities of the erosion control in the Apátkút Valley.] MSc thesis. University of West Hungary, Faculty of Forestry, Sopron. (in Hungarian)

Kiss, E. – Volford, P. (2013): Depth and areal distribution of Cs-137 in the soil of a small water catchment in the Sopron Mountains. Acta Sylv. Lign. Hung. 9: 147-159.

Kitka, G. (2009): Az Erosion 3D modell magyarországi adaptálása és alkalmazhatóságának vizsgálata kisvízgyűjtők tájhasználati tervezésében. [Adaptation and applicability of the EROSION-3D soil erosion model in Hungary to the land use planning of small catchments.] PhD thesis. University of Sciences, Szeged. (in Hungarian)

Kontur, I. – Koris, K. – Winter, J. (2003): Hidrológiai számítások. [Hydrological calculations.] Linográf, Gödöllő, Hungary. (in Hungarian)

Kosky, K. (1999): GIS and Watershed Project Management. In: URISA proceedings: Papers from the annual conference of the urban and regional information association. 406-415.

Krishnaswamy, J. – Halpin, P.N. – Richter, D.D. (2001): Dynamics of sediment discharge in relation to land-use and hydro-climatology in a humid tropical watershed in Costa Rica. J. Hydrol. 253: 91-109

Kucsara, M. (1996): Csapadék és lefolyás erdészeti kisvízgyűjtőn. [Rainfall and runoff in a small forested catchment.] PhD thesis. University of Forestry and Wood Sciences, Sopron. (in Hungarian)

Kucsara, M. – Rácz, J. (1988): A fajlagos évi eróziós talajveszteség vizsgálata a Tacsi-árok erdővel borított vízgyűjtő területén. [Examination of specific annual soil loss in the forested catchment of Tacsi Valley.] Erdészeti és Faipari Közlemények (1-2): 81-88. (in Hungarian)

Kucsara, M. – Rácz, J. (1991): Eróziós talajveszteség vizsgálata erdőterületeken. [Soil loss by water erosion in forested regions.] Hidrológiai Tájékoztató, April 1991: 22-24. (in Hungarian)

Lee, S. (2004): Soil erosion assessment and its verification using the Universal Soil Loss Equation and Geographic Information System: a case study at Boun, Korea. Environ. Geol. 45: 457-465.

Lefrancois, J. – Grimaldi, C. – Gascuel-Odoux, C. – Gilliet, N. (2007): Suspended sediment and discharge relationships to identify bank degradation as a main sediment source on small agricultural catchments. Hydrol. Process. 21: 2923-2933.

Lenzi, M.A. – Marchi, L. (2000): Suspended sediment yield during floods in a small stream of Dolomites (Northeastern Italy). Catena 39: 267-282.

Lewis, J. (1998): Evaluating the impacts of logging activities on erosion and suspended sediment transport in the Caspar Creek watersheds. In: Proceedings of the "Conference on coastal watersheds: The Caspar Creek story". Ukiah, USA. 1998. Technical report PSW GTR-168. Albany, CA, Pacific Southwest Research Station, Forest Service, USDA. 55-69.

Lidén, R. (1999): A new approach for estimation suspended sediment yield. Hydrol. Earth Syst. Sc. 3 (2): 285-294.

Lim, K.J. – Sagong, M. – Engel, B.A. – Tang, Z. – Choi, J. – Kim, K.S. (2005): GIS-based sediment assessment tool. Catena 64: 61-80.

Lisle, T.E. – Napolitano, M.B. (1998): Effects of recent logging on the main channel of North Fork Caspar Creek. In: Proceedings of the "Conference on coastal watersheds: The Caspar Creek story". Ukiah, USA. 1998. Technical report PSW GTR-168. Albany, CA, Pacific Southwest Research Station, Forest Service, USDA. 81-85.

López-Tarazón, J.A. – Batalla, R.J. – Vericat, D. – Balasch, J.C. (2010): Rainfall, runoff and sediment transport relations in a mesoscale mountainous catchment: The River Isábena (Ebro Basin). Catena 82: 23-34.

Lu, D. – Li, G. – Valladares, G.S. – Batistella, M. (2004): Mapping soil erosion risk in Rondonia, Brazilian Amazonia: Using RUSLE, remote sensing and GIS. Land Degrad. Develop. 15: 499-512.

Luce, C.H. – Black, T.A. (1999): Sediment production from forest roads in Western Oregon. Water Resour. Res. 35 (8): 2561-2570.

Ma, J. (2001): Combining the USLE and GIS/ArcView for Soil Erosion Estimation in Fall Creek Watershed in Ithaca, New York. CSS620- Spatial Modeling and Analysis. Online: http://www.docstoc.com/docs/52400644/Combining-the-USLE-and-GISArcView-for-Soil-Erosion-Estimation (Access date: 02.12.2011)

Ma, J.W. – Xue, Y. – Ma, C.F. – Wang, Z.G. (2003): A data fusion approach for soil erosion monitoring in the Upper Yangtze River Basin of China based on Universal Soil Loss Equation (USLE) model. Int. J. Remote Sensing 24 (23): 4777-4789.

MacDonald, L.H. – Sampson, R.W. – Anderson, D.M. (2001): Runoff and road erosion at the plot and road segment scales, St John, US Virgin Islands. Earth Surf. Proc. Land. 26: 251-272.

Márkus, B. – Wojtaszek, M. (1993a): A talajerózió becslése [Soil erosion estimation]. Vízügyi Közlemények 75 (2): 192-200.

Márkus, B. – Wojtaszek, M. (1993b): Estimation of soil erosion using USLE and applying ARC/INFO and remote sensing. BME Newsletter, Budapest.

Marosi, S. – Somogyi, S. (ed.) (1990): Magyarország kistájainak katasztere. [Cadastre of the Hungarian regions.] MTA Földrajztudományi Kutatóintézet. Budapest, Hungary. 379-390 ps. (in Hungarian)

Martin, A. – Gunter, J.T. – Regens, J.L. (2003): Estimating erosion in a riverine watershed Bayou Liberty-Tchefuncta River in Louisiana. Environ. Sci. & Pollut. Res. 10 (4): 245-250.

Marttila, H. – Klove, B. (2010): Dynamics of erosion and suspended sediment transport from drained peatland forestry. J. Hydrol. 388: 414-425.

Megahan W.F. (1982): Channel sediment storage behind obstructions in forested drainage basins draining the granitic bedrock of the Idaho Batholith. In: Edmonds R.L. (ed.): Analysis of coniferous forest ecosystems in the Western United States. Hutchinson Ross, Stroudsburg, Pennsylvania. 114-121 ps.

Mizuyama, T. – Egashira, S. (2010): Sediment induced disasters in the world and 1999-debris flow disasters in Venezuela. Journal of Disaster Research 5 (3): 229-235.

Moog, D.B. – Whiting, P.J. (1998): Annual hysteresis in bed load rating curves. Water Resour. Res. 34 (9): 2393-2399.

Moore, I. – Burch, G. (1986): Physical basis of the length-slope factor in the universal soil loss equation. Soil. Sci. Soc. Am. J. 50: 1294-1298.

Morehead, M.D. – Syvitski, J.P. – Hutton, E.W.H. – Peckham S.D. (2003): Modeling the temporal variability in the flux of sediment from ungauged river basins. Global Planet. Change 39: 95-110.

Mosimann, T. – Sanders, S. – Brunotte, J. (2007): Erosionsminderung in Fahrgassen – Wirkung der Intervallbegrünung in Weizen und Zuckerrüben bei verschiedenen Bodenbearbeitungsverfahren. [Erosion reduction in tractor tracks – The effects of intermittent planting in tractor tracks of wheat and sugar beet fields with different soil cultivation.] Pflanzenbauwissenschaften 11 (2): 57-66.

Nadal-Romero, E. – Regüés, D. – Latron, J. (2008): Relationships among rainfall, runoff and suspended sediment in a small catchment with badlands. Catena 74: 127-136.

Nakamura, F. – Swanson, F.J. (1993): Effects of coarse woody debris on morphology and sediment storage of a mountain stream system in Western Oregon. Earth Surf. Proc. Land. 18: 43-61.

Nearing, M.A. – Foster, G.R. – Lane, L.J. – Finkner, S.C. (1989): A process-based soil erosion model for USDA-Water Erosion Prediction Project technology. Transactions of the ASAE 32 (5): 1587-1593.

Nistor, C.J. – Church, M. (2005): Suspended sediment transport regime in a debris-flow gully on Vancouver Islands, British Columbia. Hydrol. Process. 19: 861-885.

Nováky, B. (2001): A TIM eróziós mérőpontok észleléseinek elemzése és értékelése. [Analysis and assessment of the observations on erosion sampling points of the National Information and Monitoring System for Soil Protection.] In: Dormány, G. – Kovács, F. – Péti, M. – Rakonczai, J. (eds.): A földrajz eredményei az új évezred küszöbén, Magyar Földrajzi Konferencia. SZTE-TTK Természeti Földrajzi és Geoinformatikai Tanszék, Szeged. ps. 14. (in Hungarian)

Onyando, J.O. – Kisoyan, P. – Chemelil, M.C. (2005): Estimation of Potential Soil Erosion for River Perkerra Catchment in Kenya. Water Resour. Manage. 19: 133-143.

Owens, P.N. – Collins, A.J. (ed.) (2006): Soil erosion and sediment redistribution in river catchments – Measurement, modelling and management. CAB International, NSRI Cranfield University. 1-50 ps.

Pandey, A. – Chowdary, V.M. – Mal, B.C. (2007): Identification of critical erosion prone areas in the small agricultural watershed using USLE, GIS and remote sensing. Water Resour. Manage. 21: 729-746.

Parameter catalogue for Saxony (1996): Parameterkatalog Sachsen. In: EROSION 2D/3D – Ein Computermodell zur Simulation der Bodenerosion durch Wasser. [In: EROSION-2D/3D – A computer model for simulation of soil erosion by water.] Sächsische Landesanstalt für Landwirtschaft. Dresden, Germany. (in German)

Pfaff, R.M. – Glennon, J.A. (2004): Building a groundwater protection model. ArcUser July-September 2004: 54-59.

Rácz, J. (1985): Erdővel borított lejtős területek ellenállása az erózióval szemben. [Soil erosion resistance of forested sloping areas.] In: Proceedings of the conference "The economical management of sloping areas". Gödöllő, Hungary. 1985. 196-200. (in Hungarian)

Reiczigel, J. – Harnos, A. – Solymosi, N. (2007): Biostatisztika nem statisztikusoknak. [Biostatistics for non-statisticians.] Pars Kft., Budapest. 241-290 ps.

Richards, K. (1984): Some observations on suspended sediment dynamics in Storbregrova, Jotunheimen. Earth Surf. Proc. Land. 9: 101-112.

Risse, L.M. – Nearing, M.A. – Nicks, A.D. – Laflen, J.M. (1993): Error assessment in the Universal Soil Loss Equation. Soil Sci. Soc. Am. J. 57 (3): 825-833.

Rodríguez-Blanco, M.L. – Taboada-Castro, M.M. – Taboada-Castro, M.T. – Oropeza-Mota, J.L. (2009a): Nutrient dynamics during storm events in an agroforestry catchment. Commun. Soil Sci. Plan. 40 (1): 889-900.

Rodríguez-Blanco, M.L. – Taboada-Castro, M.M. – Diéguez-Villar, A. – Taboada-Castro, M.T. (2009b): Metal fluxes from soils to surface waters at the catchment scale. Commun. Soil Sci. Plan. 40 (1): 313-326.

Rodríguez-Blanco, M.L. – Taboada-Castro, M.M. – Palleiro, L. – Taboada-Castro, M.T. (2010a): Temporal changes in suspended sediment transport in an Atlantic catchment NW Spain. Geomorphology 123: 181-188.

Rodríguez-Blanco, M.L. – Taboada-Castro, M.M. – Taboada-Castro, M.T. (2010b): Factors controlling hydro-sedimentary response during runoff events in a rural catchment in the humid Spanish zone. Catena 82: 206-217.

Sadhegi, S.H.R. – Mizuyama, T. – Miyata, S. – Gomi, T. – Kosugi, K. – Fukushima, T. – Mizugaki S. – Onda, Y. (2008): Determinant factors of sediment graphs and rating loops in a reforested watershed. J. Hydrol. 356: 271-282.

Salamin, P. (1982): Erózió elleni küzdelem és környezetvédelem. [Soil erosion and environmental protection.] Budapesti Műszaki Egyetem Mérnöki Továbbképző Intézet, Budapest. 21-112 ps. (in Hungarian)

Salant, N.L. – Hassan, M.A. – Alonso, C.V. (2008): Suspended sediment dynamics at high and low storm flows in two small watershed. Hydrol. Process. 22: 1573-1587.

Schmidt, J. – von Werner, M. – Michael, A. (1999): Application of the EROSION 3D model to the CATSOP watershed, The Netherlands. Catena 37: 449-456.

Schwertmann, U. – Vogl, W. – Kainz, M. – Auerswald, K. – Martin, W. (1987): Bodenerosion durch Wasser: Vorhersage des Abtrags und Bewertung von Gegenmaßnahmen. Ulmer, Stuttgart. 9-36 ps.

Shen, H.W. – Julien, P.Y. (1993): Erosion and sediment transport. In: Maidment, D.R. (ed.): Handbook of hydrology. McGraw-Hill. 12.1-12.61 ps.

Shieh, C.-L. – Wang C.-M. – Chen, Y.-S. – Tsai, Y.-J. – Tseng, W.-H. (2010): An overview of disasters resulted from Typhoon Morakot in Taiwan. Journal of Disaster Research 5 (3): 236-244.

Sorriso-Valvo, M. – Bryan, R.B. – Yair, A. – Iovino, F. – Antronico, L. (1995): Impact of afforestation on hydrological response and sediment production in small Calabrian catchment. Catena 25: 89-104.

Stefanovits, P. (1964): Talajpusztulás Magyarországon – Magyarázatok Magyarország eróziós térképéhez [Soil erosion in Hungary – Explanations to the erosion map of Hungary.] OMMI, Budapest, Genetikus talajtérképek 1 (7): ps. 58. (in Hungarian)

Stefanovits, P. – Filep, Gy. – Füleky, Gy. (1999): Talajtan. [Pedology.] Mezőgazda Kiadó, Budapest.

Stone, R.P. – Hilborn, D. (2000): Universal Soil Loss Equation (USLE). Series: Factsheet No. 00-001 AGDEX 572/751. Agricultural Engineering, Ministry of Agriculture, Food and Rural Affairs, Ontario. May 2000.

Stott, T. – Leeks, G. – Marks, S. – Sawyer, A. (2001): Environmentally sensitive plot-scale timber harvesting: Impacts on suspended sediment, bedload and bank erosion dynamics. J. Environ. Manage. 63: 3-25.

Surfleet, C.G. – Ziemer, R.R. (1996): Effects of forest harvesting on large organic debris in coastal streams. In: Proceedings of the "Conference on coast redwood forest ecology and management". Arcata, CA, Berkeley, CA, University of California. 18-20. June 1996. 134-136.

Syvitski, J.P.M. – Alcott, J.M. (1995): RIVER3: Simulation of river discharge and sediment transport. Comput. Geosci. 21 (1): 89-151.

Syvitski, J.P. – Morehead, M.D. – Nicholson, M. (1998): HYDROTREND: A climate-driven hydrologic-transport model for predicting discharge and sediment load to lakes or oceans. Comput. Geosci. 24 (1): 51-68.

Szabó, L. (1995): Az erózió mértékének meghatározása Délnyugat Afrikában Angola példáján. [Determination of soil erosion rate in SW Africa on the example of Angola.] Agrokémia és Talajtan 44 (3-4): 563-572. (in Hungarian)

Tetra Tech Inc. (2007): Limberlost Creek Watershed sediment and nutrient TMDL development. Indiana Department of Environmental Management. 1-38.

Thomas, R.B. (1985): Measuring suspended sediment in small mountain streams. In: General Technical Report, USDA Forest Service, Pacific Southwest Forest and Range Experiment Station. 1-9 ps.

Thyll, Sz. (ed.) (1992): Talajvédelem és vízrendezés dombvidéken. [Soil protection and melioration in hilly regions.] Mezőgazda Kiadó, Budapest. 11-64 ps. (in Hungarian)

Újvári, F. (1981): Az erdők szerepének értékelése a vízgyűjtő területek hordalék-lemosódásának megakadályozásában. [Assessment of the soil protection role of forests in the catchment areas.] Erdészeti Kutatások 74: 107-124. (in Hungarian)

US EPA (2009): Water models / Barton Springs Salamander – Meadow. US Environmental Protection Agency. Online: http://www.epa.gov/oppefed1/models/water/bs_meadow.htm (Access date: 30.05.2010)

Xu, K. – Chen, Z. – Zhao, Y. – Wang, Z. – Zhang, J. – Hayashi, S. – Murakami, S. – Watanabe M. (2005): Simulated sediment flux during 1998 big-flood of the Yangtze (Changjiang) River, China. J. Hydrol. 313: 221-233.

Van Remortel, R.D. – Hamilton, M. – Hickey, R.J. (2001): Estimating the LS factor for RUSLE through iterative slope length processing of digital elevation data. Cartography 30 (1): 27-35.

Van Remortel, R.D. – Maichle, R.W. – Hickey, R.J. (2004): Computing the LS factor for the Revised Universal Soil Loss Equation through array-based slope processing of digital elevation data using a C++ executable. Comput. Geosci. 30: 1043-1053.

Van Sickle, J. – Beschta, R.L. (1983): Supply-based models of suspended sediment transport in streams. Water Resour. Res. 19 (3): 768-778.

Várallyai, Gy. (ed.) (1992): Országos Talajvédelmi Információs és Monitoring Rendszer kialakításának megalapozása [Establishing of the development of National Information and Monitoring System for Soil Protection.] Földművelésügyi Minisztérium, Budapest. (in Hungarian)

Vinet, F. (2008): Geographical analysis of damage due to flash floods in southern France: The cases of 12–13 November 1999 and 8–9 September 2002. Appl. Geogr. 28 (4): 323-336.

von Werner (1995): GIS-orientierte Methoden der digitalen Reliefanalyse zur Modellierung von Bodenerosion in kleinen Einzugsgebieten. [GIS-based methods of the digital relief analysis for soil erosion modelling in small catchments.] PhD thesis. Freie Universität Berlin. (in German)

Walling, D.E. (1983): The sediment delivery problem. J. Hydrol. 65: 209-237.

Walling, D.E. – Webb, B.W. (1982): Sediment availability and the prediction of storm-period sediment yields. In: Proceedings of the Exeter Symposium "Recent Developments in the Explanation and Prediction of Erosion and Sediment Yield". July 1982. IAHS Publ. 137: 327-337.

Williams, G.P. (1989): Sediment concentration versus water discharge during single hydrologic events in rivers. J. Hydrol. 111: 89-106.

Wischmeier, W.H. – Smith, D.D. (1978): Predicting rainfall erosion losses – A guide to conservation planning. In: Agriculture Handbook 537. USDA, Washington DC. 3-4 ps.

Zabaleta, A. – Martínez, M. – Uriarte, J.A. – Antigüedad, I. (2007): Factors controlling suspended sediment yield during runoff events in small headwater catchments of the Basque Country. Catena 71: 179-190.

Internet references:

URL1: http://www.vasnepe.hu/cimlapon/20090624_arvizveszely_ronok_es_koszeghegyalja (Access date: 22.03.2012)

URL2: http://www.teol.hu/tolna/kozelet/iteletido-sarlavina-zudult-a-falvakra-fotok-391145 (Access date: 22.03.2012)

URL3: http://www.bbc.co.uk/news/world-europe-19767627 (Access date: 31.01.2014)

URL4: http://www.cms.fu-berlin.de/geo/fb/e-learning/geolearning/en/soil_erosion/types/ (Access date: 16.10.2012)

URL5: http://imnh.isu.edu/digitalatlas/geo/basics/massmvnt.htm (Access date: 16.10.2013.)

URL6: http://www.medcalc.org/manual/correlation.php (Access date: 02.02.2014.)

URL7: http://www.medcalc.org/manual/multiple_regression.php (Access date: 02.02.2014.)

URL8: http://www.statsoft.com/Textbook/Principal-Components-Factor-Analysis (Access date: 02.02.2014.)

URL9: http://www.yorku.ca/ptryfos/f1400.pdf (Access date: 02.02.2014.)

List of figures

Figure 1.1. Model structure of the EROSION-3D (from *Kitka* 2009)
Figure 1.2. Classification of the transported material in streams (from *Gordon et al.* 2004)
Figure 1.3. Channel bed features contributing to the postponement of bedload yield: pool-riffle sequences, armouring and imbrication (from *Gordon et al.* 2004)
Figure 1.4. Basis types of the relationship between suspended sediment concentration and discharge during a single flood event (from *Williams* 1989)
Figure 1.5. Conceptual flow chart of the major pathways through which forestry activities affect the stream sediment delivery (from *Lewis* 1998)
Figure 1.6. Sediment retention behind log jam in a forested catchment (Sopron Hills)
Figure 1.7. Erosion processes in forested catchments: soil loss from an unpaved forest road and mass movement (Sopron Hills)

Figure 3.1. Catchment of the Rák Brook with settlements, gauging stations and subcatchments belonging to the stream gauging stations
Figure 3.2. The Farkas Valley and the Vadkan Valley with the location of gauging stations
Figure 3.3. The central meteorological station and the tipping bucket rain gauges in front of the main research building in the Hidegvíz Valley
Figure 3.4. Stream gauging station at the outlet of the Farkas Valley and the Vadkan Valley
Figure 3.5. Method of the flood wave separation according to Kontur et al. (2003) – example of the flood event 15.10.2010 in the Farkas Valley
Figure 3.6. The process of gathering *SSC* data: water sampling, filtering, drying and weighing of the filter papers
Figure 3.7. The outwashed sediment deposit and GPS-survey at a shallow landslide
Figure 3.8. Conceptual flow chart for determining the USLE factors
Figure 3.9. Surface soil sampling in the Farkas Valley, pounding the soil samples and analysis of particle size distribution using Köhn pipette

Figure 4.1. Physical soil texture of the upper soil layer and the spatial distribution of *K* factor in the Farkas Valley
Figure 4.2. Precipitation categories and number of precipitation events according to the records of "$_{hhm}$" rain gauge and "$_{c1}$" rain gauge
Figure 4.3. Seasonal distribution of the precipitation categories according to the records of "$_{hhm}$" rain gauge
Figure 4.4. Boxplots of the suspended sediment concentration in different flow categories in the Farkas Valley and Vadkan Valley
Figure 4.5. Seasonal variability of the average *SSC* in different low flow categories in the Farkas Valley and in the Vadkan Valley
Figure 4.6. Boxplots of the suspended sediment concentration at low flow for the hydrological years in the Farkas Valley and Vadkan Valley
Figure 4.7. Log-log plot of suspended sediment concentration against discharge at low flow for the entire study period in the Farkas Valley and the Vadkan Valley
Figure 4.8. Semi-log plot of suspended sediment concentration against antecedent days under low flow conditions for the entire study period in the Farkas Valley and the Vadkan Valley

Figure 4.9. Semi-log plot of suspended sediment concentration against water temperature under low flow conditions for the entire study period in the Farkas Valley and the Vadkan Valley
Figure 4.10. Log-log plot of suspended sediment concentration against discharge at high flow for the entire study period in the Farkas Valley and the Vadkan Valley
Figure 4.11. Scatterplot of *SSC* against $API3_{hhm}$ at different flood events in the Farkas Valley
Figure 4.12. Semi-log plot of suspended sediment concentration against antecedent precipitation of 1-day and semi-log plot of *SSC* against soil temperature at 0cm depth at the flood event 18.07.2009 in the Farkas Valley
Figure 4.13. Semi-log plot of *SSC* against $API1_{c1}$ at the descending limb of flood event 04.08.2009 in the Farkas Valley and the Vadkan Valley
Figure 4.14. The hydrograph, the sedigraph and the rainfall data and the *SSC-Q* relationship during the flood event in the Vadkan Valley on 18th July 2009
Figure 4.15. The hydrograph, the sedigraph and the rainfall data and the *SSC-Q* relationship during the flood event in the Farkas Valley on 18th July 2009
Figure 4.16. The hydrograph, the sedigraph and the rainfall data and the *SSC-Q* relationship (right) during the flood event in the Vadkan Valley on 4th August 2009
Figure 4.17. The hydrograph, the sedigraph and the rainfall data and the *SSC-Q* relationship (right) during the flood event in the Farkas Valley on 4th August 2009
Figure 4.18. High flow suspended sediment yield response to the hydrological parameter perturbations in the year 2008-2009 in the Farkas Valley
Figure 4.19. Suspended sediment yield response to the hydrological parameter perturbations at the flood waves on 18.07.2009 and 04.08.2009 in the Farkas Valley and the Vadkan Valley
Figure 4.20. Double mass curve of bedload yield against the discharge from January 2006 to October 2009 in the Farkas Valley
Figure 4.21. Double mass curve of bedload yield and discharge against the rainfall depth between January 2006 and October 2009 in the Farkas Valley
Figure 4.22. Conceptual flow chart of the first submodel "*Relief analysis*"
Figure 4.23. Conceptual flow chart of the second submodel "*Soil and land cover*"
Figure 4.24. Conceptual flow chart of the third submodel "*Soil loss and statistics*"
Figure 4.25. The raster map of modelled soil erosion and polygons after conversion
Figure 4.26. Percent area of the soil loss categories
Figure 4.27. Average and total surface soil loss with the average *LS* factor at each land use unit
Figure 4.28. Changes of total soil loss in case of minimum or maximum USLE factor values
Figure 4.29. Erosion-accumulation risk during the rainfall event on 27-29.01.2009
Figure 4.30. Erosion-accumulation risk during the rainfall event on 18.07.2009
Figure 4.31. Area endangered by erosion as a function of maximal 1-hour precipitation

List of tables

Table 2.1. Main objectives of the dissertation and the applied methods

Table 3.1. Characteristic physical parameters of the two catchments (after the modification of the table by *Gribovszki et al.* (2006))
Table 3.2. Percentual distribution of the soil groups in the Farkas Valley and the Vadkan Valley
Table 3.3. The main descriptive *Q* values in the Farkas Valley based on the automatic *h*-records

Table 4.1. Rainfall events with high *EI* from the years 2008-2010 based on the "$_{hhm}$" rain gauge
Table 4.2. Seasonal fluctuation of the descriptive statistical variables of the rainfall parameters in the hydrological year 2008-2009 based on the "$_{hhm}$" rain gauge
Table 4.3. Descriptive statistical variables of the flood parameters for the entire study period and at seasonal scale
Table 4.4. Descriptive statistical variables of suspended sediment concentration and its control factors at high flow for the entire study period
Table 4.5. Correlation coefficients between the suspended sediment concentration data under low flow conditions and the sediment control variables for the entire study period
Table 4.6. Significant correlations between suspended sediment concentration at low flow and sediment control variables at seasonal scale
Table 4.7. Significant correlations between suspended sediment concentration at high flow and sediment control variables at different temporal scale
Table 4.8. Suspended sediment yield in the hydrological year 2008-2009
Table 4.9. Sediment yield during the two flood events in the Farkas Valley and the Vadkan Valley
Table 4.10. The factors of USLE and the predicted soil loss by surface erosion
Table 4.11. Correlation coefficients between soil loss and the USLE factors in case of land use units

Annex

Annex I.III

Annex I.III.1. Examples of different types of soil erosion models (from Kitka 2009)

Model	Reference	Spatial resolution	Temporal resolution	GIS Interface	Calculation method
USLE	Wischmeier & Smith 1987	Plot	Continuous	No or ArcInfo	Empirical
RUSLE	Renard et.al. 1991	Plot	Continuous	No	Empirical
MUSLE87	Bork & Hensel 1988	Watershed	Continuous	No	Empirical
dUSLE	Flacke et.al.1990	Watershed	Continuous	No	Empirical
AGNPS	Young et. al. 1987	Watershed	Event-based	GRASS System	Empirical
CREAMS	Knisel 1980	Watershed	Integrated events	No	Theoretical
EPIC	Williams 1997	Plot	Integrated events	GRASS System	Empirical
WEPP	Nearing et al. 1989	Slope	Event-based	ArcInfo	Physical
ANSWER	Beasly & Huggins 1982	Watershed	Event-based	GRASS System	Physical
OPUS	Diekkrüger et.al 1991	Plot	Event-based	Yes	Physical
PEPP	Schramm 1994	Slope	Event-based	No	Physical
KINEROS	Woolhiser et al.1990	Watershed	Event-based	GRASS System	Physical
EUROSEM	Morgan et al. 1998	Watershed/plot	Event-based	ArcInfo	Physical
LISEM	De Roo et al. 1996	Watershed	Event-based	Yes	Physical
SWAT	Arnold 1998	Watershed	Continuous	Arc/Info, Arc View, GRASS	Physical
GUESS	Roese et al. 1983	Plot	Event-based/annual		Mathematical
MEDRUSH	Kirkby 1992	Watershed	1 hour–100 years	GRASS System	Empirical
EROSION 3D	Von Werner 1995	Small catchment	Event-based	ArcInfo, ArcView	Physical

Annex I.IV

Annex I.IV.1. Bedload equations

The *Meyer-Peter & Müller bedload formula* (1948) simplified by *Chien* (1956, in *Julien* 2010) is based on the median size of the surface layer of the bed material. This equation is most appropriate for channels with large width-depth ratios.

$$q_{bv} = 8 \cdot (\tau * - 0.047)^{3/2} \cdot \sqrt{(G-1) \cdot g d_s^3} \,. \qquad (Eq.\ I.IV.1)$$

In *Eq. I.IV.1* G is the specific gravity (*dimensionless*); τ^* is the dimensionless shear stress, called Shields parameter, which is equal to the ratio of active horizontal force and passive vertical force acting on a non-cohesive sediment particle:

$$\tau * = \frac{\tau_0}{(\gamma_s - \gamma_m) \cdot d_s} = \frac{\rho_m \cdot u_*^2}{(\gamma_s - \gamma_m) \cdot d_s} \text{, where} \qquad (Eq.\ I.IV.2)$$

γ_m is the specific weight of the fluid mixture ($N \cdot m^{-3}$); ρ_m is the density of the water-sediment mixture ($kg \cdot m^{-3}$); u^* is the shear velocity ($m \cdot s^{-1}$).

Another idea for the bedload transport derives from *Einstein* (1942, in *Julien* 2010), who said that grains move in steps proportional to their size. Based on probability concepts, the gravel sediment discharge q_{bv} per unit width and time is transformed into a dimensionless volumetric unit sediment discharge q_{bv*} as:

$$q_{bv} * = \frac{q_{bv}}{\omega_0 \cdot d_s} = \frac{q_{bv}}{\sqrt{(G-1) \cdot g \cdot d_s^3} \left\{ \sqrt{\frac{2}{3} + \frac{36 \cdot \nu^2}{(G-1) \cdot g \cdot d_s^3}} - \sqrt{\frac{36 \cdot \nu^2}{(G-1) \cdot g \cdot d_s^3}} \right\}} \,. \qquad (Eq.\ I.IV.3)$$

In *Eq. I.IV.3* ω_0 is the Rubey's clear-water fall velocity. The dimensionless rate of sediment transport can be plotted as a function of the Shields parameter. Brown (1950, in *Julien* 2010) suggested the following relationships:

- if $\tau^* < 0.18$: $q_{bv*} = 2.15 \cdot e^{-0.391/\tau *}$,
- if $0.18 < \tau^* < 0.52$: $q_{bv*} = 40 \cdot \tau_*^3$.

Due to the usually very steep slope of the sediment rating curve, bedload yield rapidly becomes negligible at low flow ($0.1 < \tau^* < 1.0$). In this flow domain, an approximation was given by *Julien* (2002 in *Julien* 2010) for bedload yield:

- if $0.1 < \tau^* < 1.0$: $q_{bv*} \cong 18 \cdot \sqrt{g \cdot d_s^3} \tau_*^2$.

Annex I.V

Annex I.V.1. Concepts of storm runoff mechanisms (theory of Horton and Dunne)

Infiltration excess overland flow is sometimes associated with the name of *Horton* (Hortonian overland flow). This type of flow occurs when the rainfall rate is larger than the infiltration rate over the entire catchment, thus there is an excess which runs off over the surface (*Horton* 1933, in *Brutsaert* 2005). Based on this concept, all stormflow results from the overland flow of precipitation excess where the infiltration capacity is subtracted from the precipitation. Infiltration excess overland flow primarily occurs in catchments with relatively impermeable surfaces (e.g. rocky or stony areas with thin soil layer, paved urban areas). Moreover its prevalence depends on the rainfall intensity as well. Therefore, this concept is well applicable to determine the maximal rate of runoff under extremely heavy rainfall events.

Saturation excess overland flow occurs over land surfaces that are saturated by emerging subsurface outflow from below and perched water tables (*Brutsaert* 2005). Thus, the role of rainfall intensity can be neglected at the generation of this flow type, but antecedent precipitation conditions are determinant (*López-Tarazón et al.* 2010). This mechanism is most often observed over limited areas of the catchment. The measurements of *Dunne és Black* (1970, in *Brutsaert* 2005) also confirms that the stormflow originated from surface flow on limited areas along the stream channel.

Annex III.I

Annex III.I.1. Slope conditions in the Vadkan Valley and the Farkas Valley

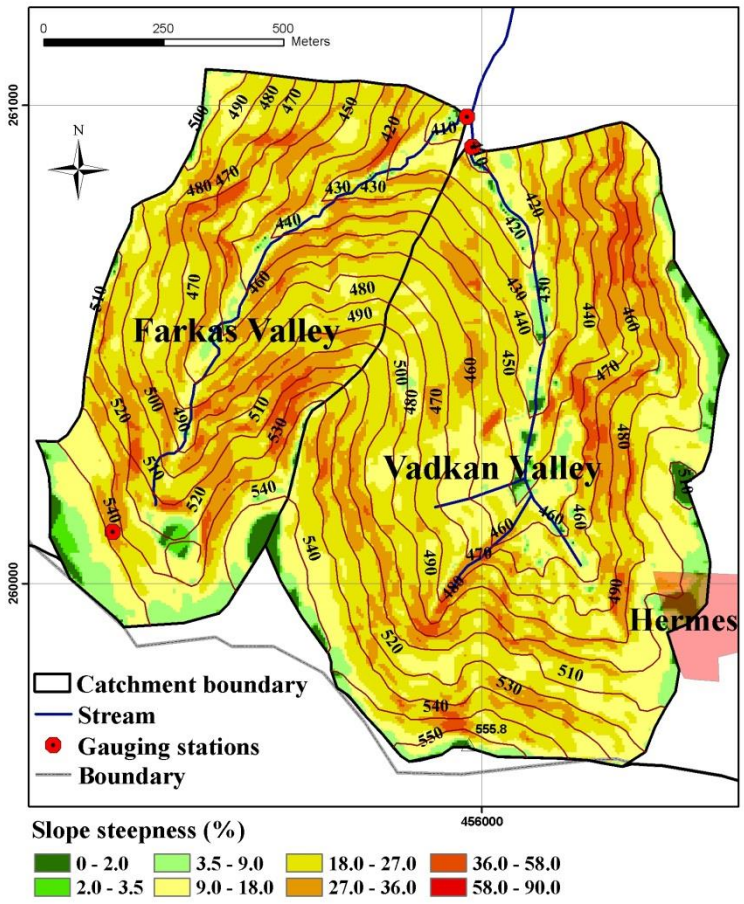

10.13147/NYME.2014.014

Annex III.I.2/a. Forestry activities in the Farkas Valley and Vadkan Valley from 1999 to 2010 (from the Forestry management plan 1994 and 2004)

Year	Subcompartment	Tree utilization method	Total area	Effected area	Reduced area	Jan	Feb	Mar	Apr	May	Jun	Jul	Aug	Sep	Oct	Nov	Dec
1999	166D	TKGY	1.1	0.2											0.2		
1999	169F	TKGY	4.5	4.5												4.5	
1999	161E	NFGY	1.1	1.1				1.1									
1999	169A	NFGY	7.3	7.3					1.5	0.5	1.5		0.5	3.3			
2000	163B	TRV	10.6	4		0.3	1.5	0.2						0.8	1.2		
2000	173B	FVB	7.1	7.1	2.1			(0.9) 4.7								0.4	1.7
2000	163A	NFGY	7.9	6.5													4
2000	163C	NFGY	2.7	2.7													2.7
2000	163E	NFGY	3.3	3.3												2.5	0.8
2000	167A	TI	1.2	1.2													
2000	167B	TI	1.5	1.5													
2000	167C	TI	3.3	3.3													
2000	167E	TI	7.3	7.3													
2001	163A	NFGY	7.9	2.5		1.3	1.2										
2001	162A	TRV	6.3	3		1.1	1.2	0.5	0.2								
2001	167F	TRV	7.5	2					0.4						0.7	0.6	0.3
2001	171A	TRV	2.3	1.6		1	0.6										
2001	171B	FVB	3.4	3.4	1	0.3	0.6		0.1								
2001	161A	NFGY	9.6	9.6									0.6	8	1		
2001	165A	NFGY	16.7	5.7									2	1	1	1.7	
2001	167G	NFGY	3.9	3.9												0.5	
2001	171C	TKGY	2.7	2.5													
2002	162A	TI			2.2			2.2									
2002	162A	EÜ						X									
2002	166D	TI			0.9											0.9	
2002	167D	EÜ										X					
2002	167G	NFGY			2.4					X	X						
2002	168A	NFGY			2.3								2.3				
2002	169A	EÜ										X					
2002	169B	NFGY			5.9									5.9			
2002	169C	NFGY			7					7							
2002	171E	NFGY			1.7								1.7				
2002	171F	NFGY			2.1									2.1			

Year	Subcompartment	Tree utilization method	Total area	Effected area	Reduced area	Jan	Feb	Mar	Apr	May	Jun	Jul	Aug	Sep	Oct	Nov	Dec
2002	171H	EÜ										X					
2003	163B	TRV	10.6	1	1		1										
2003	161C	NFGY	0.5	0.5	0.5	X	X										
2003	169E	NFGY	0.9	0.9	0.9										0.9		
2003	171I	NFGY	3.8	2.5	2.5								2.5				
2004	163F	TRV	7.1	1.5			0.3	0.5	0.2	0.1	0.1						0.3
2004	167D	TRV	4.8	2.4													
2004	169A	TRV	7.3	0.8			0.2		0.6								
2004	173B	FVB	7.1	3	0.7		0.2	0.1									
2004	161H	TKGY	2.3	2.3										2.3			
2004	169F	TKGY	4.5	4.5													
2004	170D	TKGY	4.8	4.8						4.8							
2004	171J	TKGY	4.2	4.2						3.2				1			
2005	169F	TRV		0.6										0.6			
2005	163B	TRV	3.8	1.5			0.4	0.6	1.5								
2005	169G	TRV		0.5												0.3	0.2
2005	167C	TRV	4	2.2			1.1	0.6	0.5								
2005	171C	TRV		0.6										0.6			
2005	167F	FVB	6.1	6.1	1.4							0.7	0.2	0.1			0.4
2005	174C	FVB	7.7	7.7	2.4						1					0.3	
2005	163O	NFGY	2.1	2.1								0.5				1.6	
2005	171O	TKGY	2.4	2.4											2.4		
2005	171G	TKGY	2.1	2.1										2.1			
2006	166C	FVB	3.1	3.1	1.5										0.7	0.8	
2006	167F	FVB	6.1	1.6	0.5											0.1	0.4
2006	174C	FVB	7.7	6.5	2									0.2		1.2	0.6
2007	171H	TRV		1.2					0.6	0.6							
2007	161A	FVB	3.2	3.2	1.1	1.1											
2007	170B	FVB	1.4	1.4	0.4		0.4										
2007	170E	FVB	4.4	4.4	0.9	0.9											
2007	163G	NFGY	2.6	2.6									2	0.6			
2007	169E	NFGY	4	4										1.5			
2007	167D	TKGY	7.3	7.3										1	1		2
2008	169A	TRV		0.7													0.7

Year	Subcompartment	Tree utilization method	Total area	Effected area	Reduced area	Jan	Feb	Mar	Apr	May	Jun	Jul	Aug	Sep	Oct	Nov	Dec
2008	169G	NFGY	4	3.5											0.5		1.1
2008	166E	TKGY	1.3	1.3									1		0.3		
2008	167B	TKGY	1.6	1.6									1		0.4	0.2	
2008	168C	TKGY	2.9	2.9													
2009	161C	FVB	5	5	1.56											1	0.56
2009	171B	FVB	3.3	3.3	0.58	0.2	0		0.38								-0.04
2009	173C	FVB	7	4	1.06							0.1	0.2	0.4		0.2	0.16
2009	168A	TKGY	3.5	3.5					0.8						1		1.7
2009	168C	TKGY	2.9	2.9					0.8								2.1
2010	169B	NFGY	2.5	0.5						0.3			0.2				0.3

Annex III.I.2/b. Summary of the forestry activities in the Farkas Valley and Vadkan Valley from 2000 to 2010 (from the Forestry management plan 1994 and 2004)

	Farkas Valley							Vadkan Valley						
Date	TRV	FVB	NFGY	TKGY	TI	TRV+FVB	Total area	TRV	FVB	NFGY	TKGY	TI	TRV+FVB	Total area
2000	0.0	0.4	0.0	0.0	11.1	0.4	11.5	1.9	1.3	4.1	0.0	0.0	3.2	7.3
2001	3.5	1.0	1.5	2.5	3.1	4.5	11.6	2.9	3.4	0.2	0.0	4.8	6.3	11.3
2002	0.0	0.0	5.3	0.0	0.0	0.0	5.3	0.0	0.0	14.0	0.0	2.0	0.0	16.0
2003	0.0	0.0	0.0	0.0	0.0	0.0	0.0	0.0	0.0	0.0	0.0	0.0	0.0	0.0
2004	0.0	0.1	0.0	3.1	0.0	0.1	3.2	2.6	0.3	0.0	0.0	0.0	2.9	2.9
2005	2.7	1.4	0.0	4.5	0.0	4.2	8.7	1.9	4.5	2.1	0.0	1.2	6.4	9.7
2006	0.0	0.5	0.0	0.0	0.0	0.5	0.5	0.0	3.7	0.0	0.0	0.0	3.7	3.7
2007	1.2	0.0	0.0	1.9	0.0	1.2	3.1	0.0	0.0	6.6	0.0	9.3	0.0	15.9
2008	0.0	0.0	0.0	1.6	0.0	0.0	1.6	0.7	0.0	1.6	0.0	1.6	0.7	3.9

TRV: clear cutting; FVB: shelterwood cutting; NFGY: accretion thinning; TKGY: selection thinning; TI: cleaning cutting

Annex III.I.3. Land cover and land use units in the Farkas Valley

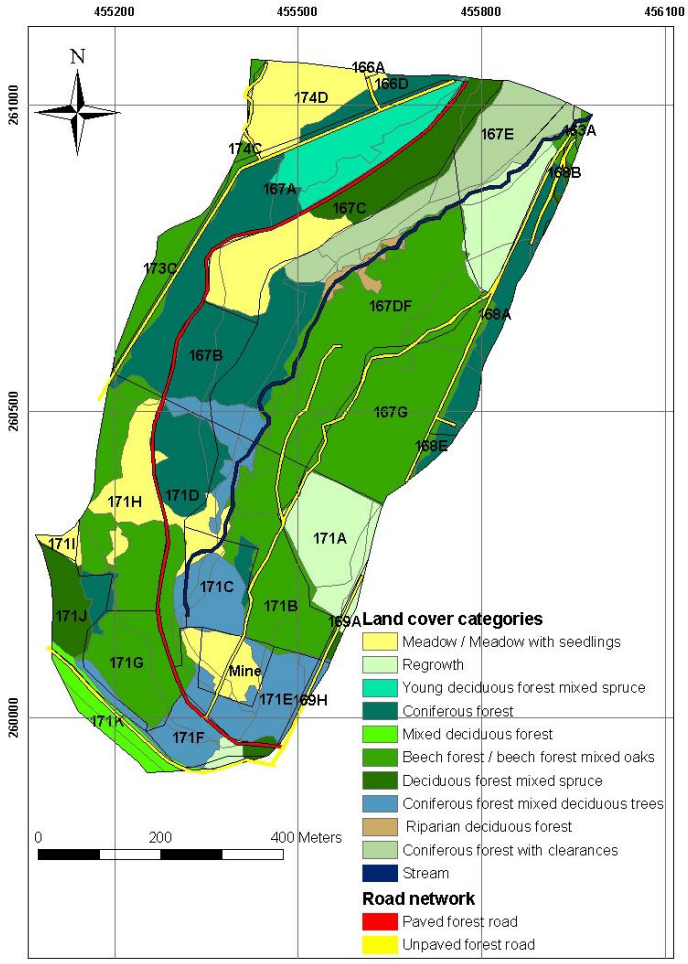

Annex III.III

Correlation analysis. This method is applied to "determine whether the values of two variables are associated. The two variables should be random samples (where the sample size *N* refers to the number of data pairs), and should have a Normal distribution" (*URL6*). Pearson correlation analysis is suitable to determine the linear relationship between two variables.

The *Pearson's correlation coefficient r* is a number between -1 and 1 which expresses "the degree that, on an average, two variables change correspondingly" (*URL6*). (If one variable increases when the second one increases, then there is a positive correlation. If one variable decreases when the other variable increases, then there is a negative correlation.) The relationship between two variables can easily be represented graphically by a scatter diagram (*Reiczigel et al.* 2007, *URL6*).

"The *p-value* is the probability that you would have found the current result if the correlation coefficient were in fact zero (null hypothesis). If this probability is lower than the conventional 5% (p<0.05) the correlation coefficient is called statistically significant" (*URL6*).

"When two variables are correlated, there may or may not be a causative connection, and this connection may moreover be indirect. Correlation can only be interpreted in terms of causation if the variables under investigation provide a logical basis for such interpretation.

95% *confidence interval* (*CI*) for the correlation coefficient: this is the range of values that contains with a 95% confidence the 'true' correlation coefficient" (*URL6*).

Multiple regression. "This statistical method is used to examine the relationship between one dependent variable y and one or more independent variables x_i. The regression parameters or coefficients b_i in the regression equation

$$y = b_0 + b_1 \cdot x_1 + b_2 \cdot x_2 + b_3 \cdot x_3 + \ldots + b_k \cdot x_k \qquad (Eq.\ III.III.1)$$

are estimated using the method of least squares. In this method, the sum of squared residuals between the regression plane and the observed values of the dependent variable are minimized. The regression equation represents a (hyper)plane in a k+1 dimensional space in which k is the number of independent variables x_1, x_2, x_3, ... x_k, plus one dimension for the dependent variable y" (*URL7*).

In the **stepwise multiple regression**, significant independent variables are entered sequentially into the model; after entering a variable in the model, the user have to check and possibly remove variables that became non-significant (*URL7*).

Coefficient of determination r^2 is the proportion of the variation in the dependent variable explained by the regression model, and is a measure of the goodness of model fitting. It ranges from 0 to 1, and is calculated as follows:

$$r^2 = \frac{explained variation}{total variation} = \frac{\sum (y_{est} - y)^2}{\sum (y - \bar{y})^2} \qquad (Eq.III.III.2)$$

where y are the observed values for the dependent variable, $\bar{y}$ is the average of the observed values and y_{est} are predicted values for the dependent variable calculated using the regression equation (*URL7*).

Residual standard deviation (*SD of res.*): the standard deviation of the residuals, where residuals are equal to the differences between observed and predicted values. It is calculated as follows (n is the sample size, the number of observed values) (*URL7*):

$$SD\ of\ res. = \sqrt{\frac{\sum (y - y_{est})^2}{n - k - 1}} \qquad (Eq.III.III.3)$$

Factor analysis. "The main applications of factor analytic techniques are to reduce the number of variables and to detect structure in the relationships between variables, that is to classify variables" (*URL8*). According to *URL9*, it is a useful "method for investigating whether a number of variables of interest (y_1, y_2, y_3, ...) are linearly related to a smaller number of unobservable factors (F_1, F_2, F_3, ...)".

The variances extracted by the factors are called the *eigenvalues*. The sum of the eigenvalues is equal to the number of variables. *Factor loadings* are the correlations between the variables of interest and the factors (or 'new' variables). We could plot the factor loadings in a scatterplot, where each variable is represented as a point. In this plot we could rotate the axes in any direction without changing the relative locations of the points to each other; however, the actual coordinates of the points, that is, the factor loadings would of course change. The goal of these rotational strategies is to obtain a clear pattern of loadings, that is, factors that are somehow clearly marked by high loadings for some variables and low loadings for others (*URL8*).

Mass curve (MC) **and double mass curve analysis** (DMC). A mass curve is a plot of cumulative values against time, while a double mass curve is a plot of cumulative values of one variable against the cumulation of another quantity during the same time period. The theory behind double mass curves is that by plotting the cumulation of two quantities the data will plot as a straight line, and the slope of

this line will represent the constant of proportionality between the two quantities. A break in slope indicates a change in the constant of proportionality (*Searcy & Hardison* 1960, in *Albert* 2004).

Annex III.V

Annex III.V.1. Spatial distribution of the LS factor (dimensionless) in the Farkas Valley

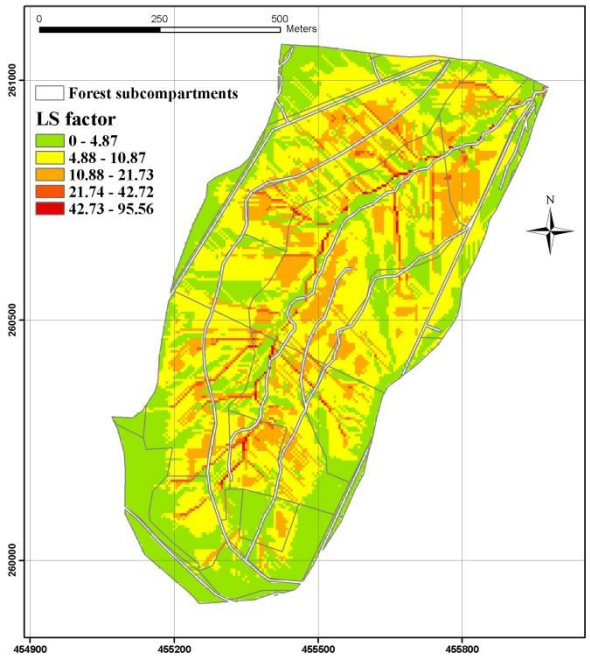

Annex III.V.2. Spatial distribution of the C factor (dimensionless) in the Farkas Valley (left)
Annex III.V.3. Spatial distribution of the P factor (dimensionless) in the Farkas Valley (right)

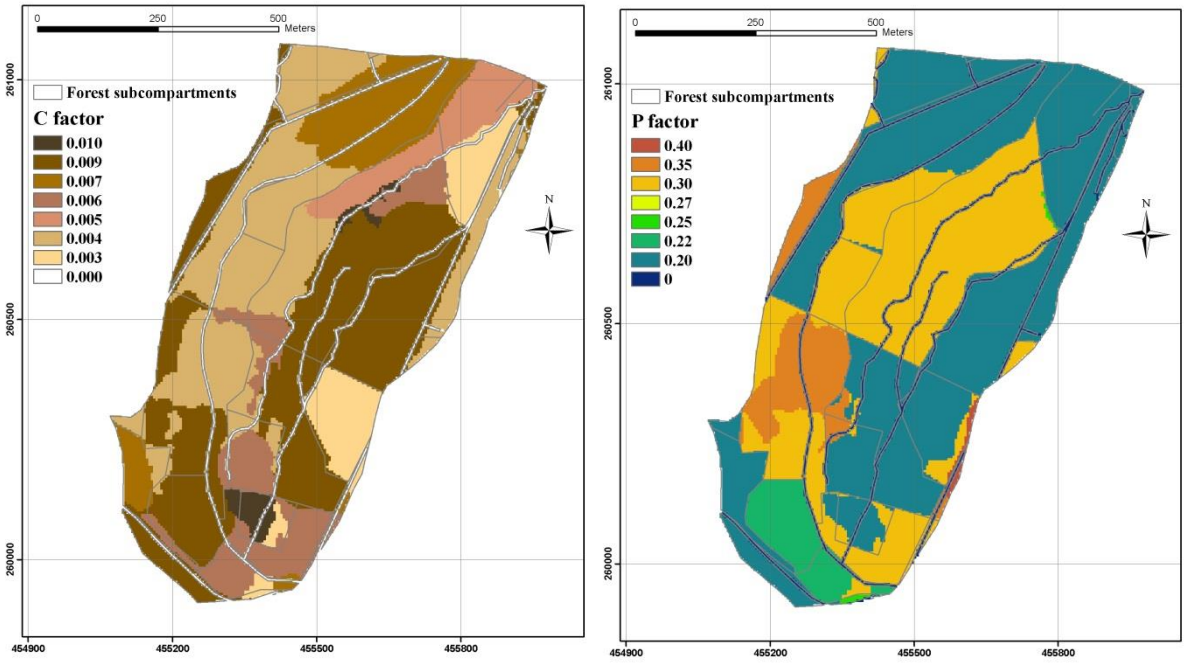

Annex III.V.4/a. Parameters for erosion modelling with the EROSION-3D derived from the Parameter catalogue for Saxony (1996) *(Jan.-Feb., June-Dec.)*

Land cover	**Soil type**	**Bulk density** ($kg \cdot m^{-3}$)	**Initial moisture** (%)	**Erodibility** ($N \cdot m^{-2}$)	**Roughness** ($s \cdot m^{-1/3}$)	**Skin factor**
Meadow / Meadow with beech seedlings mixed spruce	Ls2	1400	29.0	0.300	0.900	2.00
	Ls3	1400	30.0	0.300	0.900	2.00
	Slu	1400	30.0	0.300	0.900	2.00
	Sl4	1400	27.5	0.300	0.900	2.00
Regrowth	Ls2	1400	29.0	0.300	0.900	2.00
	Ls3	1400	30.0	0.300	0.900	2.00
	Slu	1400	30.0	0.300	0.900	2.00
	Sl4	1400	27.5	0.300	0.900	2.00
Young deciduous forest mixed spruce	Ls2	1400	29.0	0.036	0.900	2.00
	Ls3	1400	30.0	0.036	0.900	2.00
	Slu	1400	30.0	0.036	0.900	2.00
	Sl4	1400	27.5	0.036	0.900	2.00
Coniferous forest / Young coniferous forest	Ls2	1400	29.0	0.010	0.900	2.00
	Ls3	1400	30.0	0.010	0.900	2.00
	Slu	1400	30.0	0.010	0.900	2.00
	Sl4	1400	27.5	0.010	0.900	2.00
Mixed deciduous forest-borderland	Ls2	1400	29.0	0.010	0.900	2.00
	Ls3	1400	30.0	0.010	0.900	2.00
	Slu	1400	30.0	0.010	0.900	2.00
	Sl4	1400	27.5	0.010	0.900	2.00
Beech forest mixed oaks / Beech forest	Ls2	1400	29.0	0.010	0.900	2.00
	Ls3	1400	30.0	0.010	0.900	2.00
	Slu	1400	30.0	0.010	0.900	2.00
	Sl4	1400	27.5	0.010	0.900	2.00
Deciduous forest mixed spruce	Ls2	1400	29.0	0.010	0.900	2.00
	Ls3	1400	30.0	0.010	0.900	2.00
	Slu	1400	30.0	0.010	0.900	2.00
	Sl4	1400	27.5	0.010	0.900	2.00
Coniferous forest mixed deciduous trees	Ls2	1400	29.0	0.010	0.900	2.00
	Ls3	1400	30.0	0.010	0.900	2.00
	Slu	1400	30.0	0.010	0.900	2.00
	Sl4	1400	27.5	0.010	0.900	2.00
Riparian deciduous forest	Ls2	1400	29.0	0.010	0.900	2.00
	Ls3	1400	30.0	0.010	0.900	2.00
	Slu	1400	30.0	0.010	0.900	2.00
	Sl4	1400	27.5	0.010	0.900	2.00
Coniferous forest with clearances	Ls2	1400	29.0	0.010	0.900	2.00
	Ls3	1400	30.0	0.010	0.900	2.00
	Slu	1400	30.0	0.010	0.900	2.00
	Sl4	1400	27.5	0.010	0.900	2.00
Paved road	Ls2	2600	28.0	1.000	0.011	2.00
	Ls3	2600	29.0	1.000	0.011	2.00
	Slu	2600	28.5	1.000	0.011	2.00
	Sl4	2600	26.0	1.000	0.011	2.00
Dirt road	Ls2	2000	29.0	0.025	0.050	2.00
	Ls3	2000	30.0	0.025	0.050	2.00
	Slu	2000	30.0	0.025	0.050	2.00
	Sl4	2000	27.5	0.025	0.050	2.00
Stream	Ls2	1000	100.0	1.000	1.000	2.00

Ls3	1000	100.0	1.000	1.000	2.00
Slu	1000	100.0	1.000	1.000	2.00
Sl4	1000	100.0	1.000	1.000	2.00

Annex III.V.4/b. Parameters for erosion modelling with the EROSION-3D derived from the Parameter catalogue for Saxony (1996) *(March-May)*

Land cover	**Soil type**	**Bulk density** ($kg \cdot m^{-3}$)	**Initial moisture** (%)	**Erodibility** ($N \cdot m^{-2}$)	**Roughness** ($s \cdot m^{-1/3}$)	**Skin factor**
Meadow / Meadow with beech seedlings mixed spruce	Ls2	1400	40.5	0.300	0.900	2.00
	Ls3	1400	42.0	0.300	0.900	2.00
	Slu	1400	37.5	0.300	0.900	2.00
	Sl4	1400	33.0	0.300	0.900	2.00
Regrowth	Ls2	1400	40.5	0.300	0.900	2.00
	Ls3	1400	42.0	0.300	0.900	2.00
	Slu	1400	37.5	0.300	0.900	2.00
	Sl4	1400	33.0	0.300	0.900	2.00
Young deciduous forest mixed spruce	Ls2	1400	40.5	0.036	0.900	2.00
	Ls3	1400	42.0	0.036	0.900	2.00
	Slu	1400	37.5	0.036	0.900	2.00
	Sl4	1400	33.0	0.036	0.900	2.00
Coniferous forest / Young coniferous forest	Ls2	1400	40.5	0.010	0.900	2.00
	Ls3	1400	42.0	0.010	0.900	2.00
	Slu	1400	37.5	0.010	0.900	2.00
	Sl4	1400	33.0	0.010	0.900	2.00
Mixed deciduous forest-borderland	Ls2	1400	40.5	0.010	0.900	2.00
	Ls3	1400	42.0	0.010	0.900	2.00
	Slu	1400	37.5	0.010	0.900	2.00
	Sl4	1400	33.0	0.010	0.900	2.00
Beech forest mixed oaks / Beech forest	Ls2	1400	40.5	0.010	0.900	2.00
	Ls3	1400	42.0	0.010	0.900	2.00
	Slu	1400	37.5	0.010	0.900	2.00
	Sl4	1400	33.0	0.010	0.900	2.00
Deciduous forest mixed spruce	Ls2	1400	40.5	0.010	0.900	2.00
	Ls3	1400	42.0	0.010	0.900	2.00
	Slu	1400	37.5	0.010	0.900	2.00
	Sl4	1400	33.0	0.010	0.900	2.00
Coniferous forest mixed deciduous trees	Ls2	1400	40.5	0.010	0.900	2.00
	Ls3	1400	42.0	0.010	0.900	2.00
	Slu	1400	37.5	0.010	0.900	2.00
	Sl4	1400	33.0	0.010	0.900	2.00
Riparian deciduous forest	Ls2	1400	40.5	0.010	0.900	2.00
	Ls3	1400	42.0	0.010	0.900	2.00
	Slu	1400	37.5	0.010	0.900	2.00
	Sl4	1400	33.0	0.010	0.900	2.00
Coniferous forest with clearances	Ls2	1400	40.5	0.010	0.900	2.00
	Ls3	1400	42.0	0.010	0.900	2.00
	Slu	1400	37.5	0.010	0.900	2.00
	Sl4	1400	33.0	0.010	0.900	2.00
Paved road	Ls2	2600	33.5	1.000	0.011	2.00
	Ls3	2600	33.5	1.000	0.011	2.00
	Slu	2600	31.5	1.000	0.011	2.00
	Sl4	2600	28.5	1.000	0.011	2.00
Dirt road	Ls2	2000	33.5	0.025	0.050	2.00

	Ls3	2000	33.5	0.025	0.050	2.00
	Slu	2000	31.5	0.025	0.050	2.00
	Sl4	2000	28.5	0.025	0.050	2.00
Stream	Ls2	1000	100.0	1.000	1.000	2.00
	Ls3	1000	100.0	1.000	1.000	2.00
	Slu	1000	100.0	1.000	1.000	2.00
	Sl4	1000	100.0	1.000	1.000	2.00

Annex IV.I

Annex IV.I.1. Extrapolated percent values of particle fractions of each soil textures in the Farkas Valley (based on the soil samplings and analyses by the author)

Soil type	gS	mS	fS	gU	mU	fU	gT	mT	fT	C
Sl4	15.65	15.74	18.97	14.78	13.41	7.38	0.00	14.06	0.00	2.97
Ls2	8.58	10.76	16.82	19.53	17.42	7.86	0.00	19.04	0.00	3.13
Sl4	17.26	16.19	17.20	14.47	14.75	8.16	0.00	11.96	0.00	4.95
Ls3	11.72	14.69	19.44	16.52	14.21	5.97	0.00	17.45	0.00	2.42
Ls3	15.84	13.80	15.95	13.67	15.41	7.69	0.00	17.64	0.00	2.77
Ls2	10.26	12.85	16.67	17.20	16.49	8.37	0.00	18.15	0.00	2.69
Slu	15.45	11.80	12.44	19.66	17.58	8.61	0.00	14.45	0.00	3.49
Slu	13.31	15.29	17.15	15.66	15.89	8.39	0.00	14.30	0.00	3.44
Sl4	14.49	16.65	20.65	14.67	13.39	6.56	0.00	13.59	0.00	5.41
Ls2	8.88	10.81	17.33	19.40	15.96	8.80	0.00	18.83	0.00	3.24
Slu	10.82	11.28	18.74	18.80	16.43	7.92	0.00	16.01	0.00	3.07
Sl4	12.63	15.15	19.70	18.78	13.55	6.99	0.00	13.20	0.00	1.67

Symbols: gS – coarse sand; mS – middle sand; fS – fine sand; gU – coarse silt; mU – middle silt; fU – fine silt, gT – coarse clay; mT – middle clay; fT – fine clay; C – organic material content.

Annex IV.I.2. Seasonal fluctuation of the descriptive statistical variables of the rainfall depth (P) maximal 30-min rainfall intensity (I_{max30}) and erosivity index (EI) based on the "$_{hhm}$" rain gauge

		Valid N	Average	Median	Sum	Maximum	Std.Dev.
autumn	***P** (mm)*	191	5.8	1.5	1111.0	66.0	9.5
	$\boldsymbol{I_{max30}}$ *(mm·h^{-1})*	136	4.1	3.0		58.0	5.7
	***EI** (kJ·m^{-2}·mm·h^{-1})*	136	1.1	0.1	154.8	47.2	4.7
winter	***P** (mm)*	205	4.7	2.0	963.0	34.0	6.5
	$\boldsymbol{I_{max30}}$ *(mm·h^{-1})*	146	2.6	2.0		8.0	1.6
	***EI** (kJ·m^{-2}·mm·h^{-1})*	146	0.3	0.1	42.4	3.2	0.5
spring	***P** (mm)*	255	6.2	3.0	1589.0	74.0	9.9
	$\boldsymbol{I_{max30}}$ *(mm·h^{-1})*	203	4.9	3.0		74.0	6.5
	***EI** (kJ·m^{-2}·mm·h^{-1})*	203	1.4	0.1	275.0	92.0	6.7
summer	***P** (mm)*	311	9.5	3.5	2952.5	81.5	13.9
	$\boldsymbol{I_{max30}}$ *(mm·h^{-1})*	238	9.7	6.0		83.0	11.4
	***EI** (kJ·m^{-2}·mm·h^{-1})*	238	5.0	0.6	1188.6	134.0	13.9

Annex IV.I.3. Precipitation categories for each hydrological year of the study period and annual sums of rainfall depth (P) and erosivity index (EI) based on the "$_{hhm}$" rain gauge

	all categories	**< 2.0 *mm***	**2.1-5.0 *mm***	**5.1-10.0 *mm***	**10.1-20.0 *mm***	**> 20.0 *mm***
2000-2001						
No. of prec. events	113	51	25	15	17	5
P_{sum} *(mm)*	611.5	44.0	90.5	110.0	245.0	122.0
EI_{sum} $(kJ \cdot m^{-2} \cdot mm \cdot h^{-1})$	105.6	0.5	3.1	9.8	58.0	34.2
2001-2002						
No. of prec. events	95	52	13	13	8	9
P_{sum} *(mm)*	672.5	50.0	44.5	92.0	119.5	366.5
EI_{sum} $(kJ \cdot m^{-2} \cdot mm \cdot h^{-1})$	176.2	0.6	1.7	8.1	24.1	141.7
2002-2003						
No. of prec. events	48					
P_{sum} *(mm)*	123.0					
EI_{sum} $(kJ \cdot m^{-2} \cdot mm \cdot h^{-1})$	4.1					
2003-2004						
No. of prec. events	123	57	25	22	12	7
P_{sum} *(mm)*	679.0	53.5	87.5	169.5	178.5	190.0
EI_{sum} $(kJ \cdot m^{-2} \cdot mm \cdot h^{-1})$	85.0	0.8	2.9	22.9	18.7	39.7
2004-2005						
No. of prec. events	84	38	14	11	15	6
P_{sum} *(mm)*	575.0	35.0	51.0	77.5	234.5	177.0
EI_{sum} $(kJ \cdot m^{-2} \cdot mm \cdot h^{-1})$	61.7	0.5	2.4	6.2	28.4	24.2
2005-2006						
No. of prec. events	122	57	26	17	11	11
P_{sum} *(mm)*	813.0	52.5	94.0	125.5	143.0	398.0
EI_{sum} $(kJ \cdot m^{-2} \cdot mm \cdot h^{-1})$	135.6	0.7	3.0	7.5	27.4	97.1
2006-2007						
No. of prec. events	97	51	13	10	11	12
P_{sum} *(mm)*	789.5	45.5	50.0	76.5	163.0	454.5
EI_{sum} $(kJ \cdot m^{-2} \cdot mm \cdot h^{-1})$	141.2	0.5	2.6	7.6	38.8	91.7
2007-2008						
No. of prec. events	81	36	12	11	10	12
P_{sum} *(mm)*	816.0	32.0	42.5	83.5	149.5	508.5
EI_{sum} $(kJ \cdot m^{-2} \cdot mm \cdot h^{-1})$	366.3	0.3	2.8	8.0	26.4	328.8
2008-2009						
No. of prec. events	96	37	20	19	10	10
P_{sum} *(mm)*	723.5	35.0	69.5	137.0	144.0	338.0
EI_{sum} $(kJ \cdot m^{-2} \cdot mm \cdot h^{-1})$	133.9	0.4	3.2	23.2	28.1	79.1
2009-2010						
No. of prec. events	130	53	25	20	20	12
P_{sum} *(mm)*	1035.0	44.5	82.5	147.0	301.0	460.0
EI_{sum} $(kJ \cdot m^{-2} \cdot mm \cdot h^{-1})$	478.8	0.3	3.7	8.9	44.0	421.9

Annex IV.I.4. The linear relation between the discharges in the Farkas Valley and Vadkan Valley (equivalent water-levels)

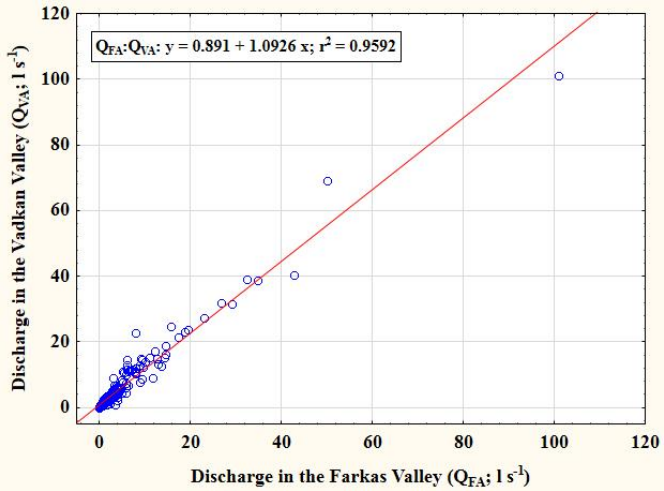

Annex IV.I.5. Descriptive statistical variables of the flood parameters for the hydrological years

	Valid N	Mean	Median	Minimum	Maximum	Std.Dev.
2000-2001						
Q_{start} ($l \cdot s^{-1}$)	50	0.9	0.9	0.2	1.4	0.3
Q_{end} ($l \cdot s^{-1}$)	51	1.2	1.2	0.6	2.8	0.4
SumQ (l)	51	103193	66641	14963	389044	96361
Q_{max} ($l \cdot s^{-1}$)	51	6.5	3.0	1.2	80.9	11.7
2001-2002						
Q_{start} ($l \cdot s^{-1}$)	34	1.0	0.9	0.1	2.5	0.6
Q_{end} ($l \cdot s^{-1}$)	34	1.5	1.2	0.2	5.0	0.9
SumQ (l)	34	193105	87517	5267	1357264	288884
Q_{max} ($l \cdot s^{-1}$)	34	10.2	4.7	0.5	98.0	17.4
2003-2004						
Q_{start} ($l \cdot s^{-1}$)	47	1.2	1.0	0.4	2.5	0.5
Q_{end} ($l \cdot s^{-1}$)	49	1.4	1.2	0.5	3.4	0.6
SumQ (l)	49	141203	57415	12655	1546717	286878
Q_{max} ($l \cdot s^{-1}$)	49	5.4	3.1	0.9	52.0	8.0
2004-2005						
Q_{start} ($l \cdot s^{-1}$)	35	0.9	0.7	0.3	2.6	0.4
Q_{end} ($l \cdot s^{-1}$)	35	1.1	0.9	0.5	2.6	0.5
SumQ (l)	35	226458	64642	9224	2559110	448864
Q_{max} ($l \cdot s^{-1}$)	35	6.1	3.5	0.9	34.0	7.1
2005-2006						
Q_{start} ($l \cdot s^{-1}$)	43	1.6	1.4	0.6	6.3	0.9
Q_{end} ($l \cdot s^{-1}$)	43	2.1	1.8	0.8	6.9	1.3
SumQ (l)	43	314931	80373	13571	2601384	570839
Q_{max} ($l \cdot s^{-1}$)	43	16.7	4.2	1.5	176.2	36.5
2006-2007						
Q_{start} ($l \cdot s^{-1}$)	58	1.0	1.0	0.1	2.4	0.4
Q_{end} ($l \cdot s^{-1}$)	58	1.3	1.1	0.5	3.3	0.6
SumQ (l)	58	281414	66152	7227	4381220	773703

Q_{max} $(l \cdot s^{-1})$	58	7.9	2.4	0.8	109.7	15.8
2007-2008						
Q_{start} $(l \cdot s^{-1})$	47	2.6	2.3	1.1	5.8	1.0
Q_{end} $(l \cdot s^{-1})$	48	3.1	2.6	1.6	10.7	1.7
SumQ *(l)*	48	727732	201566	35888	8469136	1441256
Q_{max} $(l \cdot s^{-1})$	48	35.7	7.7	2.4	214.0	58.5
2008-2009						
Q_{start} $(l \cdot s^{-1})$	58	3.5	2.6	1.8	11.4	2.1
Q_{end} $(l \cdot s^{-1})$	57	4.5	2.9	2.0	19.2	3.9
SumQ *(l)*	58	688244	116550	22813	14752272	2647100
Q_{max} $(l \cdot s^{-1})$	58	19.0	7.2	2.4	281.4	40.1
2009-2010						
Q_{start} $(l \cdot s^{-1})$	43	2.9	2.9	1.9	4.7	0.6
Q_{end} $(l \cdot s^{-1})$	44	3.4	3.1	2.0	11.0	1.5
SumQ *(l)*	44	502182	188603	33823	4984116	864122
Q_{max} $(l \cdot s^{-1})$	44	20.7	8.1	3.0	190.6	37.4

Annex IV.II

Annex. IV.II.1/a. Time series of the observed suspended sediment concentration (SSC) and manually measured discharge (Q) in the Farkas Valley under low flow conditions (without the identified outliers from 2008)

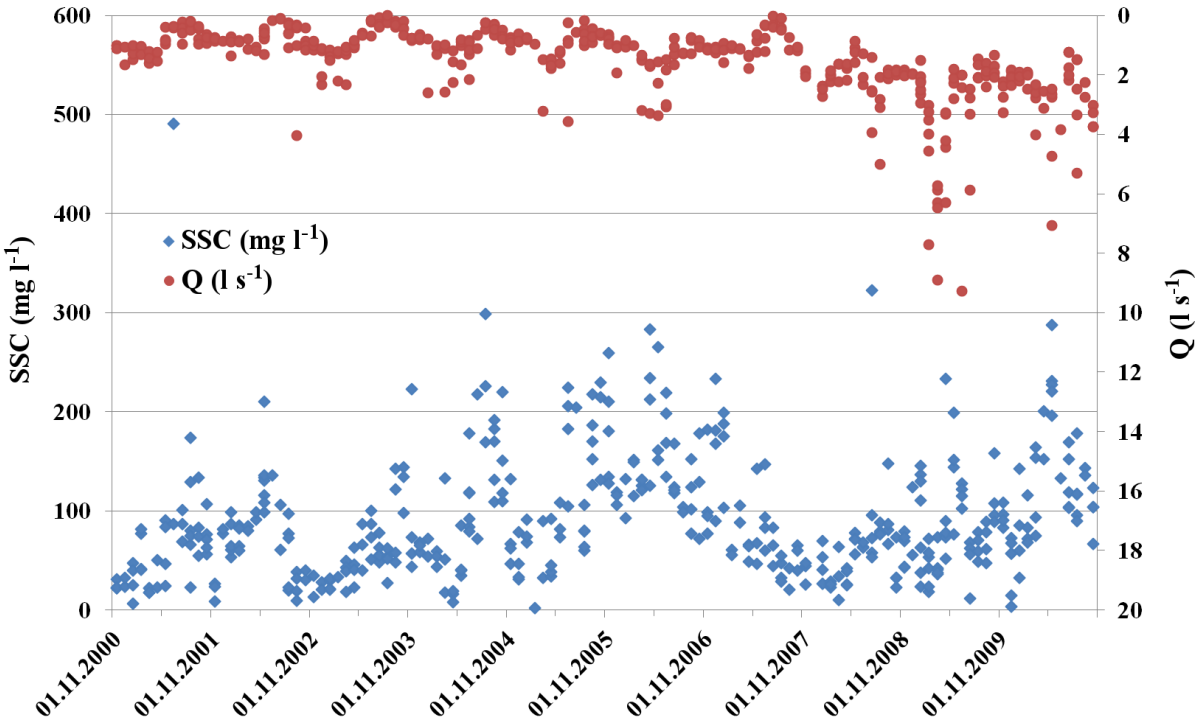

Annex. IV.II.1/b. Time series of the observed SSC and manually measured Q in the Vadkan Valley under low flow conditions (without the identified outliers from 2008)

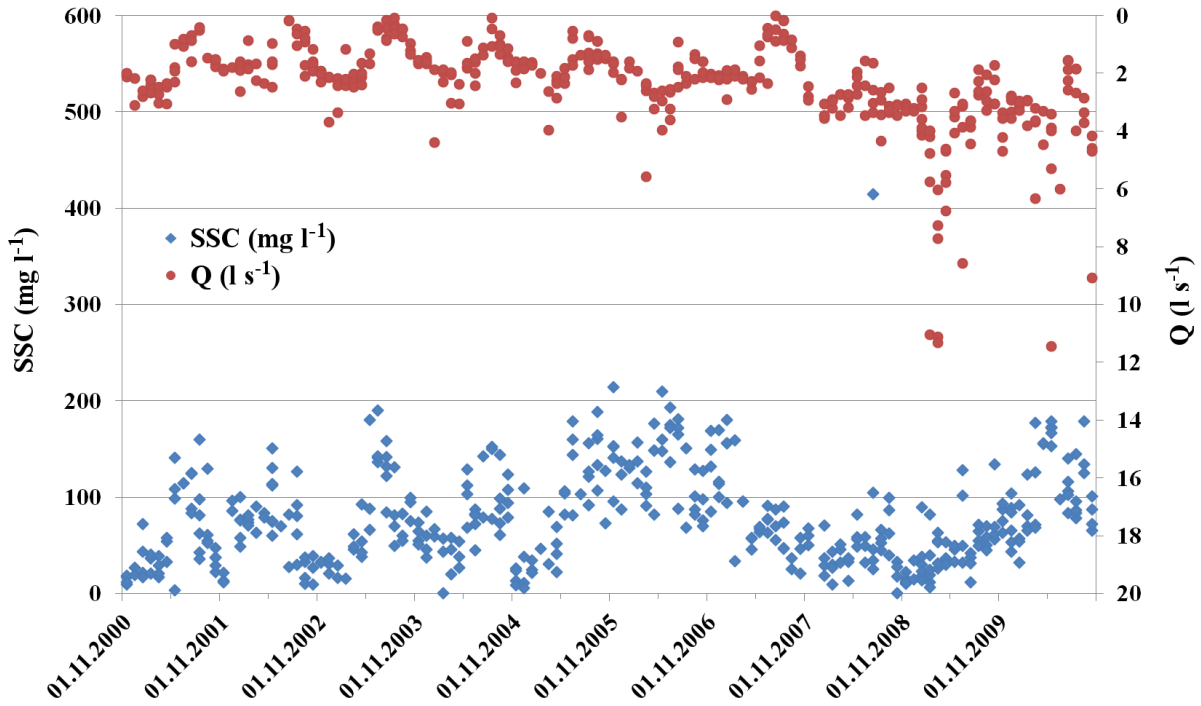

Annex IV.II.2. Descriptive statistics of the suspended sediment concentration (SSC, $mg \cdot l^{-1}$) in different flow categories (List of symbols: SSC – suspended sediment concentration; AD – antecedent days; Valid N – sample size)

Descriptive statistics of *SSC*	**low flow *AD*<2**	**low flow 2≤*AD*<8**	**low flow 8≤*AD***	**high flow rising limb**	**high flow falling limb**
			Farkas Valley		
Average	91.1	87.6	134.2	991.5	515.2
Min	8.0	8.6	19.3	31.3	24.9
Max	233.9	322.9	298.7	4005.3	3371.2
Median	87.7	72.7	131.5	429.1	173.0
Std.Dev.	48.5	61.2	73.0	1254.0	760.7
Valid N	70	142	57	33	54
			Vadkan Valley		
Average	84.9	77.3	91.4	1314.5	460.2
Min	9.2	3.4	0.0	31.2	7.5
Max	171.7	414.8	214.0	7635.9	2928.2
Median	80.5	65.5	77.3	288.3	156.4
Std.Dev.	42.2	55.6	52.1	2044.5	615.2
Valid N	71	142	58	34	52

Annex IV.II.3. Descriptive statistics of suspended sediment concentration (SSC) and its control factors at low flow (entire period and seasonal scale). (List of symbols: Q – discharge; WT – water temperature; ST0, ST5, ST10 – soil temperature at the depths 0cm, 5cm, 10cm)

		Farkas Valley				Vadkan Valley			
		Average	**Median**	**Min**	**Max**	**Average**	**Median**	**Min**	**Max**
SSC *($mg \cdot l^{-1}$)*	**entire period**	89.8	76.7	2.3	322.9	77.3	69.6	0.0	414.8
	autumn	94.9	82.9	8.6	259.1	70.6	62.8	0.0	214.0
	winter	71.3	61.7	2.3	233.0	61.7	48.7	0.0	180.0
	spring	91.1	74.2	8.0	287.4	78.6	63.4	3.4	209.4
	summer	100.3	83.7	11.9	322.9	96.9	85.4	11.4	414.8
Q *($l \cdot s^{-1}$)*	**entire period**	1.6	1.2	0.0	9.3	2.4	2.2	0.0	11.4
	autumn	1.2	1.0	0.2	4.1	2.1	1.8	0.5	9.1
	winter	1.6	1.3	0.6	7.7	2.7	2.4	0.9	11.0
	spring	2.0	1.6	0.4	8.9	3.1	2.5	0.9	11.4
	summer	1.4	1.0	0.0	9.3	1.8	1.6	0.0	8.6
WT *(^oC)*	**entire period**	9.5	10.3	0.0	20.4	9.3	10.1	0.0	20.0
	autumn	9.9	10.1	0.5	17.1	9.8	9.9	0.8	18.2
	winter	2.1	1.3	0.0	9.0	2.4	1.8	0.0	7.8
	spring	10.5	11.2	0.5	19.9	9.9	10.6	0.3	16.9
	summer	16.0	16.2	9.8	20.4	15.7	15.6	10.6	20.0
ST0 *(^oC)*	**entire period**	11.0	11.2	0.2	25.0	11.0	11.3	0.2	25.9
	autumn	10.4	10.1	2.3	18.8	10.5	10.4	2.4	17.9
	winter	3.0	2.3	0.2	8.6	3.0	2.4	0.2	8.6
	spring	10.5	11.1	0.2	18.4	10.5	11.0	0.2	18.3
	summer	17.3	17.3	7.5	25.0	17.2	16.9	7.6	25.9
ST5 *(^oC)*	**entire period**	10.0	10.3	-0.1	21.8	10.0	10.4	-0.1	22.6
	autumn	9.9	9.6	3.0	16.9	10.0	9.7	3.0	16.6
	winter	2.8	2.4	-0.1	6.7	2.8	2.5	-0.1	6.7
	spring	9.2	9.9	0.4	15.4	9.1	10.0	0.4	15.4
	summer	15.9	16.3	7.6	21.8	15.9	16.0	7.5	22.6
ST10 *(^oC)*	**entire period**	9.8	10.2	0.3	20.3	9.9	10.3	0.3	21.1
	autumn	9.9	9.6	3.5	16.4	10.0	10.0	3.5	16.4
	winter	2.9	2.8	0.3	6.2	3.0	2.8	0.3	6.4
	spring	8.8	9.5	0.6	14.6	8.8	9.5	0.6	14.5
	summer	15.5	15.9	7.8	20.3	15.5	15.8	7.4	21.1

Annex IV.II.4. Descriptive statistics of the suspended sediment concentration (SSC) and the SSC control factors at low flow for the hydrological years (List of symbols: Q – discharge; WT – water temperature; ST0, ST5, ST10 – soil temperature at the depths 0cm, 5cm, 10cm)

		Farkas Valley				Vadkan Valley			
		Average	**Median**	**Min**	**Max**	**Average**	**Median**	**Min**	**Max**
SSC *($mg \cdot l^{-1}$)*	**2000-2001**	58.8	55.7	6.5	173.8	56.3	41.6	3.4	159.7
	2001-2002	74.9	77.1	8.6	209.9	66.6	74.2	9.2	150.4
	2002-2003	57.5	50.7	12.8	143.8	80.5	72.5	15.8	189.7
	2003-2004	102.8	79.6	8.0	298.7	76.1	73.2	0.0	152.1
	2004-2005	104.3	81.9	2.3	229.3	83.2	83.3	5.9	188.3
	2005-2006	149.3	131.7	72.0	282.8	132.2	134.8	68.0	214.0
	2006-2007	92.2	72.2	20.5	233.0	87.7	77.2	20.8	180.0
	2007-2008	61.7	57.0	10.5	322.9	54.4	45.2	0.0	414.8
	2008-2009	81.0	72.5	11.9	233.1	43.4	37.6	6.5	134.2
	2009-2010	116.7	104.1	3.3	287.4	102.7	92.1	31.8	178.7
Q *($l \cdot s^{-1}$)*	**2000-2001**	0.9	1.0	0.2	1.7	1.9	2.0	0.4	3.1
	2001-2002	0.8	0.8	0.1	4.1	1.5	1.7	0.2	2.6
	2002-2003	0.8	0.9	0.0	2.3	1.5	1.7	0.1	3.7
	2003-2004	1.0	0.8	0.3	2.6	1.7	1.6	0.1	4.4
	2004-2005	1.0	0.8	0.2	3.6	1.7	1.6	0.5	4.0
	2005-2006	1.5	1.3	0.6	3.4	2.3	2.2	0.9	5.6
	2006-2007	0.9	1.1	0.0	1.8	1.6	1.9	0.0	2.9
	2007-2008	2.1	2.0	0.9	5.0	2.9	3.0	1.6	4.4
	2008-2009	3.2	2.3	1.3	9.3	4.3	3.6	1.7	11.3
	2009-2010	2.6	2.4	1.2	7.1	3.7	3.4	1.5	11.4
WT *(^oC)*	**2000-2001**	9.8	11.5	0.0	18.2	10.0	11.4	0.1	17.6
	2001-2002	10.4	10.2	0.2	19.9	9.5	10.0	0.2	17.7
	2002-2003	9.3	9.3	0.2	19.8	9.0	9.2	0.2	18.5
	2003-2004	9.3	10.5	0.4	17.9	9.0	9.5	0.2	17.6
	2004-2005	9.3	10.2	0.2	18.2	9.8	10.6	0.0	19.5
	2005-2006	8.6	9.7	0.0	19.2	8.6	9.9	0.0	20.0
	2006-2007	10.4	10.4	0.6	17.1	10.5	9.8	2.3	18.8
	2007-2008	10.5	10.7	0.1	18.3	10.1	10.5	0.1	17.0
	2008-2009	8.7	10.0	0.0	18.6	8.4	8.6	0.0	17.7
	2009-2010	9.1	9.7	0.1	20.4	8.9	10.0	0.0	19.3
ST0 *(^oC)*	**2006-2007**	10.8	10.5	2.2	20.2	10.7	10.5	2.2	20.2
	2009-2010	8.9	9.6	0.2	21.3	9.0	9.6	0.2	21.3
ST5 *(^oC)*	**2006-2007**	9.5	8.9	2.1	17.6	9.4	8.9	2.2	17.6
	2009-2010	8.6	9.0	0.4	19.9	8.7	8.9	0.4	19.9
ST10 *(^oC)*	**2006-2007**	9.4	8.6	2.1	17.2	9.3	8.6	2.2	17.2
	2009-2010	8.5	8.9	0.6	19.1	8.6	9.0	0.6	19.2

Annex IV.III

Annex IV.III.1. Relations between suspended sediment concentration (SSC) and discharge (Q) as a function of antecedent days (AD) in the Farkas Valley and the Vadkan Valley (Marked correlations are significant at p<0.05)

		Farkas Valley				Vadkan Valley			
		Average	**Std.Dev.**	**r_Q**	**r_{AD}**	**Average**	**Std.Dev.**	**r_Q**	**r_{AD}**
AD<2	***SSC***	91.1	48.5	-0.1	-0.1	84.9	42.2	-0.2	-0.1
	Q	1.8	1.7		0.0	2.5	1.5		-0.1
2≤AD<8	***SSC***	87.6	61.2	0.1	-0.1	77.3	55.6	0.0	-0.1
	Q	1.7	1.2		0.0	2.4	1.3		0.0
8≤AD	***SSC***	134.2	73.0	**-0.4**	**0.3**	91.4	52.1	-0.3	0.3
	Q	1.1	0.8		-0.2	1.9	1.0		-0.2

Annex IV.III.2/a. Correlation coefficients between the suspended sediment concentrations (SSC) under low flow conditions and the sediment control variables in autumn (Marked correlations are significant at p<0.05) (List of symbols: N – sample size; Q – discharge; AD – antecedent days; WT – water temperature; ST0, ST5, ST10 – soil temperature at the depths 0 cm, 5 cm, 10 cm)

		Q	***AD***	***WT***	***ST0***	***ST5***	***ST10***
Farkas Valley	***SSC***	***-0.23***	***0.48***	0.14	0.10	0.11	0.09
	N	111	92	107	35	35	35
Vadkan Valley	***SSC***	-0.07	***0.30***	***0.20***	-0.06	-0.05	-0.06
	N	106	93	109	37	37	37

Annex IV.III.2/b. Correlation coefficients between the SSC data under low flow conditions and the sediment control variables in winter

		Q	***AD***	***WT***	***ST0***	***ST5***	***ST10***
Farkas Valley	***SSC***	-0.15	0.47	0.03	0.16	0.17	0.17
	N	96	15	100	32	32	32
Vadkan Valley	***SSC***	-0.18	0.18	0.06	0.18	0.21	0.19
	N	93	15	99	32	32	32

Annex IV.III.2/c. Correlation coefficients between the SSC data under low flow conditions and the sediment control variables in spring

		Q	**AD**	**WT**	**ST0**	**ST5**	**ST10**
Farkas Valley	***SSC***	0.09	0.04	***0.27***	***0.33***	***0.44***	***0.45***
	N	104	70	100	44	44	44
Vadkan Valley	***SSC***	0.01	-0.11	***0.25***	0.14	0.23	0.24
	N	98	71	100	44	44	44

Annex IV.III.2/d. Correlation coefficients between the SSC data under low flow conditions and the sediment control variables in summer

		Q	***AD***	***WT***	***ST0***	***ST5***	***ST10***
Farkas Valley	***SSC***	0.06	***0.35***	0.06	0.09	0.07	0.02
	N	106	92	96	47	47	47
Vadkan Valley	***SSC***	-0.13	0.08	***0.22***	0.19	0.16	0.11
	N	99	92	98	47	47	47

Annex IV.III.3. Correlation coefficients between the SSC data under low flow conditions and the sediment control variables in each hydrological year (Marked correlations are significant at p<0.05 and N shows the sample size)

		Farkas Valley						**Vadkan Valley**					
		Q	**WT**	**AD**	**ST0**	**ST5**	**ST10**	**Q**	**WT**	**AD**	**ST0**	**ST5**	**ST10**
2000-2001	**SSC**	***-0.70***	***0.54***	0.12	-	-	-	***-0.59***	***0.56***	-0.25	-	-	-
	N	41	42	30	-	-	-	35	45	31	-	-	-
2001-2002	**SSC**	-0.22	0.22	0.18	-	-	-	0.11	0.05	-0.13	-	-	-
	N	38	38	25	-	-	-	31	39	26	-	-	-
2002-2003	**SSC**	***-0.51***	***0.47***	0.47	-	-	-	***-0.69***	***0.80***	-	-	-	-
	N	38	36	3	-	-	-	34	34	3	-	-	-
2003-2004	**SSC**	***-0.55***	***0.53***	***0.45***	-	-	-	***-0.57***	***0.68***	0.14	-	-	-
	N	43	41	27	-	-	-	41	41	27	-	-	-
2004-2005	**SSC**	-0.23	***0.59***	***0.56***	-	-	-	***-0.58***	***0.78***	0.29	-	-	-
	N	39	39	26	-	-	-	38	38	25	-	-	-
2005-2006	**SSC**	0.22	0.16	0.32	-0.06	-0.07	-0.11	0.20	0.16	0.16	0.19	0.20	0.16
	N	39	39	27	20	20	20	38	39	28	21	21	21
2006-2007	**SSC**	0.19	***-0.57***	***0.46***	***-0.48***	***-0.49***	***-0.49***	***0.43***	***-0.57***	0.25	***-0.61***	***-0.60***	***-0.59***
	N	38	35	38	36	36	36	38	36	38	36	36	36
2007-2008	**SSC**	0.13	***0.51***	-0.25	***0.51***	***0.50***	***0.51***	-0.04	0.21	-0.27	0.36	0.36	0.37
	N	41	40	32	29	29	29	41	40	32	29	29	29
2008-2009	**SSC**	-0.25	0.26	0.06	-0.04	-0.05	-0.06	0.14	***0.31***	0.07	-0.01	0.03	0.05
	N	54	50	33	27	27	27	54	50	33	27	27	27
2009-2010	**SSC**	***0.32***	***0.52***	0.16	***0.45***	***0.45***	***0.44***	0.15	***0.50***	0.10	***0.41***	***0.40***	***0.40***
	N	46	43	28	46	46	46	46	44	28	47	47	47

Annex IV.III.4/a. Correlation coefficients between the suspended sediment concentration (SSC) at high flow and sediment control variables for the entire study period (Marked correlations are significant at p<0.05) (List of symbols: N – sample size; FA – Farkas Valley; VA – Vadkan Valley; Q – discharge; WT – water temperature; ST0, ST5, ST10 – soil temperature at the depths 0 cm, 5 cm, 10 cm; API1, API3, API7 – antecedent precipitation index for 1, 3 and 7 days; EI – erosivity index; SumQ – total volume of the flood event; Q_{max} – peak discharge; $_{c1}$ –rain gauge 0.1mm; $_{hhm}$ rain gauge 0.5mm)

	Q	***WT***	***ST0***	***ST5***	***ST 10***	***API1 $_{c1}$***	***API3 $_{c1}$***	***API7 $_{c1}$***	***EI_{c1}***	***API1 $_{hhm}$***	***API3 $_{hhm}$***	***API7 $_{hhm}$***	***EI $_{hhm}$***	***Sum Q***	***Q_{max}***
SSC $_{FA}$	***0.65***	***0.46***	***0.30***	***0.32***	***0.34***	***0.46***	***0.35***	0.21	***0.39***	***0.35***	***0.30***	***0.23***	***0.33***	0.01	***0.31***
N	86	42	61	61	61	48	60	60	59	79	80	80	80	79	79
SSC $_{VA}$	***0.62***	***0.38***	***0.26***	0.25	0.25	***0.60***	***0.56***	***0.40***	***0.42***	***0.42***	***0.61***	***0.56***	***0.29***	-	-
N	81	42	59	59	59	46	59	59	58	76	78	79	79	-	-

Annex IV.III.4/b. Correlation coefficients between the SSC data under high flow conditions and the sediment control variables for summer

	Q	***WT***	***API1$_{c1}$***	***API3$_{c1}$***	***API 7$_{c1}$***	***EI$_{c1}$***	***API 1$_{hhm}$***	***API 3$_{hhm}$***	***API 7$_{hhm}$***	***EI$_{hhm}$***	***SumQ***	***Q$_{max}$***
SSC$_{FA}$	***0.62***	***0.66***	0.15	***0.43***	0.34	0.29	***0.30***	***0.31***	0.25	0.22	0.07	0.26
N	50	10	21	32	32	32	51	51	51	51	51	51
SSC$_{VA}$	**0.59**	0.53	0.28	***0.56***	***0.45***	***0.38***	***0.38***	***0.66***	***0.61***	0.17	-	-
N	48	10	21	32	32	32	51	51	51	51	-	-

Annex IV.III.4/c. Correlation coefficients between the SSC data at rising limb and the sediment control variables for the entire study period

	Q	***WT***	***ST0***	***ST5***	***ST 10***	***API 1$_{c1}$***	***API 3$_{c1}$***	***API 7$_{c1}$***	***EI$_{c1}$***	***API 1$_{hhm}$***	***API 3$_{hhm}$***	***API 7$_{hhm}$***	***EI$_{hh m}$***	***Sum Q***	***Q$_{max}$***
SSC FA	***0.68***	***0.62***	0.43	0.42	0.42	***0.61***	0.41	0.20	0.34	***0.59***	***0.52***	***0.44***	***0.57***	***0.53***	***0.64***
N	33	18	20	20	20	19	19	19	19	27	27	27	27	28	28
SSC VA	**0.54**	**0.49**	0.36	0.33	0.32	**0.77**	**0.75**	**0.51**	0.32	**0.59**	**0.81**	**0.76**	**0.46**	**-**	**-**
N	32	18	22	22	22	15	20	20	20	28	29	29	29	-	-

Annex IV.III.4/d. Correlation coefficients between the SSC data at falling limb and the sediment control variables for the entire study period

	Q	***WT***	***ST0***	***ST5***	***ST 10***	***API1 $_{c1}$***	***API3 $_{c1}$***	***API 7$_{c1}$***	***EI$_{c1}$***	***API1 $_{hhm}$***	***API3 $_{hhm}$***	***API 7$_{hhm}$***	***EI$_{hh m}$***	***Sum Q***	***Q$_{max}$***
SSC FA	***0.68***	0.28	0.25	0.29	***0.31***	***0.48***	***0.35***	0.21	***0.53***	-	-	-	***0.31***	-0.15	0.04
N	53	24	41	41	41	32	41	41	40	-	-	-	53	51	51
SSC VA	***0.86***	0.31	0.28	0.29	0.30	***0.60***	***0.42***	0.27	***0.59***	***0.43***	***0.28***	0.19	***0.48***	**-**	**-**
N	49	24	37	37	37	38	39	39	39	48	49	50	50	-	-

Annex IV.III.4/e. Correlation coefficients between suspended sediment concentration (SSC) at the rising limb and the sediment control variables for summer

	Q	**API1$_{c1}$**	**API3$_{c1}$**	**API7 $_{c1}$**	**EI$_{c1}$**	**API1 $_{hhm}$**	**API3 $_{hhm}$**	**API7 $_{hhm}$**	**EI$_{hhm}$**	**SumQ**	**Q$_{max}$**
SSC$_{FA}$	***0.67***	***0.70***	0.27	0.60	0.21	***0.64***	***0.55***	0.44	***0.71***	***0.56***	***0.62***
N	20	9	9	9	9	20	20	20	20	20	20
SSC$_{VA}$	***0.55***	0.57	***0.65***	0.37	0.28	***0.64***	***0.86***	***0.79***	***0.49***	-	-
N	19	6	10	10	10	21	21	21	21	-	-

Annex IV.III.4/f. Correlation coefficients between the SSC data at falling limb and the sediment control variables for summer

	Q	**API1$_{c1}$**	**API3$_{c1}$**	**API7$_{c1}$**	**EI$_{c1}$**	**API1$_{hhm}$**	**API3$_{hhm}$**	**API7$_{hhm}$**	**EI$_{hhm}$**	**SumQ**	**Q$_{max}$**
SSC$_{FA}$	***0.63***	-0.31	0.24	0.22	0.26	0.12	-0.04	-0.08	0.16	-0.14	-0.05
N	30	16	24	24	24	31	31	31	31	31	31
SSC$_{VA}$	***0.89***	0.22	***0.56***	***0.52***	***0.54***	***0.38***	0.33	0.28	***0.38***	**-**	**-**
N	29	15	22	22	22	30	30	30	30	**-**	**-**

Annex IV.III.4/g. Correlation coefficients between the SSC and sediment control factors at the flood wave 18.07.2009 (Marked correlations are significant at p<0.05)

	Q	***ST0***	***ST5***	***ST10***	***API1$_{hhm}$***	***API3$_{hhm}$***	***EI$_{hhm}$***	***SumQ***	***Q$_{max}$***
SSC$_{FA}$	***0.88***	***-0.63***	***-0.62***	***-0.58***	***0.78***	***0.78***	***0.72***	***0.63***	***0.75***
N	23	24	24	24	24	24	24	24	24
SSC$_{VA}$	***0.77***	***-0.52***	***-0.52***	***-0.47***	***0.74***	***0.74***	***0.70***	-	-
N	24	24	24	24	24	24	24	-	-

Annex IV.III.4/h. Correlation coefficients between the SSC data at the rising and the descending limb and the sediment control variables at the flood wave 18.07.2009

	Q	***ST0***	***ST5***	***ST10***	***API1$_{hhm}$***	***API3$_{hhm}$***	***EI$_{hhm}$***	***SumQ***	***Q$_{max}$***
	Rising limb								
SSC$_{FA}$	***0.97***	***-0.66***	-0.59	-0.56	***0.71***	***0.71***	***0.70***	***0.72***	***0.98***
N	10	10	10	10	10	10	10	10	10
SSC$_{VA}$	***0.74***	-0.59	-0.56	-0.49	***0.74***	***0.74***	***0.75***	-	-
N	11	11	11	11	11	11	11	-	-
	Descending limb								
SSC$_{FA}$	***0.93***	***-0.70***	-	-	***0.89***	***0.89***	***0.84***	***0.78***	***0.86***
N	13	14	-	-	14	14	14	14	14
SSC$_{VA}$	***0.99***	***-0.71***	***-0.69***	***-0.65***	***0.97***	***0.97***	***0.99***	-	-
N	13	13	13	13	13	13	13	-	-

Annex IV.III.4/i. Correlation coefficients between the SSC data at falling limb and the sediment control variables at the flood wave 04.08.2009

	Q	***API1$_{c1}$***	***EI $_{c1}$***	***API1$_{hhm}$***	***EI$_{hhm}$***	***SumQ***
SSC$_{FA}$	***0.99***	***-0.98***	***-0.98***	***-0.93***	***-0.93***	***-0.93***
N	12	12	12	12	12	12
SSC$_{VA}$	***0.99***	***-0.99***	***-0.99***	***-0.80***	***-0.80***	-
N	12	12	12	12	12	-

Annex IV.III.5/a. Log-log plot of suspended sediment concentration (SSC) against total volume of the flood event (SumQ) at the rising limb (left) and the falling limb (right) for the entire study period in the Farkas Valley (FA)

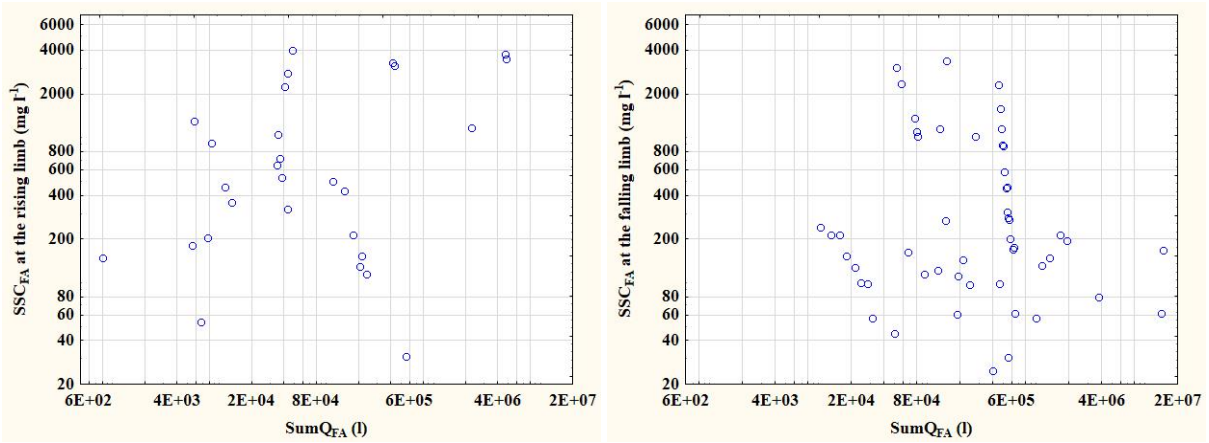

Annex IV.III.5/b. Log-log plot of suspended sediment concentration (SSC) against peak discharge (Q_{max}) at the rising limb (left) and the falling limb (right) for the entire study period in the Farkas Valley (FA)

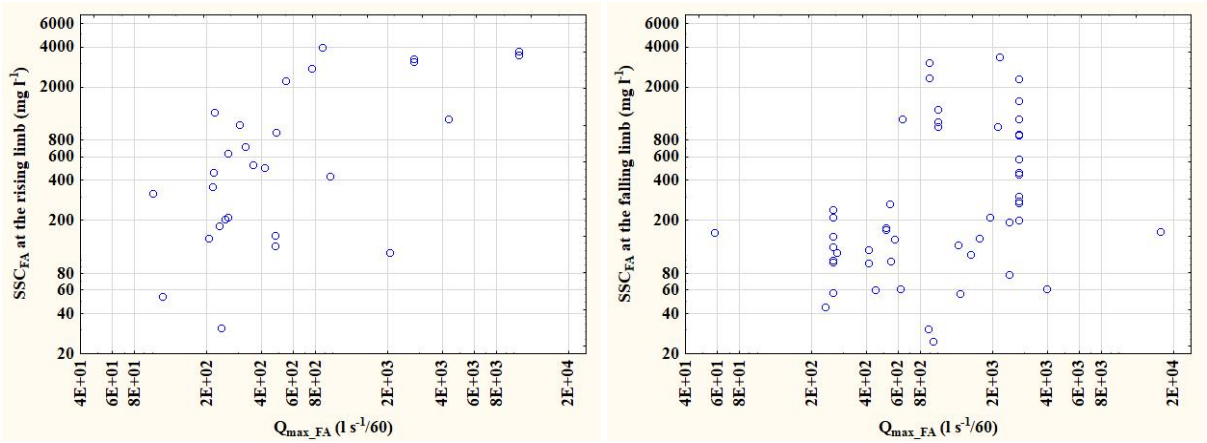

Annex IV.IV

Annex IV.IV.1/a. Results of the factor analysis based on the entire low flow dataset of the Farkas Valley and the Vadkan Valley

	Farkas Valley			Vadkan Valley		
	Factor 1	**Factor 2**	**Factor 3**	**Factor 1**	**Factor 2**	**Factor 3**
Eigenvalue	3.911	1.153	0.834	4.014	1.074	0.813
% Total variance	65.177	19.214	13.899	66.897	17.902	13.545
Factor loadings						
Q	-0.056	***-0.995***	0.076	-0.169	0.050	***-0.984***
WT	***0.970***	-0.048	0.028	***0.970***	0.036	0.063
AD	-0.065	0.076	***-0.995***	-0.062	***-0.997***	0.047
ST0	***0.989***	0.078	0.009	***0.980***	0.007	0.156
ST5	***0.991***	0.060	0.066	***0.984***	0.060	0.140
ST10	***0.983***	0.070	0.092	***0.975***	0.082	0.148

Annex IV.IV.1/b. Results of the factor analysis based on the entire high flow dataset of the Farkas Valley and the Vadkan Valley

	Farkas Valley			Vadkan Valley		
	Factor 1	**Factor 2**	**Factor 3**	**Factor 1**	**Factor 2**	**Factor 3**
Eigenvalue	5.618	3.388	1.292	5.418	2.682	0.618
% Total variance	51.072	30.802	11.741	60.197	29.799	6.868
Factor loadings						
Q	0.467	0.061	***0.837***	0.032	0.648	***0.719***
WT	0.189	***0.977***	0.057	***0.961***	0.063	0.258
ST0	0.078	***0.992***	0.026	***0.983***	0.068	0.158
ST5	0.016	***0.997***	0.053	***0.989***	0.063	0.131
ST10	0.003	***0.993***	0.099	***0.986***	0.083	0.137

$API1_{hhm}$	0.084	-0.054	***0.958***	-0.125	***0.857***	0.410
$API3_{hhm}$	***0.836***	0.237	0.395	0.253	0.307	***0.893***
$API7_{hhm}$	***0.808***	0.354	0.340	0.391	0.294	***0.857***
EI_{hhm}	0.318	0.284	***0.791***	0.296	***0.895***	0.240
SumQ	***0.952***	-0.174	-0.025	-	-	-
Q_{max}	***0.813***	0.104	0.500	-	-	-

(Notes: Non-availability of SumQ and Q_{max} data in the Vadkan Valley induces differences in the eigenvalues and the characters of the factors as well.)

Annex IV.IV.2/a. Regression models for predicting SSC under low flow conditions

Autumn:

- Farkas Valley (1.): $SSC = b_0 + b_1 \cdot Q^{b2} + b_3 \cdot WT + b_4 \cdot AD$
- Vadkan Valley (2.): $SSC = b_0 + b_1 \cdot WT^{b2} + b_3 \cdot AD^{b4}$

Winter:

- Farkas Valley (3.): $SSC = b_0 + b_1 \cdot Q^{b2} + b_3 \cdot AD^{b4} + b_5 \cdot ST0$
- Vadkan Valley (4.): $SSC = b_0 + b_1 \cdot AD^{b2} + b_3 \cdot ST0^{b4} + b_5 \cdot ST10^{b6}$

Spring:

- Farkas Valley (5.): $SSC = b_0 + b_1 \cdot WT^{b2} + b_3 \cdot ST0^{b4} + b_5 \cdot ST5^{b6}$
- Vadkan Valley (6.): $SSC = b_0 + b_1 \cdot WT^{b2} + b_3 \cdot ST0^{b4} + b_5 \cdot ST5^{b6}$

Summer:

- Farkas Valley (7.): $SSC = b_0 + b_1 \cdot Q^{b2} + b_3 \cdot WT^{b4} + b_5 \cdot AD^{b6}$
- Vadkan Valley (8.): $SSC = b_0 + b_1 \cdot WT^{b2} + b_3 \cdot ST0^{b4} + b_5 \cdot ST5^{b6}$

Annex IV.IV.2/b. Summary of the low flow regression model parameters and the coefficients of model efficiency (List of symbols: r^2 – determination coefficient; NSCE – Nash-Sutcliffe coefficient; N – sample size; SD of res. – standard deviation of residuals; b0-b6 – model parameters)

Eq.	***r^2***	***NSCE***	***N***	***SD of res.***	***b0***	***b1***	***b2***	***b3***	***b4***	***b5***	***b6***
1.	0.297	0.297	88	49.8	11.087	33.049	-0.390	2.474	3.490	-	-
2.	0.193	0.193	89	43.4	52.221	0.001	3.738	0.043	2.126	-	-
3.	0.715	0.756	13	43.8	255.949	-47.271	0.980	2.072	1.407	-22.813	-
4.	0.368	0.735	13	37.4	160.503	0.234	1.892	-11.021	0.803	-0.014	4.745
5.	0.383	0.419	42	57.3	94.886	-11.242	0.815	-0.024	3.313	0.968	2.287
6.	0.215	0.216	42	48.4	47.266	-0.083	2.505	-0.186	2.449	3.183	1.694
7.	0.225	0.235	83	46.0	-1927.347	2097.726	0.005	-29.804	0.374	3.454	1.202
8.	0.284	0.317	38	37.5	250.056	-3.990	0.033	-12.907	1.140	0.054	2.895

Annex IV.IV.3. Summary of the high flow regression model parameters and the coefficients of model efficiency (List of symbols: r^2 – determination coefficient; NSCE – Nash-Sutcliffe coefficient; N – sample size; SD of res. – standard deviation of residuals; b0-b6 – model parameters)

Eq.	***r^2***	***NSCE***	***N***	***SD of res.***	***b0***	***b1***	***b2***	***b3***	***b4***	***b5***	***b6***
4.1	0.785	0.790	27	607.2	-5621.238	409.574	0.610	-2.302	1.588	5207.038	0.033
4.2	0.730	0.735	26	745.0	-345.892	66.046	1.247	-0.009	3.610	8.267	1.433
4.3	0.667	0.668	50	449.2	-961.076	319.376	0.618	-35.101	1.105	646.091	0.229

4.4	0.831	0.832	45	260.9	-49.080	12.505	1.473	-2.453	1.590	61.280	0.468
4.5	0.983	0.983	10	169.9	-1712.356	-0.407	4.318	2.602	2.833	7.785	0.994
4.6	0.971	0.971	13	203.0	-655.460	105.574	1.327	-0.330	3.166	11.058	0.496
4.7	0.793	0.793	11	561.3	-1594.718	396.044	0.926	-18.704	3.161	3.193	2.590
4.8	0.997	0.997	13	40.8	-378.354	62.270	1.108	57.858	0.611	35.761	0.038
4.9	0.961	0.961	14	206.2	12742.499	18.163	1.315	-17.561	1.836	23.551	0.973
4.10	0.996	0.996	14	47.9	-8212.771	21.982	1.337	11.399	1.864	-16.571	1.059

Annex IV.IV.4. Monthly precipitation and bedload yield (BY) in the hydrological year 2008-2009 in the Farkas Valley

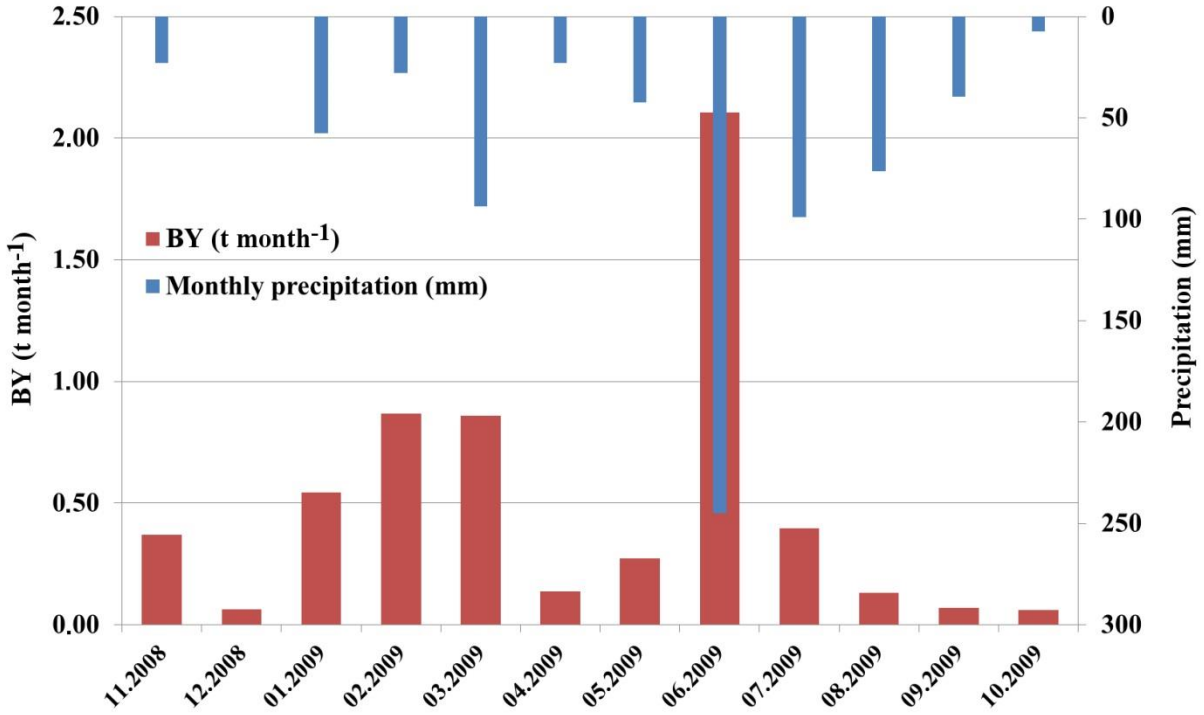

Annex IV.IV.5. Results of the sensitivity analysis for suspended sediment yield (SSY) under high flow conditions in the hydrological year 2008-2009 from one at a time parameter perturbations (List of symbols: Q – discharge; API1, API3 – antecedent precipitation of 1 and 3-days; EI – erosivity index; Q_{max} – peak discharge)

Para-meter	Perturbation +10%		Perturbation +20%		Perturbation -10%		Perturbation -20%	
	SSY_high flow (t)	Change (%)	SSY_high flow (t)	Change (%)	SSY_high flow (t)	Change (%)	SSY_high flow (t)	Change (%)
Q	131.8	19.0	154.2	39.2	91.2	-17.6	73.3	-33.9
API1	106.4	-4.0	101.9	-8.0	115.0	3.8	119.2	7.6
API3	110.4	-0.3	110.1	-0.6	111.1	0.3	111.4	0.6
EI	111.3	0.5	111.9	1.0	110.1	-0.6	109.4	-1.2
Q_{max}	110.8	0.0	110.8	0.0	110.8	-0.0	110.7	-0.0

The reference (control) SSY output is 110.8 t.

Annex IV.IV.6. Mass curve of bedload yield and discharge from January 2006 to October 2009 in the Farkas Valley

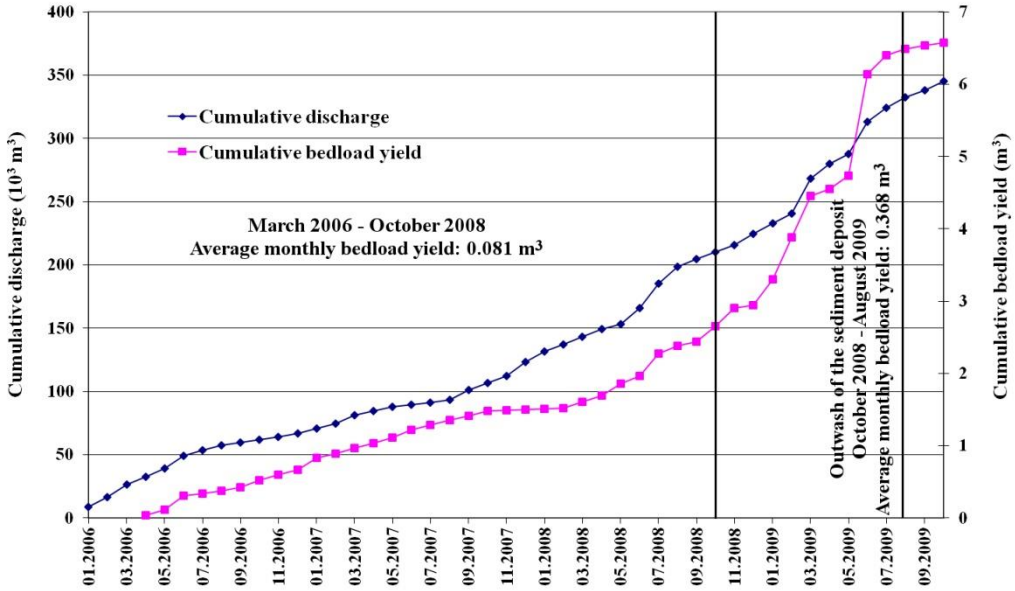

Annex IV.V

Annex IV.V.1. Attributes of the feature layer combining rainfall, soil, land cover, land use, and elevation data

Attributes of Full soil and coverage_08

OBJECTID *	SoilType	K factor	LU_units	LU_practice	P factor	LC_category	LC_category_text	C factor	Shape_Area	R factor
152	Ls2	0,39	174D		0,2	1	Meadow with seedlings (beech mixed spruce)	0,004	17903,48	108,4
153	Ls2	0,39	174D		0,2	3	Young deciduous forest mixed spruce	0,007	2529,55	108,4
154	Ls2	0,39	166A		0,2	1	Meadow with seedlings (beech mixed spruce)	0,004	156,95	108,4
155	Slu	0,42	167C	EÜ04 TRV05	0,2	7	Coniferous forest mixed deciduous trees	0,007	2218,34	108,4
156	Slu	0,42	167DF	EÜ04,07 FFV05-06 TKGY07 EÜ09	0,3	10	Coniferous forest with clearances	0,005	1624,33	108,4
157	Slu	0,42	167DF	EÜ04,07 FFV05-06 TKGY07 EÜ09	0,3	7	Coniferous forest mixed deciduous trees	0,007	307,9	108,4
158	Slu	0,42	167E		0,2	10	Coniferous forest with clearances	0,005	15799,57	108,4
159	Slu	0,42	167E		0,2	7	Coniferous forest mixed deciduous trees	0,007	956,03	108,4
160	Slu	0,38	167DF	EÜ04,07 FFV05-06 TKGY07 EÜ09	0,3	6	Beech forest	0,009	4683,15	108,4
161	Slu	0,38	167G		0,2	6	Beech forest	0,009	33712,27	108,4
162	Slu	0,38	168A	TKGY09	0,2	4	Coniferous forest	0,004	749,68	108,4
163	Slu	0,38	168A	TKGY09	0,2	4	Coniferous forest	0,004	677,25	108,4
164	Slu	0,38	168A	TKGY09	0,2	4	Coniferous forest	0,004	3346,87	108,4
165	Slu	0,38	168A	TKGY09	0,2	6	Beech forest	0,009	1111,62	108,4
166	Slu	0,38	168E	EÜ08	0,3	6	Beech forest	0,009	80,19	108,4
167	Slu	0,38	168E	EÜ08	0,3	4	Coniferous forest	0,004	1338,47	108,4
168	Slu	0,38	168E	EÜ08	0,3	6	Beech forest	0,009	612,87	108,4
169	Slu	0,38	171A		0,2	6	Beech forest mixed oaks	0,009	710,45	108,4
170	Slu	0,38	171A		0,3	2	Regrowth	0,003	231,72	108,4
171	Slu	0,38	171A		0,2	6	Beech forest	0,009	462,44	108,4
172	Slu	0,38	171A		0,2	2	Regrowth	0,003	17461,43	108,4
173	Slu	0,38	171B	FVB09	0,2	4	Coniferous forest	0,004	369,07	108,4
174	Slu	0,38	171B	FVB09	0,2	8	Coniferous forest mixed deciduous trees	0,006	19,43	108,4
175	Slu	0,38	171B	FVB09	0,2	6	Beech forest mixed oaks	0,009	14451,32	108,4
176	Slu	0,38	171B	FVB09	0,2	8	Coniferous forest mixed deciduous trees	0,006	8,65	108,4
177	Slu	0,38	171B	FVB09	0,2	6	Beech forest	0,009	6325,66	108,4
178	Slu	0,38	171B	FVB09	0,2	2	Regrowth	0,003	2,02	108,4
179	Slu	0,38	171C	TRV05	0,35	1	Meadow	0,004	32,43	108,4
180	Slu	0,38	171C	TRV05	0,2	8	Coniferous forest mixed deciduous trees	0,006	7750,64	108,4
181	Slu	0,38	171C	TRV05	0,2	1	Meadow	0,01	19,42	108,4

Record: 152 Show: All Selected Records (0 out of 292 Selected) Options

Annex IV.V.2. Average and total surface soil loss with the average LS factor at each land cover type

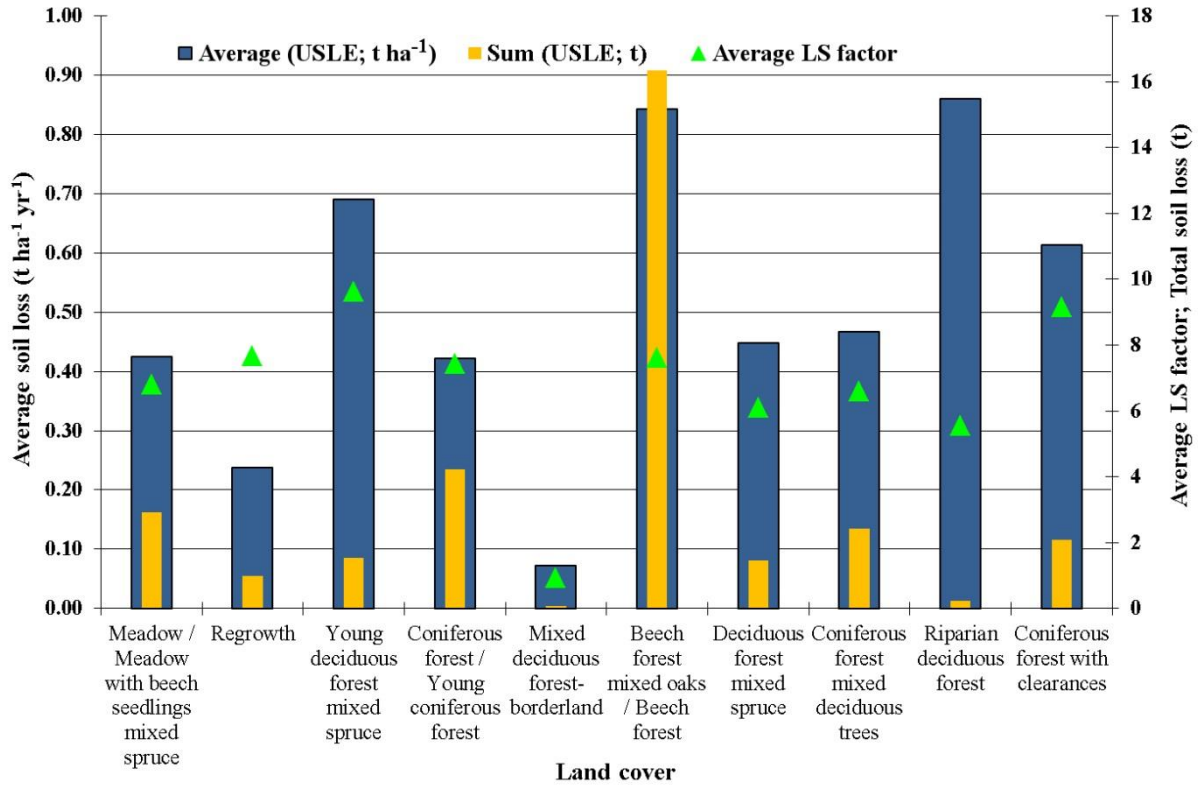

Notes: Categories “riparian deciduous forest” and “beech forest mixed oaks / beech forest” show the highest average soil loss assumedly referring to the steep slopes, the sparse canopy closure, undergrowth and litter layer. The highest average soil loss value is also six times lower than the tolerance limit, emphasizing the soil protection role of forest vegetation. As for the regions of meadow and regrowth, soil erosion risk is diminished by the dense undergrowth and its root system.

Annex IV.V.3. Correlation coefficients between soil loss and the USLE factors in case of land cover categories (Marked correlations are significant at p<0.05)

	Area	***LS*-average**	***LS*-max**	***K*-average**	***K*-max**	***C*-average**	***C*-max**	***P*-average**	***P*-max**
Soil loss-average	0.31	0.54	0.12	0.44	0.34	0.41	0.30	0.53	-0.04
Soil loss-sum	***0.96***	0.25	0.23	0.07	0.15	0.19	0.23	0.21	0.30

Notes: No significant correlation has been obtained between the average specific soil loss and average and maximal values of the USLE factors at the land cover categories. The area of each unit shows only significant linear relation the cumulative surface soil loss per land cover category.

Annex IV.V.4. Rainfall events selected for the erosion modelling (italic letters: intensive events)

Date	**Duration (h)**	**P (mm)**	**Phmax (mm)**	**I_{max30} (mm·h^{-1})**	**EI (MJ·ha^{-1}·mm·h^{-1})**
27-29.01.2009	46.5	26.5	2	3	8.8
19.03.2009	14.5	19	4	6	16.3
24.06.2009	*9.9*	*44.5*	*10.5*	*17*	*154.0*
18.07.2009	*7.5*	*23*	*12*	*21*	*104.5*
03-04.08.2009	*18.0*	*42*	*8*	*21*	*176.9*
04-05.09.2009	24.0	22.5	6	10	32.6

Annex IV.V.5. Comparison of the average soil loss by the USLE and EROSION-3D at each land cover category

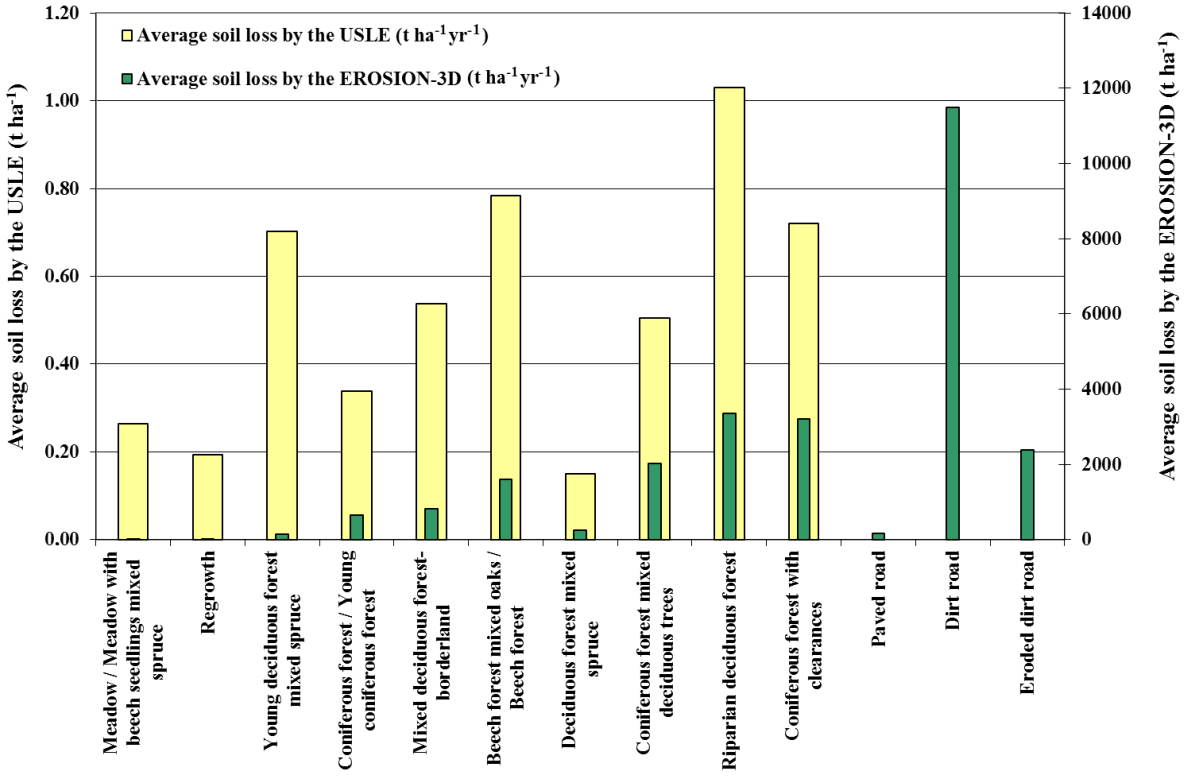

Annex IV.V.6. Observed soil loss in the Farkas Valley in autumn 2010